UNIVERSITAT POLITÈCNICA DE CATALUNYA BARCELONATECH

# *Obtaining micro- and nanotextured functional surfaces on thermoplastics via injection moulding techniques using laser textured metallic inserts and NIL (nano-imprint lithography) -textured polymeric films*

**Carlos Sáez Comet**

PhD program in Polymers and Biopolymers

# Obtaining micro- and nanotextured functional surfaces on thermoplastics via injection moulding techniques using laser textured metallic inserts and NIL (nano-imprint lithography) -textured polymeric films

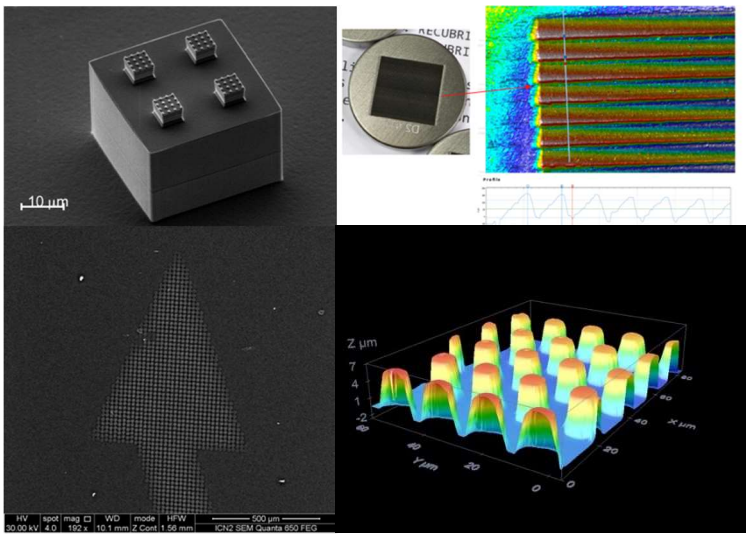


**Doctoral thesis by:**
Carlos Sáez Comet

**Thesis advisor:**

Dr. Jordi Puiggali Bellalta – Dr. Luis Javier del Valle Mendoza
Departament d'Enginyeria Química. Escola d'Enginyeria de Barcelona Est (EEBE). Universitat Politècnica de Catalunya

**Industrial manager/supervisor**:

Dr. Enric Fontdecaba Baig (EURECAT)


Barcelona, 12 de Junio de 2023

## ABSTRACT

Surfaces with special functionalities owed to their surface topographies or textures are present all around us in nature. Millions of living organisms around us profit from those special functionalities thanks to the features existing on the interfaces that separate them from the surrounding environment. These functionalities, such as special wettability or antibacterial properties, for example, arise from the micro- and nanometre periodically organized features present on those interfaces.

These properties that arise from the specific interactions of the micro- and nanotextures present on the surfaces with the surrounding environment (light, liquids, infectious agents, etc.), constitute a powerful inspiration towards the functionalization of the surfaces of plastic parts. The possibility of functionalizing the surface of plastic parts using a replication-based technique applied to a high-volume and low-cost-per-part well-known production technology such as injection moulding has acquired a lot of scientific interest during the last years. This technology allows for the production of such parts without the need of using special coatings or treatments. This in turn reduces their complexity and also the resources and times needed for the manufacturing, while also lowering their environmental footprint.

The production of such surfaces through injection moulding requires the use of micro- and nanotextured mould inserts that serve as negative template tooling for the obtention of the textured features on the surface of the final plastic produced part. In this regard, the usage of two different types of tooling have been researched in this study: first, metallic micro- and nanotextured inserts and second, flexible polymeric inserts.

In the first part of this research, the use of micro- and nanotextured metallic materials as injection mould inserts, a thoroughly studied technology for the production of micro- and nanotextured surfaces on polymeric parts, is studied.

In this case, the influence of the process parameters on the obtained results been carried out using mainly transparent thermoplastic polymers (PC, PMMA, PET, TPU). Along with it, various process technology improvements and functional characterization techniques to determine the functionality of the obtained plastic parts has been researched. Also, practical applications of the obtained results within the frame of a publicly financed project are shown within this section.

The main results show that mould temperature and holding pressure played a major role in the degree of replication (*DR%*) of the micro/nanostructures

obtained in the surface of the polymeric parts manufactured via isothermal injection moulding (IIM). Also, the improvements in the *DR%* achieved when using advanced injection moulding techniques such as variothermal injection moulding (VIM) and injection compression moulding (ICM) were researched, and the relevant functional characteristics promoted by the micro- and nanotextures replicated (special wetting, optical and mechanical properties) were thoroughly characterized.

In the second part of the research, the use of flexible polymeric materials as mould inserts, a more innovative and potentially more cost-effective technology, has been studied. In this section, the influence of the process parameters on the obtained results and the improvement of the flexible insert materials, along with a characterization of all the results obtained has been studied. Also, several complementary topics have been researched: the enhancement of the functional properties of the obtained plastic parts via secondary treatments (coatings, ionic implantation), the study of the thermoforming of such textured films to be used as 3D mould inserts and the extension of the used injectable materials to current polymers of crescent industrial interest (biopolymers).

The results showed the suitability of the method to replicate micro- and nanostructures of various levels of hierarchy and its limitations when using common transparent thermoplastics and biopolymers of high interest. The functionalities of the surfaces replicated were thoroughly characterized, and their evolution when the nanostructures were practiced on flat films latter thermoformed to 3D shapes was also analysed. A predictive model based on the change of the nanostructure geometries upon thermoforming was also established.

Some of the works presented within this industrial PhD have been carried out within the publicly financed PLASTFUN project *(Planta Pilot de Peces Plàstiques amb Superficies Funcionals Avançades)*, supported by the European Regional Development Fund (ERDF), as part of the operative frame FEDER of Catalonia 2014-2020 EC [COMRDI 16-1-0018].

**Keywords:** Injection moulding, laser-textured inserts, polymeric inlays, hierarchical micro/nanotextures.

RESUMEN

Las superficies con funcionalidades especiales debidas a sus topografías o texturas superficiales están muy presentes en la naturaleza aque nos rodea. Millones de organismos vivos a nuestro alrededor se benefician de dichas funcionalidades especiales gracias a las características existentes en las interficies que los separan del entorno. Estas funcionalidades, tales como la humectabilidad especial o las propiedades antibacterianas, por ejemplo, surgen de las características micro y nanométricas organizadas periódicamente presentes en esas interfaces.

Estas propiedades que surgen de las interacciones específicas de las micro y nanotexturas presentes en las superficies con el entorno circundante (luz, líquidos, agentes infecciosos, etc.), representan una poderosa fuente de inspiración hacia la funcionalización de las superficies de las piezas plásticas. La posibilidad de funcionalizar la superficie de piezas de plástico mediante una técnica basada en la replicación aplicada a una tecnología de producción de alto volumen y bajo coste por pieza tal como el moldeo por inyección ha adquirido un gran interés científico en los últimos años. Esta tecnología permite la producción de dichas piezas sin necesidad de utilizar recubrimientos o tratamientos especiales. Esto a su vez reduce la complejidad de dichas piezas y también los recursos y tiempos necesarios para la fabricación, al tiempo que reduce su huella ambiental.

La producción de dichas superficies a través del moldeo por inyección requiere el uso de insertos de molde micro y nanotexturizados que sirven como herramientas de plantilla negativa para la obtención de las características texturizadas en la superficie de la pieza plástica final producida. En este sentido, en este estudio se ha investigado el uso de dos tipos diferentes de herramientas: en primer lugar, insertos metálicos micro y nanotexturizados y, en segundo lugar, insertos poliméricos flexibles.

En la primera parte de esta investigación se estudia el uso de materiales metálicos micro y nanotexturizados como insertos de moldes de inyección, una tecnología muy estudiada para la producción de superficies micro y nanotexturizadas en piezas poliméricas.

En este caso, la influencia de los parámetros del proceso en los resultados obtenidos se ha llevado a cabo utilizando principalmente polímeros termoplásticos transparentes (PC, PMMA, PET, TPU). Paralelamente, se han investigado diversas mejoras tecnológicas de proceso y técnicas de

caracterización funcional para determinar la funcionalidad de las piezas plásticas obtenidas. Además, en esta sección se muestran aplicaciones prácticas de los resultados obtenidos en el marco de un proyecto financiado con fondos públicos.
Los principales resultados muestran que la temperatura del molde y la presión de mantenimiento jugaron un papel importante en el grado de replicación (DR%) de las micro/nanoestructuras obtenidas en la superficie de las piezas poliméricas fabricadas mediante moldeo por inyección isotérmica (IIM). Además, se investigaron las mejoras en el DR% logradas al utilizar técnicas avanzadas de moldeo por inyección, tales como el moldeo por inyección variotérmica (VIM) y el moldeo por inyección- compresión (ICM), y se caracterizaron minuciosamente las características funcionales relevantes promovidas por las micro y nanotexturas (humectación especial, propiedades ópticas y mecánicas).
En la segunda parte de la investigación se ha estudiado el uso de materiales poliméricos flexibles como insertos de molde, una tecnología más innovadora y potencialmente más rentable. En este apartado se ha estudiado la influencia de los parámetros del proceso en los resultados obtenidos y la mejora de los materiales de inserto flexible, junto con una caracterización de todos los resultados obtenidos. Además, se han investigado varios temas complementarios: la mejora de las propiedades funcionales de las piezas plásticas obtenidas mediante tratamientos secundarios (recubrimientos, implantación iónica), el estudio del termoformado de dichos films texturizados para su uso como insertos de moldes 3D y la extensión de desde los materiales inyectables utilizados hasta los polímeros actuales de creciente interés industrial (biopolímeros).
Los resultados mostraron la idoneidad del método para replicar micro y nanoestructuras de varios niveles de jerarquía y sus limitaciones cuando se utilizan termoplásticos transparentes comunes y biopolímeros de alto interés. Se caracterizaron minuciosamente las funcionalidades de las superficies replicadas y se analizó su evolución cuando se practicaban las nanoestructuras sobre películas planas, estas últimas termoformadas a formas 3D. También se estableció un modelo predictivo basado en el cambio de las geometrías de las nanoestructuras tras el termoformado.
Algunos de los trabajos presentados dentro de este doctorado industrial se han realizado dentro del proyecto PLASTFUN (Planta Pilot de Peces Plàstiques amb Superficies Funcionals Avançades), financiado con fondos públicos y apoyado

por el Fondo Europeo de Desarrollo Regional (FEDER), como parte del marco operativo FEDER de Cataluña 2014-2020 CE [COMRDI 16-1-0018].

**Palabras clave:** Moldeo por inyección, linsertos texturizados por láser, insertos de films poliméricos, micro/nanotexturas jerárquicas.

The production of micro- and nanotextured surfaces on all sort of materials using effective production methods has been a topic of high interest in the applied sciences and engineering world during the last decades. Such surfaces can be obtained by replication of micro- and nanotextured templates using injection moulding processes.

In those processes, the textured inserts are placed inside the injection moulds as templates, commonly referred as inlays, and they are usually produced using high-cost and low productivity techniques currently limited to 2D shapes, such as the case of lithography, chemical etching, or micromachining. Furthermore, athey are mainly manufactured using expensive metallic materials such as Nickel or Silicon.

The results published around these investigations mainly concern high flowing and low melt viscosity polymers such as PP, PE, or ABS, of little interest in the context of optical and/or high surface quality applications in the automotive or consumer electronics industries.

Adding to that, limited works have been published with focus on the use of textured inserts produced by high productivity and flexible technologies on readily available materials, such as laser texturing on steel inserts. This technique allows for he potential extension to 3D surfaces and it's been studied in this research with a focus on transparent polymers of higher value and more challenging rheological properties.

Therefore, the first main topic of this research focuses on studying the replication of micro- and nanotextures on the surface of transparent thermoplastics of high interest in the mentioned industries (such as PC and PMMA) via isothermal injection-moulding using laser textured inserts. Additionally, the improvement possibilities on the degree of replication *(DR%)* of the textures achieved by using advanced injection moulding technologies such as infrared mould heating or injection compression moulding (*ICM)* are explored.

Then, the second part of this thesis focuses on the study of a low-cost and flexible tooling alternative of higher resolution and recyclability: the use of flexible polymeric micro- and nanotextured inserts as mould inlays produced by an innovative low-cost alternative based on intermediate PDMS replicas. This second part is extended to the exploration of an enhancement of properties.

produced by the application of secondary treatments to the obtained micro- and nanotextures such as coatings and ion implantation techniques. Furthermore, the usage of these flexible inserts-based technique is also explored for biopolymers of crescent interest (PHA, PBS, PLA) in the industry within the current scenario of climate crisis.

Finally, such nanotextured polymeric films and how their functional surface properties vary when they undergo a pronounced 3D deformation produced by another typical plastic transformation process, such as thermoforming, are studied. This well-known technique is paramount to the production of high-value added plastic parts in the previously mentioned industries using the currently developing and highly strategic *IME* (in-mould electronics) technology, one of the most relevant R+D lines of the technological centre of Catalonia EURECAT.

## ACKNOWLEDGEMENTS

To Rosa, Mar and Mila, my beloved family, for supporting me during the whole time taken for this PhD Thesis.

To my PhD advisors, Jordi Puiggali and Luis Javier del Valle, for allowing me full freedom to implement and develop my ideas and the continuous support they have shown along the process.

To Enric Fontdecaba, industrial PhD advisor at EURECAT, who turned out to be the best and closest supervisor I have had along my career, for his continuous and friendly support.

To AGAUR and to the Program of *Doctorats Industrials* of the *Generalitat de Catalunya*, for the creation of the industrial PhD's program and the support offered along the whole project, providing the neccessary means and advice to successfully complete the project.

# SCIENTIFIC PRODUCTION ASSOCIATED TO THIS THESIS

## Peer-Reviewed Articles in Scientific Journals

- Carlos Sáez-Comet, Olga Muntada, Achille Francone, Nekane Lozano, Marta Fernandez-Regulez, Jordi Puiggali, Nikolaos Kehagias, Clivia M. Sotomayor Torres, Francesc Perez-Murano, Introducing surface functionality on thermoformed polymeric films, Micro and Nano Engineering Volume 14, 2022. https://doi.org/10.1016/j.mne.2022.100112.
- Carlos Sáez-Comet, E. Fontdecaba, N. Cuadrado & Jordi Puiggali (2022): Injection molding and characterization of microtextures on polycarbonate using laser textured inserts, Materials and Manufacturing Processes, https://doi.org/10.1080/10426914.2022.2075888
- Sáez Comet, Carlos & Muntada, Olga & Lozano, Nekane & Fontdecaba, Enric & Sousa, Patrícia & Llobet Sixto, Jordi & Perez-Murano, Francesc & Puiggalí, Jordi & Del Valle, Luis. (2022). Three-level hierarchical micro/nanostructures on biopolymers by injection moulding using low-cost polymeric inlays. https://doi.org/10.21203/rs.3.rs-1928926/v1

## Contributions to International Conferences

- Polymer Replication at Nanoscale congress 2019. University of Dublin – UCD School of materials and mechanical engineering. Dublin, Ireland. 9-10 May 2019
- “Replication of hierarchical nanostructures on Polycarbonate via Isothermal injection moulding using NIL-textured films”. Polymer Replication at Nanoscale congress 2021. University of Dublin – UCD School of materials and mechanical engineering. Windisch, Switzerland, 28 May 2021
- “Plastronics and Nanotexturing in EURECAT” INNOMAT MEXICO. Mexico. 16.11.2020
- “Biomimetic micro- and nanotextures on polymers via injection moulding”. (International Biomimicry Weekend in Granada, Spain, 5-7.11 2021

## University Lectures

- “Replication of micro- and naotextures on the surface of polymers”- Master in design through new materials. 11.01.2019/2020
- “Micro y nanotexturizado de pieza plástica”. Curso online para Universidad de Navarra. 23.02.2021

## Participation in research projects

- Coordinator of PLASTFUN / RIS3CAT project, dealing with the development and manufacturing of injection moulded parts with printed electronics (IME) and functional micro- and nanotextured surfaces. Project supported by (IDF) RIS3CAT supported by the European Regional Development Fund (ERDF) as part of the operative frame FEDER of Catalonia 2014-2020 EC [COMRDI 16-1-0018], included in the 7th Framework Program and also within the Industrial

Doctoral Program of Generalitat de Catalunya.

- Coordinator of EURECAT's internal NANOTEXT project, dealing with the development and manufacturing of injection moulded parts with printed functional micro- and nanotextured surfaces, and the technologies complementary to optimise their manufacturing.

# TABLE OF CONTENTS


ABSTRACT 4
PREFACE 9
ACKNOWLEDGEMENTS 11
SCIENTIFIC PRODUCTION ASSOCIATED TO THIS THESIS 12
GLOSSARY OF ABBREVIATIONS 17
LIST OF FIGURES 19
LIST OF TABLES 27

**1. INTRODUCTION 29**

1.1 STATE OF THE ART 30
1.2 OBJECTIVES 43
REFERENCES 45

**2. INJECTION MOULDING AND CHARACTERIZATION OF MICROTEXTURES ON POLYCARBONATE USING LASER-TEXTURED INSERTS 54**

ABSTRACT 55
INTRODUCTION 56
MATERIALS AND METHODS 57
RESULTS AND DISCUSSION 65
CONCLUSIONS 75
REFERENCES 77

**3. EXPERIMENTS ON THE REPLICATION OF MICRO-NANOTEXTURES ON POLYMERS USING ADVANCED INJECTION MOULDING TECHNOLOGIES 80**

3.1 INJECTION COMPRESSION MOULDING EXPERIMENTS 81
INTRODUCTION 81
MATERIALS AND METHODS 82
RESULTS AND DISCUSSION 86
CONCLUSIONS 88
3.2 INFRARED MOULD-SURFACE HEATING EXPERIMENTS 90
INTRODUCTION 90
MATERIALS AND METHODS 90
RESULTS AND DISCUSSION 93
CONCLUSIONS 97
3.3 APPLICATION CASE: PLASTFUN PROJECT 98
INTRODUCTION 98
3.3.1 PART 1: IME CAR INTERIOR BUTTON PANEL WITH MICROTEXTURED CENTRAL BUTTON'S SURFACE 98
MATERIALS AND METHODS 98
RESULTS 100
3.3.2 PART 2: IME CAR INTERIOR TOUCH PANEL WITH MICROTEXTURED CENTRAL SURFACE 101
MATERIALS AND METHODS 101
RESULTS AND DISCUSSIONS 102
REFERENCES 104

**4.INJECTION MOULDING OF MICRO/NANOTEXTURED SURFACES USING NIL (NANO-IMPRINT LITHOGRAPHY) – TEXTURED POLYMERIC FILMS 105**

INTRODUCTION 106
4.1 FIRST EXPLORATORY WORKS TO EVALUATE REPLICATION ABILITY AND PROCESS CAPACITY OF CURRENT METHOD 107
MATERIALS AND METHODS 107
4.1.1 NANOTEXTURING PROCESS VIA NANO IMPRINT LITHOGRAPHY 108
4.1.2 INITIAL INJECTION MOULDING TRIALS – DETERMINATION OF COATED FILM/INJECTED POLYMER COMPATIBILITY AND OVERALL PROCESS STABILITY 113
RESULTS AND DISCUSSION 116
CONCLUSIONS 116
4.2 DOE FOR DETERMINATION OF MAIN PROCESS PARAMETERS AFFECTING REPLICATION DEGREE DR% 118
MATERIALS AND METHODS 118
RESULTS AND DISCUSSION 121
CONCLUSIONS 125
4.3 REPLICATION OF THREE-LEVEL HIERARCHICAL MICRO/ NANOSTRUCTURES ON TRANSPARENT POLYMERS OF INTEREST (PC, PMMA) USING POLYMERIC INLAYS. 126
MATERIALS AND METHODS 126
RESULTS AND DISCUSSION 128
CONCLUSIONS 131
4.4 FINITE ELEMENT MODELLING OF THE FILLING PROCESS DURING THE INJECTION MOULDING OF TWO-LEVEL HIERARCHICAL MICROTEXTURES PRACTICED ON TO ORMOSTAMP® COATED PET FILMS 133
MATERIALS AND METHODS 133
RESULTS AND DISCUSSION 136
CONCLUSIONS 140
REFERENCES 141

**5. THREE-LEVEL HIERARCHICAL MICRO/NANOSTRUCTURES ON BIOPOLYMERS BY INJECTION MOULDING USING LOW COST POLYMERIC INLAYS 142**

ABSTRACT 143
INTRODUCTION 144
MATERIALS AND METHODS 146
RESULTS AND DISCUSSION 150
CONCLUSIONS 155
REFERENCES 157

**6. INTRODUCING SURFACE FUNCTIONALITY ON THERMOFORMED POLYMERIC FILMS 159**

ABSTRACT 160
INTRODUCTION 160
MATERIALS AND METHODS 162
RESULTS AND DISCUSSION 169
CONCLUSIONS 173
REFERENCES 174

**7. ION IMPLANTATION AND PVD-COATING OF MICRO/NANOTEXTURED SURFACES OF THERMOPLASTIC MATERIALS. 177**

INTRODUCTION 178
MATERIALS AND METHODS 178
RESULTS AND DISCUSSION 181
CONCLUSIONS 194
REFERENCES 195

**8. FINAL DISCUSSION AND OVERALL CONCLUSIONS 196**

**ANNEXES 204**

1.SUPPLEMENTARY INFORMATION TO "INJECTION MOULDING AND CHARACTERIZATION OF MICROTEXTURES ON POLYCARBONATE USING LASER TEXTURED INSERTS" 205

2.SUPPLEMENTARY INFORMATION ON "INFRARED MOULD-SURFACE HEATING EXPERIMENTS" 211

3.SUPPLEMENTARY INFORMATION TO "INTRODUCING SURFACE FUNCTIONALITY ON THERMOFORMED POLYMERIC FILMS" 215

4.SUPPLEMENTARY INFORMATION TO "THREE-LEVEL HIERARCHICAL MICRO/NANOSTRUCTURES ON BIOPOLYMERS BY INJECTION MOULDING USING LOW COST POLYMERIC INLAYS" 220

## GLOSSARY OF ABBREVIATIONS

| | |
|---|---|
| AR | Aspect ratio (ratio of feature's height to its width or diameter) |
| ABS | Acrylonitrile butadiene styrene |
| COP | Cyclic olefin polymer |
| DR% | Degree of replication |
| DOE | Design of experiments |
| FEM | Finite element modelling |
| LDPE | Low density polyethylene |
| HDPE | High density polyethylene |
| ICM | Injection compression moulding |
| IIM | Isothermal injection moulding |
| IME | In mould electronics |
| IML | In mould labelling |
| IMD | In mould decoration |
| IR | Infrared heating |
| NIL | Nano imprint lithographie |
| PC | Polycarbonate |
| PMMA | Poly (methyl methacrylate) |
| PS | Polystyrene |
| PP | Polypropylene |
| PET | Polyethylene terphtalate |
| PUA | Poly (urethane acrylate) |
| PVD | Physical vapour deposition |

| | |
|---|---|
| SEM | Scanning electron microscope |
| TPU | Thermoplastic urethane |
| TPFS | Trichloro (1H,1H,2H,2H-perfluorooctylsilane |
| UV | Ultraviolet |
| UV-NIL | Ultraviolet radiation assisted Nano imprint lithography |
| VIM | Variothermal injection moulding |
| VICM | Variothermal injection compression moulding |

## LIST OF FIGURES

CHAPTER 1

Figure 1.1. Schematic representation of the insert manufacturing process and the replication of its surface micro/nanotexture by the injected polymer. Image credit: Micro-nanostructured polymer surfaces using injection molding: A review; K. Maghsoudi R. Jafari, G. Momen, M. Farzaneh [14]..... 31
Figure 1.2. Schematic representation of the in a Variothermal Injection moulding process (VIM), in which the system that causes the hot and cold fluid flow through the temperature control system is shown. Image credit: The use of variotherm systems for microinjection moulding- Su Q., Zhang N., Gilchrist M.D. [16]..... 33
Figure 1.3. Schematic representation of the UV-assisted Nano Imprint lithography process to obtain nanotextured polymeric surfaces. Image credit: Fabrication of difficult nanostructures by injection moulding-John-Moir Stormonth Darling..... 37
Figure 1.4. Schematic representation of the Injection-compression moulding process (ICM).Image credit: Keisuke Nagato, Tetsuya Hamaguchi, and Masayuki Nakao - *Injection compression moulding of high-aspect-ratio nanostructures* [30]..... 39
Figure 1.5. Schematic representation of the In mould electronics process technology, showing the presence of a thermoformed polymeric film to give 3D shape to the final injected part's surface. Image credit: NISSHA connect. ..... 41

CHAPTER 2

Figure 2.1. Scheme of the controlled laser switch-off (red lines) along a small zone in one of the passes to create the textured area, on which the normal laser functioning can be observed in black lines..... 59
Figure 2.2 Composed images showing the details of the D1, D2, D3, D5 microstructures. Each of the images is composed by: a scheme of the intended observing direction for each functionality (upper left corner); a confocal image showing the microstructure general appearance (upper right corner) with a line drawn on it showing a linear profile (lower right corner) and the place from which is extracted. Finally, a picture of each disc that shows red dots marking the places in which replication degree and uniformity are investigated (lower left corner). ..... 60
Figure 2.3. Composed image showing the injection mould insert developed to hold the microtextured disc in position during the injection moulding stage (upper left), pointing its specific placement on the injection mould cavity with a red-dotted arrow and line (upper

right CAD-image). Below, a 3D-CAD image of the injected specimen and a processed specimen with a replicated microtextured disc on its centre. ..... 61
Figure 2.4. Results of DOE showing the critical factors and interactions between them in the replication process carried out with PC (*Tm*=mould temperature / *Vinj*= injection speed / *Pcompac*= holding pressure). ..... 66
Figure 2.5. Linear profile extracted from confocal images of the microtextured D1, D2, D3 and D5 steel inserts (left column), and from PC injected specimens (right column). The general appearances of the injected specimens are shown on the right margin... 67
Figure 2.6. Image of the measured luminance on LED-source and a microtextured sample. Measured values are displayed in a logarithmic colour- scale. ..... 71
Figure 2.8. Evolution of the coefficient of the measured friction COF (left y-axis) coefficient and Str values with load and speed levels of indentation. ..... 73
Figure 3.1. Microstructure of holes laser textured on the mould insert-cavity (above) and a CLSM-profile image of the blue line marked (below) CAD drawing of the mould half containing the microstructure in its top section (right)..... 82

CHAPTER 3

Figure 3.2. Compression-springs based ICM mould used and diagram showing the specific forces involved in the process (left) – Image credit: [6]. CAD drawing of the mould half containing the microstructure in its top section (right) – EURECAT ..... 83
Figure 3.3. Picture of the Engel 3K injection moulding machine used in the experiments. Image credit: EURECAT ..... 84
Figure 3.4. Picture of the microtextured insert used in the experiments (left) and the resulting injected part (right)– Image credit: EURECAT ..... 84
Figure 3.5. Confocal images of an area analysed in one of the samples (above), showing the lines marking the two parallel height profiles analysed in the part, and profile extracted from the confocal image showing the curvature produced in the injected samples (below)..... 87
Figure 3.6. Confocal 3D image showing the curvature and flattening of the micrometer-sized pillars of the microtextured area on the injected samples..... 88
Figure 3.7 Image showing the overall configuration of the IR-heater. source: EURECAT ..... 91
Figure 3.8. Image showing the position on which the thermocouples were placed..... 93
Figure 3.9. Confocal image of a part injected without IR-heating with the mould set temperature of 80ºC; Confocal image of the profiles analysed on the area selected

(above); linear height profiles extracted from the area analysed (centre), and 3D confocal image of the area analysed (below). ..... 94
Figure 3.10. Confocal image of a part injected without IR-heating with the mould set temperature of 120ºC; Confocal image of the profiles analysed on the area selected (above); linear height profiles extracted from the area analysed (centre), and 3D confocal image of the area analysed (below). ..... 95
Figure 3.11. Confocal image of a part that reached 45% DR% injected with IR-heating (45” heating to 180ºC mould surface temperature) with the mould set temperature of 120ºC; Confocal image of the profiles analysed on the area selected (above); linear height profiles extracted from the area analysed (centre), and 3D confocal image of the area analysed (below)..... 96
Figure 3.12. 3D CAD Image of the injection moulded part, displaying the LED and the microtextured zone on the central button’s back surface on the part’s back view (above-left). CAD design of the parts central button, showing the placement of the microstructure (above-right) and simulated light-guiding path followed by the LED embedded inside the injection moulded part (below). Picture courtesy of KOSTAL ELECTRICA S.A..... 99
Figure 3.13. Details of the custom-developed microtextured steel insert, shown right next to a non-textured steel insert for comparison (above), and its specific placement on the injection mould cavity (below). ..... 100
Figure 3.14. XY profile (above) of the replicated light-guiding microstructures of the injected plàstic part (above) and 3D CLSM image of the characterized section (below). ..... 101
Figure 3.15. Image of the injection moulded part containing the IME electronically printed film, (above-left). Image of the injection mould used, showing the central microtextured part (right) and picture of the injection moulded part (below-left) without IME film, shown in perspective to highlight the presence of the microstructure. Picture courtesy of Walterpack PPT..... 102
Figure 3.16. XY profile (above) of the replicated anti-scratch microstructure of the injected plastic part (above) and 3D CLSM image of the characterized section (below). ..... 103

CHAPTER 4

Figure 4.1. Features present in the 3x3 and 4x4 stamps used (above), picture of the actual stamps (centre) and table shared by the manufacturer with the relevant dimensional characteristics of the stamps (below). ..... 109

Figure 4.2. Details of the PDMS replica stampers onto the Ormostamp® coated polymeric film, right before UV curing (left), and detail of the UV-curing equipment used (right). ..... 112
Figure 4.3. Details of the Ormostamp® coated polymeric films to be later used as polymeric inlays, obtained using the UV-NIL process. ..... 112
Figure 4.4. 3D CAD file of the injection moulding used during the initial trials. ..... 113
Figure 4.5. Detail of the film fixation inside the injection mould applied for the initial injection moulding trials. ..... 114
Figure 4.6. Details of the Ormostamp®-coated PET nanotextured films (left), and a resulting TPU injection moulded part. ..... 117
Figure 4.7. Details of the 2-level hierarchical microstructures present on the Si-stamps developed by ICN2 and CNM, that were later replicated onto intermediate PDMS stampers to manufacture the final coated polymeric inlays. ..... 118
Figure 4.8. Details of the coated and textured film as delivered by ICN2-CNM (left), and 2-level hierarchical negative microstructures present in the replicated Ormostamp® coated films (right). Pictures courtesy of CNM. ..... 119
Figure 4.9. Details of the custom designed tool insert for textured film inlay placement during the injection moulding process (above-centre), and actual placement of the steel insert in the injection mould (below-left). Lower-Right image: final part resulting after injection. ..... 120
Figure 4.10. CLSM XY profiles extracted from an injected PMMA sample (corresponding to the DOE exp. number 5 – above image), and corresponding reconstructed 3D image of the section analysed on this injected sample (below). ..... 122
Figure 4.11. CLSM 3D constructed image of a PMMA sample showing the truncated pyramid shape of the microfeatures. ..... 123
Figure 4.12. Pictures of the cracked polymeric film inlay. ..... 123
Figure 4.13. Pareto diagram (above) and effect interaction (below) plots of the DOE carried out. ..... 124
Figure 4.14. Details of the three level hierarchical micro/nanofeatures on the Si-stamp (left) and transverse section of it (right). Pictures courtesy of CNM- PLASTFUN project. ..... 127
Figure 4.15. Details of the three hierarchical levels of the macro-micro-nano features present in the Si-stamp developed for the project. A high level of dimensional accuracy and uniformity can be observed (Image courtesy: CNM – project PLASTFUN) ..... 128
Figure 4.16. 3D reconstruction from the CLSM image of one of the PC injected samples (above), showing extracted X and Y profiles of the observed feature and of a plurality of

features across a larger area (2nd image below top one). SEM image of a replicated PC feature next to a small fragment of film inlay (below)..... 129
Figure 4.17. 3D reconstruction from the CLSM image of one of the PMMA injected samples (above), showing extracted X and Y profiles of the observed feature and of a plurality of features across a larger area (2nd image below upper one). SEM image of a replicated PC feature next to a small fragment of film inlay (below). ..... 131
Figure 4.18. 3D drawings showing the three submodel geometries (macro-meso-micro) simulated, and the final two level hierarchical microstructure to be filled during the injection moulding. ..... 134
Figure 4.19. Details of the different mesh sizes used at the three different macro-meso-microscales in the simulation. ..... 135
Figure 4.20. 3D images of the initial macroscale simulations run to validate the use of ANSYS Fluent to run the rest of the multiscale simulations. The virtual sensors placed on multiple points of the geometry can be seen on the MOLDEX3D simulation (right). ..... 136
Figure 4.21. Results of the DOE performed (above) and effect on the filling of microcavities observed at both levels of the selected parameters (below). ..... 137
Figure 4.22. Placement of the virtual sensor point in MOLDEX3D (above) and evolution of the pressure levels observed. ..... 138
Figure 4.23. Evolution of the mould filling (microfeature) obtained from the ANSYS Fluent simulations by monitoring the volume fraction of PMMA vs Air (above) and qualitative comparison of the results obtained. ..... 139

CHAPTER 5

Figure 5.1. (Top) Sketches of each individual process step of the method to obtain plastic inlay stamps from a silicon mould. (Bottom) Photographs (upper row) and micrographs (lower raw) at each step of the process: silicon stamp (a), replicas (b-c) and a final polycarbonate injected plastic piece (e). Micrographs images a), d) and e) are obtained by SEM while the micrographs of the images b) and c) are obtained by confocal microscopy. The scale bar is 10 □m for all the images. ..... 147
Figure 5.2. Details of the inlay stamp consisting of a micro/nano textured polymer coated pet film (left) and sem image detail of the 3-level hierarchical negative structures on it (right). ..... 148
Figure 5.3. PHB injected part. Hierarchical micro/nanotextured zone (left). Detailed single feature of the same PHB part (right). ..... 150

Figure 5.4. Extracted confocal profiles (black line= horizontal profile across features/red line= vertical line along features) of the surface of the micro/nanotextured replicated polymeric parts via injection moulding. The confocal optical image in the left presents the position of extraction of the horizontal (1) and vertical (2) profiles. ..... 151
Figure 5.5 Charts showing the storage modulus measurements obtained of both textured and non textured zones at various frequencies for PBI (above), PHB (centre) and PLA (below). ..... 154

CHAPTER 6

Figure 6.1. (a) Graphical representation of the Young equation and contact angle for a droplet on a surface. (b) Graphical representation of the Wenzel and Cassie-Baxter states for a micro-structured surface. ..... 163
Figure 6.2. Micro-structured texture design. The pattern consists of 4 areas of 30 × 30 mm each that contain arrays of holes pillars diameters d ranging from 4 μm to 10 μm and pitches *p* = 2d for all of therthethem. diameters d ranging from 4 μm to 10 μm and pitches *p* = 2d for all of them. ..... 164
Figure 6.3. Scheme of the overall fabrication process which includes the fabrication of the silicon stamp (steps 1–4) the replication of the stamp in a polycarbonate film by thermal NIL (steps 5–6) and the thermoforming of the film (step 7). ..... 166
Figure 6.4. (a) Design of the thermoforming mold geometry showing the placement of the microstructured areas in red. Dimensions are in millimeters. (b) Photograph of the polycarbonate film on top of the mold prior to the thermoforming process. (For interpretation of the references to colour in this figure legend, the reader is referred to the web version of this article.) ..... 167
Figure 6.5. Detail of the strain in the thermoformed film obtained with the Digital Image Correlation technique. (a): Direction of the major (black lines) and minor (white lines) strain directions. A confocal microscopy image corresponding to each of the imprinted thermal NIL areas illustrates how the microstructure deforms. The values of the major and minor strains at each point of the thermoformed film are represented in Figures (b) and (c), respectively. ..... 169
Figure 6.6. Chart showing the experimental and theoretical (Cassie-Baxter) contact angles in relation to the local major/minor strains for each of the micro-structured zones considered. To calculate the Cassie-Baxter contact angle, the procedure described in [28] was followed. ..... 171
Figure. 6.7. (a) Geometrical deformation suffered by the pillars at each zone of the thermoformed film. (b) Scheme to refer to each of the geometrical parameters. ..... 172

CHAPTER 7

Figure 7.1. Image of the nanoindentation equipment used for the experiments (above), and amplified SEM image of the Berkovich tip used (below). ..... 179
Figure 7.2. Schematic representation (left) and actual picture of the ion implantation source and device (right). ..... 181
Figure 7.3. Hardness increase produced by the CrN coating (left), and image of the PC sample before and after being coated with CrN (right). ..... 181
Figure 7.4. Penetration depth profiles during scratching of the PC and PC + CrN samples (above), and residual morphology profile (below) of the same samples, clearly showing the differences in depths registered for the coated vs the non-caoted sample. ..... 182
Figure 7.5. Penetration depth profiles during scratching of the PC and PC + CrN samples, taken using the CLSM images. ..... 183
Figure 7.6. 3D CLSM images of the residual scratches produced on PC (above) and PC + CrN (below), clearly showing the differences on morphology created, caused by different scratch resistances. ..... 184
Figure 7.7 SEM images at 250X (above) and 2000X (below) of the PC samples before (left) and after (right) Ag+ ion implantation ..... 185
Figure 7.8. EDX images and data of the Ag+ implanted PC samples at 3kV and low vacuum pressure of $2,6 \cdot 10^{-2}$ Pa at two different magnifications, showing the presence of O, Zn and other foreign elements apart from the implanted Ag+. ..... 186
Figure 7.9. Graph of the XPS measurements on the Ag+ implanted PC sample, showing a significant % of Ag3d onthe initial nanometers of sample's depth. ..... 187
Figure 7.10. Picture of the micro/nanotextured TPU sample before (left) and after (right) the ion implantation. ..... 187
Figure 7.11. CLSM images of the TPU sample before (left) and after (right) the ion implantation process. The images show the 1µm diameter micropillars (above) and the 2 µm width vertical lines (below) from the experimental stamps initially used in chapter 3. ..... 188
Figure 7.12. CLSM images of the TPU sample before (left) and after (right) ion implantation, showing the subtle change of the top of the lines after implantation on the profiles extracted (below). ..... 189
Figure 7.13. CLSM images of the TPU sample before (left) and after (right) ion implantation, showing the subtle change of the top of the pillars after implantation on the profiles extracted (below). ..... 190

SUPPLEMENTARY INFORMATION

Figure s1.1. Detail of the points (in red) on the microstructured surfaces of the disks that were used to check the overall morphological uniformity of the microstructure. *note that the points are marked on the original steel discs and not on the injected parts for a simpler representation and better contrast* ..... 205
Figure s1.2. Details of the test set-up utilized for the characterization of light-diffusive microstructures, in which it can be observed how the textured surface is illuminated 206
Figure s1.3. Details of the test set-up utilized for the characterization of light-guiding microstructures. ..... 207
Figure s1.4. Confocal (200X) and SEM images (250X) of the scratches produced on the D3 textured samples at load levels of 2, 5, 7 and 10 N and speed of 8 mm/min..... 208
Figure s1.5. Confocal (200x) and sem images (250x) of the scratches produced on the d3 textured samples at load levels of 2, 5, 7 and 10 n and a common speed of 500 mm/min. ..... 209
Figure s1.6. Picture of the set-up used during the *easy to clean* functionality tests (left), and diagram showing the easy-to-clean test set-up. ..... 210
Figure S12. Image showing a) the lamp type used for the IR-heater, b) the bigger sized heater mounted on the framework, c) the smaller sized heater mounted on the framework, d) the electronic command system. Source: EURECAT ..... 214
Figure s4.1. Fabrication of the silicon mould containing 3-level hierarchical structures. Pattern 1L: steps 1-3; pattern 2L: steps 4-6; pattern 3L: steps 7-9 ..... 220
Figure s4.2 (Left). SEM image of one of the 3-level structures of the silicon master mould. (Right) The basic structure is periodically repeated all across a 100 mm wafer..... 221
Figure S4.3. Details of the injection mould insert and the model of the injected part to be obtained. ..... 222
Figure s4.4. Details of the deterioration of the inlay filmsafter various injection shots, showing coating delamination at its lower section. ..... 223
Figure s4.5. SEM images of deformed micro/nano structures at different magnifications on a PP injected part..... 223

# LIST OF TABLES

## CHAPTER 2

Table 2.1. technical characteristics of the injection moulding machine used for the trials. ..... 62
Table 2.2. Experimental results of the light-diffusion characterization. ..... 69
Table 2.3. Experimental results of the light-guiding measurements..... 70
Table 2.4. Initial measurements of the roughness parameters for non-textured and D3 textured samples. ..... 71
Table 2.5. Roughness parameters for D3-textured and non-textured samples..... 72
Table 2.6. Average water contact angles (5 measurement points) for microtextured pc samples 1 and 2, flat pc sample and d5 steel disc insert..... 74
Table 2.7. Values of initial sample weight, weight after dust addition and % of dust removed after the cleaning and drying process was completed. ..... 74

## CHAPTER 3

Table 3.1. Conditions applied for the Design of Experiments applied to the Injection Compression Moulding experiments. ..... 85
Table 3. 2. Results obtained on the Injection Compression Moulding experiments. .... 86
Table 3.3. Results of the experiments to measure the time taken to reach the set surface temperature. ..... 93

## CHAPTER 4

Table 4.1 Injection moulding processing parameters applied during the first moulding trials..... 115
Table 4.2. Injection moulding DOE matrix ..... 121
Table 4.3. DR% results of the Injection moulding DOE. ..... 121
Table 4.4. Summary of the injection moulding conditions applied in the experiment. 127
Table 4.5. Levels chosen for the parameters of the $2^3$ DOE ..... 135

## CHAPTER 5

Table 5.1. Processing parameters used during the injection moulding trials. ..... 148

Table 5.2: Contact angle measurements..... 153
Table 5.3: COF results obtained for PHB, PLA and PBS plastic parts after 4 days and after 30 days of the injection. ..... 153

CHAPTER 6

Table 6.1. Calculated values of Wenzel $\theta_W$ and Cassie-Baxter contact angles $\theta_{CB}$ for the designs of the stamps. A nominal pillar height of 6.5 mm is assumed for all the quadrants. ..... 163
Table 6.2. Summary of the characterization results after thermoforming. ..... 165

CHAPTER 7

Table 7.1. Details of the process conditions applied and summary of the resulting degraded samples ..... 189
Figure 7.14. Storage modulus, Loss modulus and loss factor for the PC samples. ... 191
Figure 7.15. Storage modulus, Loss modulus and loss factor for the PMMA samples. ..... 192
Figure 7.16. Evolution of the storage modulus with applied voltage for PC (above) and PMMA (below) ..... 193

ANNEXES

Table s1.1. experimental design (doe) matrix used for the injection moulding experiments. $2^3$ experiments were established with taguchi method. $t_m$ = mould temperature; $v_{inj}$ = injection speed; and p = holding pressure. ..... 206
Table s1.2 surface roughness parameters chosen for the study (extracted from https://www.michmet.com/3d_s_spatial_parameters_sal.htm) ..... 207
Table s4.1. Dimensions of the three levels of the hierarchical array in the silicon mould ..... 220

# 1. INTRODUCTION

## 1.1 STATE OF THE ART

The micro- and nanotextured surfaces offer a variety of functional properties owed to their organized periodical topographies, composition and structure. During the last years, the scientific community has shown a notable interest in them, and they are becoming more and more relevant in a wide variety of industrial sectors and applications as an improved solution to enhance the functionalities of polymeric parts.

Numerous publications are being focused nowadays on the study and manufacturing of polymeric parts with such surfaces for a variety of applications. Relevant examples correspond to microfluidic chips [1], optical lenses [2], structural coloration of polymers [3], isolation of specific cells [4] or enhancement of mechanical properties [5], amongst others.

To produce such polymeric parts, injection moulding constitutes the most effective replication method in terms of its consistency, scalability, low cost per part produced and the fact that it is a well and long known technology. To inject polymeric parts using this method, a specific mould tooling is required to generate a template for replication (Figure 1.1). Most commonly, a specific tooling in the form of a mould insert with micro- and/or nanotextured surface is introduced and held in place inside the injection mould, which allows for its replication by the incoming molten polymer once it cools down to its final solid state. This replication template can be obtained either directly on the mould surface or as a stand-alone insert that can be fitted inside the injection mould.

One of the relevant technologies with higher industrial potential is the injection moulding using laser-textured metallic mould inserts, to be latter easily integrated and held in position within the injection moulds. In this technique, the negatively patterned surface on the metallic insert (commonly nickel or steel) is carried out via lithography and plating processes [6] or laser ablation techniques [7,8, 9] to directly remove material from the metallic plate surface in a periodical fashion.

Using a textured metallic insert as an insert tool provides a quick processing route that enables a practical and repeatable approach, limiting the number of intermediate steps involved. Nevertheless, the resolution of the micro- and nanotextures achievable using pico- and femtolasers over the surface of metallic materials is currently limited to the low micrometer/high nanometer range of feature dimensions [10].

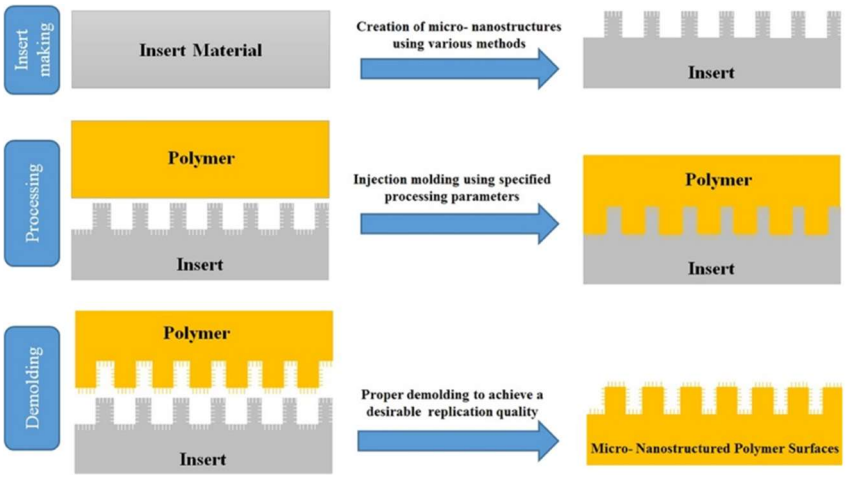


**Figure 1.1. Schematic representation of the insert manufacturing process and the replication of its surface micro/nanotexture by the injected polymer. Image credit: Micro-nanostructured polymer surfaces using injection molding: A review; K. Maghsoudi R. Jafari, G. Momen, M. Farzaneh [14]**.

These limitations associated with the resolution of laser texturing can be overcome by using electroforming and electroplating as alternative techniques to generate patterned thin metallic films out of the silicon masters (being these films latter separated from them) generated by the previously described lithographic techniques. This was shown by Gilchrist M.D. (2018), who succesfully used Ni insert tools with inverted trench patterns by electroforming and dissolving of Al to replicate nanofluidic designs for medical demonstrators [11]. Matschuk M. and. Larsen N.B (2012) also applied a similar approach using mold inserts of electroplated nickel to replicate high aspect ratio nanostructures by injection molding using cyclic olefin copolymers [12].

Zalkovskij, M. and Thamdrup, L. Højlund (2015) demonstrated the replication of sub-micron sized line diffraction gratings on injection molded parts using Nickel-coated steels and advanced steels as textured tool inserts , showing the greatest durability of the advanced steel that was used to complete 73000 injection molding cycles with no change on its topography [13].

Gilchrist M.D.(2018) demonstrated the use of stavax stainless steel, Nickel and BMG as tool inserts to manufacture nanofluidic demonstrators in HDPE using injection molding techniques [11].

The choice of the correct processing parameteres on the injection molding process to replicate micro- or nanotextured inserts is crucial for the appropriate replication of the textures on the final polymeric part. This has an even greater effect on the final replication quality of the injected polymeric parts.

For any polymer replication executed via injection molding techniques, the main factors highly influencing the quality of the replication are the mold temperature, melt temperature, injection and holding pressure, cooling time and injection speed [14]. Any small change in one of these parameters could markedly affect the quality of the replicated surface.

Srirojpinyo C. and Yoon S. (2004) showed that increasing melt temperature, mold temperature, injection velocity, and packing pressure should improve feature definition and depth ratio [15]. They replicated micro scale features using optical-grade polycarbonate (PC), polystyrene (PS), polymethylmethacrylate (PMMA) and polypropylene (PP) with isothermal injection molding, showing that higher melt temperatures allow the polymeric material to flow for longer times to complete the filling of the micro- or nanocavity.

In their study, they also showed that higher mold temperatures will slow the cooling and allow more material to flow to the end of the cavity, and that higher injection velocities lower the melt viscosity due to higher rates of shear and elongation, and to shear heating. This lower viscosity of the melt is expected to improve the depth ratio and feature definition because the material can more easily flow into the features. Rapid filling also reduces cooling of the molten polymer during filling, and thus, should improve feature replication. For this mold design, packing pressure acts like a compression force and higher pressures should force the melt closer to the cavity walls.

The choice of the correct processing parameteres on the injection molding process has a strong effect on the quality and degree of replication of the final polymeric part. The materials used for the tooling can strongly affect the final quality of the polymer replica obtained too.

In this sense, it is important to mention that the use of metals as tool inserts may arise some disadvantages such as those related to their high thermal conductivity and diffusivity of these materials. Those two properties cause a high cooling rate of the molten polymer upon contact with the metallic insert, which rapidly creates a “frozen” skin of polymer that prevents further flowing of it, therefore frequently hindering the complete filling of the micro- and/or nano-cavities by the polymer [14]. This commonly results in a poor replication of the textures contained in the tool insert, and therefore a decrease in the expected properties of the functional surface.

A potential improvement on the quality of replication on the final injected parts can be achieved by using advanced injection molded methods such as compression molding or variothermal injection molding (rapid surface temperature modulation of the injection mold) or even their combinations.

In the variothermal injection moulding, a system that allows for a precise control of the mould temperature and a rapid heating and cooling of the mould cavity is used. The heating can be carried out by means of several methods such as lasers, inductive and resistive heating, hot liquid circulation, gas vapour, or even firing the mould cavity. The cooling is usually carried out by using appropriate refrigerating pipes (most commonly using cool water) to quickly cool down the mould after the material injection has ended. A schematic representation of the system can be seen in Figure 1.2.

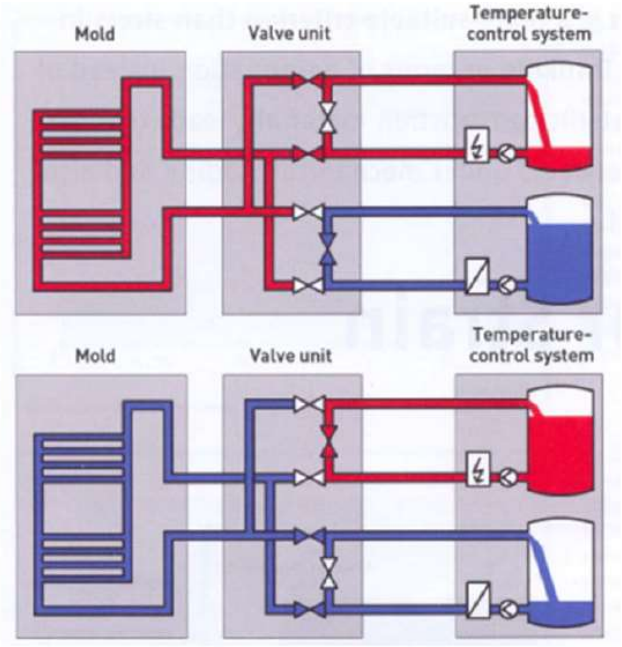


**Figure 1.2. Schematic representation of the in a Variothermal Injection moulding process (VIM), in which the system that causes the hot and cold fluid flow through the temperature control system is shown. Image credit: The use of variotherm systems for microinjection moulding- Su Q., Zhang N., Gilchrist M.D. [16].**

This system can maintain and tightly control a higher mould temperature (close to that of the melt incoming polymer) for longer time, therefore allowing an enhanced filling of the micro- and nanocavities present in the negatively patterned mould insert, and then cause a rapid cooling of the mould surface once this step is completed. The use of such system also allows for a quicker and more efficient heating of the mould that improves the quality of replication of the textures. Thus, greater geometrical accuracy and lower deformations are provided when they're compared to the features present in the tool insert. Also, the quicker cooling step allows for a potential reduction in the injection cycle times.

It should also be noted that even if this is an effective system, its wide applicability might be limited to its high implementation cost and the fact that is mould-specific, with clearly limits its flexibility. That therefore creates the need of research for other more cost-effective rapid surface heating techniques such as IR-surface mould heating.

Su Q., Zhang M. and Gilchrist M.D. (2016) analysed in their review the use of different variothermal systems and microinjection moulding process to study the existence of a quickly formed frozen polymeric layer during the filling of micro- and nanocavities [16]. This frozen layer generates quality problems on the obtained such as weld lines, incomplete filling, large residual stresses, and imperfect surface smoothness. They concluded that a variothermal system is a useful solution for these problems, as long as the appropriate heating system is selected (a greater challenge than the choice of the cooling system, due to the highest influence of the mould surface temperature upon contact with the molten polymer during injection. This happens to be the determinant factor on the filling of the micro- or nanocavity).

Liparoti S., Speranza V. and Pantani R. (2018) showed in their study the effects on the quality of the replication of micro- and nanofeatures of Nickel shims used as tool inserts by using rapid surface-temperature modulation (obtained by a heating device layered below the cavity surface) with two PLA grades of different viscosities [17].

In their study, they analysed the pressure and temperature profiles of the complete cycles and observed their effect on the accuracy of replication, showing that replication accuracy of microfeatures increases with both temperature level and heating time. On the other hand, they showed that an increase of packing pressure only marginally improves the replication.

Yu M. et al. (2017) used a two-lamp infrared heating system that were able to fit within the mould walls in between injecting cycles in order to heat a microtextured PMMA mould surface during few seconds [18]. They observed a complete mould filling when heating the microtextured mould surface during 10s. with a constant set mould temperature of 80ºC.

Berlin W. et al. (2022) developed a numerical model to try to increase the efficiency of energy input by infrared radiation into metals, using an aluminium mould with built-in infrared radiators and moveable mould surfaces [19].

The quality of the replication is also related to the pressure within the cavity mould along the injection process. Considering all the pressure contributions during the injection moulding cycle, we can estimate that during the polymer flow, the pressure exerted on the polymer has to overcome the pressure drop due to the filling of micro- or nanocavity, the one from the potentially trapped air inside the cavities and also the contribution from the surface tension.

This was shown by Matschuk, M.and Larsen, N.(2012), who succesfully replicated various micro- and nanotextures on fluorocarbon-containing thin films surface-coatied Nickel inserts using cyclic olefin copolymers [20]. This was also remarked by Rytka C. et al. (2015), who used isothermal, variothermal and injection compression moulding (and also a combination of the latter two) techniques to compare the replication of various aspect ratio 3D nanostructures with each method using various mould materials [21]. They analysed the thermal and wetting behaviour of the polymer and mould cavities, including a calculation of the mentioned frozen layer thickness, relating it with the *no flow* temperature, which was determined for the polymers studied.

The filling process taking place during the injection moulding using finite element modelling techniques has been recently studied, considering the various phenomena and characteristics of the used materials involved (injected polymer, mould material, injection parameters, etc.). Loaldi et al. studied the filling behaviour and tried to predict the replication of microfeatures using a multiscale meshing approach, obtaining reasonably good results but also showing the clear limitations on the use of this tool for the optimization of the process [22].

Rytka C. et al (2015) also simulated in their study the filling of the micro- and nanopatterns present in the mould using the software moldflow and a mulsitcale meshing approach, realising the added difficulty of the simulation when going down to the nanometer vs the micrometer feature size present in the texture [21].

Guerrier P. et al. (2016) used a special mould produced with a glass window to perform a direct visual (and other) comparison of ABS and PC injection moulded parts with simulations carried out using the Moldex 3D software and a high-speed imaging system [23]. They revealed the good agreements of the pressures registered within the cavities with those obtained in the simulations, although some discrepancies arose with lower cavity-filling times observed in the simulation vs the high-speed videos, mainly due to the non inclusion of barrel acceleration and incorrect mould cushioning size in their initial calculations.

Baldi-Boleda T. et al. (2021) used the software Polyflow with a monoscale approach to simulate the filling of hydrophobic microstructures, using PP as injected polymer [24]. They proved the effectivity of the tool to define process parameters such as temperature and cycle times and compared the effectivity of calculation of the software of Polyflow versus other relevant softwares such as Ansys Fluent.

Muntada-López O. et al. (2019) used computer fluid dynamics simulations to simulate the filling of nanostructured gratins on plastic parts using PP as injected polymer [25].

They studied replication of process parameters such as maximum injection pressure, injection time, charge and polymer temperature, demoulding, etc., and also other the geometric factors from the micro/nanostructure and their influence on the overall quality of the replication. They observed some shrinking of the nanostructured area and of the pattern period used and related them to a local young's modulus reduction and thermal contraction of the part upon demoulding.

A additional potential way of reducing the problems associated with the high thermal conductivity of metallic inserts and the creation of the frozen layer, as mentioned by the previous authors [16, 21] is the use of anti-adhesive polymeric coatings, such as those based on fluorocarbons or hydrocarbons [20]. They also show some other added benefits, like the reduction of demoulding issues such as feature damages (for high aspect ratios, *AR*), but in the end they represent and added manufacturing step on top of the already high manufacturing cost of the metallic inserts.Their lifespan can often be limited too, depending on the polymers injected and the morphology of the micro-nanotexture and the injected part itself.

Another possible injection moulding tooling technology is the use of textured polymeric inserts, which is the secondly proposed technique in this Thesis. The low thermal conductivity typical of this materials acts as a thermal barrier (between metallic mold and molten polymer) and thus reduces the cooling rate of the molten incoming polymer upon contact with it, therefore providing it with longer time for the filling of the micro- and nanocavities [26].

To use a textured polymeric material as tool insert, we use a second processing technique to produce the original textured patterned part. It starts with the manufacturing of a micro- and/or nanotextured master (most commonly in silicon or quartz) via lithographic techniques, commonly. This master is then replicated on to an intermediate stamper using the UV-assisted *Nano imprint lithography* (*NIL)* techniques, so getting a negative replica of the original master. In this process, a UV-curable material pressed under fixed pressure on top of it at room temperature and then polymerized by UV radiation [27]. The stamper thus obtained (PDMS in our case) can be then used for additional replication steps or be used as the final functional material [28].

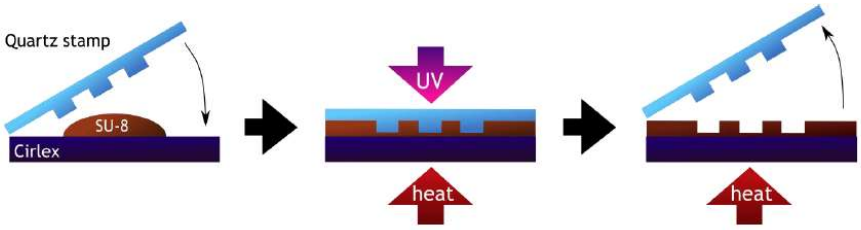


**Figure 1.3. Schematic representation of the UV-assisted Nano Imprint lithography process to obtain nanotextured polymeric surfaces. Image credit: Fabrication of difficult nanostructures by injection moulding-John-Moir Stormonth Darling**

Using this UV-assited *NIL* technique has the advantage of requiring much lower viscosity materials (and therefore lower pressure to allow the filling of nanocavities) than other types of NIL, such as Thermally-assisted NIL; and it also allows the user to operate at room temperature, too.

A possible further replication of this PDMS stamper (complementary geometry –polarity- to the original master) can be carried out using an off-the-shelf material such as a PET or PC film as a substrate. This replication is carried out in order to obtain the polarity of the original geometry of the master on the final template to be used as mould insert. The replication of the intermediate PDMS stamper onto lower cost and higher toughness polymeric materials constitutes an improvement on the mechanical properties of the polymers to be used as final tool inserts. This reverts into an improvement of the film handling and durability.

This polymeric film substrate can be then coated with a suitable material to be micro- or nanopatterned, such as shown by S. H. Park (2011), who replicated micrometer sized line patters using a PUA coated PET film as insert for the injection molding, showing the effectivity of polymeric inlays material (PUA) as an effective thermal barrier [26]. That thermal barrier can significantly hinder heat transfer into the mold during the molding process and thus may keep the melt viscosity low for longer duration.

The polymeric tooling approach is appealing, not just for its simplicity, but also for the fact that it opens up an alternative inlay material and patterning options (e.g. UV-NIL) that remove the requirement for expensive Ni electroforming and can be adapted to the individual's own fabrication capabilities.

The various polymeric materials can also be selected for other applicable properties such as temperature resistance (that might be needed upon contact with the injected polymer) and ease of demoulding once the injected polymer is cooled, therefore potentially avoiding distortions and variations in the geometry of the injection-mold replicated features.

The usage of polymeric materials for micro- and nanotextured tool inserts has also been shown by Stormonth-Darling (2013), who succesfully replicated various micro- and nanotextures (nanopits and naopillars) of high aspect ratios with various grades of PC,PP,PS and TPU, using fluorosilane -coated cirlex polymer inserts [29].

In his study, the applied inlay coatings were shown to have a clear influence on the height, shape and deformation of the micro- and nanofeatures in the final replication. It was shown that non-adhesive $Si_3N_4$+TPFS coatings prevented the stretching of low aspect ratio nanopillars. He also pointed out some of the most common fabrication defects obtained in the final polymeric replications, such as incomplete cavity filling, feature deformation and success rate (percentage of the replicated surface that was successfully replicated). These replication defects strongly depend on the correct processing parameters and methods.

As Stormonth Darling stated (2013), the filling of the microcavity implies the polymer overcoming several effects that should be taken into account: the volume of the trapped air while the cavity is being filled gets compressed and subsequently delays its complete filling [29]. The pressure due to surface tension effects also delays this filling, even if its effects become only significant as the dimension of the feature decreases (towards nm-scale), and finally the formation of a solid “frozen layer” at the polymer-air interface, which has to elastically deform to allow the replication process to proceed.

An interesting potential way of overcoming those effects contrary to the filling of the micro- and nanocavities is the use of the injection-compression moulding or ICM method. This process includes and additional step during the injection phase that applies an increased pressure inside the moulding cavity. While in regular injection moulding the polymer melt is injected in a closed mould cavity with almost same dimensions as the final part (to account for polymer shrinkage effects), in ICM the molten polymer is injected into an “open” cavity with the two mould halves initially being separated from each other by a small distance. While the polymer is injected, or once this stage has completely finished, the mould is successively closed during a compression phase, therefore reducing the space available within the cavity (the compression gap) and producing the necessary stroke to perform the compressing action.

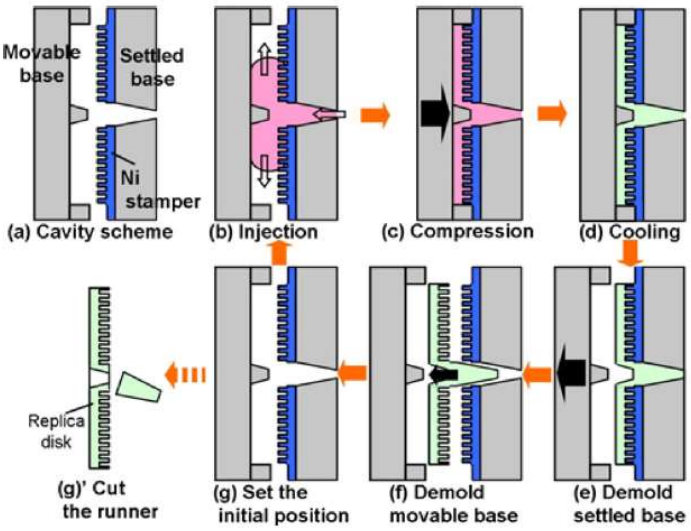


**Figure 1.4. Schematic representation of the Injection-compression moulding process (ICM). Image credit: Keisuke Nagato, Tetsuya Hamaguchi, and Masayuki Nakao - *Injection compression moulding of high-aspect-ratio nanostructures* [30].**

Nagato K. et al. (2011) showed in their study the application of this system (ICM) for the injection moulding of optical discs using electroplated Ni inserts with PC as selected polymer [30]. They successfully used this technique for the replication of high aspect-ratio nanostructures (pattern width: 200 nm, aspect ratio: 2) over the whole area of a circular disk of 120 mm diameter, demonstrating the suitability of this technique to obtain periodical nanotextured surfaces of nm-range over a relatively large area of injected PC polymer with reasonable quality.

This ICM technique offers the possibility of replicating high nm-range with good optical properties, reducing internal stresses accumulated by the polymeric part during the process.

Loaldi D. et al. (2018) used this method to assess its replication capability compared to isothermal injection moulding (IM) for the replication of a microstructured Fresnel lens [31]. Lenses in general require very limited amounts of residual stresses accumulated in them to achieve the right transparency and avoid birefringence issues.

For this purpose, these researchers used cyclic-olefin polymer (COP) and a polymethylmethacrylate (PMMA) and compared the results obtained for IM and ICM processes through the design of two factorial designs of experiments (DOE) in their study. They demonstrated the higher accuracy achieved in the replicated micro-dimensions and the advancements in terms of part warpage and process precision with respect to IM.

The pressure produced in this process is more uniform along the cavity wall, and lower for post filling stage, and therefore results in less residual stress as well as less part warpage. Potential drawbacks for this method include low productivity due to the time-consuming charging step, and the limitation for producing large complex shaped parts.

Rytka C. et al. (2015) tested isothermal injection moulding IM, injection compression moulding and a combination of both in a process known as variothermal injection-compression moulding to compare the results obtained in the replication of polymers of different viscosity and wetting behaviour [21]. They replicated three representative 2D and 3D micro- and nanostructures into polymethylmethacrylate and amorphous polyamide by isothermal and variothermal injection moulding with and without compression, respectively, using the same mould and several different mould inserts as textured templates.

By means of finite element simulation, they calculated parameters of interest such as the frozen layer thickness, the no-flow temperature and heat transfer coefficients with enough accuracy, concluding that even demoulding issues like nano-pillar breakage can be minimized using ICM because of the lower and more evenly stress generated in the injected part. This well-known benefit of reduced pressure and internal stresses in the polymer part can be nicely combined with variothermal heating for best replication accuracy, when low-range nm-structures are to be replicated.

There exist two main schools of thought for how best to tackle the problem of premature freezing induced poor mould filling: variothermal and heat retardation. Variothermal techniques offer a means of precise control that could lead to more predictable outcomes, but do not seem to be any more advantageous in that regard in the evidence presented by the current literature. Furthermore, the development of complex heating/cooling systems is time consuming and costly, which can also cause significant increases in cycle time. On the other hand, heat transfer retardation obtained by the use of polymeric micro/nanotextured inserts, which delays the creation of a frozen layer and thus improves the micro/nanopattern filling, seems to be a much lower cost, flexible and promising technique that well deserves further study.

The use of polymeric textured films via nanoimprint lithography (*NIL)* processes also constitutes an interesting low cost and affordable technology that can allow for the extension of textured film insert injection moulding technologies or simply nanotextured film technologies to the 3D domain.

There are many potential applications in industrial sectors that will clearly need to benefit from the extension to the 3D domain. Some examples of applications that will naturally require to be extend to 3D are the automotive industry (interior parts, optics), electronics like [32] as well as home and industrial lighting [33], to mention a few.

In these sectors, a novel manufacturing technology known as in-mould electronics is becoming more and more relevant [34]. In-mould labelling (IML) [35] and in-mould decoration (IMD) [36] processes allow to handle and incorporate decorative 3D formed polymeric films on final injection-moulded parts.

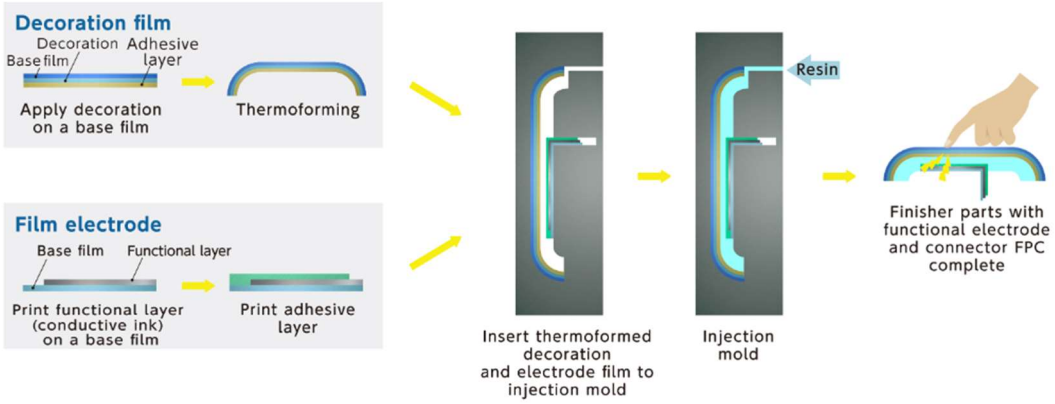


**Figure 1.5. Schematic representation of the In mould electronics process technology, showing the presence of a thermoformed polymeric film to give 3D shape to the final injected part's surface. Image credit: NISSHA connect.**

These manufacturing technologies can be further enhanced by using locally micro- and nanotextured films to obtain local and specific functionalities on the surface of the resulting injection moulded parts. Furthermore, the micro- and nano- textured polymeric films can also be directly used as replication inserts, adequately placed on the injection moulds [25].

A specific lithographic patterning technique that allows for the local 3D micro- and nanostructuring of thermoplastic films is thermal nanoimprint lithography (thermal NIL) [37], a high resolution and high-throughput lithography technique. Thermal NIL is based on the mechanical deformation of a thermoplastic material, which can be a thermoplastic resist coated on a substrate or a bulk thermoplastic sheet/film, with a stamp containing the surface topography to be replicated in a 1 to 1 scale. The achievable resolution is mainly limited by the minimum feature size that can be fabricated on the stamp and sub-10 nm lateral dimensions have been demonstrated [38].

However, most lithography methods require the printed surface to be flat. Some examples of patterning on curve surfaces exist, like for example in nanostencil lithography [39], but they are not a universal solution and present limited industrial applicability. When it comes to form micro and nano- textured films into 3D shapes, a well-known and popular transformation process is thermoforming using vacuum-assisted plugs. In this case, the surface is patterned when it is flat, and later it is given the desired

final macroscopic shape [40]. Applications of thermoforming in industry are large but so far very few examples of functional patterned thermoformed pieces have been realized [41, 42].

After thermoforming, the patterned areas in the film will suffer geometrical distortions caused by the induced macroscopic deformation. Those distortions might negatively impact the surface functionality. To understand the achievable maximum 3D-macroscale deformations that can be applied to the films without losing the surface functionality, a study of how the macroscopic deformation translates into geometrical distortions at the micro- and nano- scale is required. This will then allow to study the loss in the initial surface functionality, if any, and how it could be identified and prevented.

The micro- and nanotextured surfaces, specially on polymeric materials, commonly suffer from low mechanical durability [43], and there is still limited research on their durability and wear characteristics. An interesting possibility to further enhance and fine tune the surface properties of such micro/nanotextured materials lies in the ion implantation treatments. Properties such as hardness, adhesion, wettability, wear, and chemical resistance can be altered with these treatments, and this makes the implantation of organic-based materials an attractive approach for applications in biology and medicine, for example [44,45]. This micro- and nanotexturing process, in which ions of a material are accelerated in an electrical field and impacted into a solid surface of the material to treat, constitutes a versatile and effective surface modification technique for polymers, and is used to change the physical, chemical, or electrical properties of the solid.

In particular, the shallow metal implantation of polymers can change the mechanical and electric properties of the base polymeric material and is of importance for in mould electronics [46] or organic-based functional devices, which constitutes a relevant approach to be further investigated and put into practice within this research. Concerning the surface characterization of the injected polymeric specimens, confocal laser scanning microscopy (*CLSM)* is used to properly characterize the replicated surfaces, when dealing with characterization of polymers [47,48]. Also, scanning electron microscopy SEM and AFM are commonly used, as they constitute well known techniques for the morphological characterization of micro- and nanostructured surfaces with great detail [49,50].

## 1.2 OBJECTIVES

The main objective of this thesis is to investigate the manufacturing of micro- and nanotextured surfaces on polymeric materials via injection moulding using low cost and easy to use flexible tooling as mould inserts. As a starting point to evaluate a performance baseline, isothermal injection moulding processes using traditional mould materials as laser- textured inserts will also be researched.
As secondary objectives, several complementary aspects will be evaluated along the process:

- A comparison of the ICM-associated benefits on the replication quality of various polar and non-polar polymers (to address surface tension effects).

- The possibility of enhancing the replication degree DR% of the injected parts by evaluating VIM and similar techniques.

- Evaluate the applicability and effect of additional secondary treatments on the enhancement of various properties of the textured polymeric surface injected, such as:

- Ionic implantation treatment
- PVD treatments

- Functional characterization protocols (based on optical, confocal and SEM microscopy techniques) of the injected polymeric parts in order to assess the replication degree DR% and uniformity.

- Perform relevant mechanical characterization tests (to be defined) to evaluate the strength and other mechanical characteristics of the injection moulded textured surfaces and evaluate their behaviour with regards to the bulk of the plastic part.

- Study the thermoforming behaviour of polymeric textured inserts towards its future application as 3D polymeric inserts for injection moulding in the industry. This process can be considered as

- The incorporation of various anti-stick agents over the surface of the textured polymeric films, in order to study the appropiate textured-material-on-film/injected polymer combinations that lead to a satisfactory replication.

- Observe the replication behaviour of several of polymers and biopolymers of common use and the process parameters influencing them, developing an innovative finite-element modelling two- stage approach using a common FEM-software.

# REFERENCES


[1] Zhang, Haoyang & Fang, Fengzhou & Gilchrist, Michael & Zhang, Nan. (2018). Filling of high aspect ratio micro features of a microfluidic flow cytometer chip using micro injection moulding. Journal of Micromechanics and Microengineering. 28. 10.1088/1361-6439/aab7bf. https://www.doi.org/10.1088/1361-6439/aab7bf.

[2] Loaldi D, Calaon M, Quagliotti D, Parenti P, Annoni M, Tosello G. Tolerance verification ofprecision injection moulded Fresnel lenses. Procedia CIRP [Internet]. 2018; 75:137–42. https://www.doi.org/10.1016/j.procir.2018.05.004

[3] Højlund-Nielsen, E., Clausen, J., Mäkela, T., Thamdrup, L. H., Zalkovskij, M., Nielsen, T., Pira, N. L., Ahopelto, J., Mortensen, N. A., Kristensen, A. (2016). Plasmonic Colors: Toward Mass Production of Metasurfaces. Adv. Mater. Technol., 1 : 1600054. https://www.doi.org/10.1002/admt.201600054

[4] Islam M, Sajid A, Mahmood MA, Bellah MM, Allen PB, Kim YT, Iqbal SM. Nanotextured polymer substrates show enhanced cancer cell isolation and cell culture. Nanotechnology. 2015 Jun 5;26(22):225101. Epub 2015 May 11. PMID: 25961762. https://www.doi.org/10.1088/0957-4484/26/22/225101

[5] Hernández, J., Monclús, M., Navarro-Baena, I. et al. Multifunctional Nano-engineered Polymer Surfaces with Enhanced Mechanical Resistance and Superhydrophobicity. Sci Rep 7, 43450 (2017). https://www.doi.org/10.1038/srep43450

[6] Nikolaos Kehagias, Achille Francone, Markus Guttmann, Frank Winkler, Ariadna Fernández, and Clivia M. Sotomayor Torres , "Fabrication and replication of re-entrant structures by nanoimprint lithography methods", Journal of Vacuum Science & Technology B 36, 06JF01 (2018) https://www.doi.org/10.1116/1.5048241

[7] Aizawa T, Inohara T. Pico- and Femtosecond Laser Micromachining for Surface Texturing.In: Micromachining [Internet]. Intech Open; 2019 [cited 2020 Oct 9]. https://www.doi.org/10.5772/intechopen.83741

[8] Holzer, C., Gobrecht, J., Schift, H. and Solak, H. (2010), Replication of Micro- and Nanostructures on Polymer Surfaces. Macromol. Symp., 296: 316-323. https://www.doi.org/10.1002/masy.201051044

[9] Ebrahimi M, Konaganti VK, Moradi S, Doufas AK, Hatzikiriakos SG. Slip of polymer melts over micro/nano-patterned metallic surfaces. Soft Matter [Internet]. 2016 ;12(48) :9759–68. Available from: http:/www.doi.org/10.1039/C6SM02235A

[10] Skoulas, Evangelos & Manousaki, Alexandra & Fotakis, Costas & Stratakis, Emmanuel. (2017). Biomimetic surface structuring using cylindrical vector femtosecond laser beams. Scientific Reports. 7.

45114. https:// www.doi.org/10.1038/srep45114

[11] Zhang, N., Srivastava, A. P., Browne, D. J., & Gilchrist, M. D. (2016). Performance of nickel and bulk metallic glass as tool inserts for the microinjection molding of polymeric microfluidic devices. Journal of Materials Processing Technology, 231, 288-300. https://www.doi.org/10.1016/j.jmatprotec.2015.12.011

[12] Matschuk, Maria & Larsen, Niels. (2012). Injection molding of high aspect ratio sub-100 nm nanostructures. Journal of Micromechanics and Microengineering. 23. 025003. https:// www.doi.org/10.1088/0960-1317/23/2/025003

[13] Zalkovskij, Maksim & Thamdrup, Lasse & Smistrup, Kristian & Andén, Thomas & Johansson, Alicia & Mikkelsen, Niels & Madsen, Morten & Garnaes, J. & Kristiansen, Tommy & Diemer, Mads & Døssing, Michael & Minzari, Daniel & Tang, Peter & Kristensen, Anders & Taboryski, Rafael & Essendrop, Søren & Nielsen, Theodor & Bilenberg, B. (2015). Smart plastic functionalization by nanoimprint and injection molding. Proceedings of SPIE - The International Society for Optical Engineering. 9423. https:// www.doi.org/10.1117/12.2085766

[14] Maghsoudi K, Jafari R, Momen G, Farzaneh M. Micro-nanostructured polymer surfaces using injection molding: A review. Mater Today Commun [Internet]. 2017 ;13 :126–43. https:// www.doi.org/10.1016/j.mtcomm.2017.09.013

[15] Srirojpinyo C., Yoon S., Lee Y., Sung Ch., Mead J.L., Barry C.M.F. (2004). Processing Parameters Affecting Nanoinjection Molding. NSTI-Nanotech 2004. ISBN 0-9728422-9-2. Vol. 3, 2004

[16] Su, Q., Zhang, N., & Gilchrist, M. D. (2016). The use of variotherm systems for microinjection molding. Journal of Applied Polymer Science, 133(9). https://www. doi.org/10.1002/app.42962

[17] Liparoti S, Speranza V, Pantani R. Replication of Micro- and Nanofeatures in Injection Molding of Two PLA Grades with Rapid Surface-Temperature Modulation. Materials (Basel). 2018 Aug 15 ;11(8):1442. https://www.doi.org/10.3390/ma11081442

[18] Yu, Ming-Ching & Young, Wen-Bin & Hsu, Pe-Ming. (2007). Micro-injection molding with the infrared assisted mold heating system. Materials Science and Engineering: A. 460. 288-295. https://www.doi.org/10.1016/j.msea.2007.02.036

[19] Berlin, W., Reichel, V., Hürkamp, A. et al. Heat Control simulation for variothermal injection moulding moulds using infrared radiation. Int J Adv Manuf Technol 119, 6073–6089 (2022). https://www.doi.org/10.1007/s00170-022-08715-1

[20] Matschuk, Maria & Larsen, Niels. (2012). Injection molding of high aspect ratio sub-100 nm nanostructures. Journal of Micromechanics and Microengineering. 23. 025003. https:// www.doi.org/10.1088/0960-1317/23/2/025003

[21] Rytka, C., Kristiansen, P.M., Neyer, A., 2015. Iso- and variothermal injection compression moulding of polymer micro- and nanostructures for optical and medical applications. J. Micromech. Microeng. 25, 065008. https:// www.doi.org/10.1088/0960-1317/25/6/065008

[22] Loaldi D, Regi F, Baruffi F, Calaon M, Quagliotti D, Zhang Y, Tosello G. Experimental Validation of Injection Molding Simulations of 3D Microparts and Microstructured Components Using Virtual Design of Experiments and Multi-Scale Modeling. Micromachines. 2020; 11(6):614. https:// www.doi.org/10.3390/mi11060614

[23] Guerrier, Patrick & Tosello, Guido & Hattel, Jesper. (2016). Flow visualization and simulation of the filling process during injection molding. CIRP Journal of Manufacturing Science and Technology. 16. https:// www.doi.org/10.1016/j.cirpj.2016.08.002

[24] Baldi-Boleda T, Sadeghi E, Colominas C, García-Granada A. Simulation Approach for Hydrophobicity Replication via Injection Molding. Polymers. 2021; 13(13):2069. https:// www.doi.org/10.3390/polym13132069

[25] Muntada-López, O., Pina-Estany, J., Colominas, C., Fraxedas, J., Pérez-Murano, F., García-Granada, A., 2019. Replication of nanoscale surface gratings via injection molding. Micro and Nano Engineering 3, 37–43. https://www.doi.org/10.1016/j.mne.2019.03.003

[26] Park, S.W., Lee, W.I., Moon, S.N., Yoo, Y.-E., Cho, Y.H., 2011. Injection molding micro patterns with high aspect ratio using a polymeric flexible stamper. Express Polym. Lett. 5, 950–958. https:// www.doi.org/10.3144/expresspolymlett.2011.93

[27] Jan Haisma, Martin Verheijen, Kees van den Heuvel, and Jan van den Berg, Mold-assisted nanolithography: A process for reliable pattern replication, Journal of Vacuum Science & Technology B: Microelectronics and Nanometer Structures Processing, Measurement, and Phenomena 14, 4124-4128 (1996). https://www .doi.org/10.1116/1.588604

[28] Estévez, Ariadna. “Functional surfaces by means of nanoimprint lithography techniques.” (2016). PhD Thesis. Universitat Autónoma de Barcelona.

[29] Stormonth-Darling, John Moir (2013) Fabrication of difficult nanostructures by injection moulding. PhD thesis, University of Glasgow.

[30] Keisuke Nagato, Tetsuya Hamaguchi, and Masayuki Nakao, Injection compression molding of high-aspect-ratio nanostructures, Journal of Vacuum Science & Technology B 29, 06FG10 (2011). https:// www.doi.org/10.1116/1.3662405

[31] Loaldi D., Quagliotti D., Calaon M, Parenti P, Annoni M, Tosello G. Manufacturing Signatures of Injection Molding and Injection Compression Molding for Micro-Structured Polymer Fresnel Lens Production. Micromachines. 2018; 9(12):653. https:// www .doi.org/10.3390/mi9120653

[32] Shin, Sang Ho & Hwang, Boyeon & Zhao, Zhi-Jun & Jeon, So & Jung, JooYun & Lee, Ji-Hye & Ju, Byeong-Kwon & Jeong, Jun-Ho. (2018). Transparent Displays Utilizing Nanopatterned Quantum Dot Films. Scientific Reports. 8. https://www .doi.org/10.1038/s41598-018-20869-1

[33] Amalathas P., Amalraj & Alkaisi, Maan. (2019). Nanostructures for Light Trapping in Thin Film Solar Cells. Micromachines. https:// www.doi.org/10.3390/mi10090619

[34] Gong, Yao & Cha, Kyoung & Park, Jang Min. (2020). Deformation characteristics and resistance distribution in thermoforming of printed electrical circuits for in-mold electronics application. The International Journal of Advanced Manufacturing Technology. 108. https://www.doi.org/10.1007/s00170-020-05377-9

[35] Chen, Songmao & Zhang, Sai. (2014). Mechanical Behaviors and Thermoforming Features of PMMA Used In-Mold Decoration. Applied Mechanics and Materials. 496-500. 440-443. 10.4028. https://www.scientific.net/AMM.496-500.440.

[36] Chen, Shia-Chung & Huang, Shih-Tsun & Lin, Ming-Chung & Chien, Rean-Der. (2008). Study on the thermoforming of PC films used for in-mold decoration. International Communications in Heat and Mass Transfer 35. 967-973. https://www.doi.org/10.1016/j.icheatmasstransfer.2008.04.008

[37] Chou, Stephen & Krauss, Peter & Renstrom, Preston. (1995). Imprint of Sub-25 Nm Vias and Trenches in Polymers. Applied Physics Letters. 67. 3114-3116. https://www.doi.org/10.1063/1.114851

[38] Chou, Stephen & Krauss, Peter & Zhang, Wei & Guo, Lingjie & Zhuang, Lei. (1997). Sub-10 nm Imprint Lithography and Applications. Journal of Vacuum Science & Technology B. : Microelectronics and Nanometer Structures. 15. 2897 - 2904. https://www.doi.org/10.1116/1.589752

[39] Vazquez-Mena, O. & Gross, L. & Shenqi, Xie & Villanueva, Luis Guillermo & Brugger, Juergen. (2015). Resistless nanofabrication by stencil lithography: A review. Microelectronic Engineering. 132. 236-254. https://www.doi.org/10.1016/j.mee.2014.08.003

[40] Throne, J., Technology of Thermoforming. 1996 ISBN: 9783446402478.

[41] Senn, T. & Waberski, Ch & Wolf, J. & Esquivel, J.P. & Sabaté, N. & Löchel, Bernd. (2011). 3D structuring of polymer parts using thermoforming processes. Microelectronic Engineering. 88. 3043–3048. https://www.doi.org/10.1016/j.mee.2010.08.003

[42] Giselbrecht, Stefan & Gietzelt, T. & Gottwald, Eric & Trautmann, Chris & Truckenmüller, R & Weibezahn, K & Welle, Alexander. (2006). 3D tissue culture substrates produced by microthermoforming of pre-processed polymer films. Biomedical microdevices. 8. 191-9. https://www.doi.org/10.1007/s10544-006-8174-8

[43] Charitidis, C.A. & Dragatogiannis, D.A. & Koumoulos, Elias P. & Perivoliotis, Dimitrios. (2016). Mechanical, Tribological Properties, and Surface Characteristics of Nanotextured Surfaces. https://www.doi.org/10.1002/9781118753460.ch9

[44] Fink, D. & Muller, M. & Chadderton, Lewis & Cannington, P. & Elliman, Robert & McDonald, D. (1988). Optically Absorbing Layers on Ion-Beam Modified Polymers - a Study of Their Evolution and Properties. Nuclear Instruments & Methods in Physics Research Section B-Beam Interactions with Materials and Atoms. 32. 125-130. https://www.doi.org/10.1016/0168-583X(88)90194-2

[45] Leont'ev, A.V. Local Modification of the Optical Constants of Polymeric Films by Ion Implantation. Russian Microelectronics 30, 324–329 (2001). https://www.doi.org/10.1023/A:1011944813048

[46] Popok, Vladimir. (2012). Ion implantation of polymers: Formation of nanoparticulate materials. Reviews on Advanced Materials Science. 30. 1-26.

[47] Zhang, Yang & Mischkot, Michael & Hansen, H. & Hansen, Poul-Erik. (2015). Replication of microstructures on three-dimensional geometries by injection moulding of liquid silicone rubber. Proceedings of the 15th International Conference on Metrology and Properties of Engineering Surfaces, ASPE

[48] Loaldi, Dario & Regi, Francesco & Baruffi, Federico & Calaon, Matteo & Quagliotti, Danilo & Zhang, Yang & Tosello, Guido. (2020). Experimental Validation of Injection Molding Simulations of 3D Microparts and Microstructured Components Using Virtual Design of Experiments and Multi-Scale Modeling. Micromachines. https://www.doi.org/11.614.10.3390/mi11060614

[49] Liu, F., Wu, J., Chen, K., & Xue, D. (2010). Morphology Study by Using Scanning Electron Microscopy.
[50] Calaon, Matteo & Hansen, H. & Tosello, Guido & Garnaes, J. & Ravn, Christian & Tang, Peter. (2012). Characterization of large area nanostructured surfaces using AFM measurements. Proceedings of the 12th euspen International Conference.

[51] Zhang, Nan & su, Quanliang & Choi, Seong Ying & Gilchrist, Michael. (2015). Effects of gate design and cavity thickness on filling, morphology, and mechanical properties of microinjection mouldings. Materials and Design. 83. 835-847. http://www.doi.org/10.1016/j.matdes.2015.06.012

[52] Tofteberg, T. & Andreassen, Erik. (2008). Simulating injection moulding of microfeatured components.

[53] Rytka, Christian & Lungershausen, J & Kristiansen, Per Magnus & Neyer, A. (2016). 3D filling simulation of micro- and nanostructures in comparison to iso- and variothermal injection moulding trials. Journal of Micromechanics and Microengineering. 26. 065018. https://www.doi.org/10.1088/0960-1317/26/6/065018

[54] Oliver, W.C., & Pharr, G.M. (1992). An improved technique for determining hardness and elastic modulus using load and displacement sensing indentation experiments. Journal of Materials Research, 7(6), 1564-1583. https://www.doi.org/10.1557/JMR.1992.1564

[55] B. Bhushan, Biomimetics: Lessons from Nature - an overview, Philos. Trans. R. Soc. A Math. Phys. Eng. Sci. 367 (2009) 1445–1486. https://www.doi.org/10.1098/rsta.2009.0011.

[56] A. Malshe, K. Rajurkar, A. Samant, H.N. Hansen, S. Bapat, W. Jiang, Bio-inspired functional surfaces for advanced applications, CIRP Ann. - Manuf. Technol. 62 (2013) 607–628. https://www.doi.org/10.1016/j.cirp.2013.05.008.

[57] B. Bhushan, Y.C. Jung, M. Nosonovsky, Lotus Effect: Surfaces with Roughness-Induced Superhydrophobicity, Self-Cleaning, and Low Adhesion, in: Springer Handb. Nanotechnol., Springer Berlin Heidelberg, 2010: pp. 1437–1524. https://www.doi.org/10.1007/978-3-642-02525-9_42.

[58] Zhang, J., Rosenkranz, A., Zhang, J. et al. Modified Wettability of Micro-structured Steel Surfaces Fabricated by Elliptical Vibration Diamond Cutting. Int. J. of Precis. Eng. and Manuf. -Green Tech. 9, 1387–1397 (2022). https://www.doi.org/10.1007/s40684-021-00358-

[59] Yifang Chen, Nanofabrication by electron beam lithography and its applications: A review, Microelectronic Engineering, Volume 135,2015, pg. 57-72, ISSN 0167-9317, https://www.doi.org/10.1016/j.mee.2015.02.042.

[60] Schift, Helmut et al. “Transparent hybrid polymer stamp copies with sub-50-nm resolution for thermal and UV-nanoimprint lithography.” Journal of Vacuum Science & Technology B 27 (2009): 2846-2849. https://www.doi.org/10.1116/1.3250207 .

[61] Wu, Dongxu & Rajput, Nitul & Luo, Xichun. (2016). Nanoimprint Lithography - the Past, the Present and the Future. Current Nanoscience. 12. 712-724. https://www.doi.org/10.2174/1573413712666160530120432.

[62] Xiao, Guijian & He, Yi & Shuai, Liu & Yi, Hao & Du, Lingyan. (2021). Laser processing of micro/nano biomimetic structures. Micro & Nano Letters. 16. 10.1049/mna2.12055. https://www.doi.org/10.1049/mna2.12055

[63] Farzam, M.; Beitollahpoor, M.; Solomon, S.E.; Ashbaugh, H.S.; Pesika, N.S. Advances in the Fabrication and Characterization of Superhydrophobic Surfaces Inspired by the Lotus Leaf. Biomimetics 2022, 7, 196. https://www.doi.org/10.3390/biomimetics7040196

[64] Lee, Ho-Sang & Park, Jong-Rak. (2014). Experimental Study of Injection-Compression Molding of Film Insert Molded Plates. International Journal of Precision Engineering and Manufacturing. 15. 455-461. https://www.doi.org/10.1007/s12541-014-0357-2.

[65] Pan, Qiaofei & Cao, Yu & Xue, Wei & Zhu, Dehua & Liu, Wenwen. (2019). Picosecond laser textured stainless steel superhydrophobic surface with antibacterial adhesion property. Langmuir. 35. https://www.doi.org/10.1021/acs.langmuir.9b01333.

[66] Acikgoz, Canet & Hempenius, Mark & Huskens, Jurriaan & Vancso, Gyula. (2011). Polymers in conventional and alternative lithography for the fabrication of nanostructures. European Polymer Journal -

EUR POLYM J. 47. 2033-2052. https://www.doi.org/10.1016/j.eurpolymj.2011.07.025.

[67] Burton Z, Bhushan B.; Hydrophobicity, Adhesion, and Friction Properties of Nanopatterned Polymers and Scale Dependence for Micro- and Nanoelectromechanical Systems. Nano Lett. 2005 Aug;5(8):1607-13. https://www.doi.org/10.1021/nl050861b.

[68] Barr, C. J., Liang Wang, J. K. Coffey and Fugen Daver. “Influence of surface texturing on scratch/mar visibility for polymeric materials: a review.” Journal of Materials Science 52 (2017): 1221-1234. https://www.doi.org/10.1007/s10853-016-0423-5

[69] J.-M. Romano, M. Gulcur, A. Garcia-Giron, et al., Mechanical durability of hydrophobic surfaces fabricated by injection moulding of laser-induced textures, Applied Surface Science, https://www.doi.org/10.1016/j.apsusc.2019.01.162

[70] Broitman, Esteban. (2014). The Nature of the Frictional Force at the Macro-, Micro-, and Nano scales. Friction. 2. 40-46. https://www.doi.org/10.1007/s40544-014-0037-3.

[71] Świetlicki M, Chocyk D, Klepka T, Prószyński A, Kwaśniewska A, Borc J, Gładyszewski G. The Structure and Mechanical Properties of the Surface Layer of Polypropylene Polymers with Talc Additions. Materials (Basel). 2020 Feb 4 ;13(3):698. https://www.doi.org/10.3390/ma13030698.

[72] Zhang, Haoyang & Fang, Fengzhou & Gilchrist, Michael & Zhang, Nan. (2019). Precision replication of micro features using micro injection moulding: Process simulation and validation. Materials & Design. 177. 107829. https://www.doi.org/10.1016/j.matdes.2019.107829.

[73] Roeder, Marcel & Schilling, Peter & Fritz, Karl-Peter & Guenther, Thomas & Zimmermann, Andre. (2018). Challenges in the fabrication of microstructured polymer optics. 10.3850/978-981-11-2728-1_05.

[74] Jiang, Shaofei & Zhang, Yuansong & Ma, Haowei & Zha, Xiaoqiang & Peng, Xiang & Li, Jiquan & Lu, Chunfu. (2022). Effects of Cavity Thickness on the Replication of Micro Injection Molded Parts with Microstructure Array. Polymers. 14. 5471. https://www.doi.org/10.3390/polym14245471.

[75] Lozano, N. [et al.]. Micro- and nanotexturization of liquid silicone rubber surfaces by injection molding using hybrid polymer inlays. "Macromolecular materials and engineering", 8 Març 2022, vol. 307, núm. 3, p. 2100741. https://www.doi.org/DOI10.1002/mame.202100741.

[76] Blondiaux, Nicolas & Pugin, Raphaël & Andreatta, Gaëlle & Tenchine, Lionel & Dessors, S. & Chauvy, Pf & Diserens, Matthieu & Vuillermoz, Philippe. (2017). Fabrication of Functional Plastic Parts Using Nanostructured Steel Mold Inserts. Micromachines. 8. 179. https://www.doi.org/10.3390/mi8060179.

[77] E. Gogolides, K. Ellinas, A. Tserepi, Hierarchical micro and nano structured, hydrophilic, superhydrophobic and superoleophobic surfaces incorporated in microfluidics, microarrays, and lab on chip microsystems, Microelectron. Eng. 132

(2015) 135–155, https://www.doi.org/10.1016/J.MEE.2014.10.002.

[78] M. Lohse, M. Heinrich, S. Grützner, A. Haase, I. Ramos, C. Salado, M.W. Thesen, G. Grützner, Versatile fabrication method for multiscale hierarchical structured polymer masters using a combination of photo- and nanoimprint lithography, Micro Nano Eng. 10 (2021), 100079, https://www.doi.org/10.1016/j.mne.2020.100079.

[78] Q. Zheng, C. Lü, Size effects of surface roughness to superhydrophobicity, in:Procedia IUTAM, Elsevier B.V, 2014, pp. 462–475, https://www.doi.org/10.1016/j.piutam.2014.01.041.

[79] E. Puukilainen, T. Rasilainen, M. Suvanto, T.A. Pakkanen, Superhydrophobic polyolefin surfaces: controlled micro- and nanostructures, Langmuir. 23 (2007). 7263–7268, https://www.doi.org/10.1021/la063588h.

[80] Truckenmüller, R., Giselbrecht, S., Rivron, N.C., Gottwald, E., Saile, V., van den Berg, A., Wessling, M., & van Blitterswijk, C.A. (2011). Thermoforming of Film-Based Biomedical Microdevices. Advanced Materials, 23. https://www.doi.org/10.1002/adma.201003538

[81] Turco R, Santagata G, Corrado I, Pezzella C, Di Serio M (2021) In vivo and post-synthesis strategies to enhance the properties of Phb-based materials: a review. Front Bioeng Biotechnol 8 :619266. https://www.doi.org/10.3389/fbioe.2020.619266

[82] Rafiqah SA, Khalina A, Harmaen AS, Tawakkal IA, Zaman K, Asim M, Nurrazi MN, Lee CH (2021) A review on properties and application of bio-based poly (butylene succinate). Polymers 13 :1436. https://www.doi.org/10.3390/polym13091436

[83] Muthui ZW, Kamweru PK, Nderitu FG, Hussein SAG, Ngumbu R, Njoroge GN (2015) Polylactic acid (PLA) viscoelastic properties and their degradation compared with those of polyethylene. Int J. Phys Sci 10 :568–575. https://www.doi.org/10.568-575.10.5897/IJPS2015.4412.

[84] Muehlberger, M. 2022. "Nanoimprinting of Biomimetic Nanostructures" Nanomanufacturing 2, no. 1: 17-40.https://www.doi.org/10.3390/nanomanufacturing2010002

[85] Beltrão, Mariana & Duarte, Fernando & Viana, Julio & Paulo, Vitor. (2022). A review on in-mold electronics technology. Polymer Engineering & Science. 62. https://www.doi.org/10.1002/pen.25918.

[86] Phillips, C.O. & Claypole, Tim & Gethin, D.T. (2008). Mechanical properties of polymer films used in in-mould decoration. Journal of Materials Processing Technology. 200. 221-231. https://www.doi.org/10.1016/j.jmatprotec.2007.09.014.

[87] Jerabek, M. & Major, Zoltan & Lang, R.W. (2010). Strain Determination of Polymeric Materials Using Digital Image Correlation. Polymer Testing. 29. 407-416. https://www.doi.org/10.1016/j.polymertesting.2010.01.005.

[88] Chen, Anfu & Huang, Han-Xiong. (2016). Rapid transfer of hierarchical microstructures onto biomimetic polymer surfaces with gradually tunable water adhesion from slippery to sticky superhydrophobicity. Materials Research Express. 3. 025011. https://www.doi.org/10.1088/2053-1591/3/2/025011.

[89] Berlin, Werner & Reichel, Vicky & Hürkamp, André & Dröder, Klaus. (2022). Heat Control simulation for variothermal injection moulding moulds using infrared radiation. The International Journal of Advanced Manufacturing Technology. 119. https://www.doi.org/10.1007/s00170-022-08715-1.

[90] Piccolo L., Puleo K., Sorgato M., Lucchetta G., Masato D., Modeling the replication of submicron-structured surfaces by micro injection molding, Materials & Design, Volume 198,2021,109272. https://www.doi.org/10.1016/j.matdes.2020.109272.

[91] Vera, J. ; Brulez, A.-C.; Contraires, E.; Larochette, M.; Trannoy-Orban, N.; Pignon, M., et al. Factors Influencing Microinjection Molding Replication Quality. J. Micromech. Microeng. 2017, 28(1), 15004. https://www.doi.org/10.1088%2F1361-6439%2Faa9a4e.

[92] Hopmann, Christian & Weber, Mathias & Schöngart, M. & Schäfer, C. & Bobzin, K. & Bagcivan, Nazlim & Brögelmann, Tobias & Theiß, S. & Münstermann, Tobias & Steger, M. (2014). Injection moulding of optical functional microstructures using laser structured, PVD-coated mould inserts. https://www.doi.org/1664.10.1063/1.4918478.

[93] Attia, U.M.; Marson, S.; Alcock, J.R. Micro-Injection Moulding of Polymer Microfluidic Devices. Microfluid. Nanofluidics. 2009, 7(1), 1. https://www.doi.org/10.1007/s10404-009-0421-x.

[94] Di Benedetto F., & D'Amore A., Mosca M., Massaro M., Cassano G., Capodieci L., Esposito C., Tapfer L. (2015). on Implantation in thermoplastic polymers. https://www.doi.org/10.1109/NANOFIM.2015.8425354.

[95] Kavetskyy T., Stebeletska N., Borc J., Kravtsiv M., Graz K., Šauša O.,Švajdlenková H., Kleinová A., Kiv A., Tadeush O., Stepanov A.L., Long-range effect in ion-implanted polymers,Vacuum, Volume 200,2022,111038, https://www.doi.org/10.1016/j.vacuum.2022.111038.

[96] Guerrier, Patrick & Tosello, Guido & Nielsen, Kaspar & Hattel, Jesper. (2016). Three-dimensional numerical modeling of an induction heated injection molding tool with flow visualization. The International Journal of Advanced Manufacturing Technology. 85. https://www.doi.org/10.1007/s00170-015-7955-8.

[97] Oppelt, Thomas & Schulze, J. & Stein, H. & Platzer, B.. (2012). Comparison of Methods for Mould Surface Heating – Part 1: Review. International Polymer Science and Technology. 39. T1-T12. https://www.doi.org/10.1177/0307174X1203901201.

[98] Wang, B., Song. J., 2022. "Hydrophobic Prediction Model and Experimental Study of PMMA Surface Microstructure Prepared by Femtosecond Laser Direct Writing" Coatings 12, no. 12: 1856. https://www.doi.org/10.3390/coatings12121856.

[99] Kim, S & Jeong, J & Youn, J. (2010). Nanopattern insert molding. Nanotechnology. 21. 205302. https://www.doi.org/10.1088/0957-4484/21/20/205302.

[100] Zhou, Mingyong & Xiong, Xiang & Jiang, Bingyan & Weng, Can. (2017). Fabrication of high aspect ratio nanopillars and micro/nano combined structures with hydrophobic surface characteristics by injection molding. Applied Surface Science. 427. https://www.doi.org/10.1016/j.apsusc.2017.08.003.

# 2. INJECTION MOULDING AND CHARACTERIZATION OF MICROTEXTURES ON POLYCARBONATE USING LASER-TEXTURED INSERTS[1]

[1] * This chapter has been published as a research article in an indexed journal :
*Sáez Comet, Carlos & Fontdecaba, E. & Cuadrado, Nuri & Puiggalí, Jordi. (2022). Injection molding and characterization of microtextures on polycarbonate using laser textured inserts. Materials and Manufacturing Processes. 38. 1-11. 10.1080/10426914.2022.2075888.* [1]

## ABSTRACT

The purpose of this chapter is to demonstrate the easy manufacturing and quick characterization of several microtextured functional surfaces on two transparent thermoplastics of general interest for several industrial sectors. Microtextured polymeric surfaces with special optical, tribological and easy-cleaning properties were manufactured via isothermal injection-molding using laser-microtextured steel mold inserts. For that purpose, conventional injection molding of two chosen amorphous transparent polymers (polycarbonate, PC, and polymethyl methacrylate, PMMA) utilizing laser-microtextured steel inserts was carried out, and a detailed morphological and functional characterization of the injected specimens was conducted later. We also report on the suitable process conditions for the injection molding of these specimens using design of experiment (DOE) techniques.

The analysis of the degree of replication (DR%) on the injected samples shows that mold temperature and injection speed are the most relevant parameters to obtain a successful replication and confirm the viability of conventional injection molding as a processing technique to obtain microtextured functional surfaces in amorphous transparent thermoplastics. The success of the procedure is further checked by the confirmation of the obtained surface functionalities by various standard and self-developed methods.

***Keywords***

Injection moulding; microtextures; polycarbonate; laser textured inserts; replication

## INTRODUCTION

Injection molding of specimens with micro- and nanostructured faces, which enhance or modify their surface functionality, constitutes a technology of rising interest in a wide variety of sectors and applications within the industry. Numerous publications are being focused nowadays on the study and manufacturing of polymeric specimens for a variety of applications. Relevant examples correspond to microfluidic chips, [1] optical lenses, [2] structural coloration of polymers, [3] isolation of specific cells [4] or enhancement of mechanical properties, [5] amongst others.

To produce such specimens, one of the technologies with higher industrial potential is the injection molding using laser-textured metallic mold inserts, due to its practicality and ease of integration in standard injection molds. In this technique, the negatively patterned surface on the metallic insert (commonly nickel or steel) is carried out via lithography and plating processes [6] or laser ablation techniques [7–10] to directly remove material from the metallic plate surface in a periodical fashion.

This mastered material can then be introduced as a tool insert inside the injection mold for the manufacturing of the final polymeric specimen, which once injected will have the complementary positive texture on its surface [2,8,11].

On the injection molding phase, the main factors influencing the quality of the replication are the election of the injected polymer, the geometry of the mold and cavities to be filled, mould temperature, melt temperature, injection and holding pressure, cooling time and injection speed as shown by numerous previous studies.[12–15] While there are differences in the main processing parameters affecting replication, there seems to be a general agreement on the fact that high melt and mold temperature, high injection speed, and high holding pressure have a positive effect on the melt flow in micro- and nanometer-sized cavities. Exhaustive reviews around the influencing factors were performed by Maghsoudi et al. and Attia et al. [16,17]. Considering mould temperature, packing pressure, and injection speed as the factors with highest relevance on the process presented here (PC and PMMA injection molding over micro-textured steel inserts), a determination of the factors with the highest influence investigated via a DOE is presented in this study. Concerning the surface characterization of the injected polymeric specimens, a double testing on the surface of the resulting molded specimens (morphological and functional) is carried out to investigate both the replication degree and the acquired/enhanced surface functionality achieved by the microstructure.

Confocal microscopy is used to characterize the replicated surfaces, the reference technique when characterizing of transparent polymers [18,19] In the case of surface

functional characterization, various tests can be performed to determine the effectivity of the four functionalities designed on the lasermicrotextured steel inserts: light diffusion, light guiding, easy to clean and anti-scratch.

To evaluate the effectivity of the injected light-diffusive structures, a quick test to measure luminance, homogeneity, and percentage of change versus a non-structured surface is conducted [20]. On the other hand, the light-guiding effectivity of microstructures on the injected specimens was evaluated by a highly sensitive device that was able to register the luminance of the perpendicularly guided light (Fig. S3 on S.I.). It is well known that micro- and nanotextures can modify the tribological performance properties of polymeric surfaces [21,22]. The particular anti-scratch microstructure studied in this paper is evaluated by various micro indentation and micro-scratch tests, following previously reported techniques [23–25]. Surface roughness parameters were measured and correlated with the variations on user perceptions of the scratch-visibility. The easyto-clean functionality is qualitatively evaluated – due to the lack of suitable standard test methods – by combining water contact angle measurements [26] and a quick dust-wiping effectivity test inspired by Haines [27].

The overall objective of the work presented was to confirm the validity of conventional injection molding as a suitable method for the successful replication of functional microtextures in amorphous transparent thermoplastics and to obtain the most relevant influencing parameters. The aim was also to confirm the investigated surface functionalities using conventional and novel characterization techniques in the absence of relevant testing standards in some of the presented cases.

## MATERIALS AND METHODS

### Injection molding materials

The injection molding experiments were conducted using mainly a polycarbonate polymer, but in some cases (i.e., optical characterization) polymethyl methacrylate was also used for comparison purposes.

The specific selected polymers were:

- Polycarbonate (PC) from the company Covestro (Makrolon 2207 – grade 550115-Crystal Clear) [28].
- Polymethyl methacrylate (PMMA) from the company Evonik (Plexiglas 8N Clear) [29].

Both materials were dried prior to the injection molding trials: PC was dried at 120°C during 4 h, while PMMA was dried at 98°C during 2 h, as recommended by the technical datasheets of the manufacturers.
The injection molding tests were performed at 290°C for PC and 240°C for PMMA, as recommended by the material manufacturers.

**Microtextured steel discs**

The microtextures were manufactured on one of the sides of steel disc-shaped samples of 30 mm diameter and 5 mm thickness. Inserts were manufactured using laser-ablation techniques with a nano-laser texturing machine, using 220 ns pulse durations, a wavelength of 1068 nm, and a repetition rate of 80 KHz. The power rate and galvo speed of the laser were set to 35 W and 2000 mm/s. The laser used a circular polarization like what is stated in ref. [10], but distinctly in our research the laser source was switched on and off several thousand times per layer in a controlled manner to selectively eliminate material across the surface which allows to create a smoother microtopography.
This derived in lesser demolding issues upon the latter injection molding trials, as it can be observed in the scheme presented in Fig. 2.1. The four microstructures (named D1, D2, D3, and D5) used in the experiments were designed and manufactured by MICRORELLEUS SL., and their main morphological characteristics and expected functionalities were as follows:

(a) D1 – Homogeneous light-diffusive structure: Thismicrotexture was designed to conceal and homogenize the light coming from a LED or a focal point.
This structure followed a Gaussian roughness profile, with a matte visual appearance, an average depth of structures of 50 μm and an arithmetic mean height of line.
(Saroughness parameter) of 3,024 μm. Figure 2.2 (upper left image) shows a scheme of the working principle of this microtexture, along with a confocal image. In this case,
the microstructure was engraved within the profile of an automotive icon representing a heated seat according to the manufacturer original design.

(b) D2 – Light-guiding structure: This microtexture was designed to guide the light passing through a transparent specimen (e.g., PC or PMMA). Light refracts perpendicularly toward the observer with regards to the initial direction of illumination. It had shiny visual appearance and finishing, a peak-to-valley average height of $\Delta Z = 206 \pm 7$ μm, and an approximate distance between peaks of $\Delta L = 315$ μm. A scheme of the working principle of this microtexture, along with a confocal image of it can be seen in

Fig. 2.2 (upper right image). The microstructure lied within a 1.6 × 1.5 mm rectangle centered on the disk. face, according to the manufacturer original design.

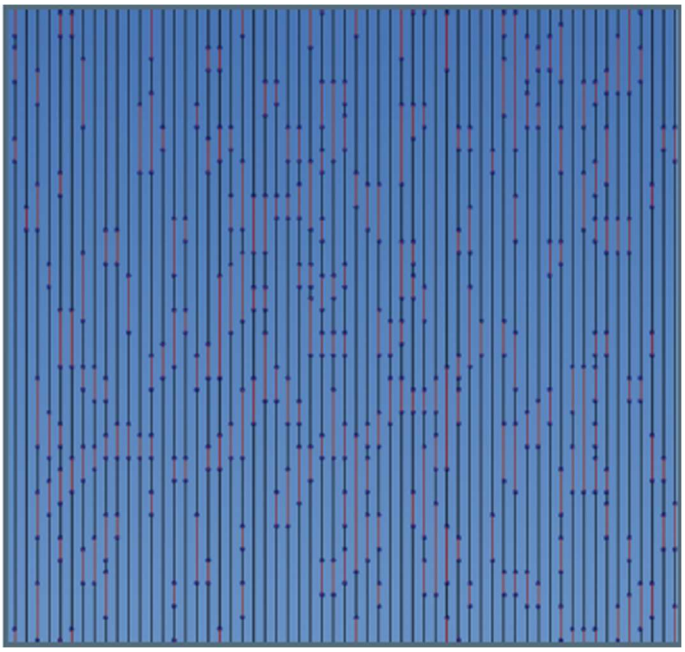

**Figure 2.1. Scheme of the controlled laser switch-off (red lines) along a small zone in one of the passes to create the textured area, on which the normal laser functioning can be observed in black lines.**

(c) D3 - Anti-Scratch: The purpose of this microstructure was to optically hide the scratches produced on the surface of the final polymeric specimen, while increasing the scratch-resistance of the polymer surface over which is practised. The structure followed a Gaussian profile and had an average feature depth of 3-4 μm with a matte-rough finish. A scheme of the working principle of this microtexture, along with a confocal image of it can be seen in Fig. 2 (lower left image).

(d) D5 – Easy-to-clean: This microstructure was conceived to give the final injected polymeric specimen a decorative finish (matte and shiny) and an easy cleaning of dust and dirt using water as wiping medium. This is due to the soft peak and valley features present on it that show an average peak-to-valley height of 10 μm. Figure 2 (lower right image) shows a scheme of the working principle of this microtexture, along with a confocal image.

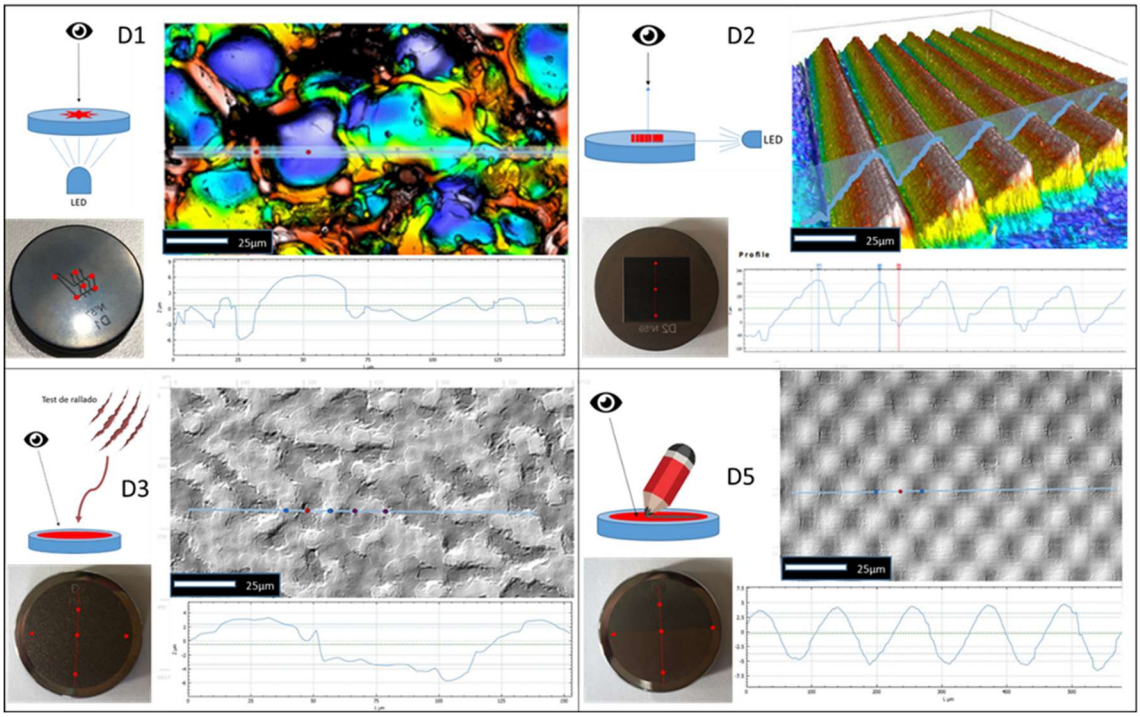


**Figure 2.2 Composed images showing the details of the D1, D2, D3, D5 microstructures. Each of the images is composed by: a scheme of the intended observing direction for each functionality (upper left corner); a confocal image showing the microstructure general appearance (upper right corner) with a line drawn on it showing a linear profile (lower right corner) and the place from which is extracted. Finally, a picture of each disc that shows red dots marking the places in which replication degree and uniformity are investigated (lower left corner).**

### Mould inserts and machinery

All the injection moulding and morphological characterization tests were carried out at the facilities of EURECAT, the technological R+D centre of Catalonia.

In order to hold in place the above-explained microtextured discs during the injection moulding process, a custom-designed injection mould insert was manufactured. The insert was designed to adapt to one of our injection moulds at EURECAT, which are used for research purposes. The insert allowed to install each of the microtextured discs indistinctly on the surface of the fixed half in the injection mould to carry out replication trials.

The insert held the disc in the appropriate position during the whole injection cycle, keeping the adequate flatness and leaving the microtextured face of the disc exposed towards the interior of the cavity at a reduced depth of 1,25 mm regarding the mould-insert surface. Both insert and injection mould can be seen in Figure 2.3.

Thus, the injected specimen (a squared plate of 70 x 70 x 2.6 mm) has a cylindrical elevation of 1.25 mm height that is centred on the specimen, on top of which the texture is replicated as can be seen in Figure 2.3 (lower left image).

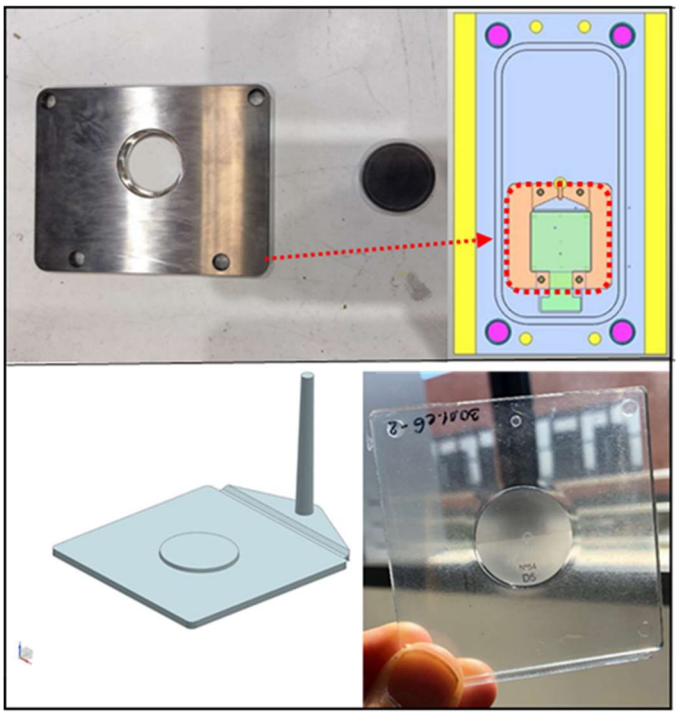

**Figure 2.3. Composed image showing the injection mould insert developed to hold the microtextured disc in position during the injection moulding stage (upper left), pointing its specific placement on the injection mould cavity with a red-dotted arrow and line (upper right CAD-image). Below, a 3D-CAD image of the injected specimen and a processed specimen with a replicated microtextured disc on its centre.**

The entry of the polymeric material during the injection molding was effectuated through a 6.44 mm diameter circular gate that delivered the molten polymer into the cavity via a fan-type entry. The distance from the circular gate centre to the edge of the injected specimen was 34.40 mm. Main flow region width, thickness, and distance from entry to the microtextured zone of the tool were carefully observed using the polymer flow simulation software MOLDEX. After a careful analysis, all those parameters were considered favorable for a successful replication, as stated in [30].

For the injection molding trials, an Engel complete E-motion 200/55 electric machine was used. The main technical characteristics of the machine can be seen in Table 2.1.

The mould inserts were cleaned with isobutanol and let drying at room temperature prior to the start of each test. Also, they were carefully inspected after each injection

round, to confirm the lack of damage or wear on their surface (already observed in the previous related project [14] using the confocal microscope.

| | Value | Unit |
|---|---|---|
| **Closing unit** | | |
| Clamping force | 550 | kN |
| Screw stroke | 270 | mm |
| Ejection stroke | 100 | mm |
| Ejection system Force | 23 | kN |
| **Injection unit** | | |
| Screw diameter | 25 | mm |
| Maximum injection volume | 59 | $cm^3$ |
| Screw maximum rotary speed | 400 | r/min |
| Injection speed | 109 | $cm^3/s$ |
| Maximum specific pressure | 2400 | bar |
| Nozzle stroke | 225 | mm |
| Nozzle force | 28 | kN |

**Table 2.1. Technical characteristics of the injection moulding machine used for the trials.**

### Morphological characterization

For the morphological characterization of the injected samples a Sensofar Plμ 2300 confocal microscope was used, and the images acquired were latter processed by the softwares MountainsMap 5.1 of Digital Surf, and Gwyddion. The main purpose of this characterization was the determination of the degree of replication (DR%):

$$DR\% = hf / dc \times 100$$

where hf is the height of features in the polymeric sample anddc is the depth of cavities in the steel insert. The DR% parameter is also interesting to check the uniformity.
of the replicated structures on the injected polymer samples. Peak heights of features Rp, along with relevant surface roughness parameters such as were measured on the injected samples according to the DIN EN ISO 4827 standard. The overall uniformities of the microtextured surfaces' profiles were further checked on several relevant points of each of the microtextured icons, as indicated in Fig. 2.2.
Once the topographies of the microtextured steel discs and the replicated injection-molded specimens were evaluated, the Design of Experiments (DOE) was completed with the help of the software MINITAB 18.

**Injection molding experiments and DOE**

A factorial design of experiments was applied to check the influence of various relevant process parameters on the replication of the microfeatures present on the insert on injected PC [12]. This method constituted a relevant alternative to check for the highest-influencing processing factor on the expected results. For our specific test setup, a $2^3$ experiment type was used, choosing three molding process factors to check their influence on the final DR% of the microstructures on the injected specimens. The chosen factors were as follows: mould temperature (Tm), injection speed (Vinj) and holding pressure (P). Details of the specific D.O.E. matrix can be seen in the Supporting Information (S.I.) document. The microtextured steel insert D3 with anti-scratch functionality was chosen for this purpose.

**Functional characterization**

For the functional characterization, different tests were chosen to determine the effectivity of each surface and found a correlation with microstructure morphology in each case:

Light diffusion (D1)

Three of the injected samples of both PC and PMMA materials with light-diffusive microstructures were tested to determine the light-diffusive functionality of the microtexture. For that purpose, maximum and minimum light luminance and homogeneity were determined for the injected samples with the highest DR% by means of illuminating the sample back face on the zone corresponding to the microtexture (placed on the front face) by using a LED light source with known characteristics.
Then, the variations on the LED-emitted light characteristics once it had gone through the microtextured sample were registered using an ultra-light-sensitive camera (LMK6–5 color TechnoTeam Bildverarbeitung) placed in front of the microtextured surface (opposite side of the sample). The results were compared with those obtained from illuminating samples of the same untextured materials.

Light guiding (D2)

Four samples of PC with light-guiding microstructures anddifferent DR% were illuminated with an LED light of known intensity on one of the sides of the sample (Fig. 4). By doing so, the light traveled through the PC sample and exited it perpendicularly, so that a high-sensitivity light-measuring system (LMK6–5 color Techno Team Bildverarbeitung GmbH) could properly be placed in order to measure the relevant light characteristics. In addition, it is important to note that the samples were cut following indications of the adequate LED light source-microstructure distance for optimal guiding supplied by the microstructure manufacturer (i.e., 10 mm).

Anti-scratch (D3)

Several surface scratches using a Micro-combi Indentation-Scratch Tester MHT (CSM) were produced on the D3 microtextured samples at the EURECAT facilities.
In order to evaluate the coefficient of friction (COF) and the visibility of the residual footprint, scratches with different applied loads (from 2 N to 10 N) and speeds (8 mm/min and 500 mm/min) using a steel ball indenter with 2.5 mm diameter as counterpart were performed. After the scratch tests, relevant surface roughness parameters were determined, and the scratch residual imprints were visually inspected and measured using confocal imaging. These results were correlated with changes in the relevant surface roughness parameters (Sa, Sdr and Str) measured before and after producing the scratch. The three selected parameters initially measured and whose evolution was followed after producing the sample scratches at different speeds and loads are shown in Table 3. They were chosen in order to be correlated with the “scratch hiding ability” of the microstructure and to analyze the visual perception of the various scratches produced.

Easy-to-clean (D5)

Due to the absence of standard procedures to check this effect, a self-made method in which a controlled quantity of very fine-grained talc powder (PRC Panreac) was deposited on the top of the microtextured surface, and then the sample was wiped by dropping ultra-clean water from a fixed distance. First, the samples were dried in an oven prior to the test (following each material datasheet recommendations) to avoid

contributions of absorbed humidity on the weighed sample prior to the test. The dust was deposited on the surface of the discs and its excess was subsequently eliminated to obtain a uniform layer. Then, samples were weighed with a high-precision scale.

After that, samples were held at an angled position (i.e., 45°) and three equal amounts of 100 µL of ultra-clean water were dropped from a height of 1.5 cm from the upper part of the textured disc, along three positions parallel to the disc horizontal diameter (details are shown in Figure S5 of supplementary information). Finally, the samples were dried for 5 min at 100°C inside an oven and weighted after complete water evaporation. This procedure was followed for all the microtextured and non-microtextured polymer samples and steel discs. After that, the weights of wiped-off dust in each case were compared. Images of samples before and after the water-drop assay were taken for visual comparison. In addition, water contact angles and their hysteresis were determined for all the injected samples and compared to those determined for the microtextured steel inserts. A tensiometer (Dataphysics OCA 15 CE) and the appropriate image processing software (SCA 2.0) were employed.

## RESULTS AND DISCUSSION

### Design of experiments DOE

The results of the design of experiments carried out for the PC material were obtained using the microtextured disc of anti- scratch functionality (D3). Figure 2.4 shows the Pareto chart- plot of the relative effects that the different considered parameters have on replication along as well as the interactions between them.
The mold temperature Tm during the injection molding was the dominant factor of influence on the DR% as expected [12,15]. The holding pressure and its interaction with injection speed represented the second and third highest influencing factors in the process, respectively. The graph also shows a smaller influence of the interaction between Tm and P, and that the actions between Tm and Vinj were not significant. As expected, for the chosen materials and process parameters, high Tm and P constituted the two most important influencing factors for maximizing DR%.

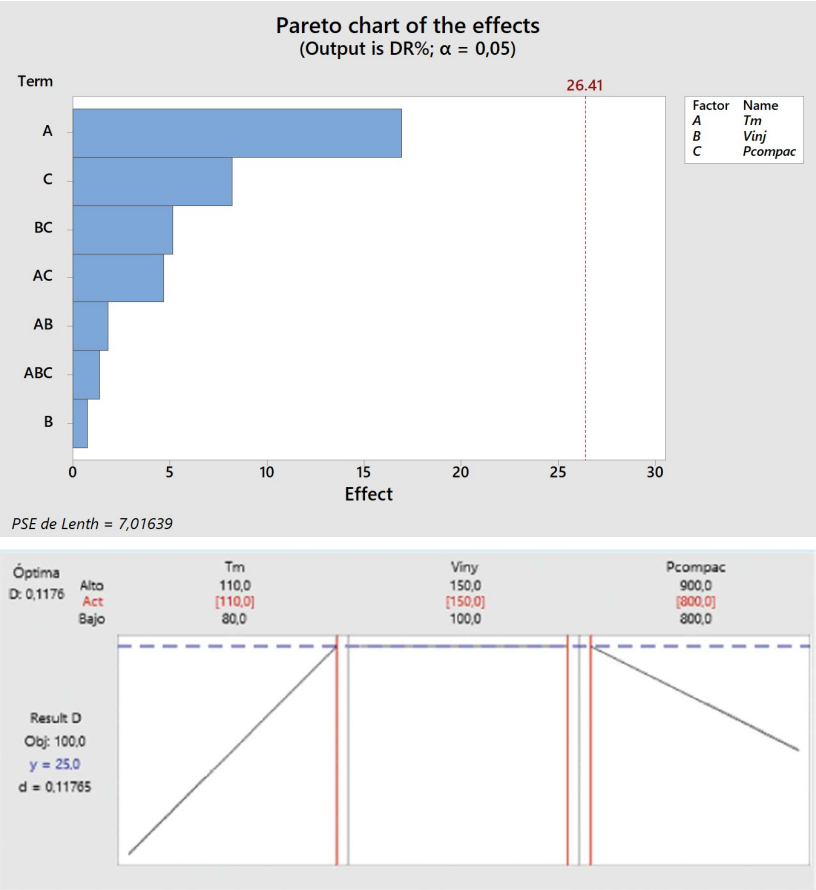


**Figure 2.4. Results of DOE showing the critical factors and interactions between them in the replication process carried out with PC (*Tm*=mould temperature / *Vinj*= injection speed / *Pcompac*= holding pressure).**

The interaction between Vinj and P had higher relevance than Vinj alone, which is the less influencing factor for the considered DOE. This suggests a very small variation of the polymer viscosity on the short interval where Vinj was tested (i.e., between 100 and 150 mm/s) for the two sets of mold temperatures. It seems that further experimentation with more spaced Vinj andTm values is necessary to check with better accuracy the influence of Vinj.

## Topographic analysis

### Light-diffusion microstructure (D1)

For all the different tested injection molding conditions, DR % reached average values between 68% and 95%. For the conditions in which the best replication was achieved (i.e., 95%), the injected PC samples showed a variation on the Sa roughness of the microtopography around ±10% between the different tested zones in the samples (see Fig. 2.5, upper left and right images). This was a clear sign of a uniform DR % across

the whole microtextured surface. Nevertheless, this small variation in the DR% may be a consequence of small differences in the thickness of the microtextured discs (reaching values of up to 0.01 mm in some points). Note that these differences could cause a non-satisfactory adjustment of the textured disc inside the manufactured custom mold.
This feature could lead to small deviations on the flatness of the injected sample and the observed DR% variations amongst the various zones of the sample.
Figure 2.5 compares the linear profiles of the D1 microtextured steel (left) and the microtextured surface of the injection molded PC sample with the highest DR% (i.e., Tm/Vinj /P molding conditions of 110°C 100 mm/s and 900 bar).

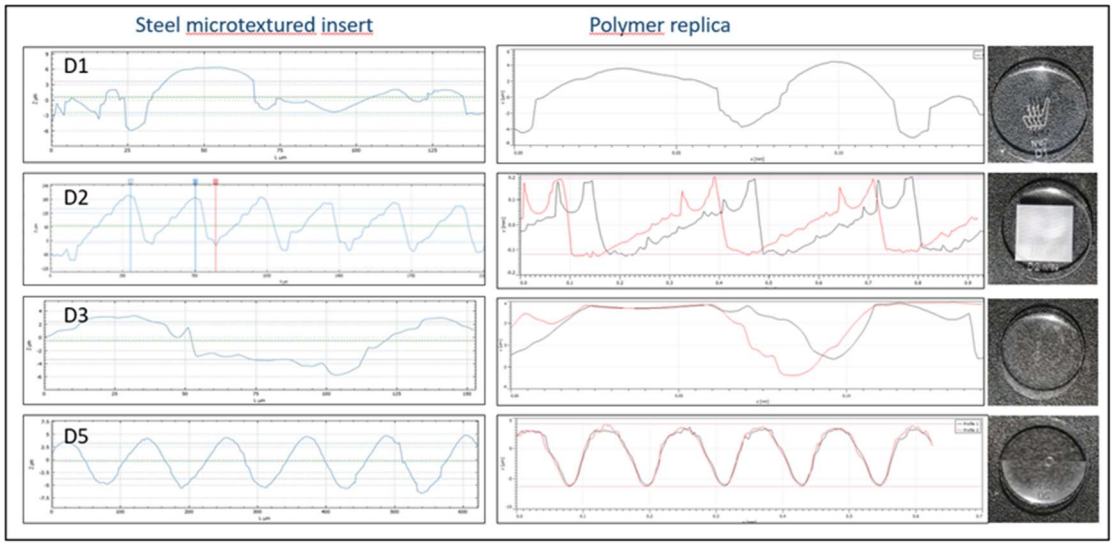


**Figure 2.5. Linear profile extracted from confocal images of the microtextured D1, D2, D3 and D5 steel inserts (left column), and from PC injected specimens (right column). The general appearances of the injected specimens are shown on the right margin.**

Light-guiding microstructure (D2)

Figure 2.5 (second row-profile on the left) compares the linear profiles of the microtextured steel insert D2 and the textured surface of the injected PC sample at the molding conditions (i.e., Tm/Vinj/P of 110°C 100 mm/s and 800 bar, respectively) that gave rise to the highest replication degree (DR%). DR% ranged from averages of 80% to 150% depending on the different conditions applied. The values obtained suggested an unusual elongation of the features in the case of injection conditions associated to the highest replication degree.
These elongations were probably due to a too short cooling time or even by an excessive surface roughness of the metallic disc of the D2 microtexture. Another possible cause could be the small “wells” with larger demolding angles present in the valleys observed

between peaks on the profile of the D2 microtextured steel insert. These two facts might have caused an undesired excessive adhesion of the polymer in the mold cavity upon demolding.
In addition to the elongation shown by the highest peaks in the replicated microstructure, a set of secondary peaks is also observed. These might also be caused by an excessive adhesion of the polymer to the irregularities present on the ridge surfaces upon demolding. As it will be shown later in the functional validation part, these deformations did not prevent the expected light-guiding functionality.
Despite the observed deformations, the microtextured surface of the injected PC samples showed a good replication uniformity for all the injection molding conditions. Variations on the peak-to-valley distance between the different tested zones were minimal (i.e., St around ±10%).

Anti-scratch microstructure (D3)

In Fig. 2.5 we can observe a linear profile of the D2 microtextured steel insert together with two parallel profiles (roughly 50 μm apart) extracted from the textured surface of the injected PC sample at molding conditions (i.e., Tm/Vinj/P of 110°C 150 mm/s and 800 bar, respectively) that correspond to the highest DR% (93%).
For all the observed injection molding conditions, the microtextured surface of the injected PC samples showed an acceptable uniformity of replication, with variations on the peak-to-valley distance St of ±15% between the different tested zones. Again, it is believed that small variations in the steel disc thickness caused an incorrect adjustment of the disc in the tool insert and flatness defects on the injected samples, which later derived into uniformities of the DR% amongst various zones of the disc.

Easy to clean microstructure (D5)

Figure 2.5 compares a linear profile of the D5 microtextured steel insert D5 with two parallel profiles (roughly 150 μm apart from each other) extracted from the textured surface of the injected PC sample at molding conditions corresponding to the highest DR% (i.e., Tm/Vinj/P of 110°C 150 mm/s and 800 bar, respectively).
The best replication degree for this test configuration reached an average 95%, while the lowest were approximately 55 and 65% for the lowest mold temperatures.

For all the observed injection molding conditions, the microtextured surface of the injected PC samples showed an acceptable uniformity of replication. Variations on the

maximum peak to valley distance St were ±10% between theent zones tested in the samples.

### Surface functionality characterization

Light-diffusion microstructure (D1)

Three samples of PC were tested and compared for an equal number of injected samples with and without microstructural features on its top face, following the method presented in the experimental section. The same experiment was carried out for the same number of PMMA-microtextured samples, which for comparison purposes were selected with a similar DR%.

Table 2.2 summarizes the results of the light diffusion measurements. Textured PC samples showed a marked increase of 96.5% in the homogeneity of the light measured sample vs the non-textured PC samples. The increase of homogeneity determined for the PMMA samples reached 19.2%, while the decrease in the main luminance was of 17.8% compared to a decrease of 29.5% for PC. As can be seen on Table 2, both materials confirmed the enhanced light-diffusive surface functionality acquired by the presence of the microtexture, markedly on a higher level for the PC material when compared to the PMMA. Nevertheless, the increase in light homogeneity measured for both materials, which is directly related to the diffusive capability of the microstructure, came at a higher decrease of mean luminance of 12% in the case of PC with regards to the PMMA.

| | | Luminance (cd/m$^2$) | | | Homogeneity min/max % | Change (%) | |
|---|---|---|---|---|---|---|---|
| | | min. | max. | mean | | Mean luminance | Homogeneity |
| PC | non-textured | 2360 | 8631 | 4622 | 30.5 | REF | REF |
| | textured | 2801 | 4701 | 3256 | 59.9 | -29.5 | 96.5 |
| PMMA | non-textured | 2638 | 9563 | 5096 | 27.6 | REF | REF |
| | textured | 2555 | 7871 | 4191 | 32.9 | -17.8 | 19.2 |

**Table 2.2.** Experimental results of the light-diffusion characterization.

Light-guiding microstructure (D2)

Four samples of injection moulded PC were illuminated from one of its sides by means of a white LED of known characteristics, and the light coming out of the D2 microstructure was evaluated and recorded at a distance of 20 cm (Figure 2S in supporting information document).

The measured luminances of the original LED-source and guided light after going through the microstructure D2 are summarized in Table 2.3.

| | | Luminance (cd/m$^2$) | | |
|---|---|---|---|---|
| | **Sample** | **Min** | **Max** | **Mean** |
| Measured on LED source | 1 | 13.84 | 14150 | 669.40 |
| | 2 | 13.88 | 14210 | 697.10 |
| | 3 | 13.93 | 13960 | 653.80 |
| | 4 | 13.96 | 14520 | 714.00 |
| After guided by microstructure D2 | 1 | 13.49 | 108.40 | 31.51 |
| | 2 | 13.44 | 71.67 | 26.39 |
| | 3 | 13.51 | 92.90 | 27.67 |
| | 4 | 13.49 | 75.23 | 25.82 |

**Table 2.3.** Experimental results of the light-guiding measurements.

It can be observed from the table that the highest efficiency of the light-guiding functionality was reached for sample 1, which corresponds to a DR% of 80%. This value contrasted with the value attained on sample 2, that had the highest DR% (i.e., 150%), but also the highest distortion on the injected features. Nevertheless, even for various different DR% and geometrical distortions of the features, the measurements of mean luminance for all samples showed similar values and confirmed the D2 surface functionality. This is consistent with the bigger dimensions of the D2 microtextures, which probably were less exigent in terms of process conditions to achieve adequate replication when compared to the other microstructures (e.g., D1, D3 and D5).

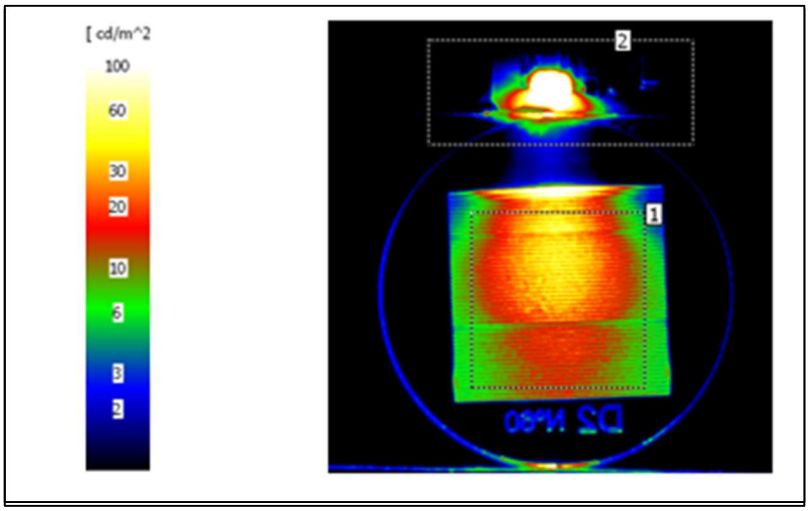


**Figure 2.6. Image of the measured luminance on LED-source and a microtextured sample. Measured values are displayed in a logarithmic colour- scale.**

Anti-scratch microstructure (D3)

The chosen roughness parameters ($S_a$, $S_{dr}$, $S_{tr}$) were initially measured for both injected textured and non-textured samples of the same material for comparison purposes. These initial values are summarized in table 2.4. Samples with a DR% of 67,5% were chosen for this evaluation in order to confirm the surface functionality at the lowest replication level obtained.

| | $S_a$ (µm) | $S_{dr}$ (µm) | $S_{tr}$ (µm) |
|---|---|---|---|
| Non textured sample | 0.035 | 0.009 | 0.011 |
| Anti-scratch Texture | 2.340 | 21.200 | 0.067 |

**Table 2.4.** Initial measurements of the roughness parameters for non-textured and D3 textured samples.

Confocal images of scratch residual imprints for two applied loads (2 N, 5 N) and speed levels (8 mm/min and 500 mm/min) in both textured and non-textured samples are shown in Figure 2.7 for comparative purposes. Table 2.5 summarizes the resulting values of the roughness parameters and Figure 2.8 the corresponding friction coefficients (COF) for the different tested load and speed scenarios. Lastly, a chart representing the evolution of the $S_{tr}$ parameter (right *y*-axis) and that of the friction coefficient COF (left *y*-axis) is also shown on Figure 2.8.

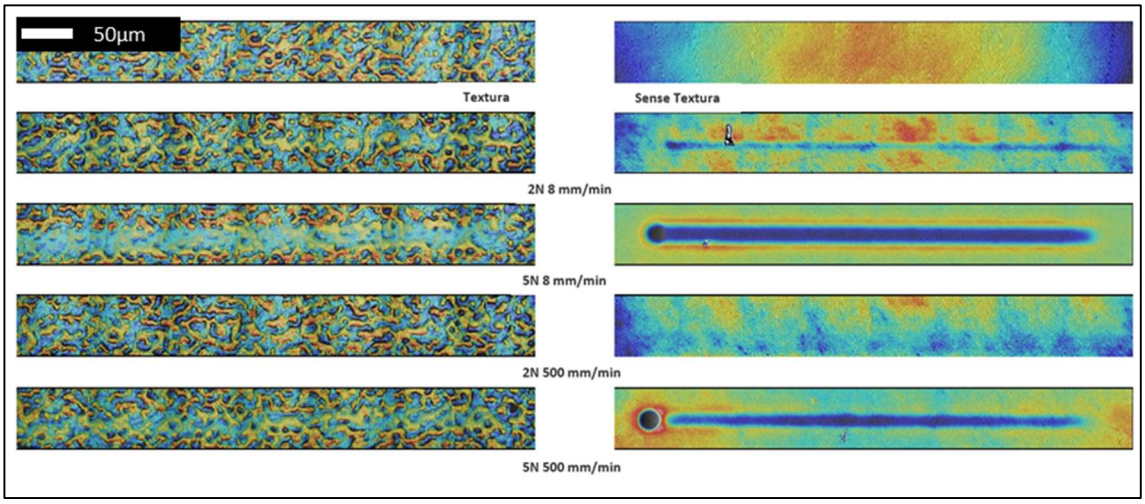


**Figure 2.7. Confocal images (200 X magnification) of the footprints produced on non-textured samples (right) and D3-microtextured samples (left) at the indicated indenter loads and speeds.**

The determined roughness parameters $S_a$, $S_{dr}$ and $S_{tr}$ have been used for the analysis of scratch visibility on this study. The parameter $S_{tr}$, related to the microstructure isotropy (Table 2.5) stays at relatively constant values for low load levels and all the load speeds tested, while strong decreases are seen for $S_a$ and $S_{dr}$. This fact correlates with the lowest visibility of the scratches produced at low load levels (2 and 5 N) at both high and low speeds (500 and 8 mm/min, 1st to 2nd lowest visibility), as perceived by the observers on the round robin run. Low perception level was defined as *hard to be perceived* or *directly not perceived*, depending on the observer age. Results clearly contrast with the much higher visibility of the scratches produced at higher load levels.

| | | 8 mm/min | | | 500 min/min | | |
|---|---|---|---|---|---|---|---|
| | **F (N)** | ***Sa*** | ***Sdr*** | ***Str*** | ***Sa*** | ***Sdr*** | ***Str*** |
| D3 microtextured samples | 2 | 1.520 | 7.690 | 0.608 | 1.540 | 9.130 | 0.801 |
| | 5 | 0.962 | 0.720 | 0.416 | 1.090 | 0.754 | 0.714 |
| | 7 | 1.280 | 0.388 | 0.023 | 1.160 | 0.390 | 0.023 |
| | 10 | 2.120 | 1.500 | 0.030 | 1.880 | 1.100 | 0.030 |
| Non-microtextured sample | 2 | 0.051 | 0.011 | 0.022 | 0.038 | 0.008 | 0.040 |
| | 5 | 0.490 | 0.342 | 0.018 | 0.216 | 0.024 | 0.026 |

**Table 2.5.** Roughness parameters for D3-textured and non-textured samples.

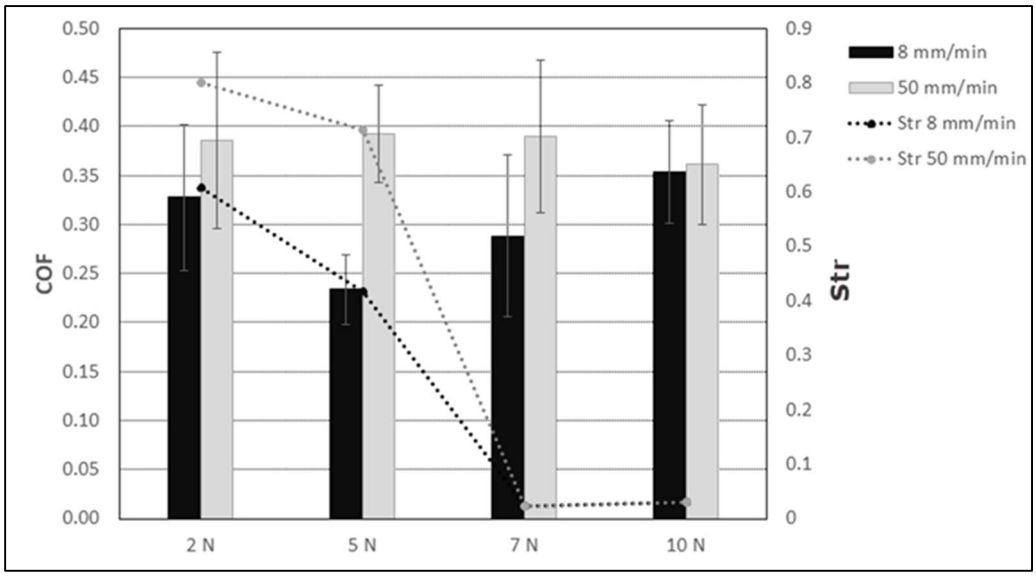


**Figure 2.8. Evolution of the coefficient of the measured friction COF (left y-axis) coefficient and Str values with load and speed levels of indentation.**

The values of $S_{tr}$ at high load (7 N and 10 N) and speed levels (8 and 500 mm/min) showed a drastic reduction when compared to those determined at low load levels for both scratching speeds. This feature can be explained by the higher damage observed when scratching the microtextured PC sample at high load and speed levels and relates well with the different scratch behaviour observed at various low and high loads and speeds for this viscoelastic material.

Confocal and SEM images of the scratches produced on the D3 microtextured samples at low and high levels of scratching load and speeds can be seen in Figures s1.4 and s1.5 of the Supporting Information.

With respect to the friction coefficient (COF*)*, measurements indicated a practically constant value for every applied load level applied when the speed is 500 mm/min, except for 10 N that led to a small decrease. On the other hand, a correlation is observed between COF and the $S_{tr}$ parameter. Specifically, COF increases for higher $S_{tr}$ values. When this roughness becomes, the surface shows less deformation when scratched and higher distances exist between peaks and valleys (correlated to $S_z$) of the structured surface. This feature may also explain the lowest visibility of scratches at high $S_{tr}$ values.

Easy to clean microstructure (D5)

First, the values of water contact angles were determined for the microtextured PC (on both shiny and matte sides), non-microtextured PC and steel D5 disc insert samples. Table 2.6 summarizes the average values obtained, which were in good agreement with reported water contact angles measured on PC surfaces [29]. The average hysteresis remained below 5° for all the samples measured.

| | **matte side** | **SD** | **Shiny side** | **SD** |
|---|---|---|---|---|
| Sample 1 | 84.62 | ± 1.38 | 83,7 | ±2.70 |
| Sample 2 | 84.37 | ±0.79 | 82,13 | ±0.61 |
| Steel Disc Insert D5 | 88.08 | ± 3.44 | 92,27 | ±2.03 |
| PC sample-No texture | 84,23 (**SD**=3.13) | | | |

**Table 2.6.** Average water contact angles (5 measurement points) for microtextured pc samples 1 and 2, flat pc sample and d5 steel disc insert.

During the process of checking the efficiency of the *easy to clean* microstructure, an additional PC sample with a D1 surface microstructure was included in the trials for comparison purposes. The values obtained for the weight measurements can be observed on Table 2.7.

| | **Initial weight (gr.)** | **Weight WITH Dust (gr.)** | **% dust removed** |
|---|---|---|---|
| Sample 1 | 16.7602 | 16.7616 | 0.0406 |
| Sample 2 | 17.0108 | 17.0122 | 0.0935 |
| Steel Disc Insert D5 | 28.7135 | 28.7169 | 0.0091 |
| PC-D1 sample | 17.0108 | 17.0122 | 0.0235 |

**Table 2.7.** Values of initial sample weight, weight after dust addition and % of dust removed after the cleaning and drying process was completed.

The values of the amount of dust removed after the specified cleaning process for samples 1 and 2 were superior to those observed for the metallic disc or even for the PC sample.

Nevertheless, these values should be taken with caution, as this is mostly a custom test set-up that gives qualitative information. The dust amounts removed represent very small quantities, and the PC samples might have gone through some hydration during the liquid drop stage, due to their different hydrophilicities.

The water contact angles were quite similar for all the samples measured, which points to a similar adhesion of water for all materials. Nonetheless, there were clear differences

between the amount of dust wiped for the D5 microtextured PC samples and the rest of the samples used in the study. In the case of the original D5 textured steel disc, the lower amount of dust removed might be caused by a higher chemical affinity between steel and water or a slightly rougher surface of the steel disc when compared to the rest of the samples shown.

Interestingly, the removed dust weight for the PC sample of the D1 microtexture was also smaller than those determined for samples 1 and 2 (“easy to clean” microtextured D5 PC samples with DR% of 75% and 95%, respectively). This eliminated the possible reasoning of having an *easy to clean* functionality on the surface of injected PC due to the mere existence of a microtextured surface. The specificity of the D5 microstructure design for easy to clean purposes appears to be confirmed by the observed results.

All these facts seemed to confirm the surface functionality easy to clean for injected PC samples and point to a higher effectivity for higher degrees of replication DR%.

## CONCLUSIONS

This chapter demonstrates a method for the replication of surface microstructures on PC using regular isothermal injection molding and confirms their functionalities based on custom and easily aplicable validation tests with interest for the industry.

The attainment of such functionalities on steel was achieved by means of laser texturing using an innovative technique that reverts into lower surface roughness of the obtained microtextures and therefore easier demolding of the latter injection molded parts. The latter obtained functional surfaces of the injection molded plastic specimens represents an interesting technology to enhance the functionality of plastic parts.

on the automotive, consumer electronics, medical devices, or lighting sectors, to cite some. Isothermal injection molding constitutes a suitable method for the replication of such low aspect-ratio structures of various physical functionalities in the micrometer range, with high applicability and uniform results for a large number of parts.

Between the process parameters chosen for the analysis, mould temperature, and holding pressure showed the highest influence on the replication degree, as shown by the factorial DOE analysis.

The surface functionalities were validated even at varied degrees of replication for the injected microtextured surfaces. Custom validation test set-ups were defined to best represent the final application potential, with a clear focus on final use properties. Measurements were taken for relevant parameters, following recommendation of the project participants in view of underlying the industrial relevance of the replicated

textures. On most cases, the best replication fidelity was obtained for the center of the microstructure and a slight deviation on the DR% between the center and the lateral ends of the injected samples was detected. These deviations reached a maximum of 15% for the case of the highest aspect ratio structures (i.e., D2 light-guiding functionality with AR = 0.73).

# REFERENCES

[1] Zhang, H.; Fang, F.; Gilchrist, M.D.; Zhang, N. Filling of High Aspect Ratio Micro Features of a Microfluidic Flow Cytometer Chip Using Micro Injection Moulding. J. Micromech. Microeng.2018 July 1, 28(7), 075005. https://www.doi.org/10.1088/1361-6439/aab7bf.

[2] Loaldi, D.; Calaon, M.; Quagliotti, D.; Parenti, P.; Annoni, M.; Tosello, G. Tolerance Verification of Precision Injection Moulded Fresnel Lenses. Procedia CIRP. 2018, 75, 137–142. https://www.doi.org/10.1016/j.procir.2018.05.004.

[3] Højlund-Nielsen, E.; Clausen, J.; Mäkela, T.; Thamdrup, L.H.; Zalkovskij, M.; Nielsen, T.; Li Pira, N.; Ahopelto, J.; Mortensen, N. A.; Kristensen, A., et al. Plasmonic Colors: Toward Mass Production of Metasurfaces. Adv. Mater. Technol. 2016, 1(7), 1600054. https://www.doi.org/10.1002/admt.201600054.

[4] Islam, M.; Sajid, A.; Mahmood, M.A.I.; Bellah, M.M.; Allen, P.B.; Kim, Y.-T.; Iqbal, S. M., et al. Nanotextured Polymer Substrates Show Enhanced Cancer Cell Isolation and Cell Culture.Nanotechnology. 2015, 26(22), 225101.https://www.doi.org/10.1088/0957-4484/26/22/225101.

[5] Hernández, J.J.; Monclús, M.A.; Navarro-Baena, I.; Viela, F.; Molina-Aldareguia, J.M.; Rodríguez, I. Multifunctional Nano-Engineered Polymer Surfaces with Enhanced Mechanical Resistance and Superhydrophobicity. Sci. Rep. 2017, 7(1), 43450. https://www.doi.org/10.1038/srep43450.

[6] Kehagias, N.; Francone, A.; Guttmann, M.; Winkler, F.; Fernández, A.; Sotomayor Torres, C.M. Fabrication and Replication of Re-Entrant Structures by NanoimprintLithography Methods. J. Vac. Sci. Technol. B. 2018 Nov 1, 36(6), 06JF01. https://www.doi.org/10.1116/1.5048241.

[7] Aizawa, T.; Inohara, T. Pico- and Femtosecond Laser Micromachining for Surface Texturing. In: Micromachining.IntechOpen,2019.https://www.intechopen.com/books/micromachining/pico-and-femtosecond-laser-micromachining-for-surface-texturing

[8] Holzer, C.; Gobrecht, J.; Schift, H.; Solak, H. Replication of Micro and Nanostructures on Polymer Surfaces. Macromol. Symp. 2010, 296(1), 316–323. https://www.doi.org/10.1002/masy.201051044.

[9] Ebrahimi, M.; Konaganti, V.K.; Moradi, S.; Doufas, A.K.; Hatzikiriakos, S.G. Slip of Polymer Melts Over Micro/nano-Patterned Metallic Surfaces. Soft Matter. 2016, 12(48),9759–9768. https://www.doi.org/10.139/C6M02235A.

[10] Skoulas, E.; Manousaki, A.; Fotakis, C.; Stratakis, E. Biomimetic Surface Structuring Using Cylindrical Vector Femtosecond Laser Beams. Sci. Rep. 2017 Mar 22, 7(1), 45114. https://www.doi.org/10.1038/srep45114

[11] Zhang, N.; Srivastava, A.; Kirwin, B.; Byrne, R.; Fang, F.; Browne, D.; Gilchrist, M. D., et al. Manufacturing Microtextured Tool Inserts for the Production of Polymeric Microfluidic Devices. J. Micromech. Microeng. 2015 Aug 10, 25(9), 95005. https://www.doi.org/10.1088/ 0960-1317/25/9/095005.

[12] Vera, J.; Brulez, A.-C.; Contraires, E.; Larochette, M.; Trannoy- Orban, N.; Pignon, M., et al. Factors Influencing Microinjection Molding Replication Quality. J. Micromech. Microeng. 2017, 28(1), 15004. https://www.doi.org /10.1088%2F1361-6439%2Faa9a4e.

[13] Pina-Estany, J.; Colominas, C.; Fraxedas, J.; Llobet, J.; Perez- Murano, F.; Puigoriol-Forcada, J.M.; Ruso, D.; Garcia- Granada, A. A., et al., A Statistical Analysis of Nanocavities Replication Applied to Injection Moulding. Int. Commun. Heat Mass Transf.2017,81,131–40. https://www.doi.org/10.1016/j.icheatmasstransfer.2016.11.003.

[14] Muntada-López, O.; Pina-Estany, J.; Colominas, C.; Fraxedas, J.; Pérez-Murano, F.; García-Granada, A. Replication of Nanoscale Surface Gratings via Injection Molding. Micro Nano. Eng. 2019, 3, 37–43. https://www.doi.org /10.1016/j.mne.2019.03.003.

[15] Liou, A.-C.; Chen, R.-H. Injection Molding of Polymer Micro- and Sub-Micron Structures with High-Aspect Ratios. Int. J. Adv. Manuf. Technol. 2006, 28(11–12), 1097–1103. https://www.doi.org /10.1007/ s00170-004-2455-2.

[16] Maghsoudi, K.; Jafari, R.; Momen, G.; Farzaneh, M. Micro- Nanostructured Polymer Surfaces Using Injection Molding: A Review. Mater. Today Commun. 2017, 13, 126–143. https://www.doi.org /10.1016/j.mtcomm.2017.09.013.

[17] Attia, U.M.; Marson, S.; Alcock, J.R. Micro-Injection Moulding of Polymer Microfluidic Devices. Microfluid. Nanofluidics. 2009, 7(1), 1. https://www.doi.org/10.1007/s10404-009-0421-x.

[18] Zhang, Y.; Mischkot, M.; Hansen, H.; Hansen, P.-E. Replication of Microstructures on Three-Dimensional Geometries by Injection Moulding of Liquid Silicone Rubber. 2015.

[19] Loaldi, D.; Regi, F.; Baruffi, F.; Calaon, M.; Quagliotti, D.; Zhang, Y.; Tosello, G., et al. Experimental Validation of Injection Molding Simulations of 3D Microparts and Microtextured Components Using Virtual Design of Experiments and Multi-Scale Modeling. Micromachines. 2020 Jun 24, 11(6), 614. https://www.doi.org 10.3390/mi11060614.

[20] Lu, Y.; Luo, W.; Wu, X.; Xu, B.; Wang, C.; Li, J., Li, L., et al. Fabrication of Micro-Structured LED Diffusion Plate Using Efficient Micro Injection Molding and Micro-Ground Mold Core. Polymers (Basel). 2020, 12(6), 1307. https://www.doi.org/10.3390/ polym12061307.

[21] Gheisari, R.; Lan, P.; Polycarpou, A.A. Efficacy of Surface Microtexturing in Enhancing the Tribological Performance of Polymeric Surfaces Under Starved Lubricated Conditions. Wear. 2020, 444–445, 203162. https://www.doi.org/ 10.1016/j.wear.2019.203162.

[22] He, B.; Chen, W.; Jane Wang, Q. Surface Texture Effect on Friction of a Microtextured Poly(dimethylsiloxane) (PDMS). Tribol. Lett. 2008, 31(3), 187. https://www.doi.org/10.1007/s11249-008-9351-0.

[23] Świetlicki, M.; Chocyk, D.; Klepka, T.; Prószyński, A.; Kwaśniewska, A.; Borc, J.; Gładyszewski, G., et al. The Structure and Mechanical Properties of the Surface Layer of Polypropylene Polymers with Talc Additions. Mater. (Basel). 2020 Feb 4, 13(3), 698.

[24] Skarmoutsou, A.; Charitidis, C.A.; Gnanappa, A.K.; Tserepi, A.; Gogolides, E. Nanomechanical and Nanotribological Properties of Plasma Nanotextured Superhydrophilic and Superhydrophobic Polymeric Surfaces. Nanotechnology. 2012, 23, 50, 505711. https://www.doi.org /10.1088%2F0957-4484%2F23%2F50%2F505711.

[25] Wong, M.; Moyse, A.; Lee, F.; Sue, H.-J. Study of Surface Damage of Polypropylene Under Progressive Loading. J. Mater. Sci. 2004, 39(10), 3293–3308. https://www.doi.org /10.1023/B:JMSC.0000026930.12462.3d.

[26] Geyer, F.; D\textquoterightacunzi, M.; Sharifi-Aghili, A.; Saal, A.; Gao, N.; Kaltbeitzel, A.; Sloot, T.-F.; Berger, R.; Butt, H.-J.; Vollmer, D., et al. When and How Self-Cleaning of Superhydrophobic Surfaces Works. Sci. Adv. 2020, 6(3). https://www.doi.org /10.1126/sciadv. aaw9727.

[27] Haines, R.S.; Ahf, W.; Zhang, H.; Coffey, J.; Huddle, T.; Lafountaine, J. S.; Lim, Z.-J.; White, E. A.; Tuong, N. T.; Lamb, R. N., et al. Self- Cleaning Surfaces: A Third-Year Undergraduate Research Project. J. Chem. Educ. 2009 Mar 1, 86(3), 365. https://www.doi.org /10.1021/ed086p365.

[28] Condition, T. Makrolon® 2207, 2019, pp 2–5.

[29] Information P. PLEXIGLAS ®8N, 2013, pp 3–5.

[30] Masato, D.; Sorgato, M.; Lucchetta, G. Analysis of the Influence of Part Thickness on the Replication of Micro-Structured Surfaces by Injection Molding. Mater. Des. 2016, 95, 219–24. https://www.doi.org /10.1016/j. matdes.2016.01.115

[31] Rios, P.F.; Dodiuk, H.; Kenig, S.; McCarthy, S.; Dotan, A. The Effect of Polymer Surface on the Wetting and Adhesion of Liquid Systems. J. Adhes. Sci. Technol. 2007 Jan 1, 21(3–4), 227–241. https://www.doi.org/10.1163/156856107780684567.

# 3. EXPERIMENTS ON THE REPLICATION OF MICRO-NANOTEXTURES ON POLYMERS USING ADVANCED INJECTION MOULDING TECHNOLOGIES

## 3.1 INJECTION COMPRESSION MOULDING EXPERIMENTS

### INTRODUCTION

As part of the research planned, using injection compression moulding methods in order to improve the replication degree for high aspect ratio microstructures was contemplated for its use with thermoplastic injection over laser microtextured steel inserts. Once the baseline performance on the regular isothermal injection moulding method in terms of DR% was established, it was interesting to check the potential improvements obtained on the micro/nanocavitiy filling by application of this method.

This method consists on injecting the molten polymer inside a mould cavity with an initial increased thickness (versus the final one that corresponds to the injected part), that is subsequently reduced to a final thickness by means of the displacement of one of the mould's lateral walls, consequently closing the mould to its final position. Therefore, the molten polymer is compressed on one of its lateral surfaces to reach the final thickness, and an extra compression of the polymer upon cooling is produced. As researched on related scientific literature [1,2], it seems proven that this injection moulding method can improve the replication degree under certain conditions.

The objective of this specific work is double:

1. To set up and dominate the injection compression moulding process as part of the applicable processes' catalogue within the EURECAT plastronics pilot plant.
2. To check the specific process conditions that allow for an increase in replication degree of high-aspect ratio micro/nanostructures.

A squared steel insert was laser-engraved with a periodic microstructure consisting of microholes with an area of 10x10mm and a depth of 20 µm and a peak-to-valley average distance of 9.93 µm was used for the experiments. This laser textured periodic microstructure was engraved on the top half of the moveable mould insert-cavity with variable thickness, at 100 mm from the gate (see place marked with a red square on the picture on the right below).

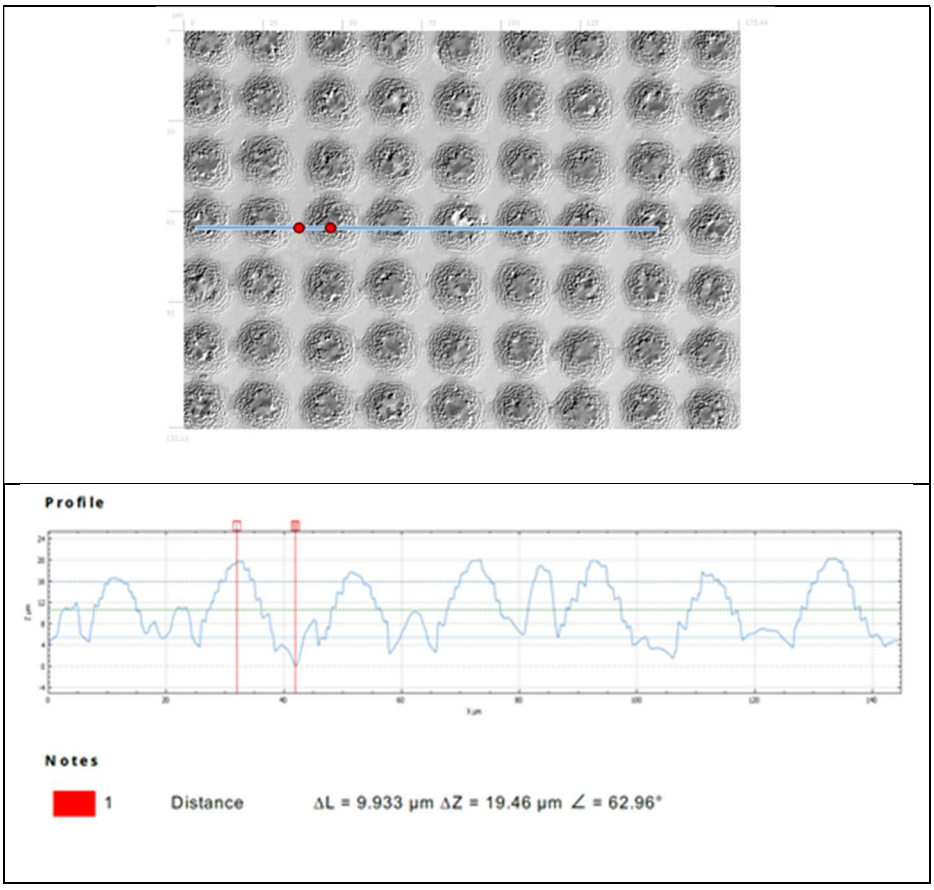


**Figure 3.1. Microstructure of holes laser textured on the mould insert-cavity (above) and a CLSM-profile image of the blue line marked (below) CAD drawing of the mould half containing the microstructure in its top section (right)**

An injection mould capable of producing injection compression effects by means of compression springs was used for the experiments. A CAD design of the mould half where the microstructure was engraved can be observed in Fig 3.2. Also, a diagram including the active forces in the process can be seen. The main forces involved in the process can be summarized as:

$F_{pP}$= Programmed compression force

$F_{wP}$= Effective compression force

$F_A$= Lifting force

$F_F$= Spring force

They have to be carefully balanced prior to the injection trials, in order not to damage the mould or to avoid producing defect-containing parts.

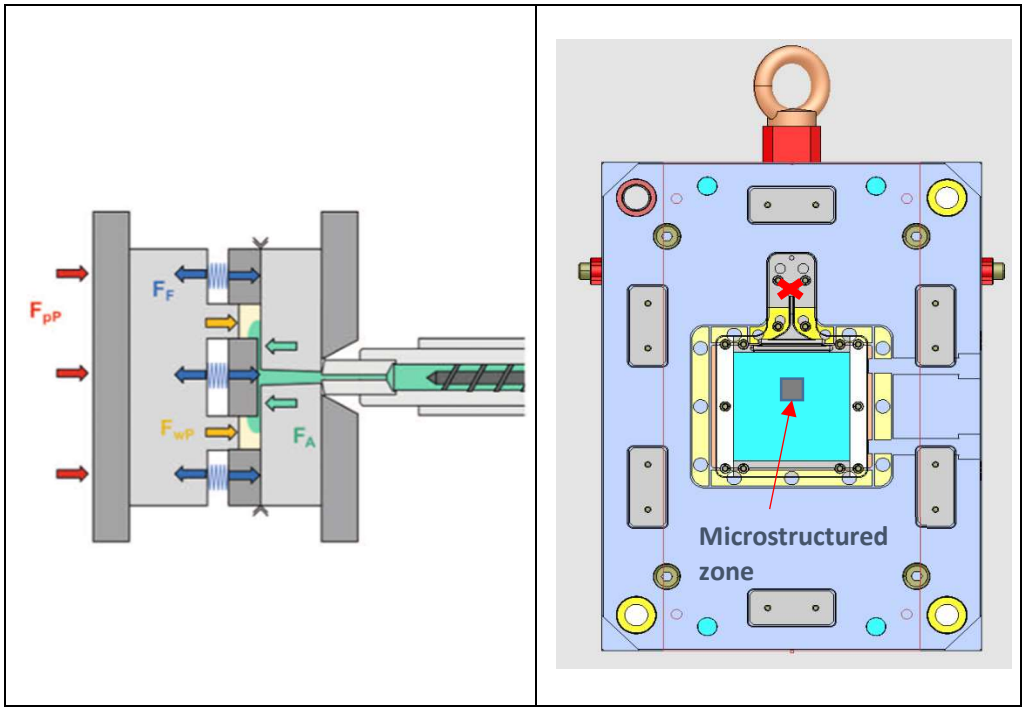


**Figure 3.2. Compression-springs based ICM mould used and diagram showing the specific forces involved in the process (left) – Image credit: [6]. CAD drawing of the mould half containing the microstructure in its top section (right) – EURECAT**

This injection mould was mounted in a 3K 160-Ton Engel injection moulding machine. Polycarbonate Makrolon 2207 was chosen as polymer material. Each injection round yields a flat square part of 122 by 120 mm and 2.2 mm in thickness, that was later characterized using confocal laser scanning imaging. Details of the mould type and microstructure placement can be observed in Figure 3.2.


**Figure 3.3. Picture of the Engel 3K injection moulding machine used in the experiments. Image credit: EURECAT**

A detailed of the obtained injected part can be observed in the figure below (Figure 3.4).

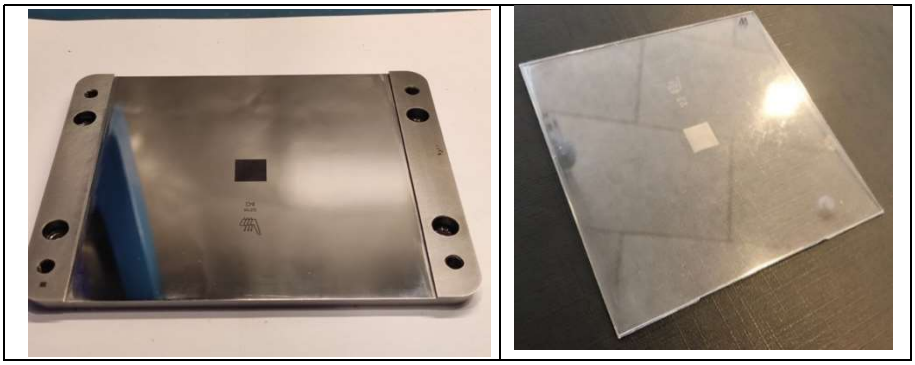

**Figure 3.4. Picture of the microtextured insert used in the experiments (left) and the resulting injected part (right)– Image credit: EURECAT**

For the experiments, Experimental Methods a custom design of experiments was conceived in order to inject material at various injection speeds, mould gaps, compression speeds and as shown in the table below.

| INSERT NUM | Order exp. | Gap (mm) | Vinj (cm3/s) | V comp (mm/s) |
|---|---|---|---|---|
| FLAT insert without texture | 0 | 0 | 57 | - |
| | 0A | 0 | 38 | - |
| | 0B | 0 | 90 | - |
| 52- super-hydrophobic texture on flat steel insert | 1 | 0,5 | 38 | 30 |
| | 2 | 0,5 | 38 | 15 |
| | 3 | 0,5 | 57 | 30 |
| | 4 | 0,5 | 57 | 15 |
| | 5 | 1 | 38 | 30 |
| | 6 | 1 | 38 | 15 |
| | 7 | 1 | 57 | 30 |
| | 8 | 1 | 57 | 15 |
| | 9 | 3 | 38 | 30 |
| | 10 | 3 | 38 | 15 |
| | 11 | 3 | 57 | 30 |
| | 12 | 3 | 57 | 15 |

**Table 3.1.** Conditions applied for the Design of Experiments applied to the Injection Compression Moulding experiments.

Aside form the injection moulding compression conditions included in the table, the following conditions were held constant during the experiments, as per the experience gathered during previous injection moulding of micro/nanotextures and as per indication of the used material's datasheet:

Screw temperature: 290ºC

Mould temperature: 80ºC

Holding pressure: 800 bar

Holding pressure time: 7''

Cooling time: 15''

Once the experiments were completed and the polymeric parts were gathered, they were carefully analysed using CLSM and the software Gwyddion, in an analogue way to what is explained in chapter 2, in order to compare DR% of the parts injected using

compression stroke with that of the uncompressed parts. That allowed therefore to determine the processing window of main compression parameters that resulted in micro/nanocavity filling improvement.

## RESULTS AND DISCUSSION

While injection compression moulding is largely demonstrated as a technique to improve part thickness uniformity, reduce stress concentrations or improve overall optical uniformity of the part, its effectivity to improve the replication degree of micro/nanostructures at typical mould temperatures for PC (80°C) is not confirmed for our settings, for any of the compression gaps/compression stroke speeds and injection speeds combinations tested.

The maximum achieved replication degree of for the chosen microstructure in isothermal injection moulding (IM) reached a maximum value of 25% (see figure YY) for the parts injected without compression stroke (0, 0A, 0B), and it largely did not improve for the parts injected with compression stroke in any of the cases except for experiments 7 and 8, when it was similar due to higher injection speeds applied. A table of the obtained results can be seen below.

| INSERT NUM | Order exp. | Avg. feature height / DR% |
|---|---|---|
| **FLAT insert without texture** | 0 | 4.8µm / 25% |
| | 0A | 2.3µm / 12% |
| | 0B | 2.6µm / 13% |
| **52- super-hydrophobic texture on flat steel insert** | 1 | 1µm / 5% |
| | 2 | |
| | 3 | 2µm / 10% |
| | 4 | |
| | 5 | 3,5µm / 18% |
| | 6 | |
| | 7 | 4,5µm / 23% |
| | 8 | |
| | 9 | Too stretched and broken pillars |
| | 10 | |
| | 11 | |
| | 12 | |

**Table 3. 2.** Results obtained on the Injection Compression Moulding experiments.

On top of that, an increased part-curvature was observed when comparing the centre with the sides of the microtextured zones and a flattening of the features tip was observed on the confocal images (see Figs. 3.5 and 3.6 below), that might be potentially caused by the process, too.

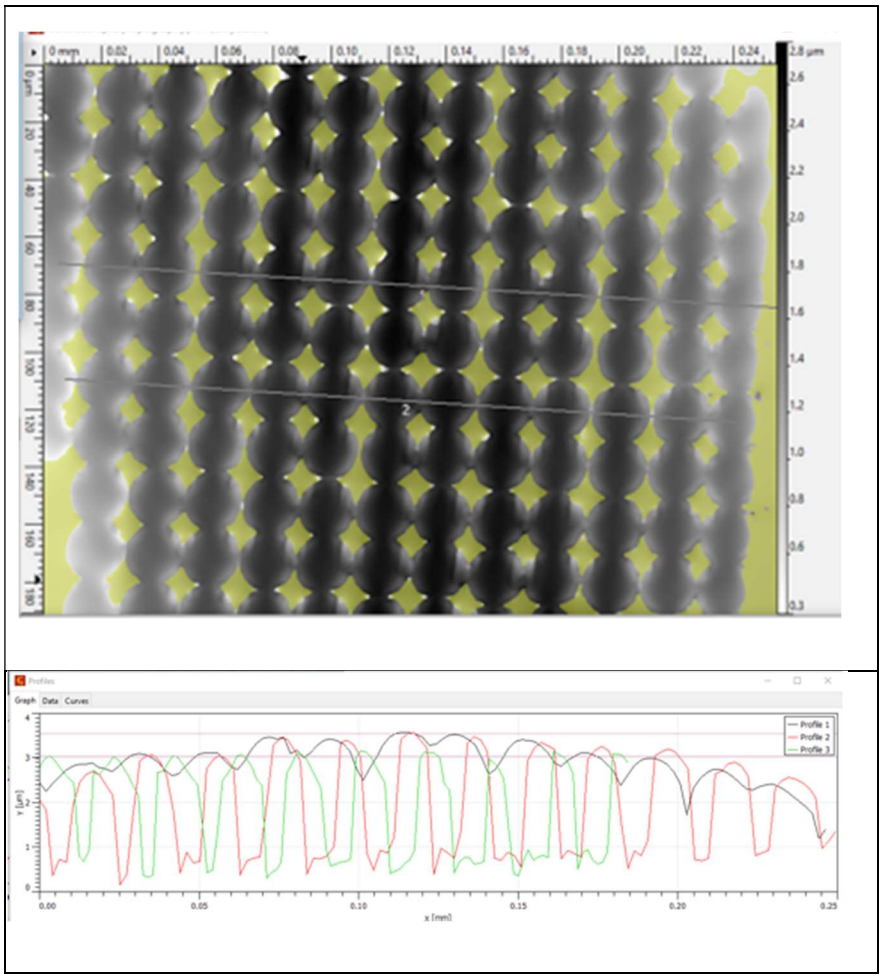


**Figure 3.5. Confocal images of an area analysed in one of the samples (above), showing the lines marking the two parallel height profiles analysed in the part, and profile extracted from the confocal image showing the curvature produced in the injected samples (below).**

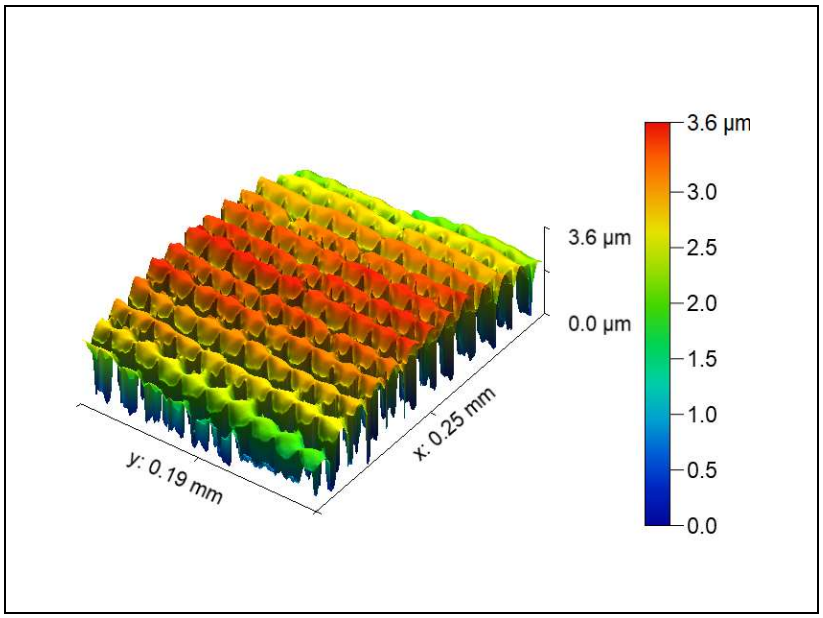


**Figure 3.6. Confocal 3D image showing the curvature and flattening of the micrometer-sized pillars of the microtextured area on the injected samples.**

All the results are based on comparing 6 different confocal-laser imaging measurements at the centre-upper half, centre-lower half, centre-left and right sides of the microstructured square practiced on the injected part.

## CONCLUSIONS

None of the DR% values obtained did not go over the value 25% when applying injection compression moulding methods, which is very comparable to the values obtained when using normal isothermal injection moulding to replicate nanotextures with laser-textured inserts.

While ICM increases replication degree for high-fluidity thermoplastics at regular mould temperature settings (as stated in extensive scientific literature), it doesn't seem to be a very effective method to increase the replication degree in HAR (high aspect ratio – 2:1 or higher) microstructures at common processing mould temperatures on high-viscosity thermoplastics, as it's the case for PC.

Another potential cause for the unexpected results obtained with these trials might be the excessive reduced area (100 $mm^2$) of the micro/nanotextured zone with regards to the overall surface exposed to compression stroke, which in fact constitutes the whole flat area of the part (122x120mm=14646 $mm^2$). This might have caused insufficient compression on the microtextured area of the injected parts. What remains also clear is that for constant compression gap and speed, the DR% improves slightly at higher

injection speeds, as expected per the interactions shown between pressure and injection speed in the chapter 2 of this research.

Replication degree can potentially be increased by adding higher mould temperatures to the compression moulding stated processes, but at the expense of process energy costs and cycle times. Anyway, even if ICM does not clearly improve replication degree for high viscosity thermoplastics in HAR microstructures, it might still be adding remarkable improvements to the optical quality & thickness uniformity of injected transparent parts. Therefore, it should be further explored for other polymer types (with lower viscosities) and also its combination with rapid mould heating methods to achieve all these effects.

## 3.2 INFRARED MOULD-SURFACE HEATING EXPERIMENTS

### INTRODUCTION

The utilization of variothermal surface heating to enhance the filling of micro/nanocavities in injection moulding has been recently demonstrated [3, 4]. It allows for the reduction or elimination of the frozen layer by increasing the mould surface temperature.

The most common way to apply this technology is using Heat & Cool systems built-in in injection moulds, that allow for the quick heating and cooling of the mould surface. Nevertheless, even if these are effective systems, their wide applicability might be limited to its high implementation cost and the fact that they're mould-specific, with clearly limits its flexibility. For an R+D institution such as EURECAT where all the tests were taking place, in order to have a non mould-specific system at lower cost available for many different experiments and configurations, an IR-surface mould heating system that has also proven its applicability to the referred problem [5] presented itself as the most convenient alternative.For that reason, a specialised company we contacted to design a custom equipment that could be suitable to be used with various moulds of different cavity sizes. The idea behind it was to have available an equipment as modular and flexible as it was possible at reasonably low cost.

Then, a series of trials comparing different mould heating levels and set temperatures were carried out and compared with the base cavity-filling level obtained when using isothermal injection moulding, by means of the *CLSM* imaging on the injected samples.

### MATERIALS AND METHODS

The same steel insert laser-engraved with a periodic microstructure consisting of microholes from the previous section 3.1. Additionally, the same machine and injection moulds were also used in the experiments. The parts obtained were identical in dimensions to the parts obtained in the previous experiment 3.1.

Concerning the specifically conceived infrared heating system, a custom device consisting of two interchangeable IR-lamps of two different sizes was manufactured. It was designed so as to fit in between the mould halves of two machines (an ENGEL 55Tm. and an ENGEL 160Tm) daily used at EURECAT's lab. The main idea behind the configuration was to have a reasonable cost, adaptable and modular system able to heat one side of a mould cavity while the mould was open, prior to the injection run. Once designed and agreed, it was outsourced for manufacturing.

It consisted of two IR-lamps with the following dimensions and characteristics:

- Big lamp: 5 short wave (SW) lamp emitters with reflector with a total power of each lamp emitter of 2530 W. The working voltage of the lamp emitters was 230 V, and the module heating area was 35x35cm. The heating heads were adjustable in height and rotation.
- Small lamp: 2 SW emitters with reflector with a total power of 500 W. the working voltage of the emitters was 115 V, and the module heating area was 35x35cm. The heating heads were adjustable in height and rotation.
- An electronic command system able to switch control between small module (up to 1kW) and big module (up to 12.65 kW) was used. This module can be regulated to control the heating by set temperature and/or time, as it incorporates an optical pyrometer to continuously monitors the desired temperature by pointing it to the right surface.
- Metallic frame of size 610x1200.65x1361 mm.

Details of the heating lamps, big and small systems and a picture of the actual assembled device with the installed cam be seen below in Figure 3.7 and the supplementary material of this section.

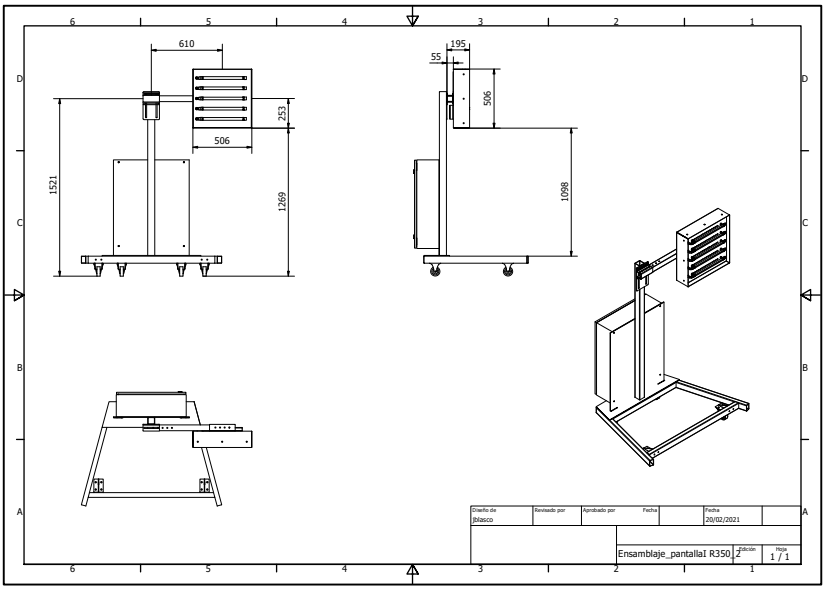


**Figure 3.7. Image showing the overall configuration of the IR-heater. SOURCE: EURECAT**

To optimize the calibration of the IR-heating device towards achieving optimized production cycles in the future, the temperatures on the the heated mould surface were

continually measured comparing the readings and deviations between the various measurement methods. The measurements were taken using the following devices:

- Thermocouples attached to the mould surface (2) and conveniently protected with high-temperature tape. They offered continuous temperature reading thanks to the connection to a multiple-channel data logger.
- Contact pyrometer (single-point instantaneous reading upon contact)
- Optical thermocouple (connected to IR device to allow for temperature-regulated settings)

Also, the mould temperature settings of the injection moulding machine were used for comparison purposes.
Prior to any IR-heating experiment five parts were injected with the same settings as the previous section 3.1, and five additional parts were obtained with a mould temperature setting of 120 ºC.
For the machine calibration, initially the IR-heating system was used on the “set by temperature” mode, fixing an input temperature at 180ºC (corresponding to the now flow temperature of PC, which is the thermal transition temperature of PC + 30ºC [16]), using the big lamp (35x35cm heating area) and setting the mould temperature at 80ºC. Then, the time taken for the thermocouples, the optical and the contact pyrometer to achieve the set temperature was measured (twice at various heated cavity locations). The IR-heater was placed at 55mm from the mould surface.

In a second experiment, the same process was carried out but setting the mould temperature at 120ºC.Once the optimal setting was achieved for the IR-heating device and a time to reach the set temperature was measured, several parts were injected using this time as heating time set in the command module.

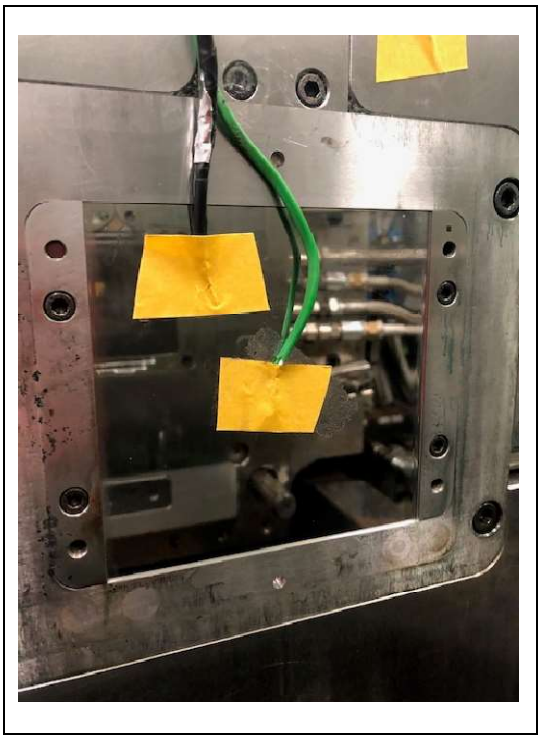

**Figure 3.8. Image showing the position on which the thermocouples were placed.**

## RESULTS AND DISCUSSION

From the initial experiments, a constant deviation of approximately 10ºC existed between the temperature measured by the IR-heater's optical pyrometer and the thermocouples, with the read from the contact pyrometer which always showed the higher value. The contact pyrometer was from then on used as the reference value, given the acceptable ±10ºC variation on the mould temperature settings which were fixed at 120ºC (and sufficient time was allowed for the mould to heat-up).

There exists a considerable deviation between the time taken for the IR-heating system to reach the set temperature depending on the starting set temperature of the machine mould, as shown in the two measurements in table 3.3.

| Mould setting | time to achieve 180℃ mould surface temperature | |
|---|---|---|
| 80ºC | 7' | 6'10" |
| 120ºC | 44" | 45" |

**Table 3.3.** Results of the experiments to measure the time taken to reach the set surface temperature.

Due to the much shorter time to reach the set temperature of 180ºC when the mould temperature is intially set at 120 ºC, it was decided to use this mould temperature for the experiments of micro/nanocavity-filling.

In terms of the baseline replications achieved for the non-heated parts the average DR% values achieved for the injected parts with the mould set at 80ºC was 20%, while it reached 22% for the parts injected with the mould set at 120ºC. Confocal images of some of these parts can be seen in the figures 3.9 and 3.10 below.

This phenomenon was probably caused by the great thermal inertia of the moulds, given by their great mass. The mould insert was not thermally isolated from the rest of the mould, and this caused the intermediate (and high) heat transfer from the heated mould surface to the rest of the mould parts.

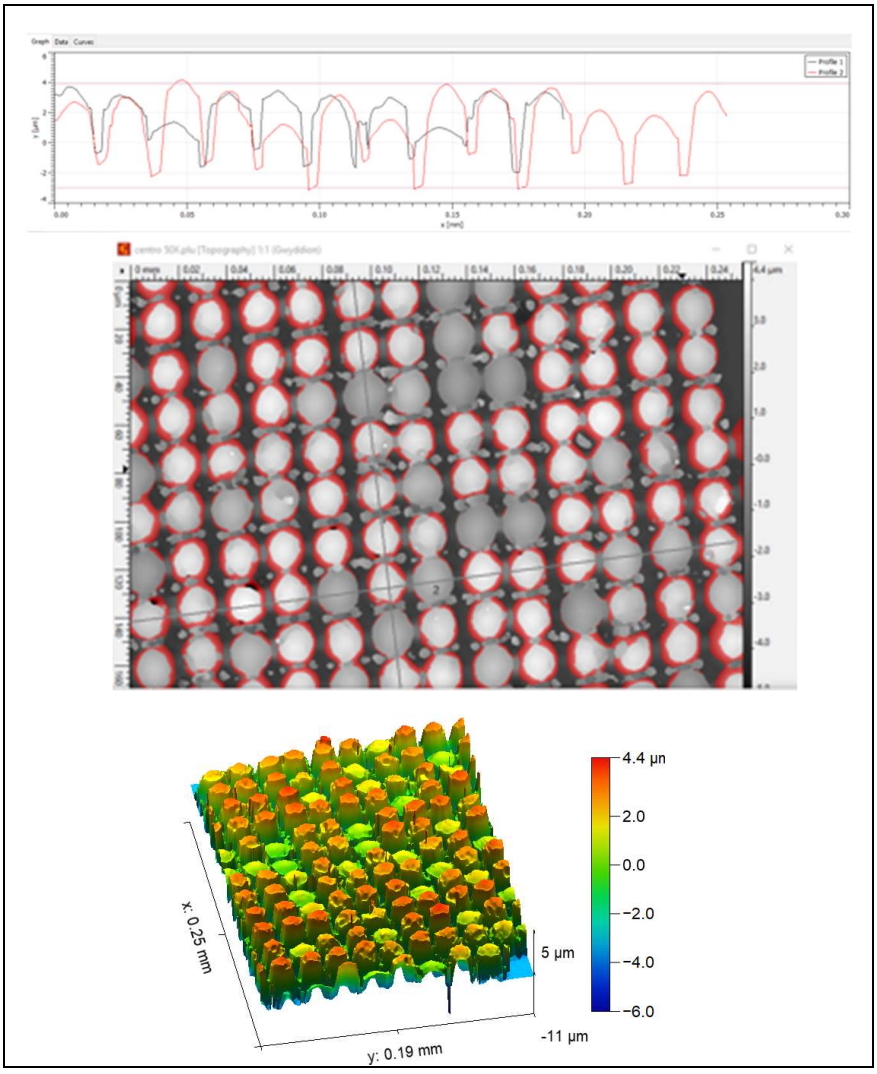


**Figure 3.9. Confocal image of a part injected without IR-heating with the mould set temperature of 80ºC; Confocal image of the profiles analysed on the area selected (above); linear height profiles extracted from the area analysed (centre), and 3D confocal image of the area analysed (below).**

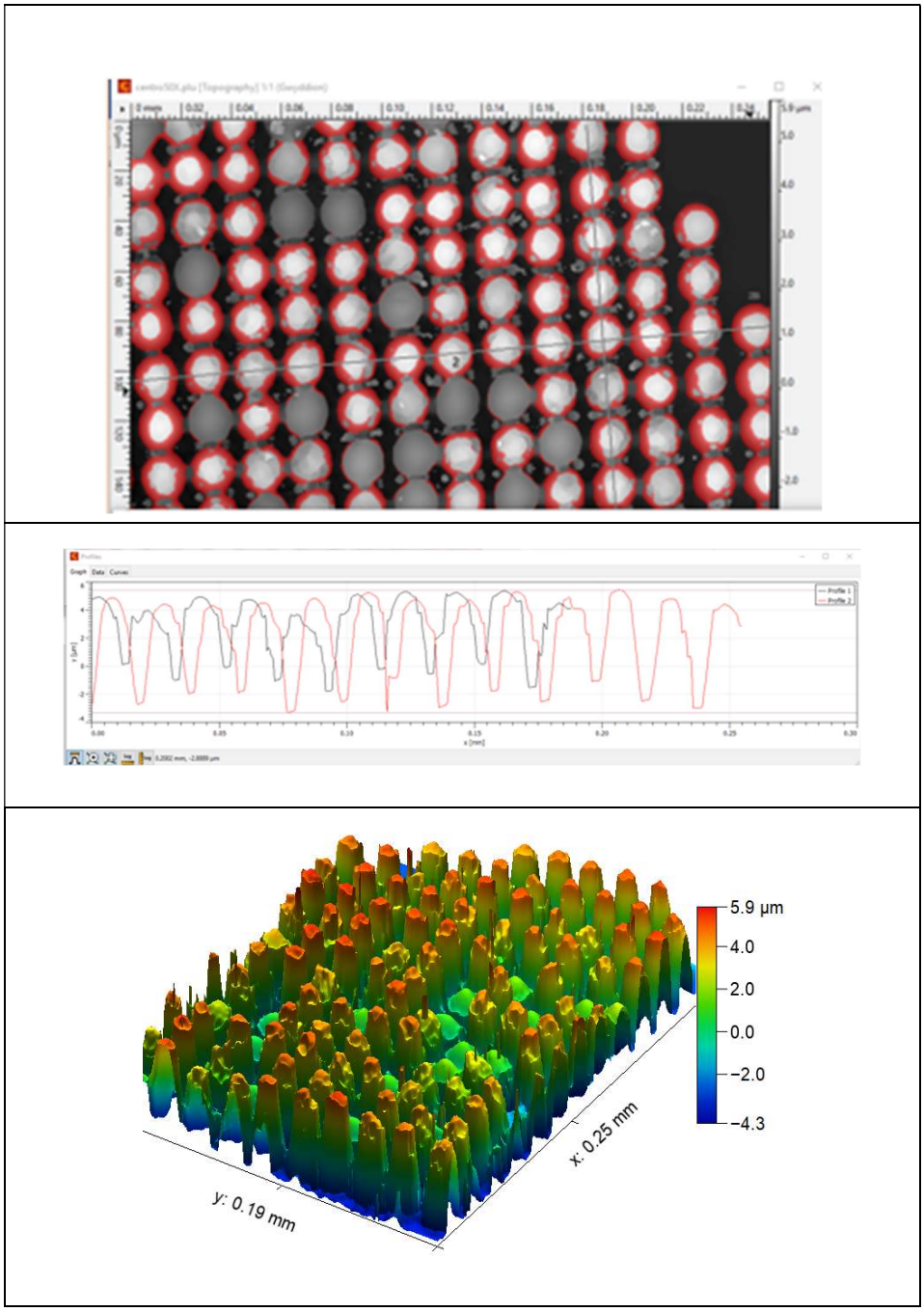


**Figure 3.10. Confocal image of a part injected without IR-heating with the mould set temperature of 120ºC; Confocal image of the profiles analysed on the area selected (above); linear height profiles extracted from the area analysed (centre), and 3D confocal image of the area analysed (below).**

Then, for the injected parts on which the IR-heating was applied, the achieved replication for the best heating conditions -setting the initial mould temperature at 120ºC and heating to 180ºC in 45”- the average DR% achieved reached 36%. Pictures of the best replicated part can be seen in Figure 3.11.

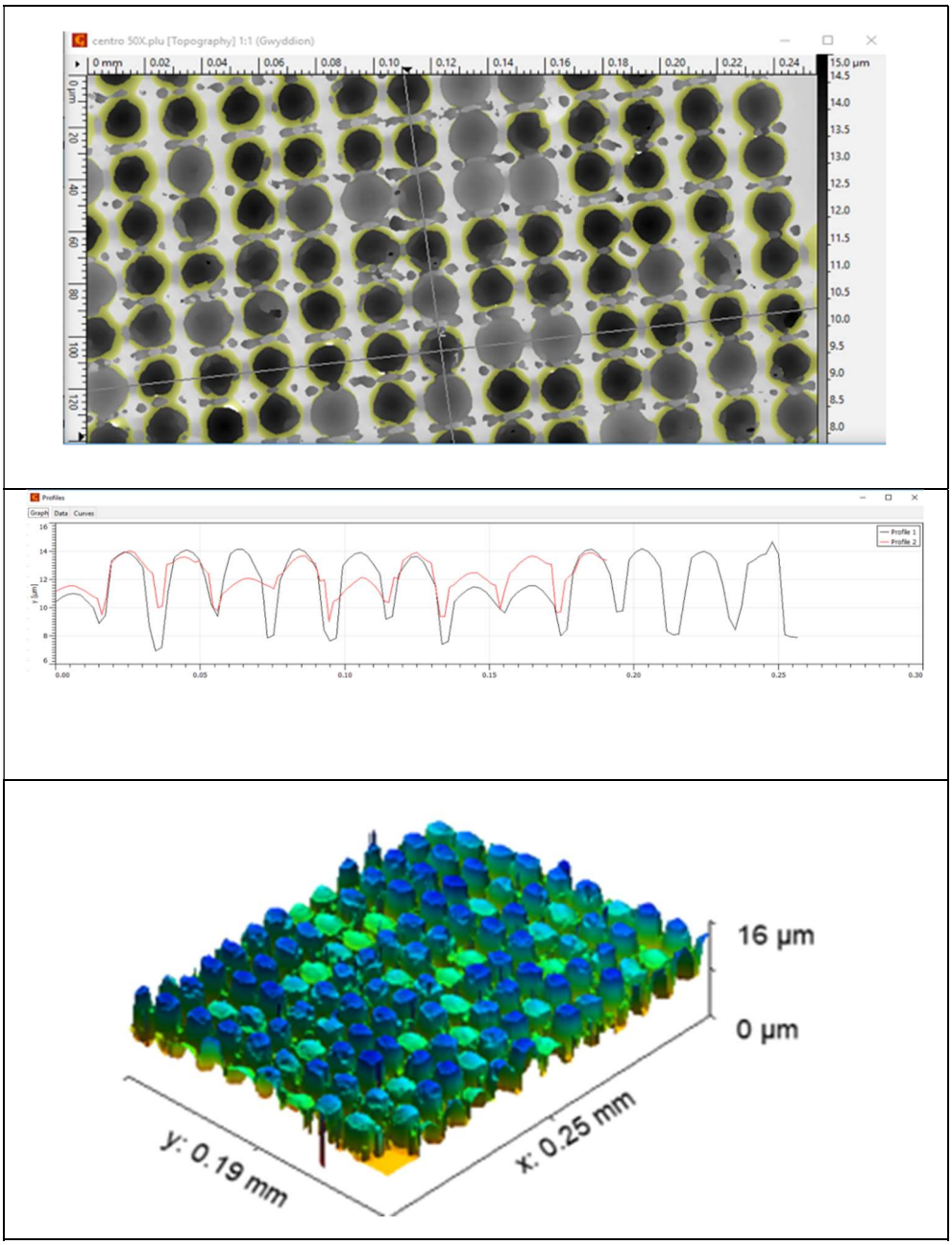


**Figure 3.11. Confocal image of a part that reached 45% DR% injected with IR-heating (45" heating to 180ºC mould surface temperature) with the mould set temperature of 120ºC; Confocal image of the profiles analysed on the area selected (above); linear height profiles extracted from the area analysed (centre), and 3D confocal image of the area analysed (below).**

The improvements reached are not very remarkable, contrary to what was expected. Although it was not possible to measure it with full accuracy, the time taken to close the mould and inject material from the moment the temperature on the mould surface reached 180ºC was around (and most probably higher) than 3". This excessive time caused an excessive temperature drop on the mould surfaces. This decrease in temperature adds to the approximate drop rate of 10ºC/s, observed by the measurements -taken once the IR-heated stopped- with the mould still in open position.

Both facts surely caused the insufficient degree of replication DR% to a large extent. This is supported by the well-known main cause for insufficient mould surface temperature, which is the insufficient mould wall temperature upon the plastic entry.

Also, some of the pillars appeared broken in most of the cases, as it can be observed on the confocal 3D images obtained. This might have been caused by insufficient cooling time (that might have been to be adjusted for such high aspect ratio features or excessive polymer-mould adherence) upon demoulding.

## CONCLUSIONS

The usefulness of application of IR-heaters in isothermal injection moulding processes to assist the improvement of the degree of replication of micro/nanotextures present in the mould has already been already demonstrated in the last years. Upon its development and implementation though, very careful adaptation of the heater characteristics and process parameters to the particular case of study is needed in order to obtain the best possible results.

In our case, the results obtained were very minor, most probably due to insufficient mould temperature upon the moment of injection. This insufficient temperature level was caused by a very quick temperature drop vs time on the micro/nanotextured mould cavity. An excessive time used by the injection moulding machine to inject the polymeric material in the cavity, counted from the moment the IR-heating system was stopped, largely contributed to the insufficient mould temperature too.

The high heat transfer rate of the steel mould surface was probably caused by the very high thermal inertia associated to the different parts constituting the steel mould. The mould parts are directly assembled to the final steel plate containing the cavity without any thermal insulation, and therefore provide a high thermal inertia to the whole mould. Most probably the relatively small, heated surface in comparison to the total mould's surface, and the cavity insulation with regards to the rest of the mould area should be revised.

It is also important to note that the microtexture considered in this case shows a considerable aspect ratio *AR*, of 2, which makes its replication more difficult compared to other not so slender microstructures.

## 3.3 APPLICATION CASE: PLASTFUN PROJECT

### INTRODUCTION

The knowledge and experience gained along this research was applied to the development and prototype production of two polymeric parts representative of interior car dashboard components, that were manufactured via the *In Mould Electronics* IME processing technology within the PLASTFUN project.

The PLASTFUN project (Planta Pilot de Peces Plàstiques amb Superficies Funcionals Avançades), that had the main objective of developing the technology and processes for the pilot production of two IME and micro/nanotextured injection moulded prototype parts typical of car interiors, was included within the Industries of the Future community (IDF) RIS3CAT and supported by the European Regional Development Fund (ERDF) as part of the operative frame FEDER of Catalonia 2014-2020 EC [COMRDI 16-1-0018], included in the 7th Framework Program.

The specific injected parts were built out of an electronically printed film to create an electronic circuit on the film's surface that contained micro-LEDs for the parts retro-illumination. Following the *In Mould Electronics* IME processing route, the specific parts were then thermoformed, precision cut and over-injection moulded. The parts resulting after the injection moulding contained a microtextured zone that provided light-guiding and anti-scratch surface functionality, in order to enhance the luminosity of a LED-back lit area of the part and to reduce the visibility of produced scratches, respectively.

### 3.3.1 PART 1: IME CAR INTERIOR BUTTON PANEL WITH MICROTEXTURED CENTRAL BUTTON'S SURFACE

### MATERIALS AND METHODS

The part mentioned was an injection moulded dashboard control panel displaying seven functional tactile-control buttons, and it contained a microtextured zone on the central key's back surface. The light-guiding microstructure applied (see chapter 2), once replicated in the injection moulded process, was designed to face the inside of the part and perpendicularly guide the light produced by the LED embedded in the part towards the user's eyes. A scheme of the injection moulded part, displaying the microtextured zone and the LED placement, together with the designed and optically simulated light-guiding path can be seen on Figure 3.12 below.

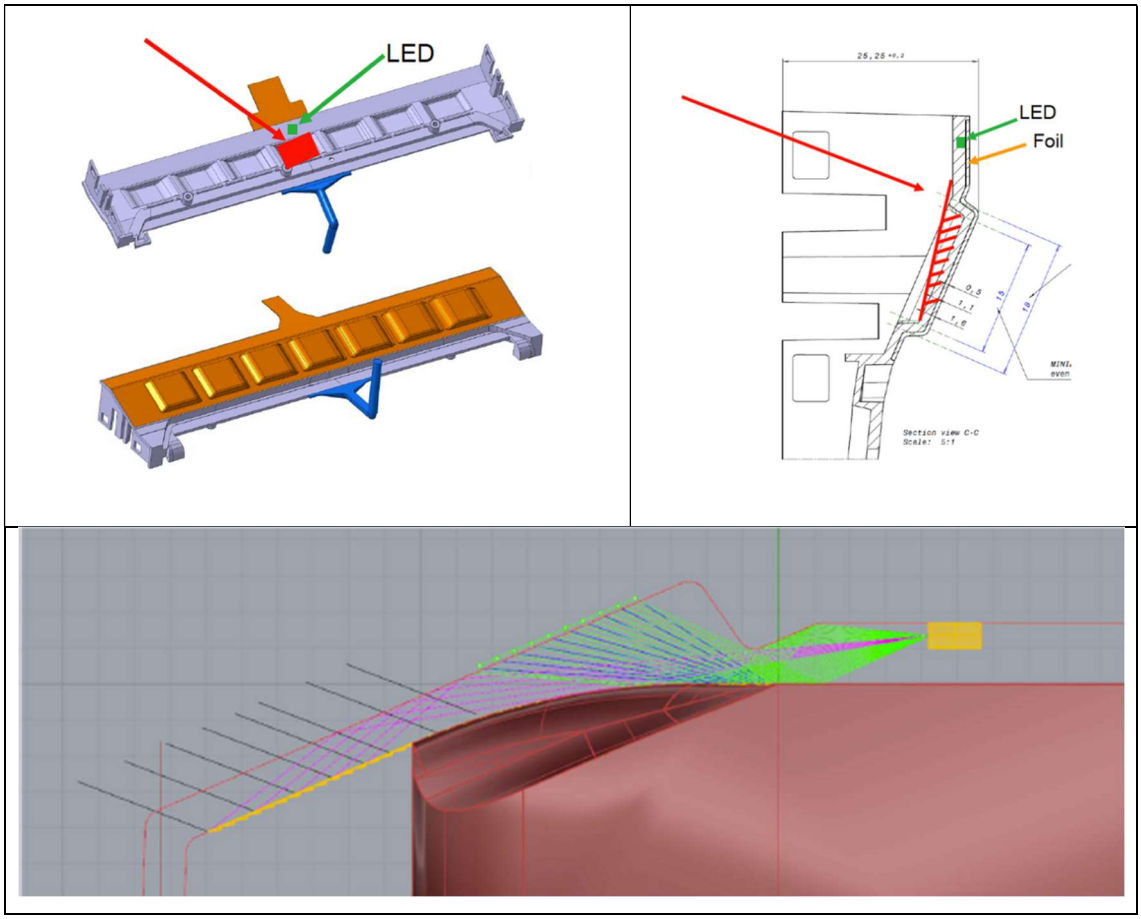


**Figure 3.12. 3D CAD Image of the injection moulded part, displaying the LED and the microtextured zone on the central button's back surface on the part's back view (above-left). CAD design of the parts central button, showing the placement of the microstructure (above-right) and simulated light-guiding path followed by the LED embedded inside the injection moulded part (below). Picture courtesy of KOSTAL ELECTRICA S.A.**

To be able to manufacture the prototype, a custom button-shaped microtextured insert of the size of the central button was manufactured via femtosecond laser ablation, and then conveniently fit in the central section –corresponding to the central button- of the injection mould prior to the injection moulding trials.


**Figure 3.13. Details of the custom-developed microtextured steel insert, shown right next to a nontextured steel insert for comparison (above), and its specific placement on the injection mould cavity (below).**

The part was then injection moulded using the materials and conditions specified in chapter 2, and then it was conveniently validated via confocal laser scanning microscopy *CLSM* and optical measurements.

## RESULTS

The *DR%* achieved reached an average value of 75% (measured over 5 injected parts), which was slightly lower than previous values reached (see chapter 2.1) due to the need of protecting the electronically printed film to avoid potential damages while injecting the polymer. To properly protect the electronically printed film, lower mould and melt temperature were required during the injection, which was not convenient in order to

optimize the *DR%.* Nevertheless, the *DR%* reached was completely satisfactory to obtain the sought functionality.

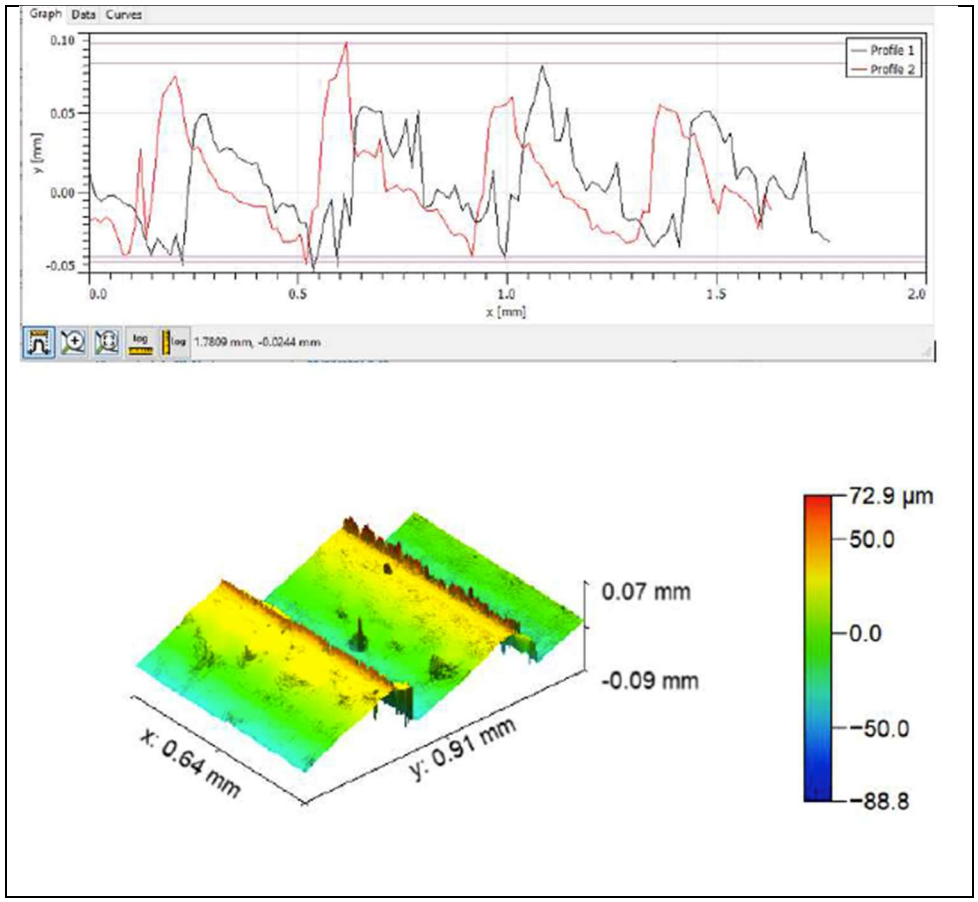


**Figure 3.14. XY profile (above) of the replicated light-guiding microstructures of the injected plàstic part (above) and 3D CLSM image of the characterized section (below).**

## 3.3.2 PART 2: IME CAR INTERIOR TOUCH PANEL WITH MICROTEXTURED CENTRAL SURFACE

### MATERIALS AND METHODS

The part mentioned was an injection moulded decorative and functional panel to be installed in a vehicle interior between the driver and the co-pilot seats, featuring a multi-touch control functional surface and it contained a microtextured zone on the part's central zone. The anti-scratch microstructure applied (see chapter 2), once replicated in the injection moulded process, was designed to face the outside of the part and reduce the visibility of scratches produced during the normal usage of the part.

A scheme of the injection moulded part, displaying the microtextured zone and injection mould can be seen on Figure 3.15 below.

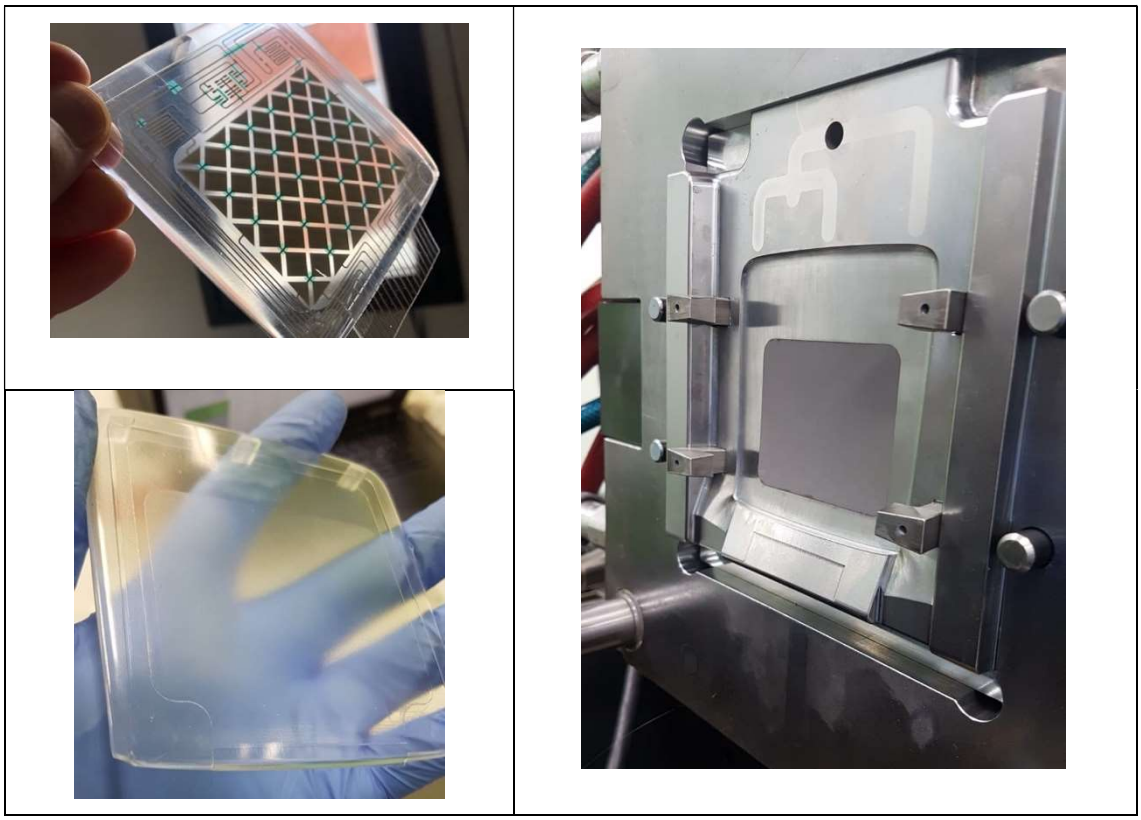

**Figure 3.15. Image of the injection moulded part containing the IME electronically printed film, (above-left). Image of the injection mould used, showing the central microtextured part (right) and picture of the injection moulded part (below-left) without IME film, shown in perspective to highlight the presence of the microstructure. Picture courtesy of Walterpack PPT.**

To be able to manufacture the prototype, a custom microtextured insert of the size of the central touch-sensitive are of the final part was manufactured via femtosecond laser ablation, and then conveniently fit in the central section of the injection mould prior to the injection moulding trials.

## RESULTS AND DISCUSSIONS

The *DR%* achieved reached an average value of 40% (measured over 5 injected parts), which was slightly lower than previous values reached (see chapter 2) due to the need of protecting the electronically printed film to avoid potential damages while injecting the polymer. To properly protect the electronically printed film, lower mould and melt temperature were required during the injection, which was not convenient in order to optimize the *DR%.*

Nevertheless, the *DR%* reached was completely satisfactory to obtain the sought functionality.

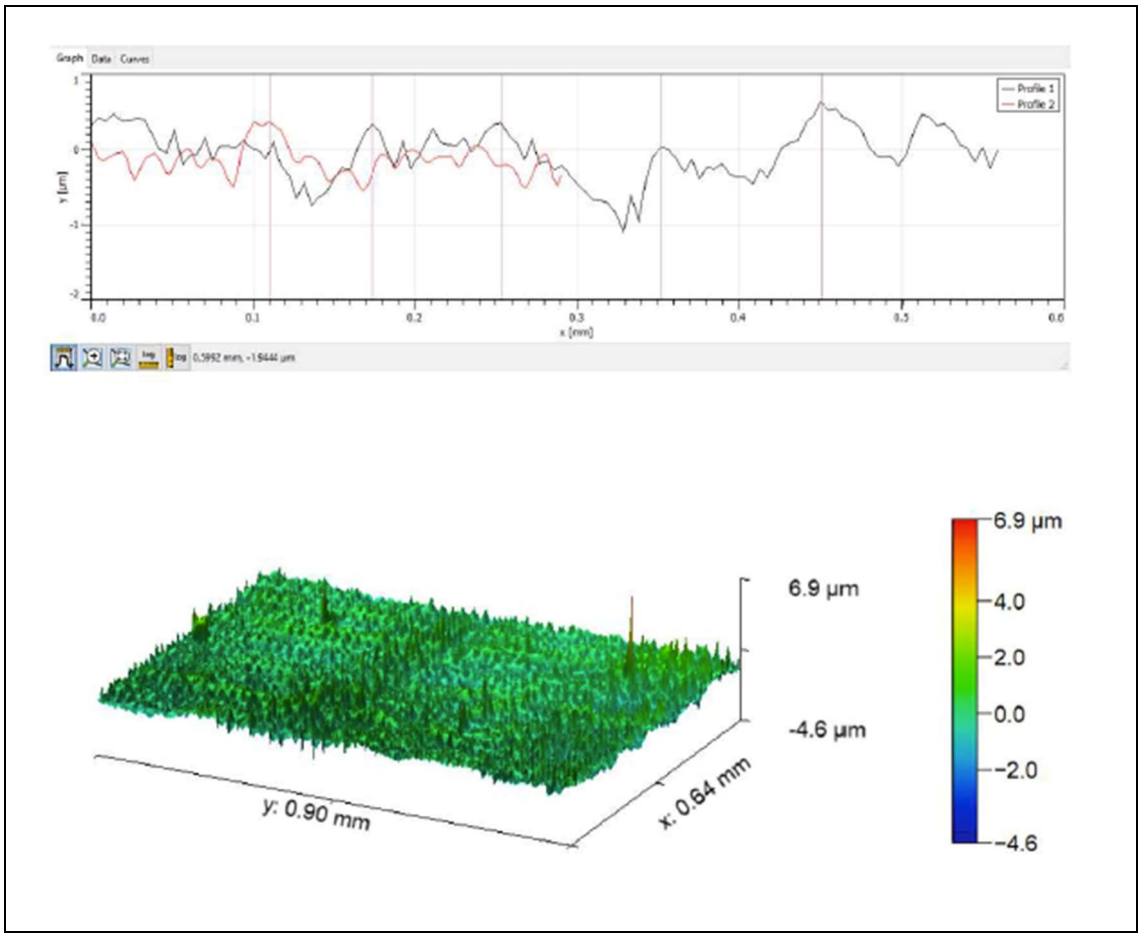


**Figure 3.16. XY profile (above) of the replicated anti-scratch microstructure of the injected plastic part (above) and 3D CLSM image of the characterized section (below) .**

# REFERENCES

[1] Keisuke Nagato, Tetsuya Hamaguchi, and Masayuki Nakao, Injection compression molding of high-aspect-ratio nanostructures, Journal of Vacuum Science & Technology B 29, 06FG10 (2011). https://doi.org/10.1116/1.3662405

[2] Loaldi D., Quagliotti D., Calaon M, Parenti P, Annoni M, Tosello G. Manufacturing Signatures of Injection Molding and Injection Compression Molding for Micro-Structured Polymer Fresnel Lens Production. Micromachines. 2018 ; 9(12) :653. https://doi.org/10.3390/mi9120653

[3] Su, Q., Zhang, N., & Gilchrist, M. D. (2016). The use of variotherm systems for microinjection molding. Journal of Applied Polymer Science, 133(9). https://doi.org/10.1002/app.42962

[4] Liparoti S, Speranza V, Pantani R. Replication of Micro- and Nanofeatures in Injection Molding of Two PLA Grades with Rapid Surface-Temperature Modulation. Materials (Basel). 2018 Aug 15 ;11(8):1442. https://www.doi.org/10.3390/ma11081442

[5] Yu, Ming-Ching & Young, Wen-Bin & Hsu, Pe-Ming. (2007). Micro-injection molding with the infrared assisted mold heating system. Materials Science and Engineering: A. 460. 288-295. https://www.doi.org/10.1016/j.msea.2007.02.036

[6 ] www.kuntstoffe-international.com; Rolf-Uwe Müller; Kuntstoffe 1-2013, pp. 36-39.

# 4.INJECTION MOULDING OF MICRO/NANOTEXTURED SURFACES USING NIL (NANO-IMPRINT LITHOGRAPHY) – TEXTURED POLYMERIC FILMS

## INTRODUCTION

The second part of this thesis focuses on researching the obtention of injection moulded micro/nanotextured polymeric surfaces using textured polymeric films as mould inlays. As previously mentioned, when compared to the usage of metallic inserts as texture templates, the use of polymeric inserts inside the injection mould as replication templates brings the advantage of reducing the cooling rate of the molten incoming polymer upon contact with it, and therefore provides longer time for the filling of the micro- and nanocavities [1].

As part of the research planned within this section, an initial set of experiments was planned in order to evaluate different parameters and conditions involved in the replication-by-injection process, with the aim of exploring the baseline performance of the whole process:

- Explore the application of different polymeric films to be used as base support materials for the deposition of the nanotextured coatings (film and coating constitute the polymeric inlays introduced in the injection mould for latter replication) and evaluate their compatibility and integrity with different transparent polymers of interest when being overinjection moulded.
- Evaluate the method used to hold the film inside the injection mould during the injection moulding process.
- Perform a *Design of Experiments DOE* in order to define the main process parameters influencing the replication.
- Explore the overall tooling set up and evaluate potential improvements.

Later on within this chapter, several subsections dealing with injection moulding of hierarchical three level micro- and nanotextures using optimized polymeric inlays and transparent injected polymers of industrial relevance will be exposed. Another section exploring the replication of these hierarchical structures with biopolymers of high interest in the current environmental crisis context constitutes the second publication belonging to this PhD thesis, and the third publication explores the transfer of micro/nanotextures obtained in flat films to 3D shapes through thermoforming processes, developing at the same time an analytical model to predict the functionality of the textured polymeric surface after the forming process. Finally, two additional sections appear at the end of this thesis: the first one deals with a new finite element modelling approach to evaluate

mould filling processes during the injection moulding of this type of micro/nanotextured parts.

There are many well known commercial softwares to simulate mould filling situations at the macroscale, but their extension to the micro- or nanoscale is rarely seen. For that reason and using the available finite element modelling tools at EURECAT, the combined application of two different softwares for the macro and micro/nanoscale simulations, respectively, was explored.

The last section explores the feasibility and properties obtained by applying postprocessing techniques such as ion implantation to the micro/nanotextured polymers. These types of post-processes are considered of high interest to improve the mechanical properties of the micro/nanotextured surfaces and/or enhance some of their special properties.

## 4.1 First exploratory works to evaluate replication ability and process capacity of current method

### Materials and Methods

During this initial exploratory works, several elements of the process were evaluated. First, and thanks to the existence of two research-purposed silicon stamps in EURECAT, the whole UV-assisted nano imprint lithography UV-NIL nanotexturing process is manually conducted to evaluate potential areas of improvement on the initial tooling manufacturing. Then, an evaluation of several potential materials to be applied as base films on which the coating (that was latter nanotextured via lithographic methods) could be deposited was carried out.

Once those initial tasks were completed, *DOE* applied to injection moulding experiments were carried out to evaluate the main influence of the most relevant process parameters. All these previous works allowed to establish critical conclusions of high interest for the rest of the sections presented in this chapter.

### 4.1.1 NANOTEXTURING PROCESS VIA NANO IMPRINT LITHOGRAPHY

*Stamps*

Initially, EURECAT had available two different stamps from the company NILT technology to complete the works planned. These are silicon stamps without an anti-stick coating mostly used for process research and optimization. It is expected that in a later stage of the study textured films with additional structures and a higher degree of accuracy (manufactured using a prototype UV-NIL machine instead of manual methods) will be used for the research.

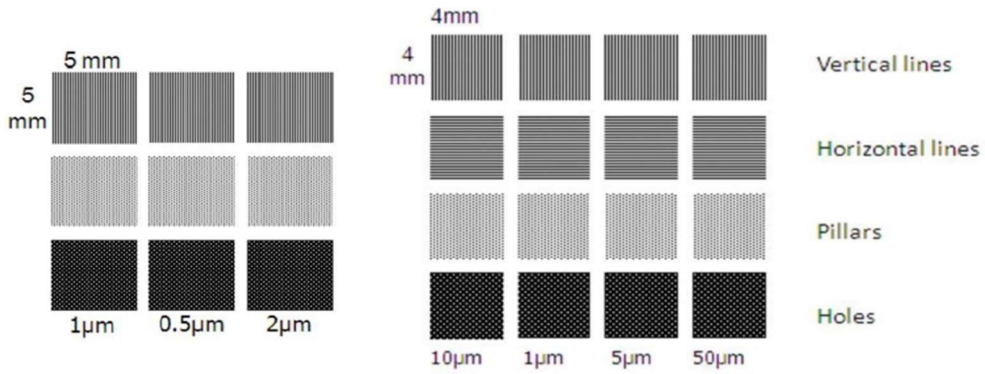


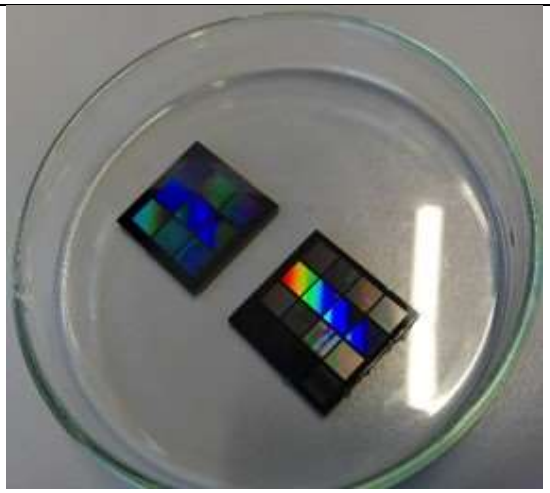

| Stamp ID | SMLA_V1 |
|---|---|
| Stamp size | 150 mm diameter |
| Stamp material | Silicon |
| Stamp thickness | 1 mm |
| Structure size | 500 nm |
| Etch depth | 1 µm |
| Pattern field size | 50 mm x 50 mm |
| Pattern | 1 µm pitch lines and spaces or triangular arranged holes or pillars |
| Delivery time | 3-4 weeks |

| Stamp ID | SMSS_SIQZ_V1 |
|---|---|
| Stamp size | 20 mm x 20 mm |
| Stamp material | Silicon or Fused Silica |
| Stamp thickness | 1 mm |
| Structure size | 500 nm - 2 µm |
| Etch depth | 1 µm or 2 µm in Silicon. 500 nm in Fused Silica |
| Pattern field size | 5 mm x 5 mm x 9 |
| Delivery time | 3-4 weeks |

**Figure 4.1. Features present in the 3x3 and 4x4 stamps used (above), picture of the actual stamps (centre) and table shared by the manufacturer with the relevant dimensional characteristics of the stamps (below).**

It is expected that in a later stage of the study textured films with additional structures and a higher degree of accuracy (manufactured using a prototype UV-NIL machine instead of manual methods) will be used for the research.

The UV-assisted Nano Imprint Lithography process (UV-NIL) to obtain nanotextured coated film inserts was performed at the EURECAT facilities, using several in-house materials. A protocol for the replication of the nanotextures onto the coated films was carefully designed within this research, which is as follows:

*UV-NIL Process*

The steps to complete the replication via *UV-NIL* of the nanotexture patterns present on the surface of a metallic stamp (SI stamps) onto coated polymeric films, the following steps have to be followed:

There re mainly two steps involved:

- Step 1: obtaining a replica of the metallic stamp patterns onto an intermediate PDMS stamper
- Step 2: Pressing/Imprinting the PDMS stampers onto the Ormostamp® coated polymeric films.

*Step 1-Generating the PDMS replica:*

1. Obtaining the mixture PDMS – Sylgard 186:

To mix these two components (base prepolymer and catalyst) a plastic glass (transparent PVC or PS) and a pipette tip need to be used. The mixing ratio is 10:1 (5:1 would also be acceptable in case of needing to increase mechanical properties). Once mixed, the resulting mix has to be thoroughly stirred for at least 3 minutes.

2. Blow the air out of the PDMS mixture:

In a degasser, place the container on a piece of paper. A vacuum is applied until the air bubbles on the surface are completely removed. Then we let the air in by checking the input key and the connection with the vacuum pump. We will repeat the two steps until no bubbles are observed on the surface when vacuuming. Another possibility to remove the bubbles is to let the mixture rest for 30 minutes. The last remaining bubbles can be "punctured" with the tip of the pipette.

3. Curing of PDMS

Pour the mixture into the mould with the stamps facing upwards, being careful not to trap any amount of air as small bubbles can cause flatness problems and the resulting curing might not be homogeneous. Put the mould on a tray covered with a foil and put it inside the oven. The curing conditions are: 150ºC/15 minutes or 80ºC/3 hours (the longer curing time can make it easier for any bubbles to come to the surface)

4. Unmoulding the PDMS stamps

After the curing time, remove the mould from the oven (with gloves) and let it cool down. To remove it from the mould, cut the edges with a cutter (being careful not to cut the silicon stamp) and pour a drop of ethanol on the edges to facilitate separation. Plastic wedges can be used as assistance so as not to scratch the metal stamps; while also trying not to stretch while separating in order to not break the PDMS replica.

5. Trim the burr from the PDMS replica

The edges of the replicas are slightly burred, which means that they are not flat and therefore do not make good contact with the UV polymer drop; This is corrected by cutting a little with the cutter. To get new PDMS replicas, steps 3,4,5 will be repeated. It

will be necessary to clean the stamps with ethanol. Drying them with compressed air or putting them in the oven for a few minutes to dry them completely. *Note:* It is interesting to get PDMS stamps that are not very thick because in case the thickness is excessive, the curing does not take place adequately: it takes longer time, and it is then difficult to separate it from the sheet. In addition, it is important to try to ensure that the thickness is homogeneous and that bubbles do not appear on the surface (so that an equal curing occurs throughout the Ormostamp® sheet).

*Step 2 - Printing the PDMS stamps in Ormostamp®*

6. Plasma treat the cut polymeric film sheets to improve adhesion

7. Pour Ormostamp® (Microresist.de) on the surface of the foil

The Ormostamp® should be first allowed to warm up to room temperature once it's removed from the refrigerator, to prevent water from entering the flask when opened. We will pour drops of about 70µL (measured with a micropipette) in the centre of the position of each stamp. Get a thin sheet of Ormostamp® onto the polymeric films on which the stamps will be pressed.

8. Placing the PDMS stamps on the Ormostamp® thin sheet

To get a good alignment, you can assist yourself with a template containing gaps that mark the positions of the stamps. It is interesting to place them with the same orientation, for better comparison purposes of the coated film inlays after the injection process (a mark can be made on them to facilitate this process).

9. Ormostamp® curing.

Switch on the UV curing lamp for about 2 minutes (the time will depend on the thickness of the PDMS stamp since a larger thickness requires longer curing time, it is also important that the thickness of the stamps be similar to obtain a homogeneous curing).

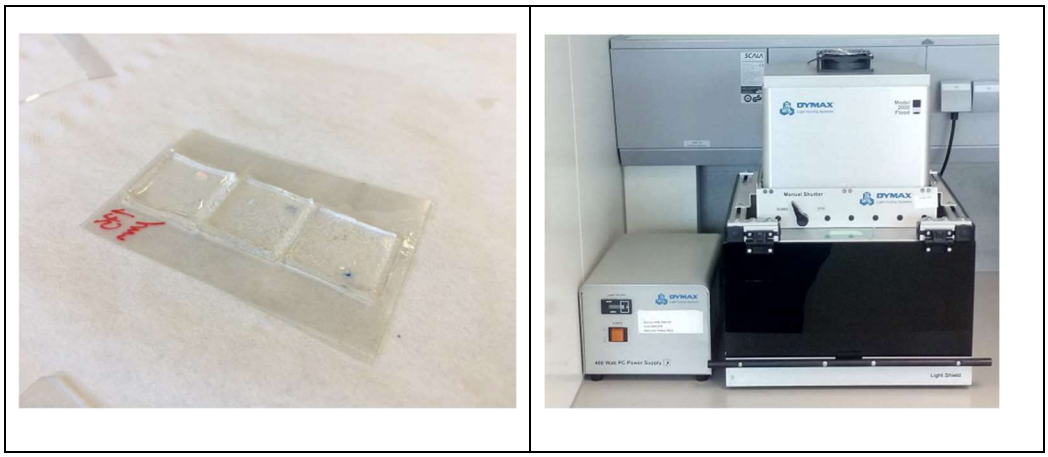


**Figure 4.2. Details of the PDMS replica stampers onto the Ormostamp® coated polymeric film, right before UV curing (left), and detail of the UV-curing equipment used (right).**

Repeat steps 6, 7, 8, 9 to obtain new replicated films. Although it is not strictly necessary, it is recommendable cleaning the PDMS stamps with ethanol and drying them before starting to imprint a new film.

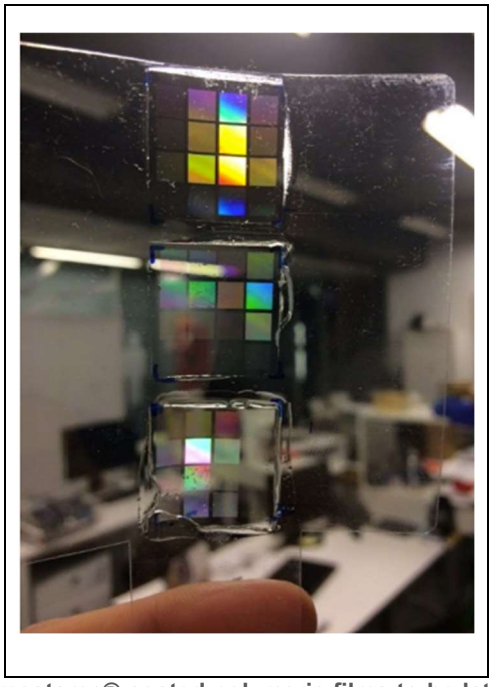

**Figure 4.3. Details of the Ormostamp® coated polymeric films to be later used as polymeric inlays, obtained using the UV-NIL process.**

*Cutting of the sheets in the plotter:*

*1. Cut large pieces with scissors (of sufficient size to obtain several films) from the PET roll. It is necessary that the ends are completely straight so that the ends of the sheet are cut with a guillotine.*

*2. Define in an Inkscape file the shape you want to cut (follow the order in which you draw them)*

*3. Place the sheet lengthwise, matching one of its corners with the upper left corner of the machine frame.*

*You have to set manually (with the controller arrows) the origin of the sheet where you want to define the cut. Fix the sheet with accuracy at the ends so that it does not move.*

*4. Select the file you want to draw, and press enter.*

### 4.1.2 INITIAL INJECTION MOULDING TRIALS – DETERMINATION OF COATED FILM/INJECTED POLYMER COMPATIBILITY AND OVERALL PROCESS STABILITY

*Machine & mould*

For the initial moulding trials, an Engel complete e-motion 200/55 electric injection moulding machine was used (see chapter 2). As mould, a steel mould with a fan-gate type entry of material and a cavity of 70x70mm size with variable thicknesses of 1.25-2.5-4 mm. was used.

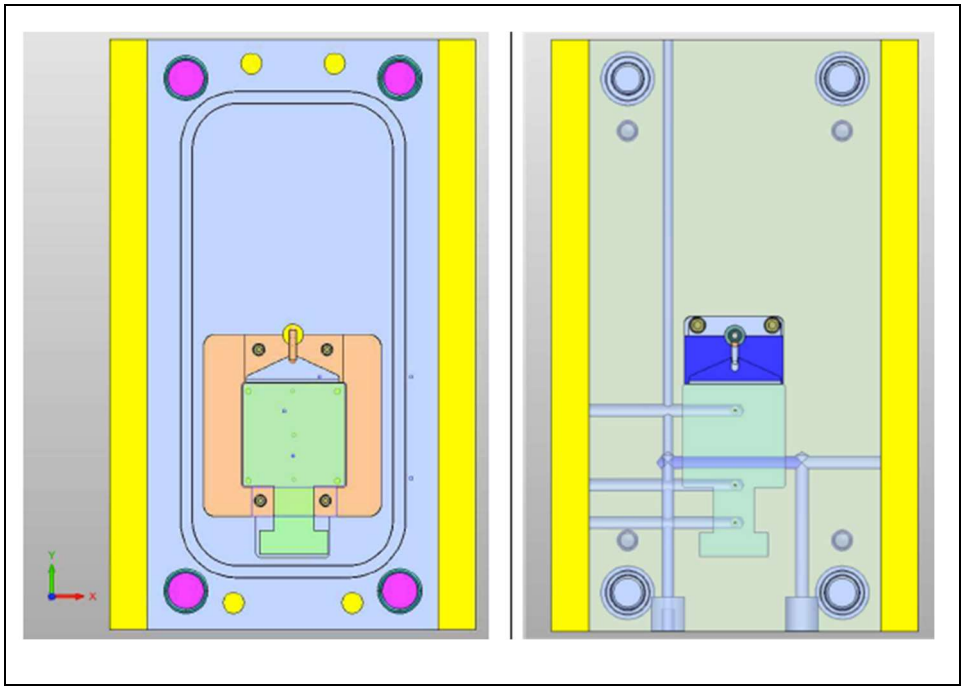

**Figure 4.4. 3D CAD file of the injection moulding used during the initial trials.**

*Film placement inside the injection mould*

Once the films to be used as inlays inside the injection mould have been textured, their placement on one of the vertical sides (machine side) of the injection moulding machine is carried out by means of 2-side high-temperature adhesive thin Kapton® film of 125 to 175 µm thickness (depending on supplier's availability). The textured film is place in a centred position, and it's expected that later during the PhD-realization, additional ways of holding the film into position while the injection moulding takes place will be tested (i.e. special tool inserts for mechanical fixation of the film, electrostatic fixing, etc.).

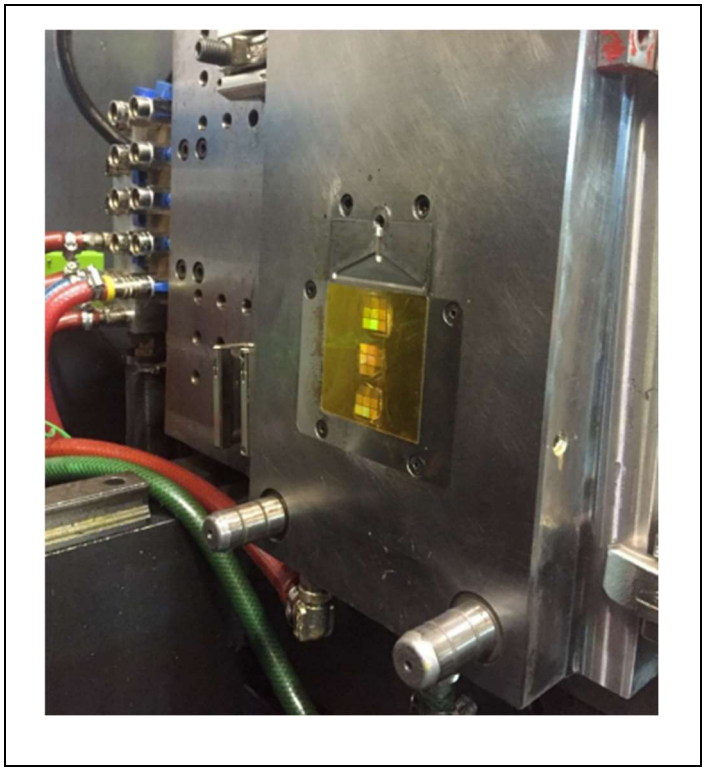

**Figure 4.5. Detail of the film fixation inside the injection mould applied for the initial injection moulding trials.**

*Polymers*

The following materials were used in the experiments.

- Films (used as support for the Ormostamp®)

PET Vivak 50µm thickness

PMMA Plexiglas 8N 125µm thickness

PC Makrolon 250µm thickness

PC Lexan 50 and 500µm thickness

- Injection moulding polymers:

PMMA Plexiglas 8N / TPU Lubrizol D91F65D

*Injection moulding conditions*

A table with the injection moulding process parameters is shown below:

| Parameter | Unit | Polymer 1 | Polymer 2 |
|---|---|---|---|
| Polymer acronym | - | PMMA | TPU |
| Degree | - | Plexiglas 8N | Estane 395A |
| colour | - | Clear | Clear |
| Manufacturer | - | Evonik | Lubrizol |
| Drying time | h | 3 | 2 |
| Drying temperature | ℃ | 95 | 90 |
| Temp. machine nozzle | ℃ | 210 | 190 |
| Temp. Zone 1 plasticizer | ℃ | 240 | 200 |
| Temp. Zone 2 plasticizer | ℃ | 235 | 195 |
| Temp. Zone 3 plasticizer | ℃ | 230 | 190 |
| Temp. Zone yoke plasticizer | ℃ | 40 | 40 |
| Nr. of circuits - fixed side | n | 1 | 1 |
| Fixed side - circuit num. 1 input | ℃ | 70 | 20 |
| Fixed side - circuit num. 1 output | ℃ | 70 | 20 |
| Temp. Moving side circuits | n | 1 | 1 |
| Moving side-circuit num.1 input | ℃ | 70 | 20 |
| Moving side-circuit num.1 output | ℃ | 70 | 20 |
| Closing force | KN | 550 | 550 |
| Injection speed 1 | mm/s | 50 | 50 |
| Post-pressure value 1 | bar | 400 | 600 |
| Post pressure time 1 | bar | 5 | 5 |
| Decompression before loading | mm/s | - | - |
| Decompression after charging | mm/s | 5 | 5 |
| Dosing speed | % | 50 | 50 |
| Switchover point | mm/s | 15 | 15 |
| Dosage level | mm/s | 50 | 50 |
| Royal cushion | mm/s | - | - |
| Hzdraulic pressure limit injection | bar | 1000 | 1000 |
| Inj. pressure peak max. | bar | 440 | 529 |
| Back pressure | bar | 50 | 100 |
| Injection time | s | 0.83 | 0.75 |
| Dosing time | s | 4.25 | - |
| Cooling time | s | 20 | 20 |

**Table 4.1** Injection moulding processing parameters applied during the first moulding trials.

## RESULTS AND DISCUSSION

*Film-positioning*

The film positioning by using double-sided Kapton® adhesive tapes presented some problems, such as partial detachment of the film from the mould surface due to ungluing of the film or also creation of wrinkles on the film (which were therefore copied on the injected parts) due to flatness deviations caused by the non constant film thickness (excess of thickness on places where Kapton® tapes were glued).
In some of the injection rounds, film displacement (sliding over the mould surface onto which it was stuck) was also appreciated due to insufficient adhesive tape effectivity.

*Film-injected material compatibility*

In this initial phase of experiments, the compatibility between injected polymer and nanotextured coated film, understood as lack of adhesion and easy demoulding between both upon mould opening, was investigated. For that, five parts were injected for each of the injected polymer-film pairs. On most of the cases, the Ormostamp® coating was satisfactorily demoulded (no significant adhesion) from the injected parts at least initially while no damage took place on the film surface.
Regarding the films, the only compatible pair was the one formed by PET as base film support material and PMMA as injected polymer, as it showed no adhesion. The other types of polymeric films showed strong adhesion with the injected polymer (PMMA – PMMA, PC – PMMA, PC –TPU), which could most probably be avoided in future testing rounds by coating the whole film's surface with Ormostamp®, leaving no uncoated film surface in contact with the injected polymer. Pictures of the textured films and an injection moulded part in TPU can be seen on Figure 4.6 below.
These problems, together with those concerning the film positioning, were solved on the experiments of the subsequent section (4.2) by manufacturing a custom film holding metallic insert.

## CONCLUSIONS

Overall, the process showed its feasibility for the replication of micro/nanostructures present in Ormostamp® coated polymeric films. Nevertheless, even if the determination of the process performance in terms of replication was not the objective of this subsection, the DR% values achieved were very low (10-15%). This was probably

caused by unwanted injected part-textured film adhesion upon demoulding, undesired local film bending and non-optimised injection moulding process parameters.

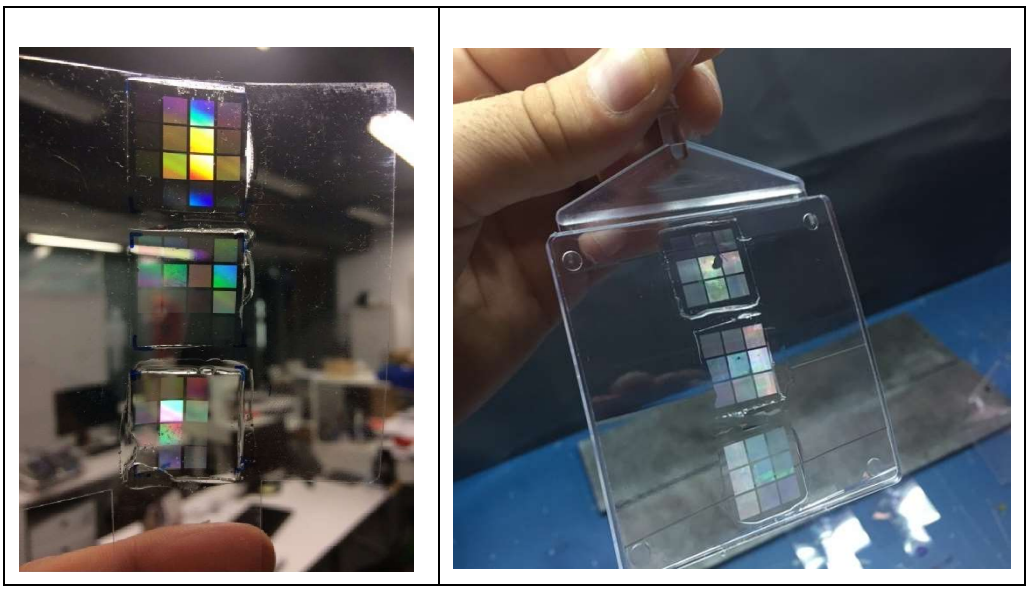

**Figure 4.6. Details of the Ormostamp®-coated PET nanotextured films (left), and a resulting TPU injection moulded part.**

It is of critical importance to hold the textured film inlay robustly and steadily in place during the whole injection moulding cycle. This avoids unnecessary fil m degradation and bending, that lead to insufficient mould filling. It also allows for the avoidance of unwanted adhesion between injected part and coated film when exposing only the coated surface of the film towards the mould cavity (which can be done due to the observed correct compatibility between Ormostamp® and injected part when using PMMA as injected polymer). All these issues were addressed in the following section (3.2) by designing a custom film holding steel tool insert.

## 4.2 DOE FOR DETERMINATION OF MAIN PROCESS PARAMETERS AFFECTING REPLICATION DEGREE DR%

### MATERIALS AND METHODS

*Micro/Nanotextured Films and polymers*

For this experiment, newly manufactured films with two level hierarchical micro/nanostructures were provided by the CNM and ICN2 as part of the tooling used within the PLASTFUN project. They were manufactured using UV-assisted NIL methods to replicate custom designed and manufactured silicon inserts developed by the CNM. Details of the manufacturing process for these films can be seen on section 3.4. Pictures of the existing hierarchical two level microtextures present on the originally developed Si-stamps and resulting textured films (after replication) can be seen in Figs. 4.7 and 4.8 below.

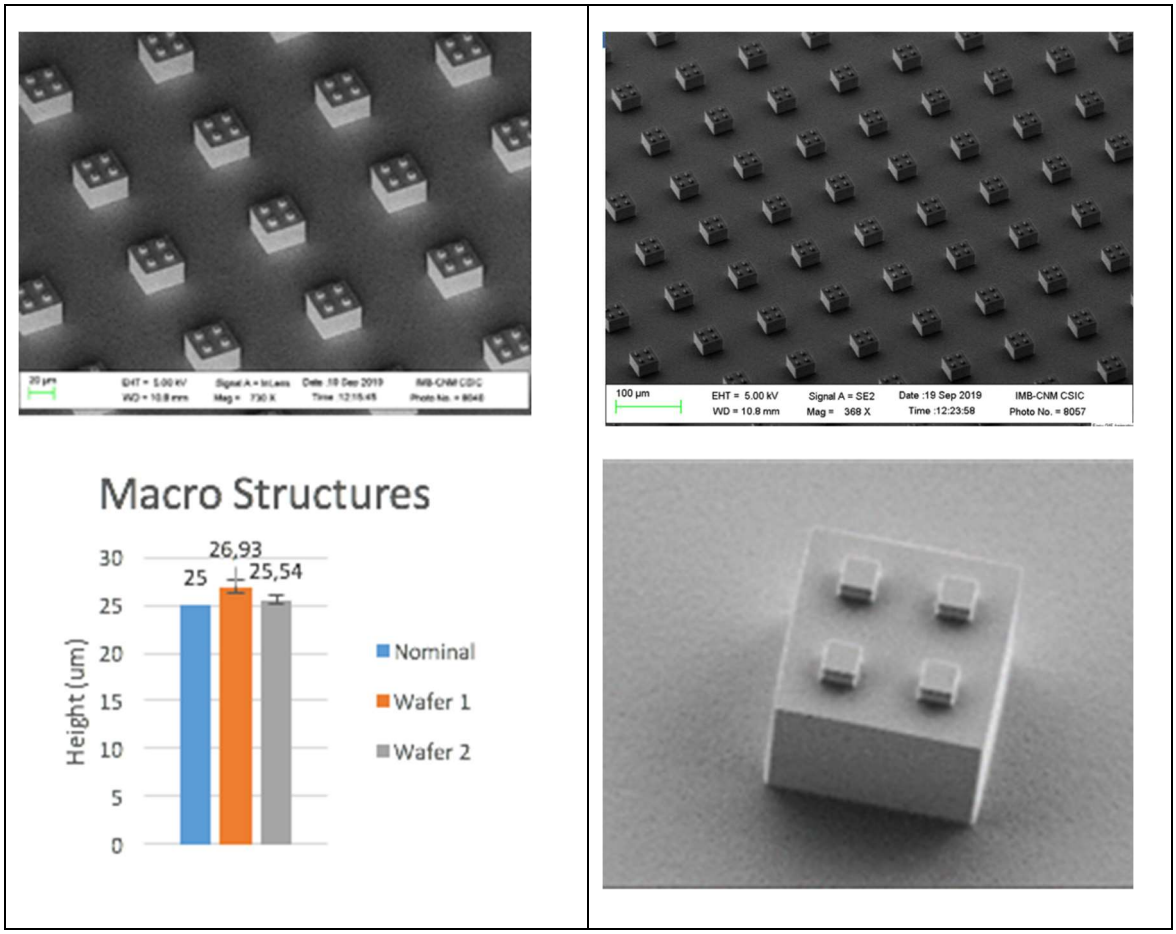


**Figure 4.7. Details of the 2-level hierarchical microstructures present on the Si-stamps developed by ICN2 and CNM, that were later replicated onto intermediate PDMS stampers to manufacture the final coated polymeric inlays.**

These films were then cut to shape so as to be fit into the specifically designed tool insert for their robust holding during the injection phase (see details in next section *Tool insert for robust film placement*). Pictures of the replicated films before being cut, and of the negative 2-level hierarchical microstructures can be seen on figure 4.8.


**Figure 4.8. Details of the coated and textured film as delivered by ICN2-CNM (left), and 2-level hierarchical negative microstructures present in the replicated Ormostamp® coated films (right). Pictures courtesy of CNM.**

In this case, PMMA Plexiglas 8N was chosen as injected material, and an Ormostamp® coated PET film (coated on its whole surface) was chosen as mould inlay, to avoid sticking of film-injected material.

*Tool insert for robust film placement.*

Also, in order to improve the overall film holding and mechanical stability during the process, a custom designed steel insert was manufactured at EURECAT's facilities. This steel insert allowed for a robust and permanent fixing of the coated film inlays during the whole injection moulding process, avoiding unwanted film sliding or bending.

This insert allowed for the placement of films in between its two component parts (insert frame and pressing pad) of up to 500µm thickness and displayed a nanotextured surface of 62x23 mm (with an increased thickness of 0,71 mm vs the rest of the resulting part) exposed towards the inside of the cavity, leaving no uncoated film exposed to it. The injection mould and machine used were the same ones as in the previous subsections.

Pictures of the custom-designed tool insert and its placement on the injection mould can be seen on the figure 4.9 below.

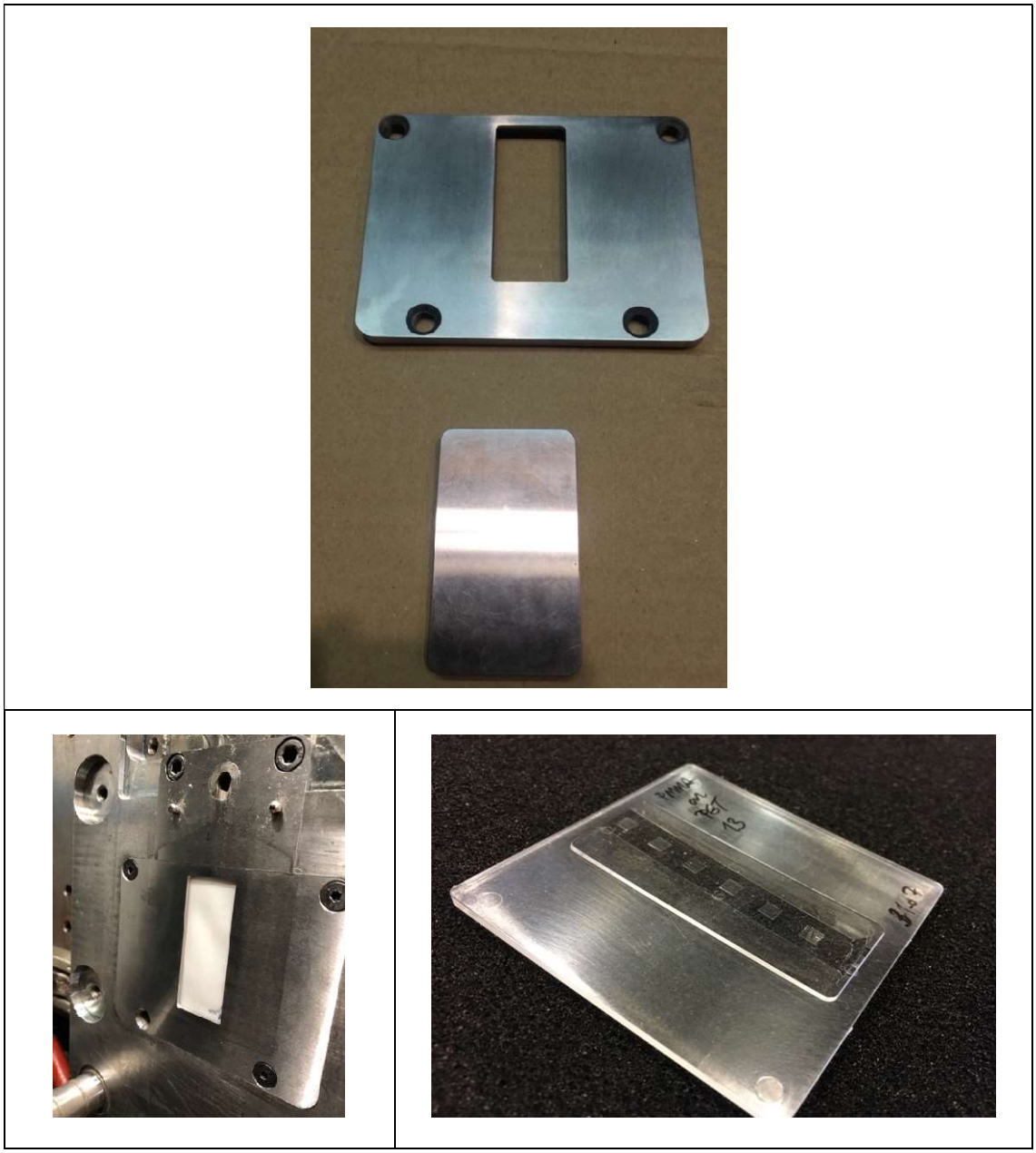

**Figure 4.9. Details of the custom designed tool insert for textured film inlay placement during the injection moulding process (above-centre), and actual placement of the steel insert in the injection mould (below-left). Lower-Right image: final part resulting after injection.**

*DOE*

A $2^3$ design of experiments *DOE* using the Taguchi method, choosing melt temperature, injection speed and holding pressure as main parameters, was carried out in order to determine their relative influence on the DR%, chosen as the process response.

The resulting matrix of experiments can be seen below:

| n | exp. Order | Tm | Inj.V | P |
|---|---|---|---|---|
| 1 | 1 | 240 | 50 | 600 |
| 2 | 2 | 240 | 50 | 800 |
| 3 | 3 | 240 | 100 | 600 |
| 4 | 4 | 240 | 100 | 800 |
| 5 | 5 | 260 | 50 | 600 |
| 6 | 6 | 260 | 50 | 800 |
| 7 | 7 | 260 | 100 | 600 |
| 8 | 8 | 260 | 100 | 800 |

**Table 4.2.** Injection moulding DOE matrix

The DOE results were later analysed using the software MINITAB by registering the DR%'s achieved, thanks to the measurements taken using CLSM images.

## RESULTS AND DISCUSSION

### *Replication and DOE*

Five parts were injected and characterized per each of the experiments. The DR%'s achieved oscillated between 41% and 78%, as it can be seen on table 4.3 below:

| n | exp. Order | Tm | Inj. V | P | DR% |
|---|---|---|---|---|---|
| 1 | 1 | 240 | 50 | 600 | 54,56 |
| 2 | 2 | 240 | 50 | 800 | 46,63 |
| 3 | 3 | 240 | 100 | 600 | 54,23 |
| 4 | 4 | 240 | 100 | 800 | 41,83 |
| 5 | 5 | 260 | 50 | 600 | 53,75 |
| 6 | 6 | 260 | 50 | 800 | 77,93 |
| 7 | 7 | 260 | 100 | 600 | 65,08 |
| 8 | 8 | 260 | 100 | 800 | 72,25 |

**Table 4.3.** DR% results of the Injection moulding DOE.

The features present on the microtextured surfaces obtained showed consistent geometrical uniformity, clearly displaying both hierarchical levels, across both x and y directions of the replicated surface, as it can be seen in Figure 4.10 below.

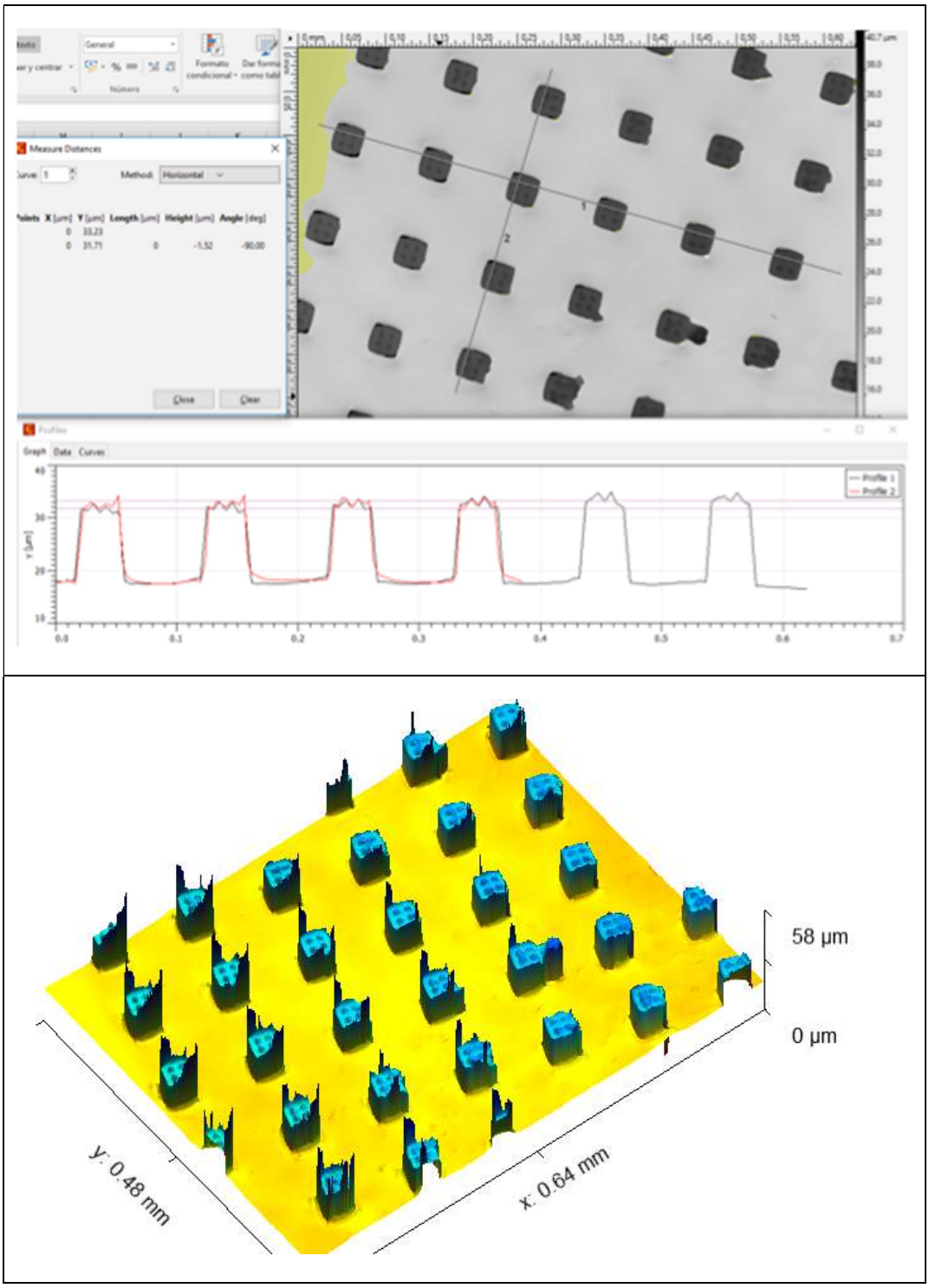


**Figure 4.10. CLSM XY profiles extracted from an injected PMMA sample (corresponding to the DOE exp. number 5 – above image), and corresponding reconstructed 3D image of the section analysed on this injected sample (below).**

In some of the cases, it was observed that the lateral walls replicated microfeatures showed some deviations from verticality, therefore displaying a truncated pyramid, as it can be observed on figure 4.11 (corresponding to a sample from the DOE exp. number 2). This could be attributed to feature-stretching caused by insufficient holding time

(under pressure), cooling time or a combination of both (Note: holding pressure time and cooling time were set at 5” and 20” for all the experiments, respectively).

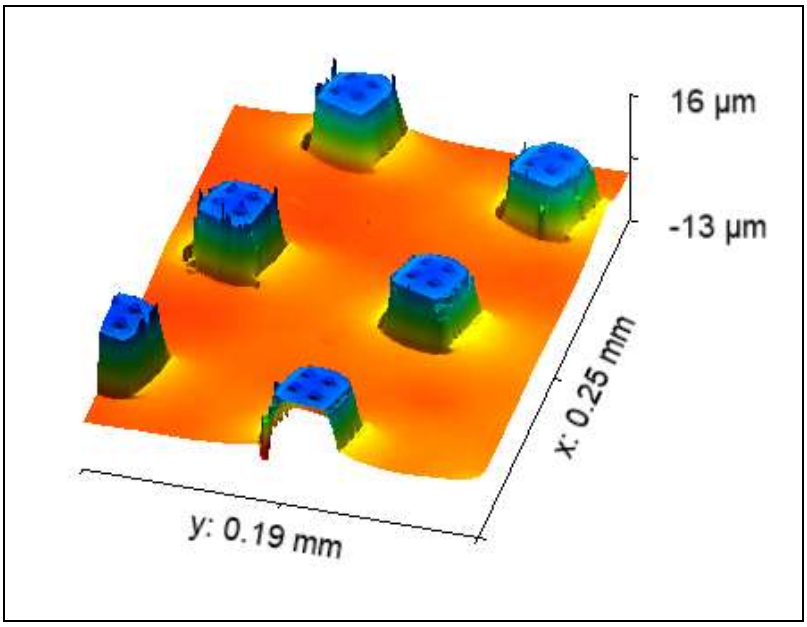


**Figure 4.11. CLSM 3D constructed image of a PMMA sample showing the truncated pyramid shape of the microfeatures.**

Only a limited number of parts (5) could be injected with each of the textured Ormostamp®-coated films, as it can be seen on figure 4.12 below.

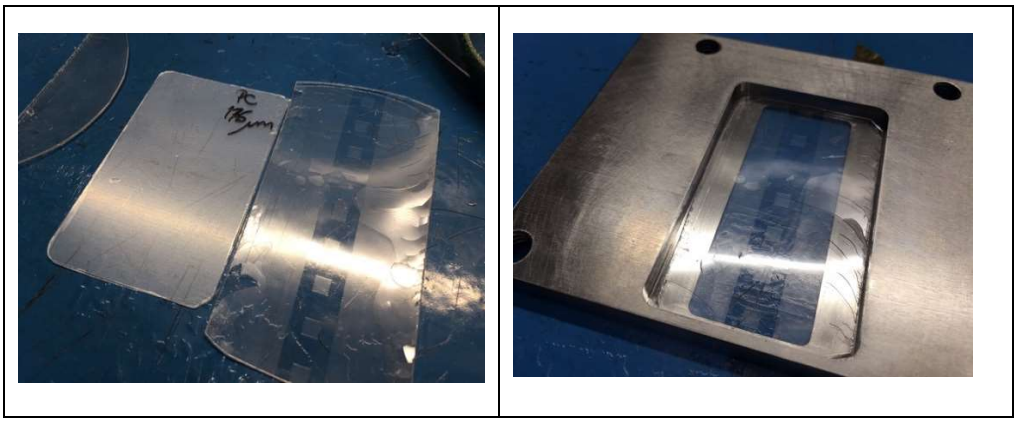

**Figure 4.12. Pictures of the cracked polymeric film inlay.**

This cracking was most probably caused by the stiffness mismatch between the Ormostamp® coating and the base polymeric film. Even though both layers were set at 50µm thickness in order to avoid such mismatch caused by differences in thicknesses, the underlaying PET film was still too flexible compared to the Ormostamp® coating.

Concerning the specific DOE results, the main influencing process parameters on the DR% achieved were the melt temperature, followed by the interaction between melt temperature and holding pressure, and the interaction between injection speed (Vinj) and holding pressure, as it can be seen on the Pareto and interaction plots on Figure 4.13 below.

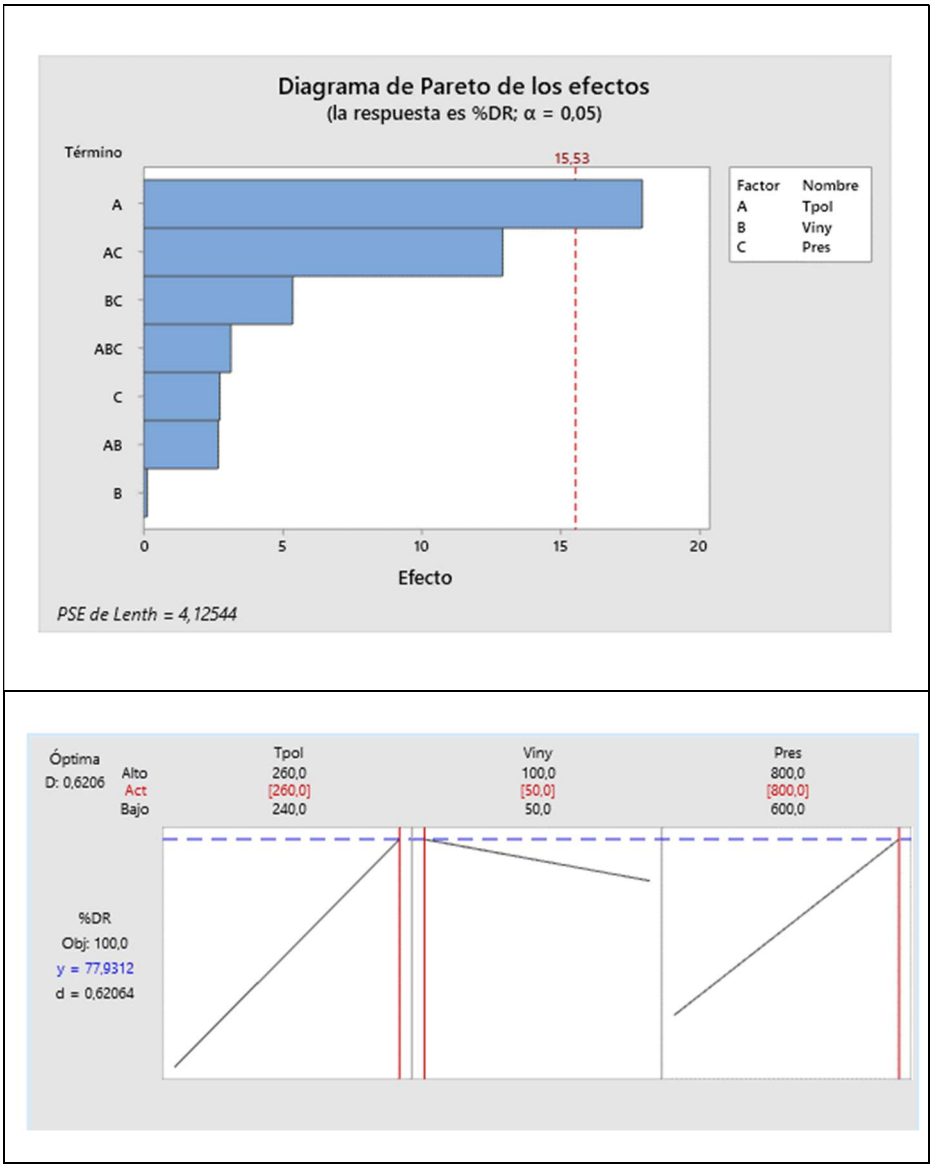


**Figure 4.13. Pareto diagram (above) and effect interaction (below) plots of the DOE carried out.**

The only critical factor of the three considered was the melt temperature, as expected, and its influence on the overall process response (DR%) was also the highest, followed by that of the holding pressure, as expected.

## CONCLUSIONS

The process to replicate 2-level hierarchical microstructures on injection moulded PMMA parts using as Ormostamp® coated polymeric inlays as templates has been demonstrated. As expected, the process parameter of all the chosen ones for the experiment set-up that showed the highest influence was the melt temperature. It constituted a critical factor as it exceeded the critical parameter level. The second influencing parameter on the overall DR% result was the interaction between the melt temperature and the holding pressure, with approximately 50% higher influence in the process result than the third influencing parameter (interaction between injection speed and holding pressure).The DR%'s reached at standard injection moulding conditions for the injected materials showed the potential improvements achieved on the replication vs the technology using laser textured inserts, even though a proper comparison should be established using the same exact micro/nanotexture geometries and injected polymers.In order to increase the number of parts replicated per film and to improve the overall replication results, it is required to pay specific attention to the mechanical and adhesive characteristics of the base polymeric film and coating, and to optimize the injection moulding parameters (with focus on holding pressure and cooling times). This was addressed in the following chapters.

## 4.3 REPLICATION OF THREE-LEVEL HIERARCHICAL MICRO/ NANOSTRUCTURES ON TRANSPARENT POLYMERS OF INTEREST (PC, PMMA) USING POLYMERIC INLAYS.

### MATERIALS AND METHODS

In the previous experiments, only a limited number of parts could be injected with each of the polymeric tool inserts before they degraded, due to extensive cracking and excessive adhesion between injected polymer and coated film.

In this round of experiments, we tried to solve these problems, while extending the compatible (meaning non adhesive upon demoulding) Ormostamp® - injected polymer range to other transparent thermoplastics of interest such as PC, of high relevance in the automotive, consumer electronics and optics industries. This was carried out by applying to main modifications to the process:

- The use of stiffer PC base films to support the Ormostamp® coating.
- The use of anti-stick fluorosilane coatings (Trichloro (1H,1H,2H,2H-perfluorooctylsilane (TPFS)) of few μm thickness (0.2-0.5μm) on top of the Ormostamp® coating.

On this experiment, three level hierarchically micro/nanostructured Ormostamp® coated films were used. They were supplied with an anti-stick fluorosilane coating by CNM, as part of the tooling used during the project PLASTFUN. The coated films were manufactured with a base PC polymeric film of 50μm, trying to delay the onset of coating cracking as per its higher stiffness vs PET films of the same thickness.

A picture of the micro/nanofeatures present in the original Si-stamp and its transverse section can be seen on the image below (Figure 4.14).

The same steel insert to hold the films in place, mould, injection moulding machine and CLSM characterization as in the previous sections were used. Some SEM images were also taken for better exploration of the third hierarchical level, not visible with the CLSM images due to its reduced size. In terms of the injection moulding processing parameters applied, the following ones were used (the rest of parameters were the same ones as those applied in 3.1):

| | Tm (ºC) | Vinj (mm/s) | P (bar) | t holding P (s) |
|---|---|---|---|---|
| PC | 310 | 120 | 600 | 12" |
| PMMA | 260 | 100 | 600 | 5" |

**Table 4.4.** Summary of the injection moulding conditions applied in the experiment.

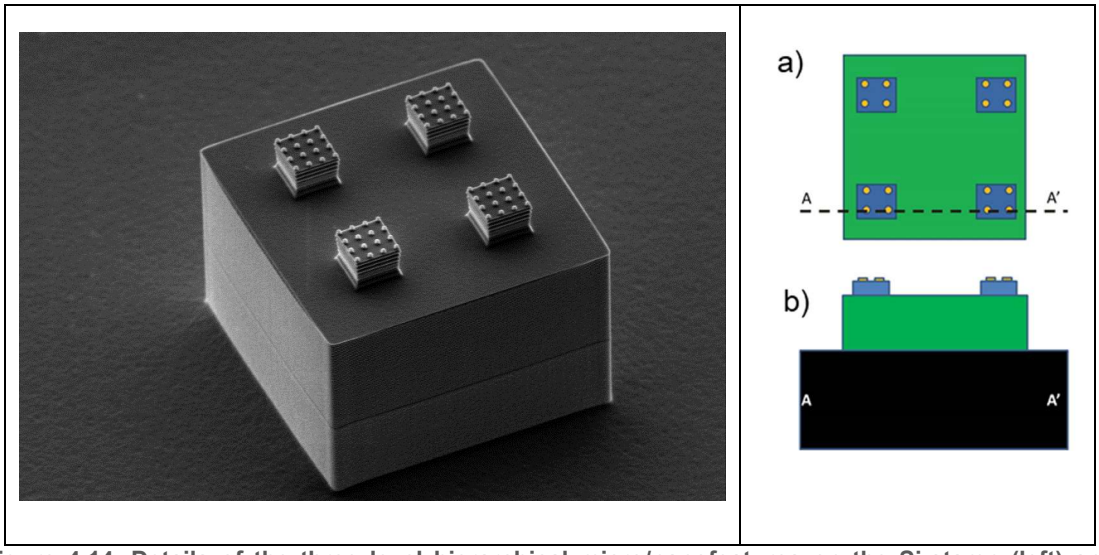


**Figure 4.14. Details of the three level hierarchical micro/nanofeatures on the Si-stamp (left) and transverse section of it (right). Pictures courtesy of CNM- PLASTFUN project.**

A scheme of the different hierarchical levels of the existing features, together with their geometrical dimensions, can be seen in figure 4.15. (Note: The Ormostamp® coated films contain the negative polarity features, i.e., the “holes” with three hierarchical levels of structure).

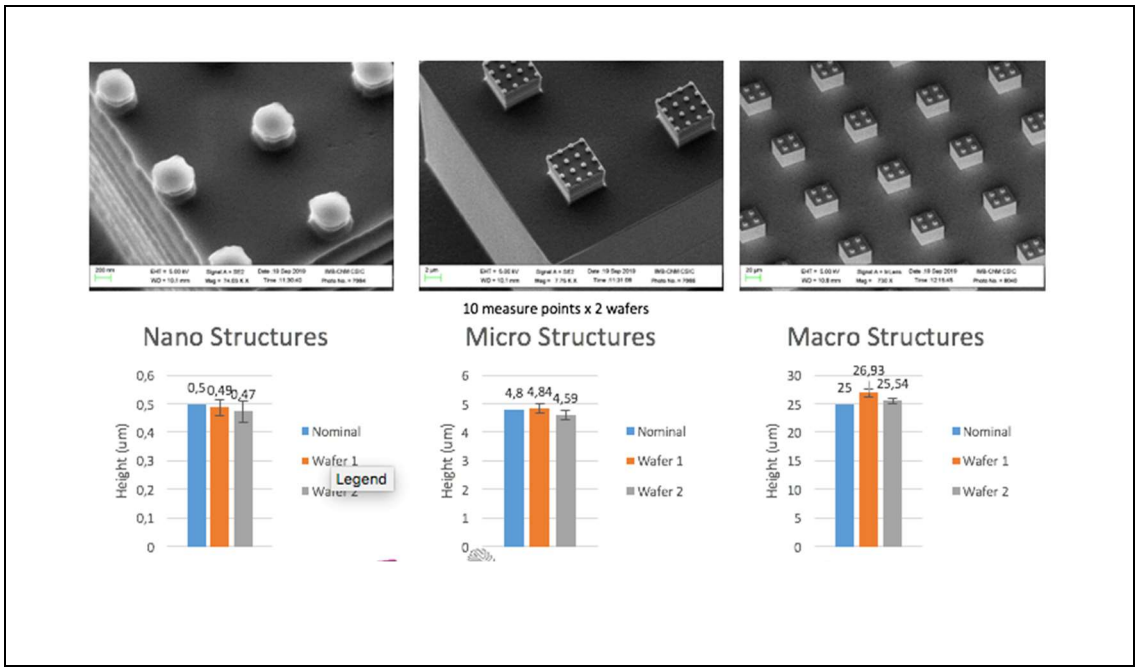


**Figure 4.15. Details of the three hierarchical levels of the macro-micro-nano features present in the Si-stamp developed for the project. A high level of dimensional accuracy and uniformity can be observed (Image courtesy: CNM – project PLASTFUN)**

The following injection moulding polymers were used:

PMMA Plexiglas 8N

PC Makrolon 2207

## RESULTS AND DISCUSSION

Up to 6 samples were injected when the PC injected polymer was used, and up to 10 in the case of the PMMA. From the sample nr. 7 and 11, respectively, the films started to crack and therefore some delamination took place upon demoulding. This caused insufficient uniformity on the textured zone of the injected parts, but nevertheless the film areas still not damaged yielded adequate replications.

In the case of PC, the average DR% (based on measurements at three distinct points of all the 6 samples injected) reached approximately 70%. The samples injected displayed an adequate verticality and an overall uniformity of replication of the first two levels of hierarchy. A slightly lower replication of the third level (better appreciated in the SEM images) could also be observed. CLSM profiles, 3D reconstructions and a SEM image of a feature on the PC sample upon demoulding can be seen on Figure 4.16.

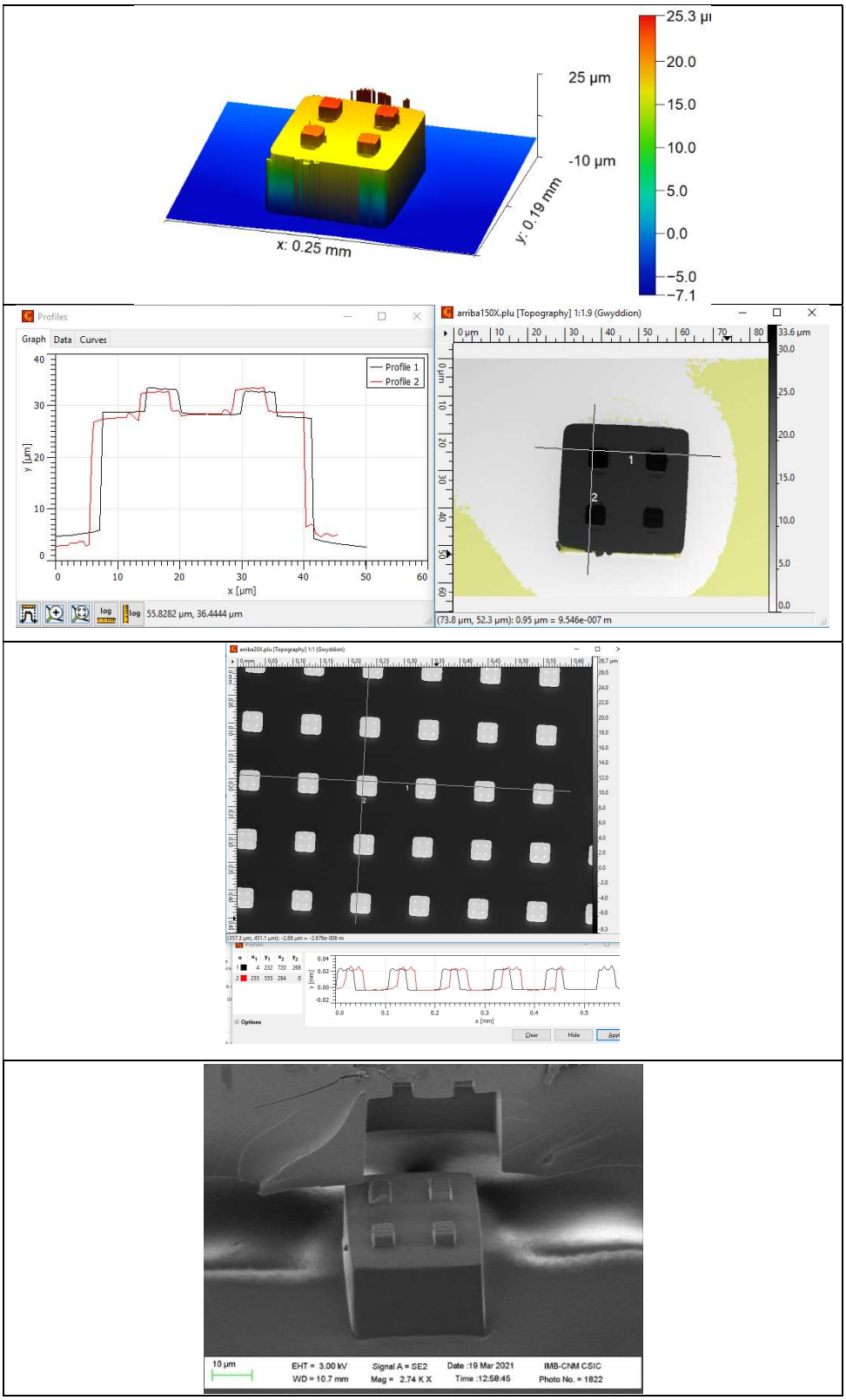


**Figure 4.16. 3D reconstruction from the CLSM image of one of the PC injected samples (above), showing extracted X and Y profiles of the observed feature and of a plurality of features across a larger area (2nd image below top one). SEM image of a replicated PC feature next to a small fragment of film inlay (below).**

For the PMMA samples, only an average DR% of 35% was reached, and the micro/nanofeatures present on the surface of the samples injected showed a truncated pyramid shape. Probably caused during the demoulding phase due to an insufficient cooling time. The first two levels of the hierarchical micro/nanotextures could be clearly observed, while the third level was rarely observed on the injected samples.

CLSM profiles, 3D reconstructions and a SEM image of a feature on one of the PMMA injected samples can be seen on Figure 4.17.

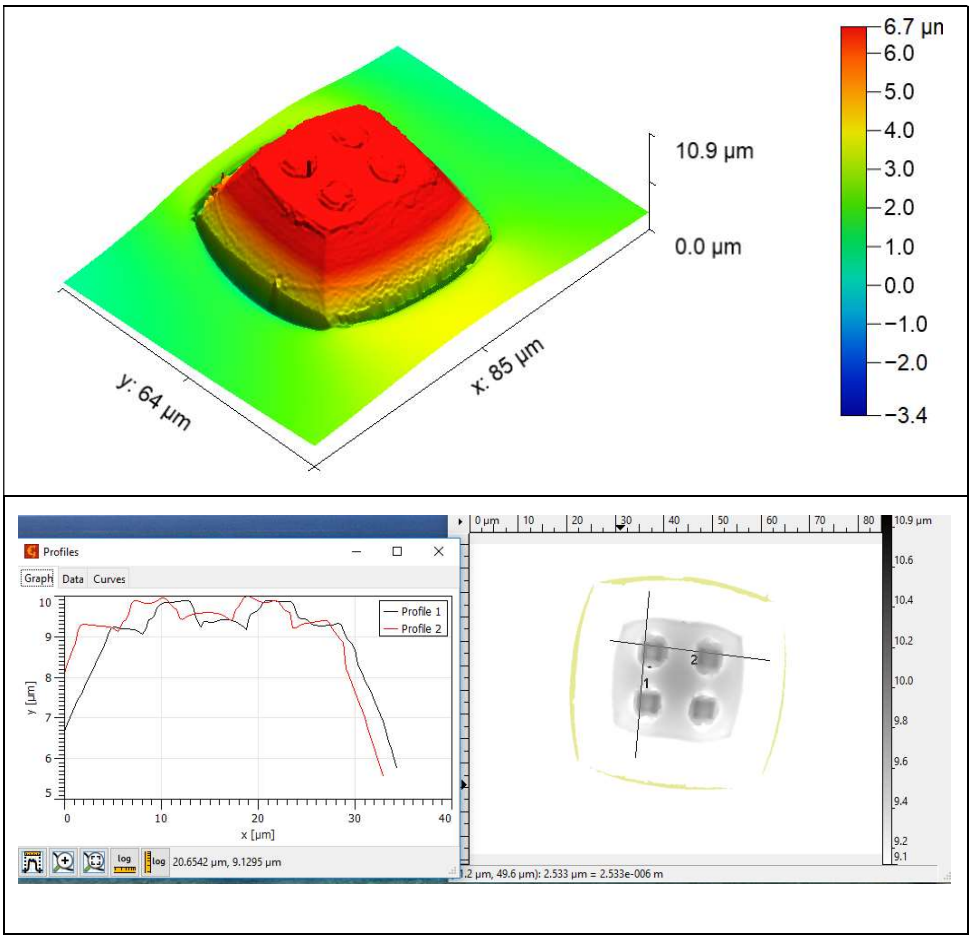

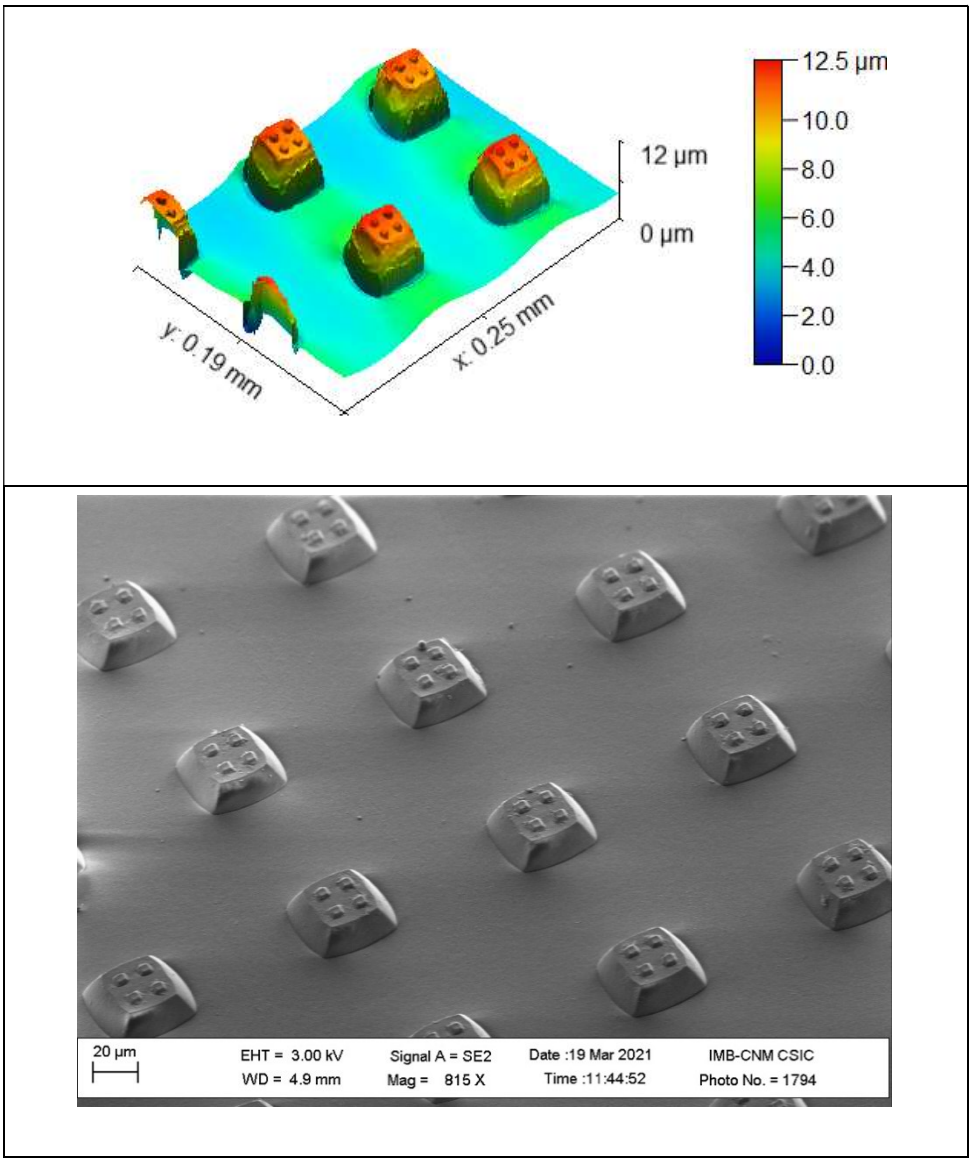


**Figure 4.17. 3D reconstruction from the CLSM image of one of the PMMA injected samples (above), showing extracted X and Y profiles of the observed feature and of a plurality of features across a larger area (2nd image below upper one). SEM image of a replicated PC feature next to a small fragment of film inlay (below).**

## CONCLUSIONS

The feasibility of the process to replicate 3-level hierarchical micro/nanotextures on PC and PMMA was proven with these experiments. While the number of parts injected per film was not much of an improvement vs section 3.2, at least the range of injectable polymers using these method and materials was extended to polycarbonate, mainly thanks to the antistick coatings.

The results obtained for the PC polymer were quite satisfactory, and they could potentially still be improved by fine-tuning the processing conditions and most probably by enhancing the coating-film adhesion.

The results obtained for the PMMA injected samples still show a significant deformation of the surface textures on the injected samples when compared to those present on the film template. They were most probably caused by feature stretching taking place during the demoulding stage, further enhanced by insufficient holding and/or cooling time.

The film handling and cracking improved slightly, although some coating-base film delamination issues still remain to be solved as per the failure modes observed in the polymeric inlays.

## 4.4 Finite Element Modelling of the filling process during the injection moulding of two-level hierarchical microtextures practiced on to Ormostamp® coated PET films

### Materials and methods

The main objective of this section was to set up a method to simulate the filling of micro/nanocavities by the injected molten polymer. While there are many well know softwares for the simulation of phenomena such as the mould filling by a molten polymer at the macroscale, not many of them deal with such a problem at the micro/nanoscale or when they do only a limited part of the whole part geometry is evaluated [2,3]. The geometric scale differences (macro to nano) are so great that a single functional meshing is not able to simulate the filling of both cavities (macro and micro/nano) at once. Therefore, in order to develop a model able to solve this problem, we explored the combination of two different finite element simulation softwares available at EURECAT: MOLDEX3D and Ansys Fluent. Initially, the filling of the part with squared geometry (70x70x2.6 mm – see section 2) was simulated using the MOLDEX3D software, only using the macrometric dimensions of the part (without micro/nanocavities) and a polyhedral self-adjusting meshing of average size of 0.6mm. The material chosen for the simulation was PMMA Plexiglas 8N, and its rheological properties were obtained from the MOLDEX3D material database. Initially, the mould material was set to regular tool steel, also present in the MOLDEX3D database.Once this step was completed, the same simulation was performed using the ANSYS Fluent software to make sure that the same results as when using MOLDEX3D were achieved (by comparing the final time need for the complete mould filling used by both softwares).Then, for the start of the multiscale modelling, an approach relying of the construction of part submodels was followed [4, 5]. For this, three different 3D geometries of the part were selected, with ever increasing level of geometric detail from the macro to the micro level. A single 2-level hierarchical microtexture (see section 3.2) was included on the centre of the micro-level geometry. Also, the output results from each submodel were transferred as inputs to the subsequent submodel, being the results of a submodel transformed into the inputs for the next smaller submodel. This part of the simulation was completed using the ANSYS Fluent software.

A 3D drawing showing a scheme of the sequence followed can be seen on Figure 4.18 below.

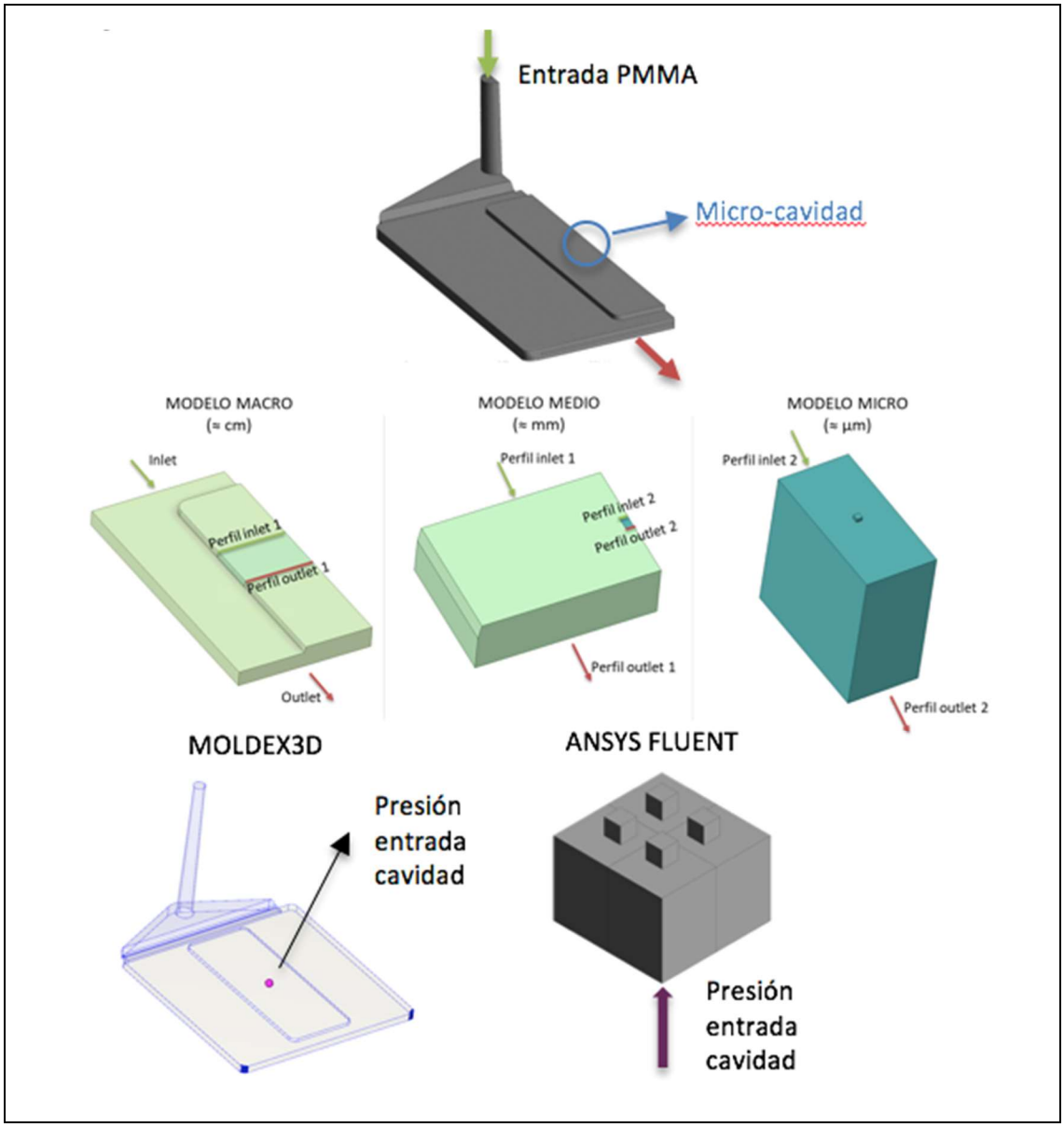


**Figure 4.18. 3D drawings showing the three submodel geometries (macro-meso-micro) simulated, and the final two level hierarchical microstructure to be filled during the injection moulding.**

The meshing chosen for each of the three macro-meso-micro scale models can be seen in Figure 4.19 below.

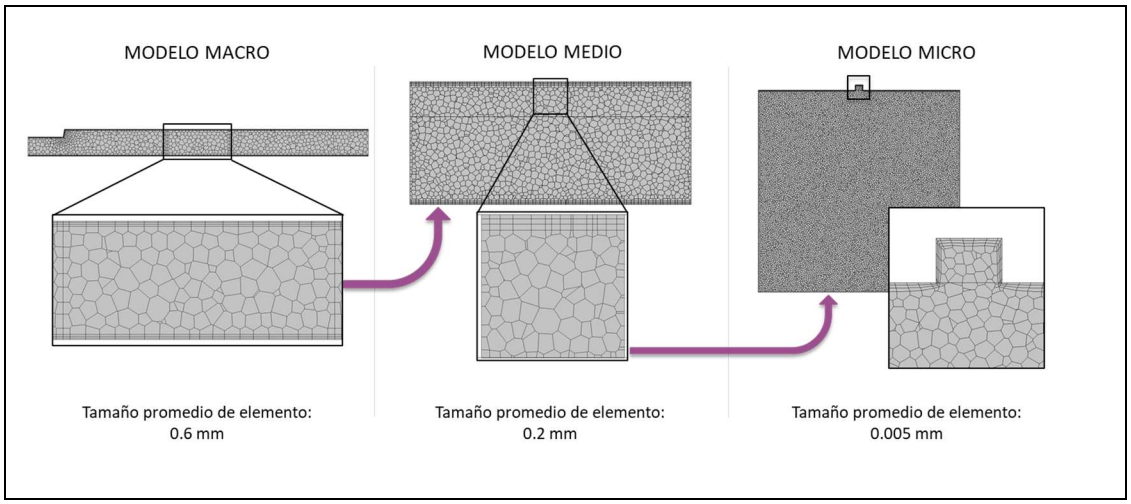


**Figure 4.19. Details of the different mesh sizes used at the three different macro-meso-microscales in the simulation.**

At this point, Ormostamp® was already selected as the mould material and symmetric half-geometries were used for the simulation in order to reduce the computing time.

At the centre of the macroscale part on its textured zone, a virtual sensor point, which is a built-in MOLDEX3D feature that allows to register the time-evolving values of several parameters such as P, T, shear stress…etc., was placed at the exact place on which the microstructure was located so that the pressure with which the polymer front arrived was registered.

Once the three steps of the multiscale simulation adequately ran, a virtual $2^3$ *DOE* was performed, choosing the melt temperature mould temperature and injection speed as factors, and the multiscale simulations were run at those upper and lower levels of the chosen parameters. The levels chosen for the specified factors can be seen on the table below:

| | Lower | Upper |
|---|---|---|
| Tp (℃) | 240 | 260 |
| Tm | 70 | 260 |
| Vinj (m/s) | 0,5 | 1 |

**Table 4.5.** Levels chosen for the parameters of the $2^3$ DOE.

Then, the filling results expressed as the DR% were obtained, and they were compared to the results of the real experiments. Finally, a simulation of microcavity filling using the two levels of pressure obtained from the virtual sensor point was carried out, to elucidate the effects of pressure on the filling of the microcavity.

*Initial Simulations*

The initial macroscale simulations run satisfactorily, achieving almost identical final filling times (0,29 s for ANSYS Fluent vs. 0,30 s for MOLDEX3D). Therefore, the use of ANSYS Fluent for the subsequent simulations was validated.

A detail of the final stage of both macroscale simulations can be seen on Figure 4.6 below.

| ANSYS Fluent | MOLDEX3D |
|---|---|
| 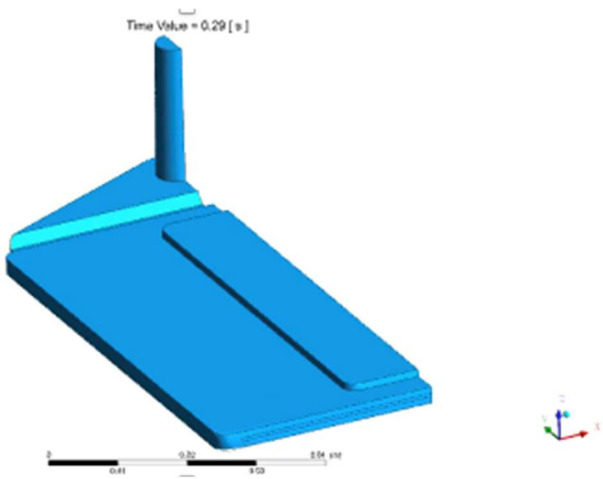 | 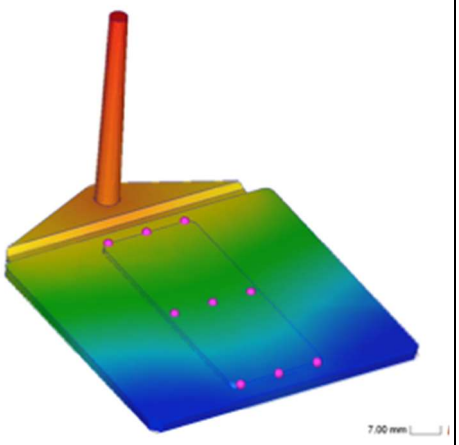 |

**Figure 4.20. 3D images of the initial macroscale simulations run to validate the use of ANSYS Fluent to run the rest of the multiscale simulations. The virtual sensors placed on multiple points of the geometry can be seen on the MOLDEX3D simulation (right).**

*DOE*

The results of the DOE showed the mould temperature as a critical parameter with the highest influence of the filling of the microstructures. The second influence parameter was marked by the interaction between mould temperature and injection speed, and the third was the injection speed.

While these results are not completely consistent with the ones shown on the DOE of section 3, they still highlight the temperature difference between melt and mould temperature as the highest influencing factor affecting the microcavity filling.

The differences observed between these results and those of section 3 can be attributed to the different factors considered for both experiments, and to the fact that mould temperature is set as a constant parameter during the simulation, while its value evolves, quickly reaching the incoming melt temperature in the real experiments [29].

In any case, the effect of increased DR% results when the temperature difference between mould and in coming melt material is reduced, which is the specific purpose sought when using a polymeric coated film inlay as a template for replication inside the mould, remains clear.

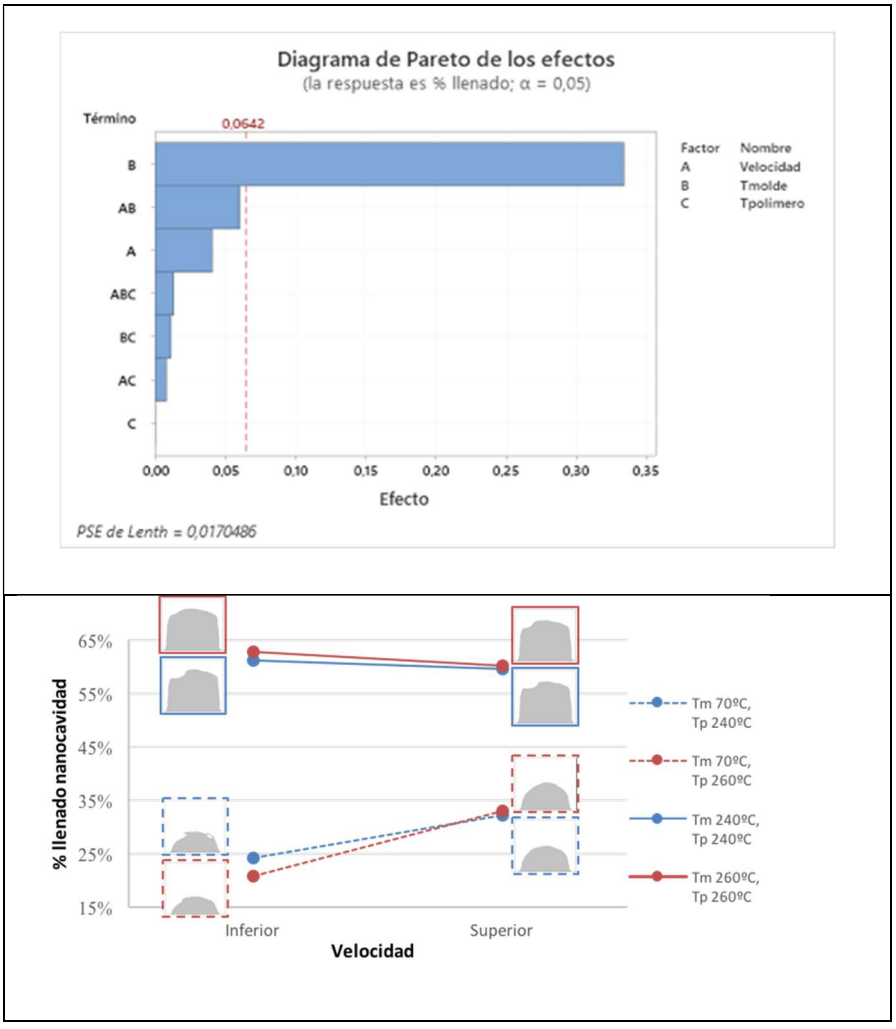


**Figure 4.21. Results of the DOE performed (above) and effect on the filling of microcavities observed at both levels of the selected parameters (below).**

*Multiscale modelling at two pressure levels*

Once the multiscale models were set up and could be properly run, the melt front pressure values were extracted from the virtual sensor point placed at the centre of the microtextured zone by running a simulation of the macroscopic part in MOLDEX3D and registering the evolution of the parameter along the whole simulation time.

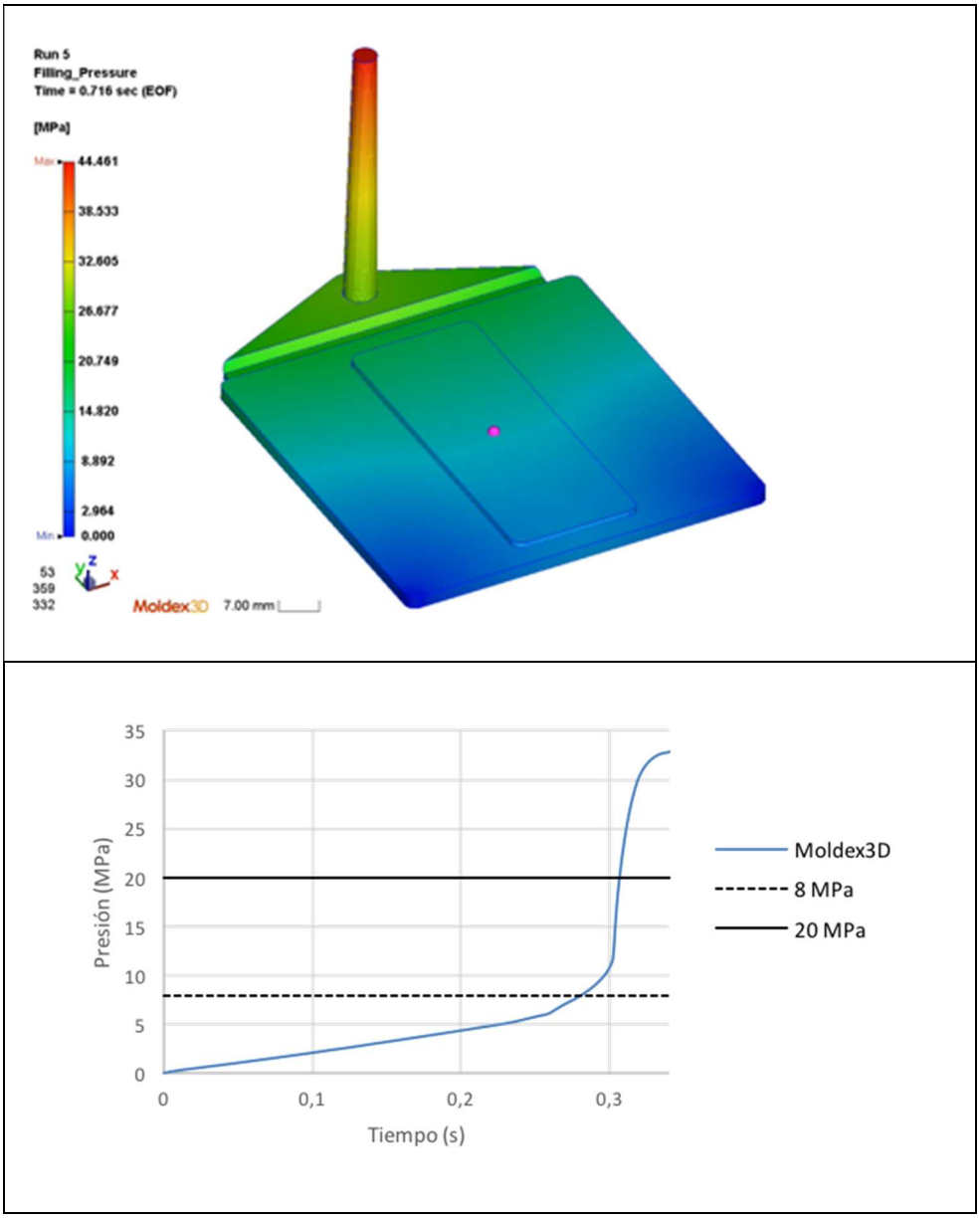


**Figure 4.22. Placement of the virtual sensor point in MOLDEX3D (above) and evolution of the pressure levels observed.**

The evolution of the pressure values, as registered by the virtual sensor showed an abrupt change, especially towards the end of the MOLDEX3D simulation. For this reason, it was decided to run the full multiscale simulation by choosing two discrete levels

(8 and 20 MPa) of the incoming melt front pressure and check the microfeature fillings in a qualitative way.

Then, a final filling simulation of the microscale geometry using the ANSYS Fluent was run, again by using half model for symmetry reasons. The filling of the microfeature was then qualitatively checked by evaluating the final microfeature 3D geometries at the end of the simulations, and also by comparing the volume fraction of PMMA within the mould cavity, as it can be seen in Figure 4.9.

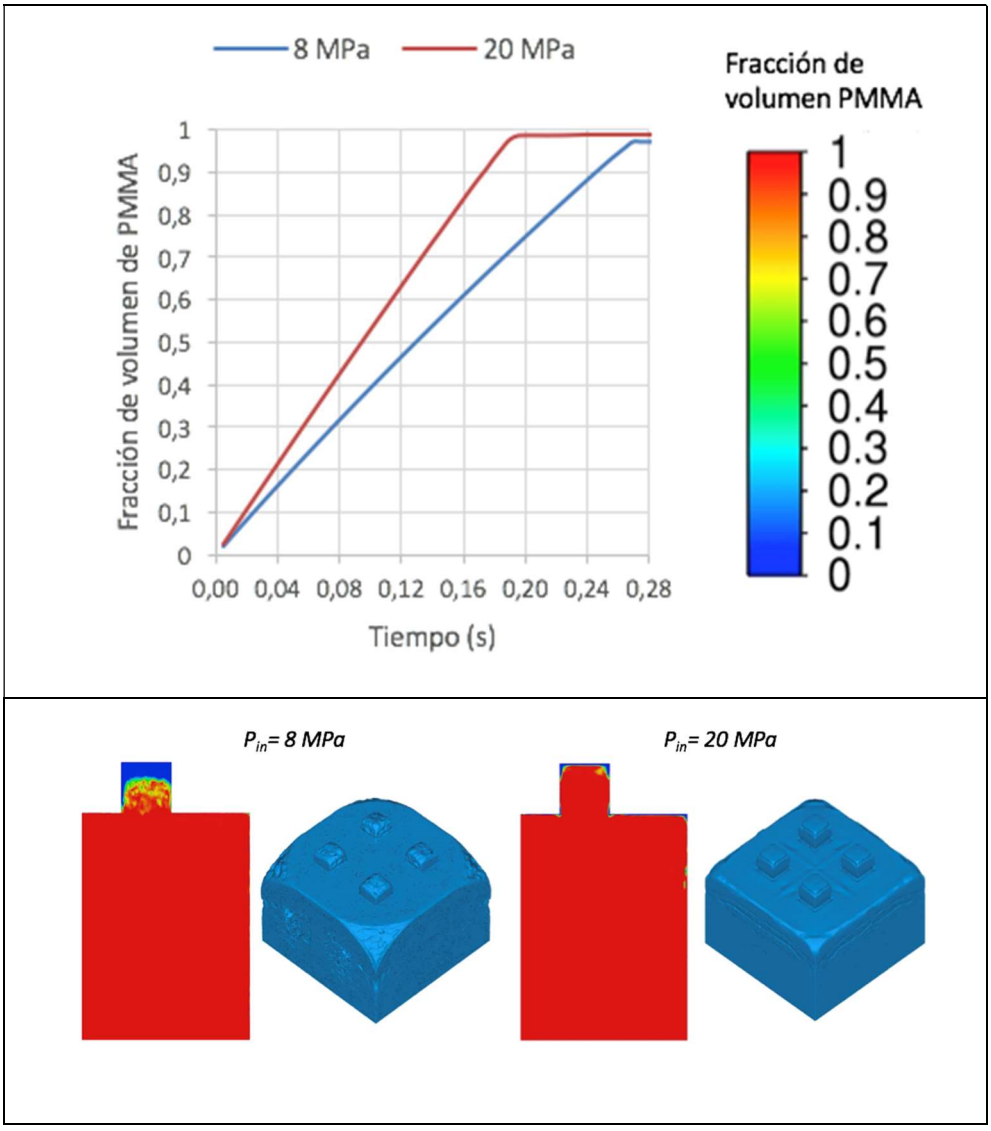


**Figure 4.23. Evolution of the mould filling (microfeature) obtained from the ANSYS Fluent simulations by monitoring the volume fraction of PMMA vs Air (above) and qualitative comparison of the results obtained.**

As observed in Figure 4.22, higher pressure levels achieve higher replication of the microfeatures, when other factors are kept constant as expected. Also, it can be observed that the final mould filling ratio was achieved at a slightly earlier time (0,08s) for the higher-pressure level than for the low-pressure level.

## CONCLUSIONS

The multiscale approach followed in order to simulate mould filling phenomena proved its feasibility, and the main influencing factors reasonably matched those observed in the real experiments.This approach allowed for the set-up of microscale mould filling simulations at EURECAT, showing that the combination of both finite element modelling softwares achieved similar results to the real experiments at reasonably short computing times.Nevertheless, these simulation model was developed and run with the main objective of checking the approach validity, and the results obtained should be carefully understood, keeping in mind their qualitative rather than quantitative nature.In the future, these simulations might be further improved by getting more accurate data of the simulated materials' properties (some of them were lacking or imprecise in the current available literature), or also by further refinement of the meshings and the boundary conditions used.

# REFERENCES

[1] Park, S.W., Lee, W.I., Moon, S.N., Yoo, Y.-E., Cho, Y.H., 2011. Injection molding micro patterns with high aspect ratio using a polymeric flexible stamper. Express Polym. Lett. 5, 950–958. https://www.doi.org/10.3144/expresspolymlett.2011.93

[2] Baldi-Boleda T, Sadeghi E, Colominas C, García-Granada A. Simulation Approach for Hydrophobicity Replication via Injection Molding. Polymers. 2021; 13(13) :2069. https://www.doi.org/10.3390/polym13132069

[3] Zhang, Nan & su, Quanliang & Choi, Seong Ying & Gilchrist, Michael. (2015). Effects of gate design and cavity thickness on filling, morphology and mechanical properties of microinjection mouldings. Materials and Design. 83. 835-847. http://www.doi.org/10.1016/j.matdes.2015.06.012

[4] Tofteberg, T. & Andreassen, Erik. (2008). Simulating injection moulding of microfeatured components.

[5] Rytka, Christian & Lungershausen, J & Kristiansen, Per Magnus & Neyer, A. (2016). 3D filling simulation of micro- and nanostructures in comparison to iso- and variothermal injection moulding trials. Journal of Micromechanics and Microengineering. 26. 065018. https://www.doi.org/10.1088/0960-1317/26/6/065018

[6] Stormonth-Darling, John Moir (2013) Fabrication of difficult nanostructures by injection moulding. PhD thesis, University of Glasgow. https://www.eleanor.lib.gla.ac.uk/record=b2985305

# 5. THREE-LEVEL HIERARCHICAL MICRO/NANOSTRUCTURES ON BIOPOLYMERS BY INJECTION MOULDING USING LOW-COST POLYMERIC INLAYS[2]

[2] * This chapter has been published as a research article in an indexed journal:
*Sáez Comet, Carlos & Muntada, Olga & Lozano, Nekane & Fontdecaba, Enric & Sousa, Patrícia & Llobet Sixto, Jordi & Perez-Murano, Francesc & Puiggalí, Jordi & Del Valle, Luis. (2022). Three-level hierarchical micro/nanostructures on biopolymers by injection moulding using low-cost polymeric inlays. 10.21203/rs.3.rs-1928926/v1.*

## ABSTRACT

The industrial interest in the patterning of polymeric surfaces at the micro/nanoscale to include new functionalities has considerably increased during the last years. Hierarchical organization of micro/nanometric surface textures yields enhanced functional properties such as hydrophobicity, hydrophilicity, antibacterial activity, optical or chromatic effects, to cite some. While high accuracy methods to pattern hierarchical surfaces at the nanoscale have been developed, only some of them have been applied for high volume manufacturing with limited success, mainly because they rely on the use of expensive machinery and moulds or complicated inserts. Therefore, a method using low-cost recyclable tooling and process conditions applicable to high volume manufacturing is currently missing.

In this work, a scalable and low-cost method to replicate hierarchical micro/nanostructured surfaces on plastic films is presented, which can be latter used as inlays for injection moulded parts with standard processing conditions. This method is used to demonstrate the feasibility of replicating three level hierarchical micro/nano textured surfaces using recyclable bio-based polymers (of high relevancy in the current plastic pollution context) achieving replication ratios above 90%, comparing the replication results with those obtained in polypropylene. The presence of the micro/nanotextures substantially increases the contact angle of all the polymers tested, yielding values higher than 90° in all the cases. Also, various mechanical properties of the replicated parts for all the polymers injected are characterized one and thirty days after the samples were manufactured, showing fairly constant values. This highlights the validity of the replicated surfaces, regardless of the biopolymer's special crystallization characteristics.



***Keywords***

Micro/nanoscale structures, Hierarchical structures. Nano-imprint lithography, Injection moulding, Flexible inserts

## INTRODUCTION

It is well understood that the presence of micro- and nanostructures in the inner structure and in the surface of materials can enhance their functional properties. Numerous examples of functionalities have been identified in the natural world [1,2] and most of the scientific principles have been successfully elucidated. Some of the existing natural micro- and nanostructures are hierarchically organized. Such arrangement is commonly manifested at several dimensional levels, that might even present different chemical composition and it is responsible for a notable improvement of key physical properties, among which self-cleaning [3] or super-hydrophobicity [4]. Hierarchical micro- and nanostructures can be found in bones, wood, plant surfaces [4] or insect cuticles [2,3] and wings [5].

Several methods have been developed to emulate these natural existing structures on the surface of polymeric parts, in view of improving their functionalities in diverse application fields. Most of them are based on laboratory scale procedures. One of the most common methods is nanoimprint lithography (NIL). NIL is a high-resolution patterning technology based on replication of the surface features of a mould into a polymer material, by mechanically moulding or embossing, using the action of temperature or UV light crosslinking. While NIL was initially originated as a nanometric resolution lithographic method, able to compete with optical lithography, it evolved to a general method to create functional nanostructured surfaces for applications beyond microelectronics. Related NIL methods have been developed, including the use of soft stamps (Soft-NIL) [6], which is particularly well suited for large, and not necessarily flat substrates NIL can be scaled-up to provide high throughput replication by means of roll-to-roll techniques. Some examples of replication of multilevel hierarchical surfaces by NIL can be found in [7].

Amongst the common replication techniques on polymers, injection moulding constitutes one of the most important methods for mass production and gathers therefore the highest industrial interest due to its reduced cost per unit and possibilities of producing versatile shapes [8].The main factors influencing the quality of the replication are the election of the injected polymer, the geometry of the mould and cavities to be filled, moulding temperature, melting temperature, injection & holding pressure, cooling time and injection velocity as shown by numerous previous studies [9-12]. The most commonly used mould tool materials in injection moulding are metallic alloys. For example, Zhang

H. [13] used microinjection moulding with Nickel inserts to study the filling behaviour of high aspect ratio microfeatures on a microfluidic flow cytometer chip by using short shots. Blondiaux et al. [14] used micro- and nanostructured steel inserts obtained by micromilling & etching processes to replicate a bio-diagnostic platform using polycarbonate material. Bhuyan et al. [15] used micromachined and hot water treated aluminium to replicate hierarchical micro/nanostructures on polypropylene.

However, it is found that although metals are highly durable and practical to be used as mould materials because of the many available processes to structure their surface, the maximum achievable filling ratios are limited due to their high thermal conductivities [16]. High thermal conductivities revert into a very quick formation of a frozen polymer layer once the molten polymer contacts the cold mould material, which impedes the further filling of the micro/nanostructure. That is why advanced injection moulding techniques such as ICM and VIM (injection compression and variothermal injection moulding) or VICM (variothermal injection compression moulding) are required [17] when using metallic moulds to achieve optimal and consistent replication rates of the micro/nanostructures. These add considerable tooling costs to the injection process and additional relevant costs, such as energy consumption-due to the extended cycle times for ICM and VIM, have to be also considered when determining the overall process costs.

An alternative technique to obtain consistent replications of micro- and nanostructures at lower tooling costs is the use of coated polymeric films as flexible mould tooling material. In this technique, the coated polymeric film acts as an effective thermal barrier that can significantly hinder heat transfer into the mould during the moulding process, which might keep the melt viscosity low (and therefore the melt flowing ability high) for longer time [18].

Stormonth-Darling [19] used polymer films patterned by NIL as mould inlay material to replicate high-aspect ratio nanostructures on common thermoplastic polymers. In his research, a photoresist typical employed in microsystems technology (SU-8 3000 series) was coated onto a highly-technical polymeric film (Kapton®) and subsequently coated with a fluorosilane–for easier part demoulding- allowing to replicate high-aspect ratio pillar-like nanostructures.

In terms of the replication of hierarchical structures on common thermoplastic materials using low-cost tooling, even though some relevant work has been carried out with two-level hierarchical micro/nanostructures [15,20], to our knowledge only few publications have been carried out combining three level hierarchical micro/nanostructures, low-cost recyclable tooling and bio-based /biodegradable thermoplastic polymers. Therefore,

further research is still needed to further reduce the cost of the tooling materials towards a potential industrialization of the technology, and also to extend the range of micro/nanostructured polymers to the family of the bio-based polymers, highly interesting [21] in the current plastic pollution and climate-change context for their bio-based origin and biodegradability.

Here, we present a method to replicate three level hierarchical micro/nanostructures on relevant bio-based and bio-degradable thermoplastic polymers using low cost and recyclable coated polymeric inlays. Additional to the quantification of the replication fidelity, we also evaluate the improvements in the contact angles experienced on the surface of the injected polymers (changing their wetting character from hydrophilic to hydrophobic), together with the comparison of the mechanical resistance of the micro/nano textured surfaces on the injected biopolymers with the non-textured ones.

## MATERIALS AND METHODS

### Fabrication of the Ormostamp® stamps

Figure 5.1 shows the overall fabrication process for obtaining the plastic inlay stamps. The process consists of 7 steps: 1) Fabrication of the silicon mould, which contains the pattern to be transferred to the final polymer sample. 2) Thermal NIL to transfer to a PMMA Film. 3) PDMS casting and 4) curing to obtain a replica of the PMMA film. 5) On this PDMS, Ormostamp® [22] is casted and 6) subsequently cured while slight a pressure with a plastic foil is applied, which will form the inlay stamp to be used in injection moulding.

The process has two main advantages: a) The PDMS film can be re-used many times, so that both Si master and thermal NIL are preserved and b) OrmoStamp® can be easily released from the PDMS film much easier than from the silicon Stamp. It is worth to note that an odd number of replicas is needed to obtain the same polarity of features in the silicon stamp and in the final injected polymer part.

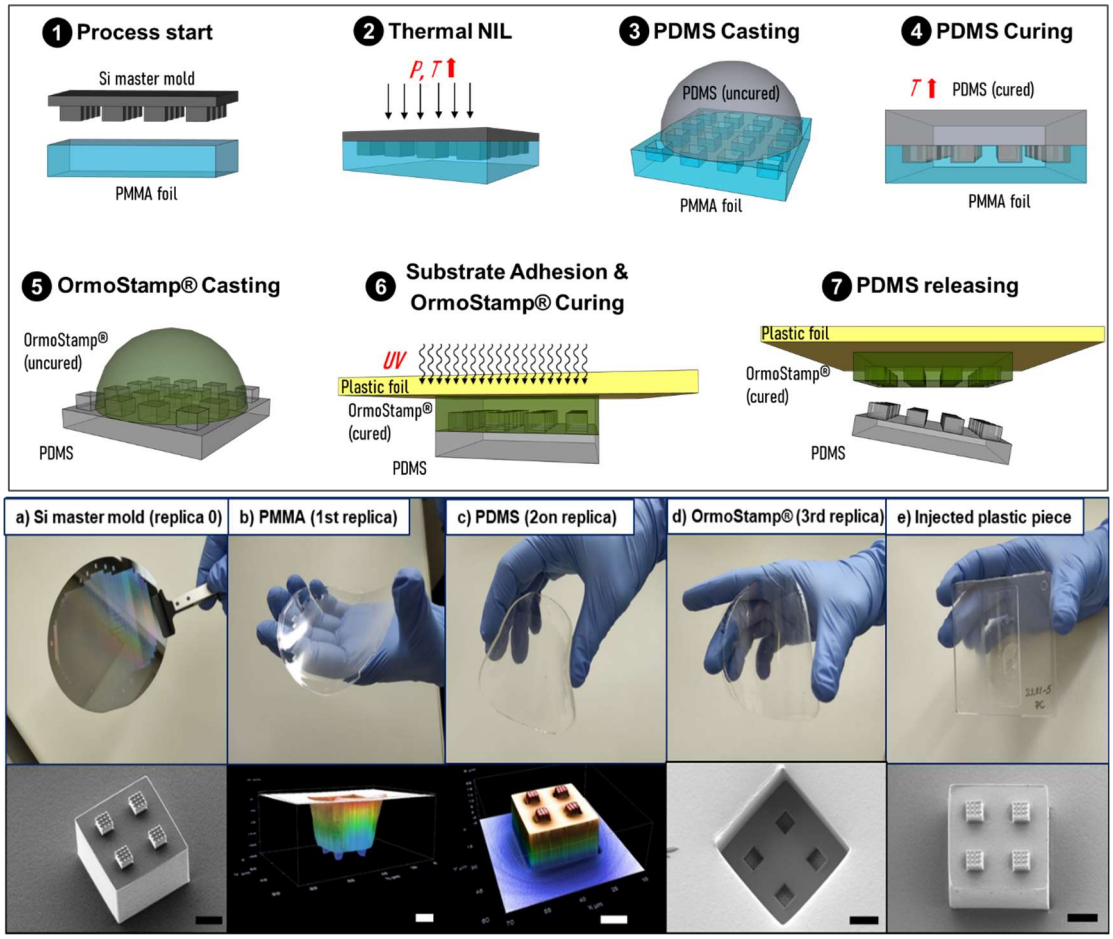


**Figure 5.1. (Top) Sketches of each individual process step of the method to obtain plastic inlay stamps from a silicon mould. (Bottom) Photographs (upper row) and micrographs (lower raw) at each step of the process: silicon stamp (a), replicas (b-c) and a final polycarbonate injected plastic piece (e). Micrographs images a), d) and e) are obtained by SEM while the micrographs of the images b) and c) are obtained by confocal microscopy. The scale bar is 10 µm for all the images.**

The details and main aspects of the stamp fabrication are presented in the supplementary information. The design of the hierarchical structure was performed in the framework of a previous study to analyse its influence on surface hydrophilicity. [23]

### Injection moulding

For the injection moulding tests, an *Engel complet E-motion 200/55* electric machine was used. The main processing parameters applied for each of the polymers injected are presented in Table 5.1.

| | PBS | PHB | PLA |
|---|---|---|---|
| Melt temperature (℃) | 130 | 175 | 205 |
| Mould temperature (℃) | 20 | 20 | 20 |
| Injection speed (mm/s) | 50 | 60 | 60 |
| Holding pressure (bar) | 700 | 500 | 600 |
| Holding pressure time (s) | 5 | 5 | 5 |
| Cooling time (s) | 20 | 15 | 20 |

**Table 5.1.** Processing parameters used during the injection moulding trials.

A photograph and an SEM image of the coated film are presented in fig. 5.2. In order to hold the micro/nano textured films during the injection moulding process, a custom-designed injection mould insert was manufactured. The insert allowed the placement of the coated films interchangeably on the surface of the fixed half in the injection mould in order to carry out replication trials (see supplementary information).

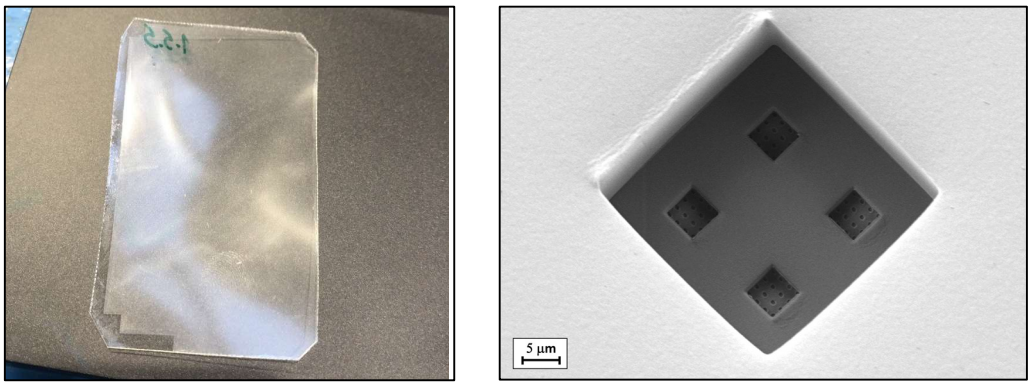


**Figure 5.2. Details of the inlay stamp consisting of a micro/nano textured polymer coated pet film (left) and sem image detail of the 3-level hierarchical negative structures on it (right).**

The following biopolymers have been used in the injection moulding experiments:

- PLA BIO LM 99004 from Ercros,
- PBS PBI 003 from Natureplast
- PHB P304 from Biomer

In addition, PP C100 CA50 from Ineos was also used for comparison purposes. All the polymers were injection moulded according to the standard processing recommendations from each of the specific manufacturers, using moulds at room temperature in all cases.

## Characterization

### Degree of replication (%) obtained with confocal microscope and SEM images

For the morphological characterization of the injected samples a Sensofar Plμ 2300 confocal microscope was used, and the images acquired were latter processed by the software MountainsMap 5.1 of Digital Surf, and Gwyddion.

The main purpose of this characterization was the determination of the degree of replication, DR%:

$$DR\% = hf / dc \times 100 \quad (1)$$

where hf is the height of features in the polymeric sample and dc is the depth of cavities in the coated polymeric inlay film.

The DR% parameter is also interesting to characterize the uniformity of the replicated structures on the injected polymer samples.

### Water contact angle

Water contact angle measurements (WCA) of the Ormostamp□ coated PET films and the micro/nanostructured zones were obtained by means of a tensiometer (Dataphysics OCA 15 CE) and image processing software (SCA 2.0). Micro-droplets of 150 μL of deionized water were used. The contact angle values were obtained as the average of 5 measurements.

### Mechanical characterization-Scratch and flat punch micro tests

In order to evaluate the different scratch resistance and quantify the coefficient of friction (COF) of the micro/nano textured zones vs the non-textured ones on the injected polymer samples, surface scratches were practiced at 0.5 N and 1.5 N load levels using a Micro-Combi Indentation-Scratch Tester MHT (CSM). Also, Flat Punch indentation measurements using an AISI 52100 steel ball of 1mm diameter were taken in order to evaluate the elastic storage modulus of the injected samples under compression in both textured and non-textured zones.

Both mechanical measurements were taken 4 days after the injection moulding took place and also after 33 days, to check the time evolution of the surface mechanical properties. It is well known that the stiffness increases due to post-crystallization (also called cold crystallization) for some of the biopolymer types used [24,25]. This increase would lead to a higher part brittleness and therefore an overall decrease of the part mechanical properties, which could affect the replicated micro/nano textures.

## RESULTS AND DISCUSSION

### Quality of the replication

The patterns replicated achieved average degrees of replication (DR%) comprised between 90% and 110% for the three polymers. The percentages higher than 100% represent excessive micro/nano texture heights and therefore considerable stretching, most probably caused during the demoulding stage. Details of the overall uniformity on the micro/nanotextures and the replication of the three hierarchical levels can be observed in Fig. 5.3 and extracted confocal profiles of the injected samples are presented in Fig. 5.4.

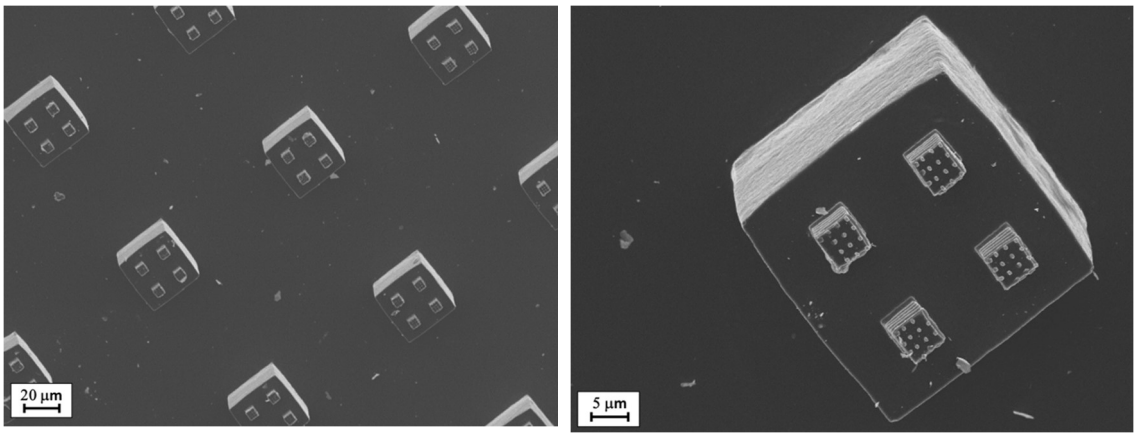


**Figure 5.3. PHB injected part. Hierarchical micro/nanotextured zone (left). Detailed single feature of the same PHB part (right).**

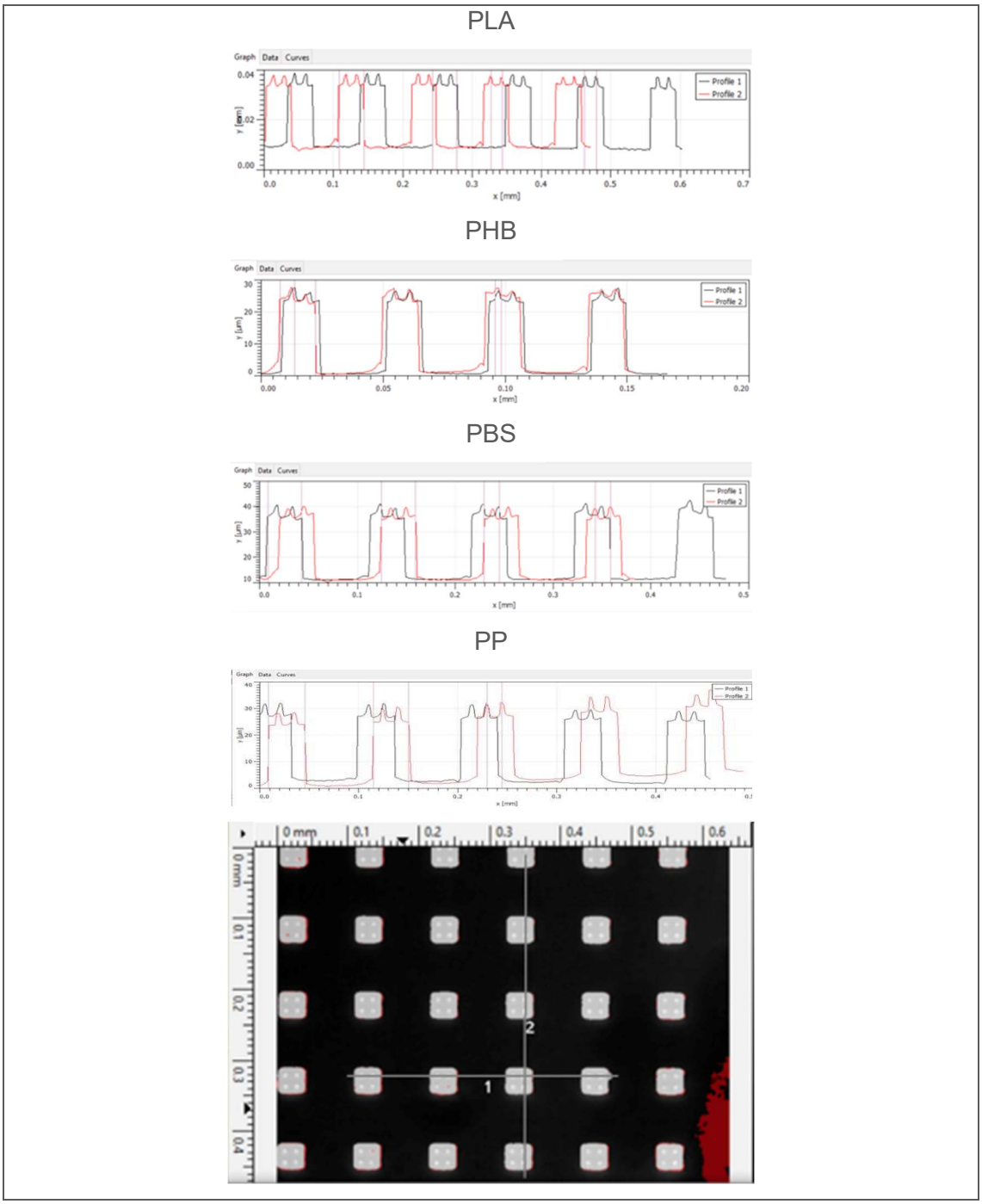


**Figure 5.4. Extracted confocal profiles (black line= horizontal profile across features/red line= vertical line along features) of the surface of the micro/nanotextured replicated polymeric parts via injection moulding. The confocal optical image in the left presents the position of extraction of the horizontal (1) and vertical (2) profiles.**

It is remarkable that the degrees of replication are always around 100 % when we compare the inlay film with the patterns in the silicon mould and also when we compare the patterns in the injected plastic parts with the patterns in the in-lay film. The variability in the measurements (±10%) are within the experimental error of the measurements.

In some of the injected samples, the micro/nano features presented an elongated and deformed shape (see supplementary information), which could have been caused by excessive adhesion between the film and the injected part due to an insufficient cooling time or to an excessive adhesion between the moulded part and the micro/nanotextured OrmoStamp®. This phenomenon took place occasionally for all the biopolymers tested, especially in the upper zone of the injected part, while it was more usual for the injected PP samples (injected at higher melt temperature as per manufacturer specifications). This could have been produced by the slightly higher temperature existing in the upper region of the plastic part with regards to the rest of it at the moment of demoulding.

This fact is also supported by the progressive delamination of the micro/nanotextured Ormostamp® coating from the base PET film that took place as the number of injection rounds increased (see supplemental information). Once initial coating delamination took place, the subsequent increased adhesion of the injected polymer to the base film PET material caused the damage of the film and therefore its deformation upon part demoulding. As an indication of this problem, using a single coated film up to twelve samples of injected plastic were replicated for PBS and PLA (when the injection process had to be stopped due to substantial film-coating delamination) while up to fifty were replicated in the case of the PHB without critical film damage by delamination.

**Water contact angle**

The contact angle measurements were taken for all the samples replicated with the same film (12 samples for PLA and PBS, 50 samples for PHB and 34 samples for PP) to account for potential variations in the hydrophobic character of the samples. The variations registered along the samples replicated were minimal as indicated in table 5.2 (the values show the averaged values amongst the samples injected per each polymer, taking 5 measurements per part and zone).
All the values show a change in wetting character of the polymers from their traditional low hydrophilic levels to slightly hydrophobic except for PP, which is already hydrophobic without the surface with micro/nano-texturing, but for which an increase in the contact angle was also measured. None of the increases in the contact angles obtained represent a dramatic change in wetting character, as the three-level hierarchical micro/nano textured were not specifically designed for that purpose. Nevertheless, the increases observed show an interesting switch in the wetting character of the biopolymers which is added to other potential surface functionalities achievable by hierarchical micro/nano textured surfaces.

| | | CA ◦ | SD |
|---|---|---|---|
| PLA | Non textured | 82,28 | ±1,55 |
| | Textured | 105,13 | ±3,22 |
| PHB | Non textured | 53,73 | ±5,66 |
| | Textured | 95,37 | ±1,77 |
| PBS | Non textured | 80,31 | ±1,1 |
| | Textured | 93,62 | ±1,74 |
| PP | Non textured | 100,35 | ±1,39 |
| | Textured | 127,7 | ±1,96 |

**Table 5.2:** Contact angle measurements.

### Mechanical characterization

The values of the coefficients of friction (COF) taken for both textured and non textured zones four days and one month after the injection moulding experiments are shown in table 5.3.

Fig. 5.5 shows the evolution of storage modulus at various frequencies for both textured and non-textured surfaces for each of the biopolymers.

| Date tested | Polymer | Textured zone | | | | Base material | | | |
|---|---|---|---|---|---|---|---|---|---|
| | | 0,5N | | 1,5N | | 0,5N | | 1,5N | |
| | | Avg | SD | Avg | SD | Avg | SD | Avg | SD |
| 01/12/2021 | PHB | 0,24 | ±0,032 | 0,19 | ±0,024 | 0,10 | ±0,015 | 0,10 | ±0,009 |
| | PLA | 0,15 | ±0,030 | 0,14 | ±0,029 | 0,07 | ±0,018 | 0,08 | ±0,011 |
| | PBS | 0,14 | ±0,040 | 0,12 | ±0,016 | 0,10 | ±0,010 | 0,09 | ±0,005 |
| 03/01/2021 | PHB | 0,26 | ±0,037 | 0,21 | ±0,029 | 0,12 | ±0,025 | 0,13 | ±0,019 |
| | PLA | 0,15 | ±0,021 | 0,15 | ±0,017 | 0,10 | ±0,028 | 0,10 | ±0,010 |
| | PBS | 0,15 | ±0,025 | 0,14 | ±0,022 | 0,06 | ±0,017 | 0,07 | ±0,008 |

**Table 5.3** COF results obtained for PHB, PLA and PBS plastic parts after 4 days and after 30 days of the injection.

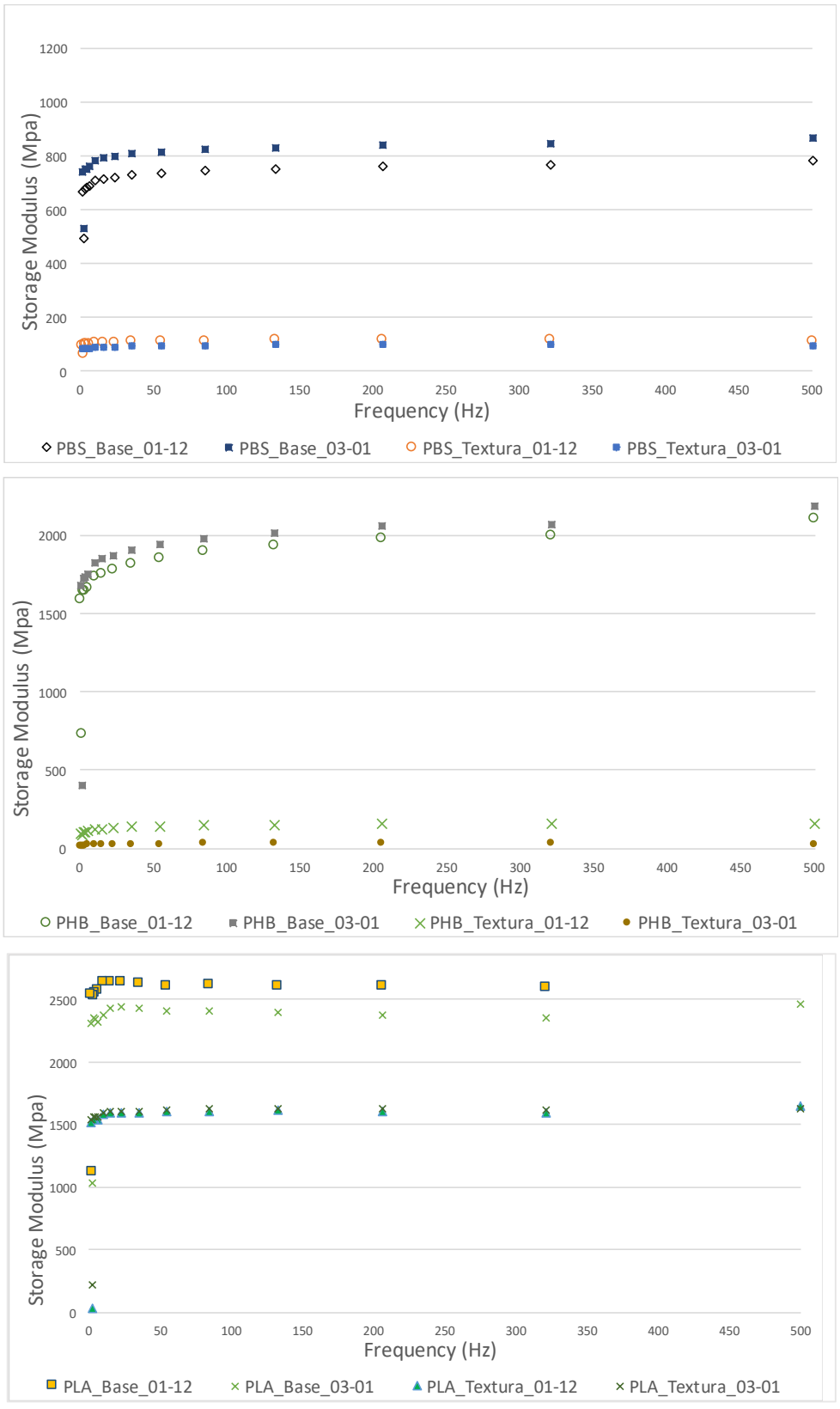


**Figure 5.5 Charts showing the storage modulus measurements obtained of both textured and non textured zones at various frequencies for PBI (above), PHB (centre) and PLA (below).**

The values observed and their differences for textured and non-textured zones remain fairly constant along the time period tested. A slight difference of the COF between non-

textured and textured zones can be observed for all the loads applied and the materials tested as expected.

Also, while a general slight increase of the COF values for both load levels along the time period tested is observed on all the textured zones of all the polymers, a small decrease is observed on values corresponding to the PBS base material. This decrease in the COF could be explained by the slight rise observed in the material's surface hardness along the defined testing time period, as appreciated in the measurements of storage modulus shown in Fig.5.5 for the PBS non-textured surface.

In Fig. 5.5, lower values of storage modulus can be observed for the textured versus the non-textured zones for all the biopolymers tested as logically expected. Slight increases of the storage modulus between both dates tested are observed for the non-textured surfaces of PBS and PHB materials, while a more marked decrease is observed for the non-textured PLA. This could be explained by the known subtle degradation of PLA material mechanical properties degradation [26], potentially enhanced by the specific additives used by the manufacturer of the specific polymer grade used in the experiments. Additionally, very small (and therefore not conclusive) or negligible changes of the values observed on the textured zones of the different biopolymer materials are shown on the graphs.

## CONCLUSIONS

A method for the fabrication of polymeric hierarchical inserts for isothermal plastic injection moulding using low cost and recyclable materials has been developed.

A method to produce high accuracy, hierarchical micro-structured moulds at wafer scale, and its replication into plastic inlays is described. The method is scalable and affordable, as once the mould is fabricated, any of the intermediate replications can be used to define additional inlays.

The high degrees of replication filling (DR%) achieved on the samples injected show the feasibility of the method presented for the replication of hierarchical micro/nanotextured on the surfaces of common thermoplastic biopolymers using standard injection moulding conditions and polymeric flexible tooling. This is further underlined by the clear replication of the three hierarchical levels in most of the cases (shown on more than 80% of total structured surfaces on replicated samples in which no damage on film had occurred).

Amongst the biopolymers tested, PHB shows the most promising characteristics, as with the method applied it achieved the highest number of parts with a constant degree of replication and contact angle using a single film inlay.

The research presented here constitutes a promising low-cost method using recyclable tooling and standard injection moulding conditions to achieve a sufficient contact angle increase on the surface of the biopolymers considered (hydrophilic on their original state) without substantial loss in surface mechanical properties, which might be of interest for applications such as packaging or the medical device industry. However, some improvements need to be made in order to enhance the film-coating durability and flatness during the injection moulding process to adequately increase the number of injected parts per film. Also, an adjustment of the cooling times and demoulding processes is required to obtain higher durability of the tooling.

# REFERENCES


[1] Malshe, A, Rajurkar, K, Samant, A, Nørgaard Hansen, H, Bapat, S, Jiang, W, Bio inspired functional surfaces for advanced applications, CIRP Annals, (Vol. 62, Issue 2,2013, P. 607-628). https://doi.org/10.1016/j.cirp.2013.05.008

[2] Watson, G.S., Watson, J.A., Cribb, B.W., 2017. Diversity of Cuticular Micro- and Nanostructures on Insects: Properties, Functions, and Potential Applications. Annu. Rev. Entomol. 62, 185–205. https://doi.org/10.1146/annurev-ento-031616-035020

[3] Bhushan, B., Jung, Y.C., Koch, K., 2009. Micro-, nano- and hierarchical structures for superhydrophobicity, self-cleaning and low adhesion. Phil. Trans. R. Soc. A. 367, 1631–1672. https://doi.org/10.1098/rsta.2009.0014

[4] Fratzl, P., Weinkamer, R., 2007. Nature's hierarchical materials. Progress in Materials Science 52, 1263–1334. https://doi.org/10.1016/j.pmatsci.2007.06.001

[5] Watson, G.S., Cribb, B.W., Watson, J.A., 2010. How Micro/Nanoarchitecture Facilitates Anti-Wetting: An Elegant Hierarchical Design on the Termite Wing. ACS Nano 4, 129–136. https://doi.org/10.1021/nn900869b

[6] Verschuuren, M.A., Megens, M., Ni, Y., van Sprang, H., Polman, A., 2017. Large area nanoimprint by substrate conformal imprint lithography (SCIL). Advanced Optical Technologies 6. https://doi.org/10.1515/aot-2017-0022

[7] Rodríguez I., Hernández J., Soft thermal nanoimprint and hybrid processes to produce complex structures, in: Nanofabrication, IOP Publishing, 2020. https://doi.org/10.1088/978-0-7503-2608-7ch7

[8] Maghsoudi, K., Vazirinasab, E., Momen, G., Jafari, R., 2020. Advances in the Fabrication of Superhydrophobic Polymeric Surfaces by Polymer Molding Processes. Ind. Eng. Chem. Res. 59, 9343–9363. https://doi.org/10.1021/acs.iecr.0c00508

[9] Vera, J., Brulez, A.-C., Contraires, E., Larochette, M., Trannoy-Orban, N., Pignon, M., Mauclair, C., Valette, S., Benayoun, S., 2018. Factors influencing microinjection molding replication quality. J. Micromech. Microeng. 28, 015004. https://doi.org/10.1088/1361-6439/aa9a4e

[10] Pina-Estany, J., Colominas, C., Fraxedas, J., Llobet, J., Perez-Murano, F., Puigoriol-Forcada, J.M., Ruso, D., Garcia-Granada, A.A., 2017. A statistical analysis of nanocavities replication applied to injection moulding. International Communications in Heat and Mass Transfer 81, 131–140. https://doi.org/10.1016/j.icheatmasstransfer.2016.11.003

[11] Muntada-López, O., Pina-Estany, J., Colominas, C., Fraxedas, J., Pérez-Murano, F., García-Granada, A., 2019. Replication of nanoscale surface gratings via injection molding. Micro and Nano Engineering 3, 37–43. https://doi.org/10.1016/j.mne.2019.03.003

[12] Liou, A.-C., Chen, R.-H., 2006. Injection molding of polymer micro- and sub-micron structures with high-aspect ratios. Int J Adv Manuf Technol 28, 1097–1103. https://doi.org/10.1007/s00170-004-2455-2

[13] Zhang, H., Fang, F., Gilchrist, M.D., Zhang, N., 2018. Filling of high aspect ratio micro features of a microfluidic flow cytometer chip using micro injection moulding. J. Micromech. Microeng. 28, 075005. https://doi.org/10.1088/1361-6439/aab7bf

[14] Blondiaux, N., Pugin, R., Andreatta, G., Tenchine, L., Dessors, S., Chauvy, P.-F., Diserens, M., Vuillermoz, P., 2017. Fabrication of Functional Plastic Parts Using Nanostructured Steel Mold Inserts. Micromachines 8, 179. https://doi.org/10.3390/mi8060179

[15] Bhuyan, M. & S., Mika & Saarinen, J. (2019). Replication of hierarchical nano- and microstructures on polymers. Academics World International Conference on Nanoscience, Nanotechnology and Advanced Materials 2019,7. 76-81.

[16] Liu, Y. (2015). Heat transfer process between polymer and cavity wall during injection molding. January 2015. Phd Thesis for: Doctoral Degree.

[17] Rytka, C., Kristiansen, P.M., Neyer, A., 2015. Iso- and variothermal injection compression moulding of polymer micro- and nanostructures for optical and medical applications. J. Micromech. Microeng. 25, 065008. https://doi.org/10.1088/0960-1317/25/6/065008

[18] Park, S.W., Lee, W.I., Moon, S.N., Yoo, Y.-E., Cho, Y.H., 2011. Injection molding micro patterns with high aspect ratio using a polymeric flexible stamper. Express Polym. Lett. 5, 950–958. https://doi.org/10.3144/expresspolymlett.2011.93

[19] Stormonth-Darling, J.M., Pedersen, R.H., How, C., Gadegaard, N., 2014. Injection moulding of ultra high aspect ratio nanostructures using coated polymer tooling. J. Micromech. Microeng. 24, 075019. https://doi.org/10.1088/0960-1317/24/7/075019

[20] Estévez, Ariadna. Functional surfaces by means of nanoimprint lithography techniques. (2016). http://hdl.handle.net/10803/400142

[21] Verma, Ashish & Chowdhury, Suvam & Nag, Sananda & Tripathi, Kumud. (2017). Recent Advances in Biopolymers for Innovative Food Packaging. 8N. 2013;3–5.

[22] Ormostamp® technical datasheet. https://www.microresist.de/en/produkt/ormostamp/

[23] Achille Francone, Olga Muntada, Gemma Rius, Clivia M. Sotomayor Torres, Francesc Perez-Murano, Nikolaos Kehagias. Nano, micro, or combination: design rules for self-cleaning surfaces. Nanimprint and Nanoprimt Technologies 2019. https://nnt2019.org/

[24] Turco, R., Santagata, G., Corrado, I., Pezzella, C., Di Serio, M., 2021. In vivo and Post-synthesis Strategies to Enhance the Properties of PHB-Based Materials: A Review. Front. Bioeng. Biotechnol. 8, 619266. https://doi.org/10.3389/fbioe.2020.619266

[25 Rafiqah, S.A., Khalina, A., Harmaen, A.S., Tawakkal, I.A., Zaman, K., Asim, M., Nurrazi, M.N., Lee, C.H., 2021. A Review on Properties and Application of Bio-Based Poly (Butylene Succinate). Polymers 13, 1436. https://doi.org/10.3390/polym13091436

[26] Muthui, Z.W., Kamweru, P.K., Nderitu, F.G., Hussein, S.A.G., Ngumbu, R., Njoroge, G.N., 2015. Polylactic acid (PLA) viscoelastic properties and their degradation compared with those of polyethylene. Int. J. Phys. Sci. 10, 568–575. https://doi.org/10.5897/IJPS2015.4412

# 6. INTRODUCING SURFACE FUNCTIONALITY ON THERMOFORMED POLYMERIC FILMS[3]

[3] [3] * This chapter has been published as a research article in an indexed journal:
*Carlos Sáez-Comet, Olga Muntada, Achille Francone, Nekane Lozano, Marta Fernandez-Regulez, Jordi Puiggali, Nikolaos Kehagias, Clivia M. Sotomayor Torres, Francesc Perez-Murano, Introducing surface functionality on thermoformed polymeric films, Micro and Nano Engineering, Volume 14,2022,100112, ISSN 2590-0072, https://doi.org/10.1016/j.mne.2022.100112*

## ABSTRACT

We present a fabrication process for the production of 3-dimensional micro-structured polymeric films. The microstructures are fabricated in a single step using thermal nanoimprint lithography as patterning technique. The micro-structured polymer films are then transformed into a 3D shape by means of a plug-assisted thermoforming process, while keeping the functionality of the micro-patterned areas. The preserved functionality is characterized by water contact angle measurements, while the deformation of the micro-structured topographies due to the thermoforming process is analyzed using confocal microscopy and Digital Image Correlation (DIC) techniques. This combined fabrication process represents a promising solution to complement in-mold decoration approaches, enabling the production of new functional surfaces. As the microstructures are fabricated by means of a mechanical modification of the surface, without the need of chemical treatments or coatings, the presented technique represents a promising, simple and green solution, suitable for the industrial fabrication of 3D nonplanar shaped functional surfaces.

***Keywords***

Thermoforming, Nanoimprint lithography, Plastic injection molding, Surface functionalization

## INTRODUCTION

The industrial interest in micro/nm scale patterning of surfaces is broad due to the wide range of applications. Micro / nano-metric texturing makes it possible to provide surfaces with functional properties, such as, for example, hydrophilicity, hydrophobicity, greater adherence, antibacterial, optical, or chromatic effects, among others [1]. Several high accuracy methods to pattern surfaces at the micro and nanoscale have been developed [2,3]. However, a methodology for high volume manufacturing at affordable cost is still missing for many applications, especially to define accurate and deterministic patterns on arbitrary and or curved surfaces. In recent years functional micro- and nano- textured surfaces on 3D formed polymeric films with potential in various applications have been a subject of investigation [4–7]. Among them, micro fluidics [8] and tissue culture [9] are some that attract the most interest.

Furthermore, there are other potential applications in other industrial sectors such as the automotive industry (interior parts, optics) [10] as well as home and industrial lighting

[11], to mention but a few. In these sectors, a recent manufacturing technology known as in-mold electronics is becoming more and more relevant [12]. In-mold labelling (IML) [13] and in-mold decoration (IMD) [14] processes allow to handle and incorporate decorative 3D formed polymeric films on final injection-molded parts. These manufacturing technologies can be further enhanced by using locally micro- and nano-textured films to obtain local and specific functionalities on the surface of the resulting injection molded parts. Furthermore, the micro- and nano- textured polymeric films can also be used as replication inserts, adequately placed on the injection molds [15]. The most widely extended methods to pattern a surface incorporate a lithography process, which defines the lateral dimensions [16]. The tremendous progress in lithography made over several decades has delivered a robust and reliable technology, covering wide dimensions range from few nanometers to millimeters. A patterning technique that allows local 3D micro- and nano- structuring of thermoplastic films is thermal nanoimprint lithography (thermal NIL) [17], a high-resolution and high-throughput lithography technique. Thermal NIL is based on the mechanical deformation of a thermoplastic material, which can be a thermoplastic resist coated on a substrate or a bulk thermoplastic sheet/ film, with a stamp containing the surface topography to be replicated in a 1 to 1 scale. The achievable resolution is mainly limited by the minimum feature size that can be fabricated on the stamp and sub-10 nm lateral dimensions have been demonstrated [18]. In order to overcome possible adhesion issues between the stamp and the surface to be patterned, generally an anti-adhesion treatment is applied on the stamp surface [19]. In this work, thermal NIL was used in a step-and-repeat mode, a manufacturing process with potential for high-volume and low-cost manufacturing [20–22]. After imprinting a die, the stamp is released from the substrate, displaced to the next die, put again into contact with the substrate, and thermally imprinted [23]. However, most lithography methods require the printed surface to be flat. Some examples of patterning on curve surfaces exist, like for example in nanostencil lithography [24], but they are not a universal solution and present limited industrial applicability. When it comes to form micro- and nano- textured films into 3D shapes, a well-known and popular transformation process is thermoforming using vacuum-assisted plugs. In this case, the surface is micro-patterned when it is flat, and later it is given the desired final macroscopic shape [25]. Applications of thermoforming in industry are large but so far very few examples of functional patterned thermoformed pieces have been realized [8,9]. After thermoforming, the patterned areas in the film will suffer geometrical distortions caused by the induced macroscopic deformation.

Those distortions might negatively affect the surface functionality. To understand the achievable maximum 3D- macroscale deformations that can be applied to the films without losing the surface functionality, a study of how the macroscopic deformation translates into geometrical distortions at the micro- scale is required. This will then allow to study the loss in the initial surface functionality, if any, and how it could be identified and prevented. In this article, we present the patterning of polycarbonate (PC) films by thermal-NIL to obtain hydrophobic surfaces. We investigate how their structural and functional properties change when the film is thermoformed. The local changes in the geometries of the various micro-structured zones are monitored using confocal scanning microscopy. The result is compared with to macroscopic deformations and draw ratios obtained by digital image correlation (DIC) [8,26]. A further correlation with surface functionality is carried out by evaluating the wetting behavior of the micro-structured areas of the film before and after the thermoforming process.

## MATERIALS AND METHODS

### Pattern design

For investigating the change of the functional properties of a surface submitted to a thermoforming process, we have chosen as test patterns arrays of pillars, because they are relatively simple structures that would allow us to relate the deformation at macroscale due to the thermoforming process with the deformation at the microscale. As a change in the morphology implies a change of the functional properties, we have quantified the variation of the hydrophobicity by measuring the contact angle before and after thermoforming. The hydrophobicity of a surface is commonly defined from the

contact angle of a water droplet in contact with the surface as described in the Young's equation [27]:

$$\gamma_{SG} = \gamma_{SL} + \gamma_{LG} \cos(\theta)$$

Where $\gamma_{SG}$ is the interfacial tension between solid and gas phases, $\gamma_{SL}$ between gas and liquid, $\gamma_{LG}$ between liquid and gas and $\theta$ is the angle of a droplet on a solid surface.

To increase the surface contact angle, the interfacial free energy must be increased. This is possible to be achieved by micro-structuring the surface: specific geometries allow air pockets to be trapped between the droplet and the surface. The ideal case where this occurs is known as Cassie-Baxter state and is preferable to the Wenzel state in which the droplet completely wets the surface (Fig. 6.1.b) [28]. (See Table 6.1.)

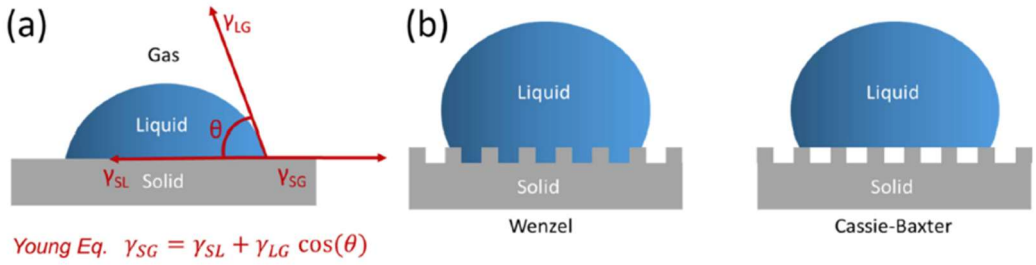


**Figure 6.1. (a) Graphical representation of the Young equation and contact angle for a droplet on a surface. (b) Graphical representation of the Wenzel and Cassie-Baxter states for a micro-structured surface.**

| Quadrant | d (μm) | p (μm) | $\theta_W$ | $\theta_{CB}$ |
|---|---|---|---|---|
| Q1 | 4 | 8 | 59° | 139° |
| Q2 | 6 | 12 | 59° | 139° |
| Q3 | 8 | 16 | 59° | 139° |
| Q4 | 10 | 20 | 59° | 139° |

**Table 6.1.** Calculated values of Wenzel θW and Cassie-Baxter contact angles θCB for the designs of the stamps. A nominal pillar height of 6.5 mm is assumed for all the quadrants.

Fig. 6.2 describes the geometrical parameters of the microstructures that will be transferred to the polycarbonate films, which will induce an increment of the water contact angle. Four designs have been selected, each one consisting of an area of 30 mm × 30 mm covered by pillars with diameters (d) of 4 μm, 6 μm, 8 μm and 10 μm. In each area, the pitch (p) is defined to be 2d. This design will result on four stamps with arrays of holes that, after the thermal-NIL process, will produce pillars in the polycarbonate films.

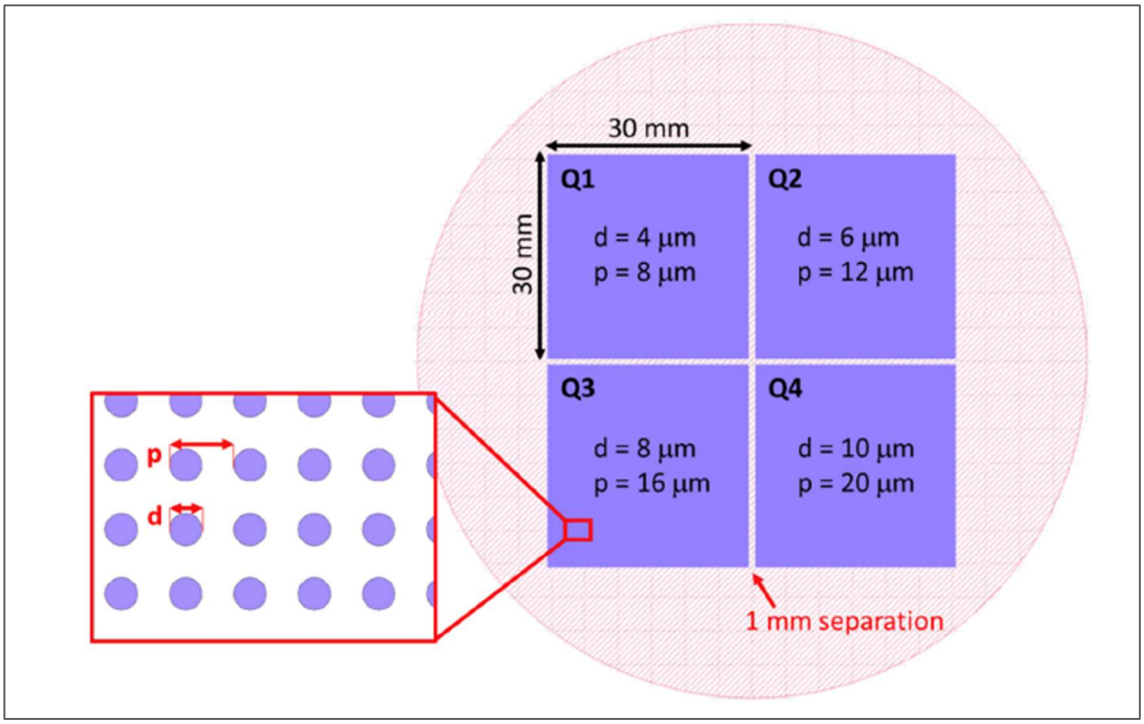


**Figure 6.2. Micro-structured texture design. The pattern consists of 4 areas of 30 × 30 mm each that contain arrays of holes pillars diameters d ranging from 4 µm to 10 µm and pitches *p* = 2d for all of therthethem. diameters d ranging from 4 µm to 10 µm and pitches *p* = 2d for all of them.**

The Wenzel and Cassie-Baxter water contact angles can be estimated according to the following relations [29]:

$$\cos\theta_W = r\cos\theta \quad (1)$$

$$\cos\theta_{CB} = \Phi_s(1+\cos\theta) - 1 \quad (2)$$

where $\theta_W$ and $\theta_{CB}$ are the apparent contact angle for Wenzel and Cassie-Baxter states respectively, r is the roughness factor, $\Phi_s$ is the areafraction of the solid surface for micro/nanostructured surfaces and θ is the water contact angle on flat –non nanostructured & non- thermoformed PC. r and Φs can be calculated as follows [30]:

$$\frac{r=[(p)^2+\pi dh]}{(p)^2} \quad (3)$$

$$\Phi S = \frac{\pi d^2}{4(p)^2} \quad (4)$$

Next table shows the values for the expected Wenzel and Cassie- Baxter contact angles for each quadrant of the design, assuming a height of 6.5 μm for the pillars, and a contact angle of 77◦ for the flat and non- textured surface:

| | Water contact angle (◦) | Standard deviation | Curvature Radius (mm) | Linear Draw Ratio AVG | AVG major strain (%) | AVG minor strain (%) |
|---|---|---|---|---|---|---|
| Non-textured PC | 77.0 | ±5.3 | - | - | - | - |
| Textured PC (flat) | 150.6 | ±1.6 | - | - | - | - |
| Zone 1 | 147.7 | ±4.3 | 314.5 | 2.79 | 2.8 | 0.3 |
| Zone 2 | 146 | ±2.4 | 211.3 | 2.98 | 7.1 | 1.2 |
| Zone 3 | 135.9 | ±8.0 | 59.8 | 2.57 | 11.6 | 4.6 |
| Zone 4 | 127.1 | ±3.1 | 58.6 | 2.85 | 12.1 | -1.8 |
| Zone 5 | 107.1 | ±5.1 | 50.1 | 4.63 | 97.4 | -15.5 |

**Table 6.2.** Summary of the characterization results after thermoforming.

Cassie-Baxter states are expected for the textured surfaces, resulting to be more hydrophobic after the patterning process in comparison to the un-patterned ones. Upon deformation, the change of the geometrical parameters of the microstructures will induce a variation in the corresponding water contact angle values, which eventually could imply a deviation from a pure Cassie-Baxter state.

## Pattern and Process design

The overall process for the fabrication of the thermoformed micro-structured film is shown in Fig. 6.3. The first part of the process is the fabrication of the stamp. Four stamps from the same silicon wafer are fabricated following the designs shown in Fig. 6.2 by means of optical lithography and reactive ion etching (steps 1–4). After Step 4, the wafer is dived in the four dices, each one containing one of the array designs, which will be used as a master stamp. The master stamp is then pressed and heated against a PC sheet by step and repeat thermal NIL (Step 5). Five micro- structured dies (see Fig. 6.4.a) of equal dimensions were fabricated in several selected locations of the flat polycarbonate film that was subsequently thermoformed in order to obtain the final 3D shape (see Fig. 6.4.b).

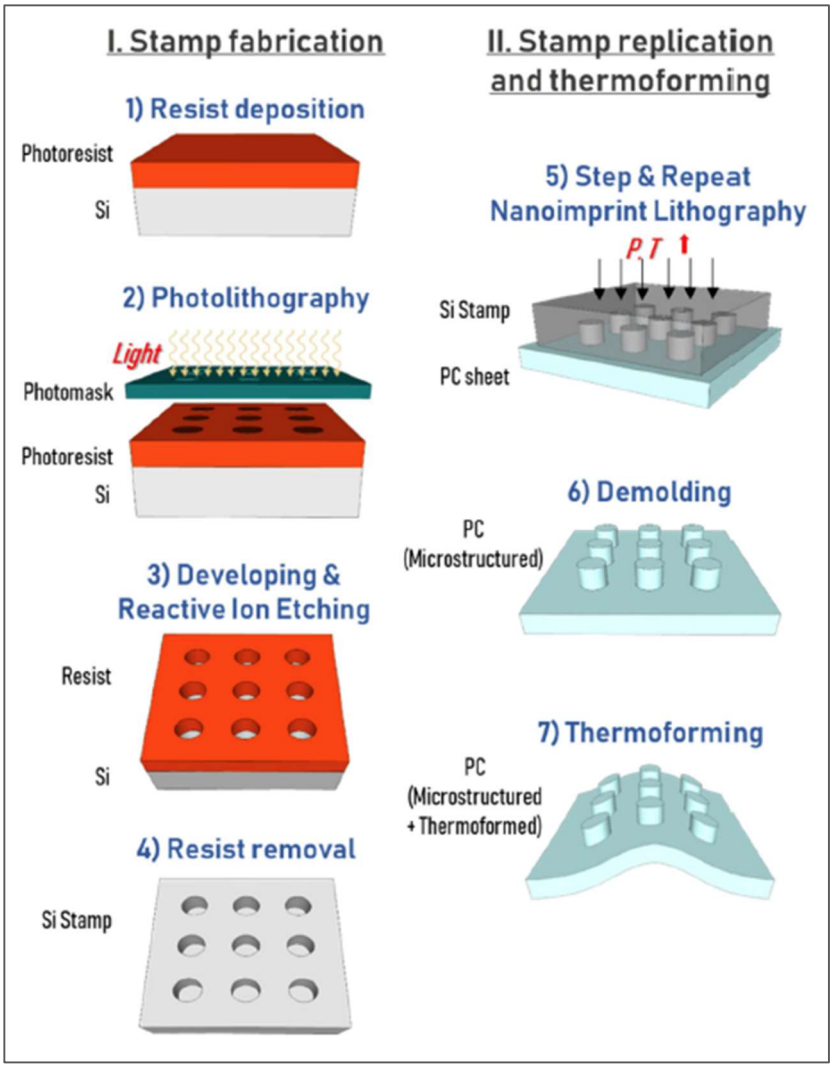


**Figure 6.3. Scheme of the overall fabrication process which includes the fabrication of the silicon stamp (steps 1–4) the replication of the stamp in a polycarbonate film by thermal NIL (steps 5–6) and the thermoforming of the film (step 7).**

After the demolding (step 6) we obtain a planar micro-structured PC sheet that is thermoformed into a 3D shape using a thermoforming process (step 7). The conditions of these processes are further detailed in the Materials and Methods section. The geometrical shape chosen for the thermoforming mold is a half-cylinder with decreasing curvature radius, down to 50 mm, a length of 195 mm and a constant width of 100 mm (Fig. 6.4.a). The placement of the micro-structured zones on the flat film was carefully selected to observe the effects caused by the film deformation in relation to the increasing linear draw ratios and decreasing curvature radii. The mold employed for the thermoforming process, together with the microstructured film on top of it, is shown in Fig. 6.4.b.

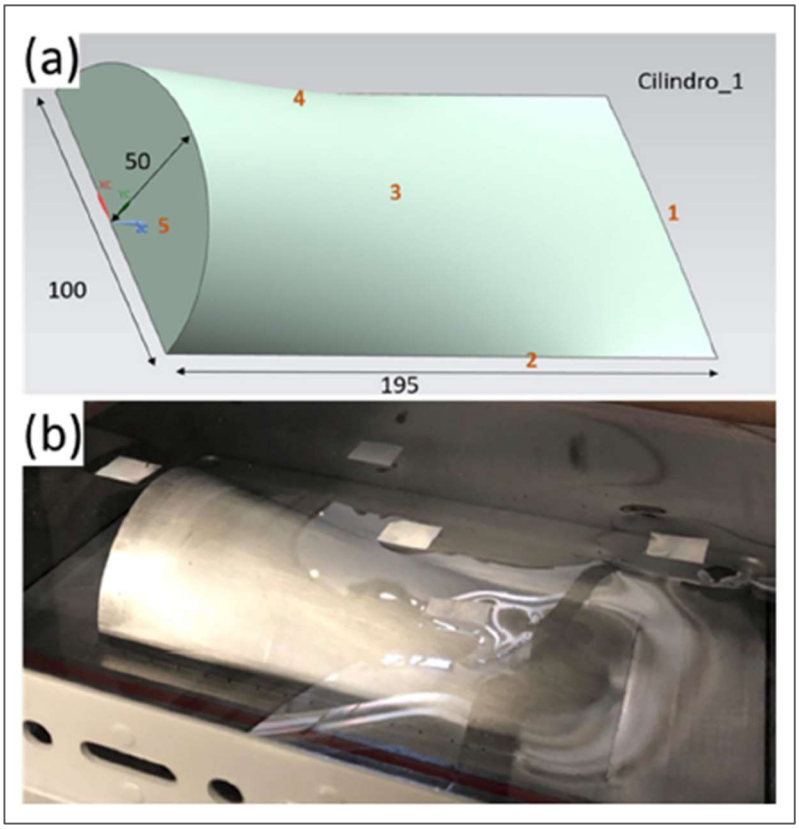


**Figure 6.4. (a) Design of the thermoforming mold geometry showing the placement of the microstructured areas in red. Dimensions are in millimeters. (b) Photograph of the polycarbonate film on top of the mold prior to the thermoforming process. (For interpretation of the references to colour in this figure legend, the reader is referred to the web version of this article.)**

### Silicon stamps fabrication

The first step for the fabrication of the silicon wafers is a 10 min standard cleaning with a piranha solution ($H_2SO_4$:$H_2O_2$ 2:1) and a rinse with 5% hydrofluoric acid (HF) followed by a photolithography process. The photolithography starts with by spin coating 2 μm of standard positive photoresist HIPR 6512 (Fujifilm) on the wafer, followed by a light exposure through a photomask using a photolithography equipment (Karl Suss MA6 Mask Aligner). Then, the wafer is immersed in OPD 4262 developer (Fujifilm) that dissolves the areas that have been exposed. The remaining photoresist is used as a mask in a modified reactive etching Bosch process (in an Alcatel 601-E equipment) that uses combined pulses of SF6 as the etching gas and C4F8 for the passivation step.

The alternation of both gases results in “wells” _craved in the silicon with a scalloping contour (Fig. S1 Supplemental). The depth of the wells is designed to be 7 μm for the smallest well. The depth is different for each array as the silicon etching rate depends

on the diameter of the wells (Table S1-Supplemental). After the etching process, the remaining resist is stripped from the wafer by means of an oxygen plasma (Power = 600 W; O2 flow = 600 ml/min; Time = 20 min).

**Thermal NIL patterned films**

Transparent 500 μm thick polycarbonate sheets were used as thermoplastic substrates. A NPS 300 stepper (SET) was used as imprinting tool for the step-and-repeat thermal NIL process, using the following process parameters: 190–220 ◦C as imprinting temperature, 50–80 kg as applied weight, 1–2 min as imprinting time, 60 ◦C as demolding temperature.

**Thermoforming process**

Thermal NIL micro-structured films were thermoformed using a vacuum-assisted aluminum mold with a half-cylinder geometry, as shown in Fig. 6.4 (b), in which the micro-structured zones are pointing outwards. During the thermoforming process, the heating stage parameters were set at 430 ◦C for 11.5 s (upper heaters) and 500 ◦C for 12.5 s (lower heaters), and the deformation stage had a duration of 1 s. The mold was kept at 80 ◦C during the whole cycle and pre-vacuum and vacuum times were set at 4″ and 3″, respectively, using a vacuum power of 15 W (pressure in the circuit 6 bar).

**Structural characterization**

The local strains and thickness reductions taking place on the films were assessed using *Digital Image Correlation (DIC)* technique [26], comparing digital images of the same films (taken from exactly the same place) before and after thermoforming. The DIC technique allows the identification of the position of each object point in the two images (before and after thermoforming) by applying a correlation algorithm based on the tracking of the grey value pattern G (x, y) in small local neighbourhood facets. Then, the characterization of local in-plane deformations can be determined by the position of these points. Prior to performing the DIC analysis, a stochastic dot-based intensity pattern was defined on the thermoplastic film's surface via serigraphy and a stereoscopic sensor setup was used for the photographic process. In addition, the local linear draw ratios, representative of the degree of geometrical deformation and local film stretching of the different micro-structured zones, were determined in order to check the effects on the microstructures produced by varying deformations. Local linear draw ratios are defined as the ratio of the projected length of a line crossing the centre of the

thermoformed zone to the length in the unformed sheet and were calculated by DIC for each of the micro-structured zones and for the two orthogonal strain directions (major and minor) as shown in Figure 6.5.

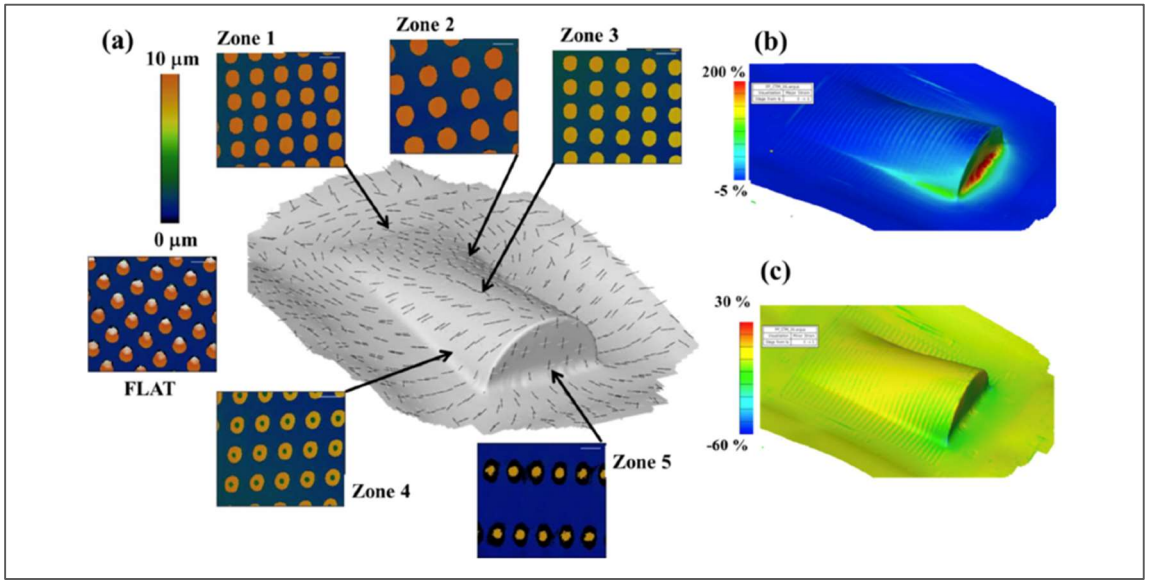


**Figure 6.5. Detail of the strain in the thermoformed film obtained with the Digital Image Correlation technique. (a): Direction of the major (black lines) and minor (white lines) strain directions. A confocal microscopy image corresponding to each of the imprinted thermal NIL areas illustrates how the microstructure deforms. The values of the major and minor strains at each point of the thermoformed film are represented in Figures (b) and (c), respectively.**

### Contact angle characterization.

Finally, water contact angle measurements (WCA) of the virgin PC film and the micro-structured zones before and after thermoforming were taken using a tensiometer (Dataphysics OCA 15 CE) and image processing software (SCA 2.0). Micro-droplets of 150 µL of deionized water were used. The contact angle values are obtained as the average of 5 measurements.

## RESULTS AND DISCUSSION

The study of the effect of the thermoforming process on the microstructure has been carried out using the stamp with the array Q2 (lateral dimensions' *d =6 µm* and *p =12 µm*; Fig. 6.2) for all the zones depicted in Fig. 6.4.b except for zone 2, where the array Q3 was used (*d =8 µm* and *p =16 µm)*. As both arrays have the same *d/p* ratio, the theoretical Cassie- Baxter contact angle remains unaffected, and in consequence, this zone is also considered in the analysis. Before the thermoforming, the five zones were

imprinted by thermal NIL and characterized by confocal microscopy in areas of 250 × 190 μm2. The height of the pillars ranged between 9.4 and 10.4 μm and the pillar diameter resulted to be 6.6 μm ± _0.3 μm. Representative optical and SEM images of the microstructured zones are included in the supplemental information (Figs. S3 and S4). Table 6.2 summarizes the results of the characterization of the textured PC films for the zones 1 to 5 depicted in Fig. 3. In order to determine the wettability behavior for the imprinted areas (prior to thermoforming), the water contact angle was measured, showing an average value of 150.6º. This represents almost a two-fold increase compared to the value of 77 º obtained for the nonmicrostructured PC film. The micro-structuring therefore modifies the surface wetting behavior of the PC, making it superhydrophobic [31]. After thermoforming, the hydrophobic character of the surfaces is preserved even at curvature radius of 50.1 mm and a linear draw ratio of 4.63. The experimental contact angles and the local deformation (strain) observed via the DIC technique are represented in Fig. 6.6 for each of the five selected zones. The zone that suffered the highest stretching is Zone 5, where the water contact angle value descended to 107.1 º compared to the original value before thermoforming (150.6°). This indicates a loss of the hydrophobic character, but still representing an improvement when compared to that of the unformed flat PC film. Representative optical images of the water droplets for measuring the contact angle are displayed in the supplemental information (Fig. S5). Initially, a theoretical estimation of the water contact angle for the different deformed microstructures after the thermoforming was conducted applying the analytical method described in [30]. In this model, the variation of the contact angle shown by different low aspect ratio pillar geometries (almost barrel-shaped) can be estimated as a function of the nanostructure roughness parameters, a, b and h; being *a* the diameter at the top of the nanopillar, *b* the distance between the top corners of a pillar and *h* the height of the nanopillar. In our case, these parameters were carefully extracted from confocal microscopy images of each of the flat and thermoformed nanostructures. However, the images of the confocal microscope show a more elliptical size for the pillars, as well as an asymmetric deformation of the pillar array, in accordance with the difference between major and minor strains. Because of this, we modelled the expected contact angle from the deformed microstructures following the procedure described in [28], which accounts for an irregular pillar shape (data is shown in the supplemental information).

The result is displayed in the red curve of Fig. 6.6. Even using this second formalism, it is obtained that the Wenzel and Cassie-Baxter contact angle theoretical estimation does not follow the trend determined by the experimental contact angle. The discrepancy

between the experimental contact angle and the contact angle estimation assuming a Cassie-Baxter state can be explain attending to the specific deformation that the microstructures suffer when submitted to deformation.

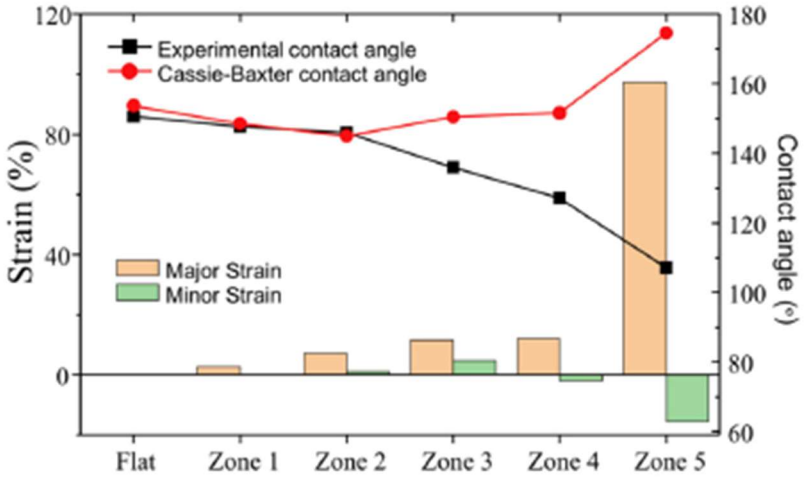


**Figure 6.6. Chart showing the experimental and theoretical (Cassie-Baxter) contact angles in relation to the local major/minor strains for each of the micro-structured zones considered. To calculate the Cassie-Baxter contact angle, the procedure described in [28] was followed.**

A detailed characterization by confocal microscopy of the pillars after the thermoforming process reveals that the base of the pillar increases significantly with the strain at which the plastic film is submitted to. We have quantified this deformation recording the most significant geometrical parameters, as displayed in Fig. 6.7, for the direction of major strain (Data is shown numerically in the supplemental information). It is remarkable that the slope angle of the pillar decreases significantly for the zones 4 and 5, following the same trend than the experimental water contact angle.

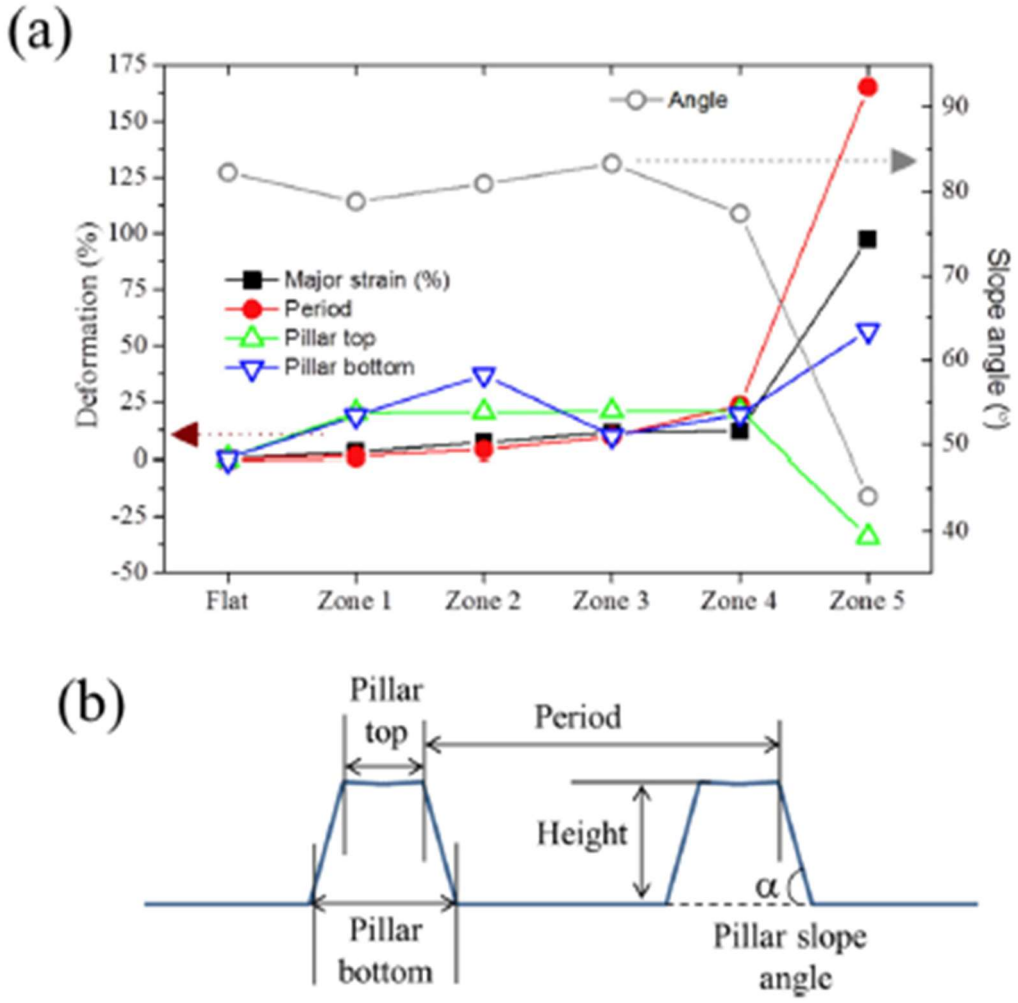


**Figure. 6.7. (a) Geometrical deformation suffered by the pillars at each zone of the thermoformed film. (b) Scheme to refer to each of the geometrical parameters.**

According to the above observation, we hypothesize that the deformation of the pillars increases the actual surface area that is wet by water. The fact that the pillar slope angle decreases implies that the water wets not only the top of pillar, but it also occupies part of the volume between the pillars. Consequently, the contact angle behavior separates from a pure Cassie-Baxter state and approaches to a Wenzel like state. This observation brings us to conclude that that the macroscopic determination of the strain caused by the thermoforming process is not enough to predict the change of the surface properties when the functionalization is generated by an array of microstructures. It implies that in order to predict the final functional of a textured surface after being submitted to a thermoforming process, the manner that the microstructures deform must be accurately investigated.

## CONCLUSIONS

We have presented the controlled incorporation of hydrophobicity in PC films by a combination of thermal-NIL patterning and thermoforming. An initial super-hydrophobic contact angle of 150° is achieved for the flat micro-structured patches on the films (which represents a twofold increase with respect to the non-patterned films (77°). The contact angles of the micro-structured patches after the macroscopic deformations suffered by the film during thermoforming have been measured and correlated with the local major and minor in-plane strains, using the DIC technique. For extreme deformations during the thermoforming process, the hydrophobic character decreases but a substantial hydrophobicity is still retained compared to that of the initial non-micro-structured film. An analytical model developed by Zheng and Lü [28] to predict the water contact angle as a function of micro-pillar geometry based on the Cassie-Baxter equation is applied to the particular case of geometrical variations produced by in-plane deformations resulting from the thermoforming process. This prediction seems to work well for most of the thermoforming induced deformation. However, it deviates for areas where the strain is larger. This deviation might be explained by the fact that, for a very large deformation, either the surface presents a more Wenzel state or the Cassie Baxter modelling does not capture the asymmetric deformation experienced by the pillars. In conclusion, the methodology we have presented here can be used to predict the change in functional properties of a microtextured surface film when subjected to a thermoforming process. Consequently, it could be used, for example, to define geometric parameters of patterns on the NIL stamps to bestow a given texture to the surface prior to thermoforming, knowing a priori the local deformation each area of the surface will experience. It can also provide clues of which maximum strain a thermoformed film can sustain to retain its functional properties.

# REFERENCES


[1] K. Ellinas, A. Tserepi, E. Gogolides, Durable superhydrophobic and superamphiphobic polymeric surfaces and their applications: a review, Adv. Colloid Interf. Sci. 250 (2017) 132–157, https://doi.org/10.1016/j.cis.2017.09.003.

[2] E. Gogolides, K. Ellinas, A. Tserepi, Hierarchical micro and nano structured, hydrophilic, superhydrophobic and superoleophobic surfaces incorporated in microfluidics, microarrays and lab on chip microsystems, Microelectron. Eng. 132 (2015) 135–155, https://doi.org/10.1016/J.MEE.2014.10.002.

[3] M. Lohse, M. Heinrich, S. Grützner, A. Haase, I. Ramos, C. Salado, M.W. Thesen, G. Grützner, Versatile fabrication method for multiscale hierarchical structured polymer masters using a combination of photo- and nanoimprint lithography, Micro Nano Eng. 10 (2021), 100079, https://doi.org/10.1016/j.mne.2020.100079.

[4] A. Fern´andez, A. Francone, L.H. Thamdrup, A. Johansson, B. Bilenberg, T. Nielsen, M. Guttmann, C.M. Sotomayor Torres, N. Kehagias, Hierarchical surfaces for enhanced self-cleaning applications, J. Micromech. Microeng. 27 (2017), 045020, https://doi.org/10.1088/1361-6439/aa62bb.

[5] A. Fern´andez, A. Francone, L.H. Thamdrup, A. Johansson, B. Bilenberg, T. Nielsen, M. Guttmann, C.M. Sotomayor Torres, N. Kehagias, Design of hierarchical surfaces for tuning wetting characteristics, ACS Appl. Mater. Interfaces 9 (2017) 7701–7709, https://doi.org/10.1021/acsami.6b13615.

[6] A. Perez-Gavilan, J.V. de Castro, A. Arana, S. Merino, A. Retolaza, S.A. Alves, A. Francone, N. Kehagias, C.M. Sotomayor-Torres, D. Cocina, R. Mortera, S. Crapanzano, C.J. Pelegrín, M.C. Garrigos, A. Jim´enez, B. Galindo, M.C. Araque, D. Dykeman, N.M. Neves, J.M. Marim´on, Antibacterial activity testing methods for hydrophobic patterned surfaces, Sci. Rep. 11 (2021) 6675, https://doi.org/10.1038/s41598-021-85995-9.

[7] N. Kehagias, A. Francone, M. Guttmann, F. Winkler, A. Fern´andez, C.M. Sotomayor Torres, Fabrication and replication of re-entrant structures by nanoimprint lithography methods, J. Vac. Sci. Technol. B. 36 (2018) 06JF01, https://doi.org/10.1116/1.5048241.

[8] T. Senn, C. Waberski, J. Wolf, J.P. Esquivel, N. Sabat´e, B. L¨ochel, 3D structuring of polymer parts using thermoforming processes, Microelectron. Eng. 88 (2011)11–16, https://doi.org/10.1016/j.mee.2010.08.003.

[9] S. Giselbrecht, T. Gietzelt, E. Gottwald, C. Trautmann, R. Truckenmüller, K. F. Weibezahn, A. Welle, 3D tissue culture substrates produced by microthermoforming of pre-processed polymer films, Biomed. Microdevices 8 (2006) 191–199, https://doi.org/10.1007/s10544-006-8174-8.

[10] S.-H. Shin, B. Hwang, Z.-J. Zhao, S.H. Jeon, J. Jung, J.-H. Lee, B.-K. Ju, J.-H. Jeong, Transparent displays utilizing nanopatterned quantum dot films, Sci. Rep. 8 (2018) 2463, https://doi.org/10.1038/s41598-018-20869-1.

[11] A. Peter Amalathas, M.M. Alkaisi, Nanostructures for light trapping in thin film solar cells, Micromachines. 10 (2019), https://doi.org/10.3390/mi10090619.

[12] Y. Gong, K.J. Cha, J.M. Park, Deformation characteristics and resistance distribution in thermoforming of printed electrical circuits for in-mold electronics application, Int. J. Adv. Manuf. Technol. 108 (2020) 749–758, https://doi.org/10.1007/s00170-020-05377-9.

[13] S. Chen, S. Zhang, Mechanical Behaviors and Thermoforming Features of PMMA Used In-mold Decoration 500, 2014, pp. 440–443, https://doi.org/10.4028/www.scientific.net/AMM.496-500.440.

[14] S.-C. Chen, S.-T. Huang, M.-C. Lin, R.-D. Chien, Study on the thermoforming of PC films used for in-mold decoration, Int. Commun. Heat Mass Transf. 35 (2008) 967–973, https://doi.org/10.1016/j.icheatmasstransfer.2008.04.008.

[15] O. Muntada-L´opez, J. Pina-Estany, C. Colominas, J. Fraxedas, F. Pérez-Murano, A. García-Granada, Replication of nanoscale surface gratings via injection molding, Micro Nano Eng. 3 (2019) 37–43, https://doi.org/10.1016/J.MNE.2019.03.003.

[16] J.M.D.T. Nogueras, Nanofabrication, IOP Publishing Ltd, 2020, https://doi.org/10.1088/978-0-7503-2608-7.

[17] S.Y. Chou, P.R. Krauss, P.J. Renstrom, Imprint of sub-25 nm vias and trenches in polymers, Appl. Phys. Lett. 67 (1995) 3114, https://doi.org/10.1063/1.114851.

[18] P.R. Krauss, S.Y. Chou, Sub-10 nm imprint lithography and applications, in: Annu. Device Res. Conf. Dig, IEEE, 1997, pp. 90–91, https://doi.org/10.1116/1.589752.

[19] A. Francone, Materials and anti-adhesive issues in UV-NIL. PhD Thesis. Institut National Polytechnique de Grenoble-INPG, 2010.

[20] S.V. Sreenivasan, Nanoimprint lithography steppers for volume fabrication of leading-edge semiconductor integrated circuits, Microsyst. Nanoeng. 3 (2017) 1–19, https://doi.org/10.1038/micronano.2017.75.

[21] M. Otto, Reproducibility and homogeneity in step and repeat UV-nanoimprint lithography, Microelectron. Eng. 73–74 (2004) 152–156, https://doi.org/10.1016/j.mee.2004.02.032.

[22] T. Haatainen, P. Majander, T. M¨akel¨a, J. Ahopelto, Imprinted 50 nm features by UV step and stamp imprint lithography method, in: Dig. Pap. - Microprocess. Nanotechnol. 2007; 20th Int. Microprocess. Nanotechnol. Conf. MNC, 2007, pp. 280–281, https://doi.org/10.1109/IMNC.2007.4456213.

[23] A. Francone, T. Kehoe, I. Obieta, V. Saez-Martinez, L. Bilbao, A. Khokhar, N. Gadegaard, C. Simao, N. Kehagias, C. Sotomayor Torres, Integrated 3D hydrogel waveguide out-coupler by step-and-repeat thermal nanoimprint lithography: a promising sensor device for water and pH, Sensors. 18 (2018) 3240, https://doi.org/10.3390/s18103240.

[24] O. Vazquez-Mena, L. Gross, S. Xie, L.G. Villanueva, J. Brugger, Resistless nanofabrication by stencil lithography: a review, Microelectron. Eng. 132 (2015) 236–254, https://doi.org/10.1016/j.mee.2014.08.003.

[25] J. Throne. Technology of Thermoforming (eBook) Hanser Publications, (n.d.). https://www.hanserpublications.com/Products/388-technology-of-thermoforming-ebook.aspx (accessed August 16, 2021).

[26] M. Jerabek, Z. Major, R.W. Lang, Strain determination of polymeric materials usingdigital image correlation, Polym. Test. 29 (2010) 407–416, https://doi.org/10.1016/j.polymertesting.2010.01.005.

[27] B. Thomas Young, An essay on the cohesion of fluids, Philos. Trans. R. Soc. Lond. A 95 (1805) 65–87, https://doi.org/10.1098/rstl.1805.0005.

[28] Q. Zheng, C. Lü, Size effects of surface roughness to superhydrophobicity, in: Procedia IUTAM, Elsevier B.V, 2014, pp. 462–475, https://doi.org/10.1016/j.piutam.2014.01.041.

[29] C.I. Park, H.E. Jeong, S.H. Lee, H.S. Cho, K.Y. Suh, Wetting transition and optimal

design for microstructured surfaces with hydrophobic and hydrophilic materials, J. Colloid Interface Sci. 336 (2009) 298–303, https://doi.org/10.1016/j.jcis.2009.04.022.

[30] E. Puukilainen, T. Rasilainen, M. Suvanto, T.A. Pakkanen, Superhydrophobic polyolefin surfaces: controlled micro- and nanostructures, Langmuir. 23 (2007)

7263–7268, https://doi.org/10.1021/la063588h.

[31] X.J. Feng, L. Jiang, Design and creation of superwetting/antiwetting surfaces, Adv.

Mater. 18 (2006) 3063–3078, https://doi.org/10.1002/adma.200501961.

# 7. ION IMPLANTATION AND PVD-COATING OF MICRO/NANOTEXTURED SURFACES OF THERMOPLASTIC MATERIALS.

## INTRODUCTION

Within this section of the research, the mechanical properties enhancement of micro/nanotextured polymeric parts through the application of hard coatings and ionic implantation treatments was explored.

Initially, samples of polycarbonate were coated with CrN using physical vapour deposition PVD techniques, and the resulting mechanical properties were evaluated and compared to those of the bare PC.

In a second stage of this subsection, ionic implantation tests of two different ions of interest, argon, and silver, potentially enhancing diverse surface properties such as mechanical properties [1] were carried out on the surface of various transparent thermoplastics of interest. The changes produced on the surfaces after the implantation of the first ion (Ar) were then evaluated, including the determination of the morphology variations produced on a micro/nanotextured surface of one of the transparent thermoplastics tested (TPU).

Then, a nanomechanical analysis was conducted on the surface of the other two transparent thermoplastics of interest (PC and PMMA) that were implanted with silver ions.

## MATERIALS AND METHODS

### *Hard CrN coating on PC samples*

The treatment of a small PC sample (approx. 20x10x3mm) by means of a cathodic arc PVD source using an ARC-TECH2 equipment was carried out at the EURECAT facilities was performed, coating the mentioned sample with at thickness of 160nm (10 min exposure time). In order to improve the adhesion of the CrN coating onto the PC sample surface, an anchoring layer of CrN of few nanometers (70 to 90 nm) was coated onto the sample prior to the final CrN application.

Then, the sample overall visual aspect was evaluated, and the mechanical properties (hardness and scratch resistance) of the resulting coated sample were evaluated using a Nanoindenter XP equipment. Details of the equipment and an amplified SEM image of the pyramidal tip can be seen in Figure 7.1.

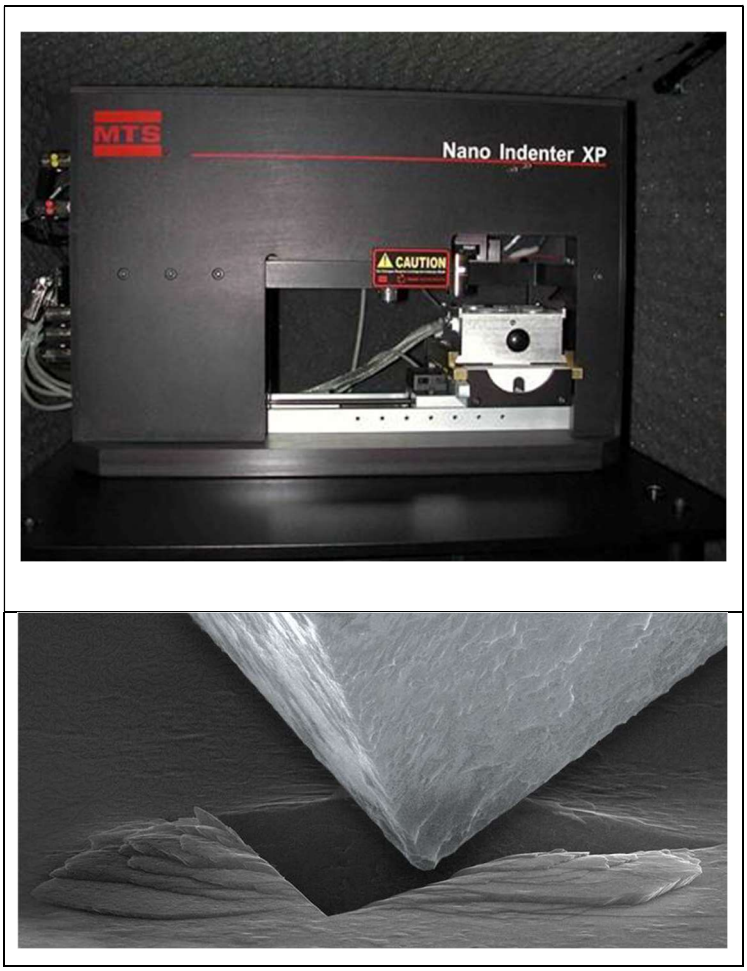


**Figure 7.1. Image of the nanoindentation equipment used for the experiments (above), and amplified SEM image of the Berkovich tip used (below).**

With such equipment, 15 indentations per sample in CSM mode (continuous stiffness measurement) were carried out in order to measure the hardness and young's modulus as per the *Oliver and Phar method* [54]. A pyramidal Berkovich tip C0045048-11-11-19-1000 nm, with an approximation speed of 10nm/s and harmonic oscillation frequency and amplitude of 45 Hz and 2nm, respectively, was used for the tests. The strain rate applied was 0.05 $s^{-1}$ and the maximum depth of penetration was 500nm.For the measurement of the scratch resistance, a scratching speed of 5μm/s was applied, and the load applied on the indenter increased incrementally along the scratching path from 0 to 50mN. The total scratch length was 200 μm.

*Ion implantation of transparent thermoplastics*

In this subsection, samples of non-textured PC of approximately 10x10mm were implanted with Ag+ ions at a voltage of 3kV, using a PFCA-450 equipment, with an

assembled high-voltage source HVPM 30. Then, visual inspection of the samples and their in-depth characterization using SEM, EDX and XPS methods was carried out in order to verify the feasibility of the treatment. Then, a sample of 20x30x3 mm of TPU with micro/nanotextured surfaces (with the topographies present in the stamp 3x3 ) was also ion-implanted under the same process conditions as the previous case, and the morphology variations on the micro/nanostructures were observed. Finally, samples of PC and PMMA were implanted with Ar ions and their nanomechanical properties were analysed. For that, the *dynamic flat punch complex modulus* using a *Nanomechanics iMicroindenter* was utilized. In this method, the indenter contacts the material surface penetrating at a certain depth (3μm by default). The oscillation force amplitude will be that one producing an oscillation of aprox. 50nm @ 100Hz of frequency. The system applies the frequencies programmed and measures the resulting oscillatory displacement and the phase delay at each frequency.

The main measuring parameters applied were:

-Cylindrical flat punch of 50 μm diameter

-Pre-test compression depth: 3 μm

-Minimum frequency: 1Hz

-Maximum frequency 500Hz

-Number of tested frequencies: 15

The main variables of interest analysed for the polymeric samples tested were:

-Storage modulus (E'): related to a material's ability to store energy elastically

-Loss modulus (E''): related to a material's ability to thermally dissipate energy; and accounts for the viscous character of the material.

-Loss factor (tan $\delta$): the fraction E'/E'', defined as tan $\delta$, where $\delta$ constitutes the phase delay existing between applied stress and the resulting deformation. For a purely elastic material, the phase delay is 0 and therefore, the loss factor is 0. For a viscoelastic material, the phase delay will reach some value between 0 and 90°. For a equally elastic and viscous material, the phase delay will be of 45° and the tan $\delta$=1.

The sequence of steps followed for the visual inspections and the implantation processes was as follows:

CLSM initial inspection/cleaning with solvents/ CLSM inspection/ion implantation/CSLM final inspection

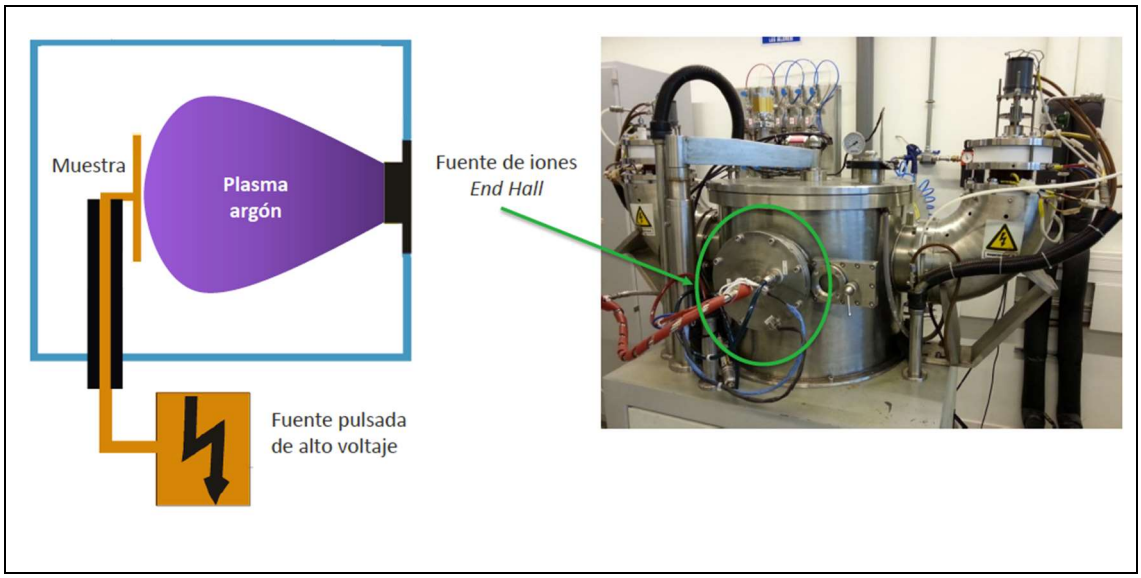


**Figure 7.2. Schematic representation (left) and actual picture of the ion implantation source and device (right).**

## RESULTS AND DISCUSSION

### *Hard CrN coating on PC samples*

First, the variation of hardness as function of penetration depth was evaluated on the PC sample. It was clearly shown that the CrN coating increases the surface's hardness in an order of magnitude, as shown in Figure 47 below.

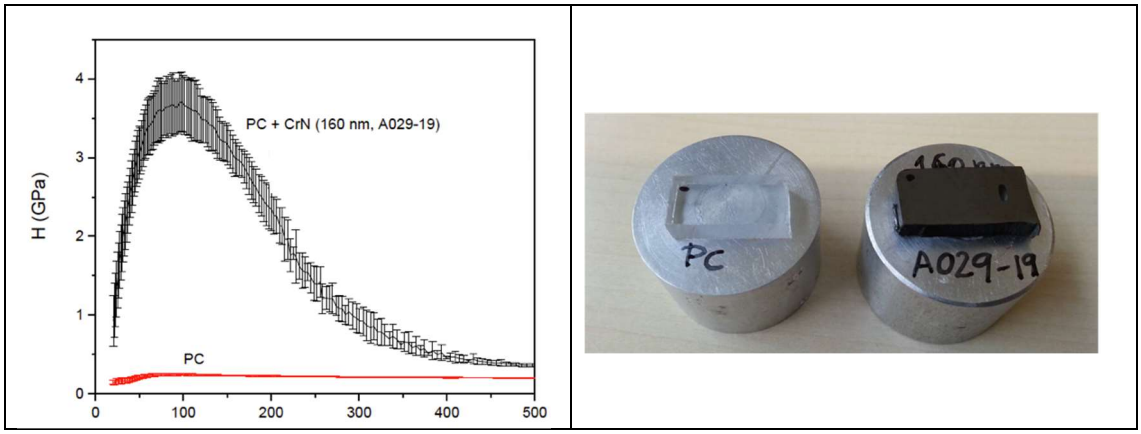


**Figure 7.3. Hardness increase produced by the CrN coating (left), and image of the PC sample before and after being coated with CrN (right).**

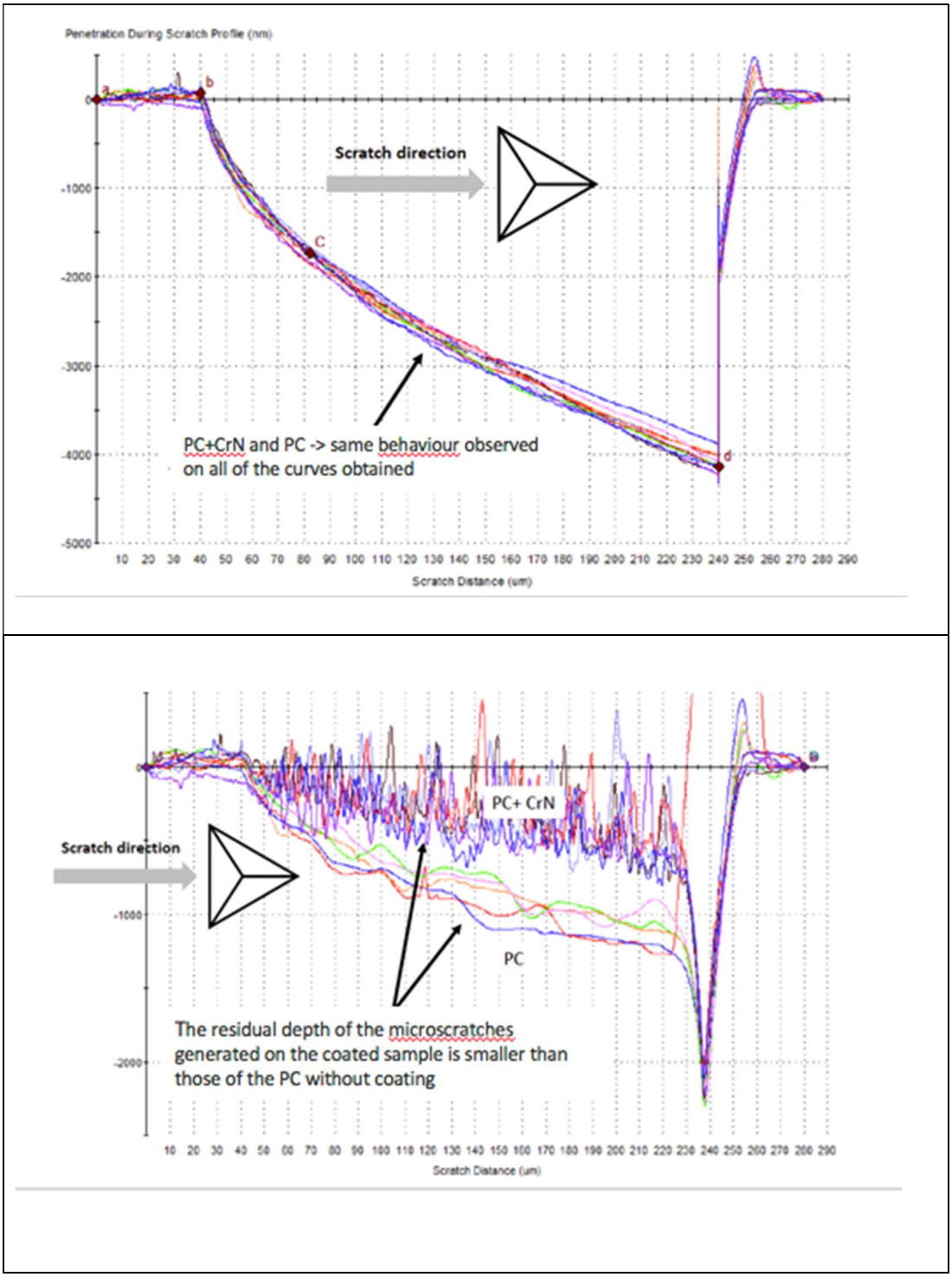


**Figure 7.4. Penetration depth profiles during scratching of the PC and PC + CrN samples (above), and residual morphology profile (below) of the same samples, clearly showing the differences in depths registered for the coated vs the non-caoted sample.**

Nevertheless, the residual depth observed for the scratches produced clearly differs between coated and non-coated samples, as it can be observed on Figure 7.5 below (i.e., lower depth for coated samples).

This fact is further confirmed by the residual depth profiles taken with CLSM, as it can be seen on Figure 7.6.

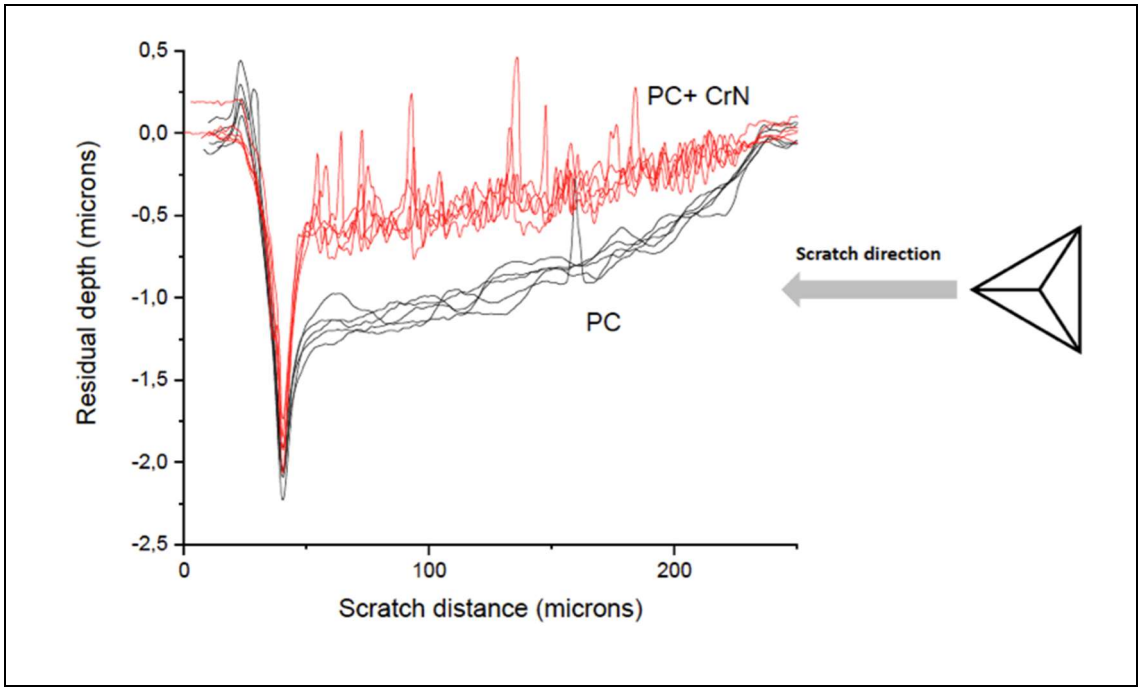


**Figure 7.5. Penetration depth profiles during scratching of the PC and PC + CrN samples, taken using the CLSM images.**

By observing the CLSM 3D constructed images (Figure 7.6), we can also confirm the differences in residual depth produced on the coated samples under the same parameters, which clearly confirms the higher scratch resistance of the coated samples.

*Ion implantation of transparent thermoplastics*

Regarding the initial implantation of PC samples, although major changes in the surface topography were not observed after the ion implantation at 3kV and low vacuum pressure of $2{,}6 \cdot 10^{-2}$ Pa (see Figure 7.7), some white spots and a slightly larger surface roughness was observed.

These areas corresponded to the presence of O, Zn and other elements existing prior to the ion implantation treatment, as revealed by the elemental composition shown by the

EDX measurements at two length scales (100 and 10µm, respectively). This can be observed in Figure 7.8. The presence of these elements can probably be attributed to impurities present during the injection moulding process or else during the later sample handling.

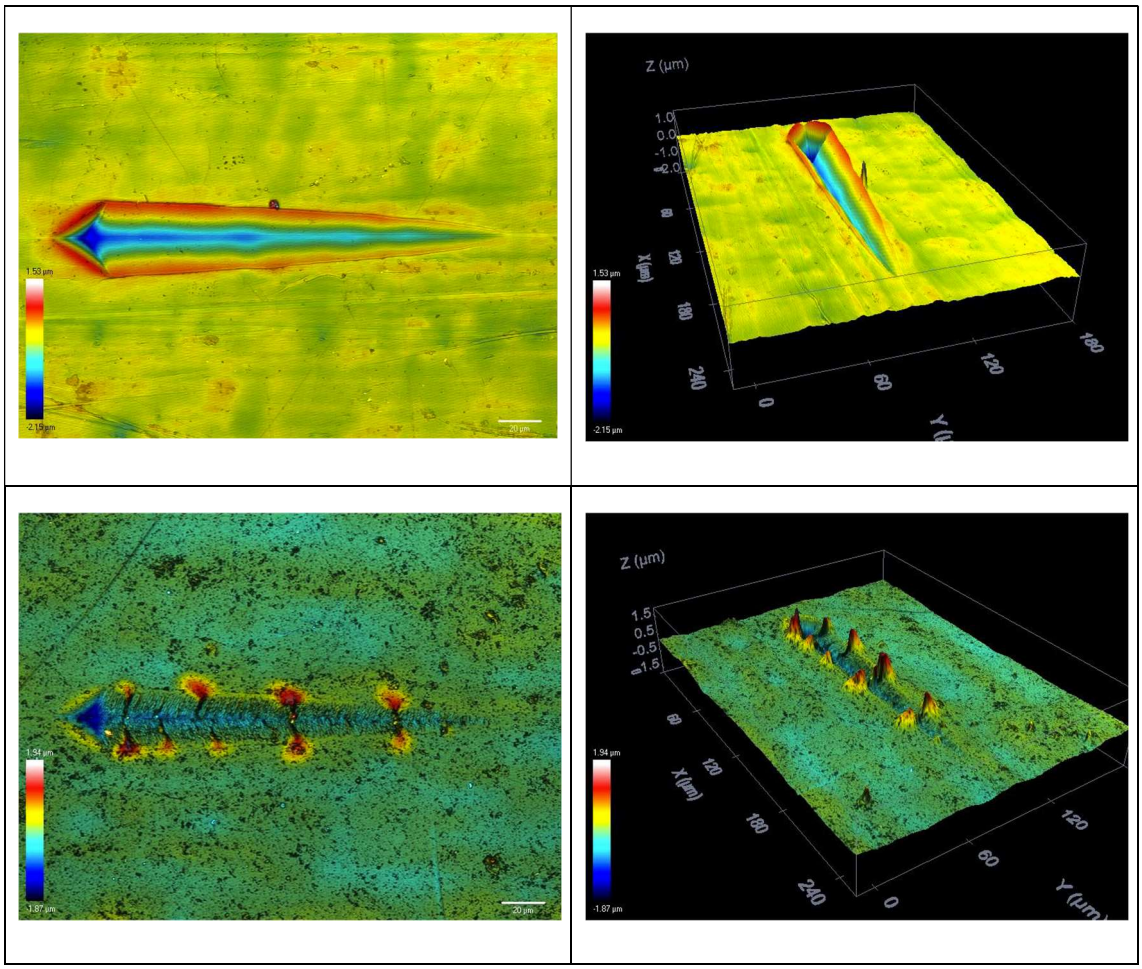


**Figure 7.6. 3D CLSM images of the residual scratches produced on PC (above) and PC + CrN (below), clearly showing the differences on morphology created, caused by different scratch resistances.**

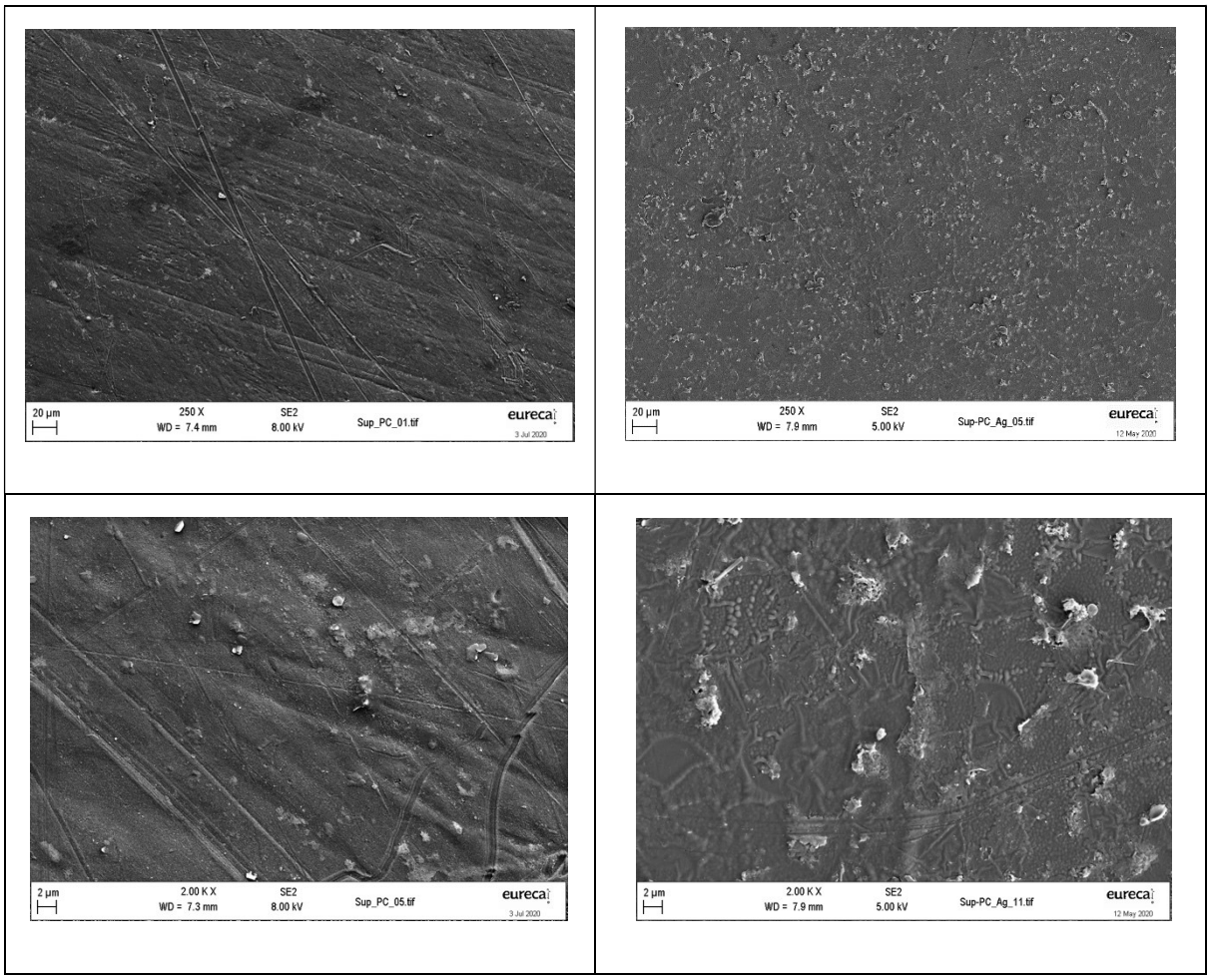


**Figure 7.7 SEM images at 250X (above) and 2000X (below) of the PC samples before (left) and after (right) Ag+ ion implantation**

Finally, the XPS measurements clearly show a percentage of Ag accumulation in the first nm of thickness of the implanted sample, compatible with the process and conditions applied.

After the initial measurements following the first ion implantation trials, a micro/nanotextured TPU sample (injection moulded using a 3x3 micro/nanotextured film inlay as per section 4.1.1) was also ion implanted with Ag+, at a voltage of 3 kV and a vacuum pressure of $2{,}7 \cdot 10^{-2}$ Pa.

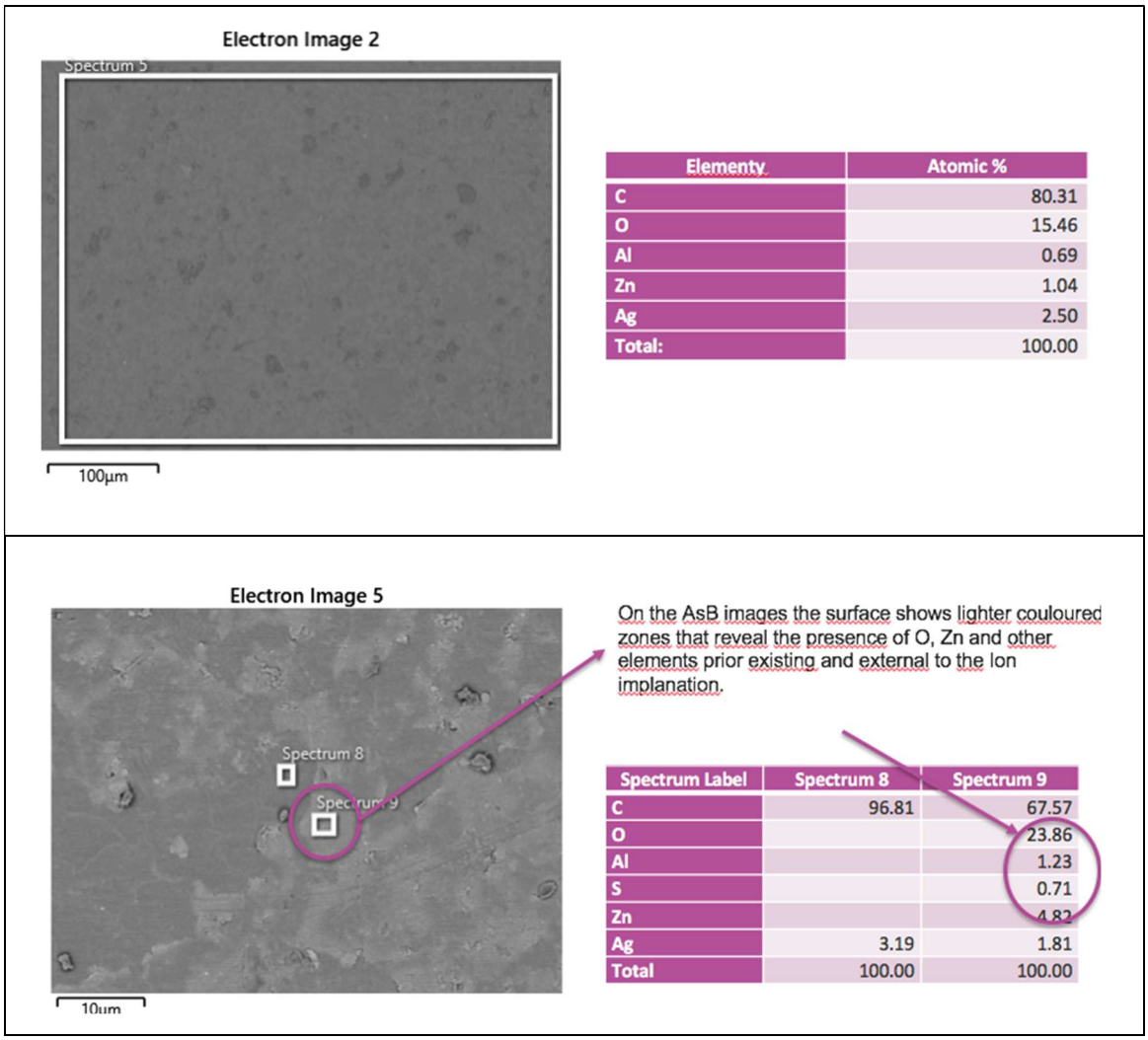


| Elementy | Atomic % |
|---|---|
| C | 80.31 |
| O | 15.46 |
| Al | 0.69 |
| Zn | 1.04 |
| Ag | 2.50 |
| Total: | 100.00 |

| Spectrum Label | Spectrum 8 | Spectrum 9 |
|---|---|---|
| C | 96.81 | 67.57 |
| O | | 23.86 |
| Al | | 1.23 |
| S | | 0.71 |
| Zn | | 4.82 |
| Ag | 3.19 | 1.81 |
| Total | 100.00 | 100.00 |

**Figure 7.8. EDX images and data of the Ag+ implanted PC samples at 3kV and low vacuum pressure of $2{,}6 \cdot 10^{-2}$ Pa at two different magnifications, showing the presence of O, Zn and other foreign elements apart from the implanted Ag+.**

From a general visual inspection, it could be clearly appreciated a darkening and loss of transparency of the implanted sample (Figure 7.11). Also, when looking at the confocal images at 50X magnification, it could be observed that even the general aspect of the microstructures remained intact, a small amount of the micro/nanofeatures were damaged or missing, most probably due to disruptions caused on them by micro-electric arcs.

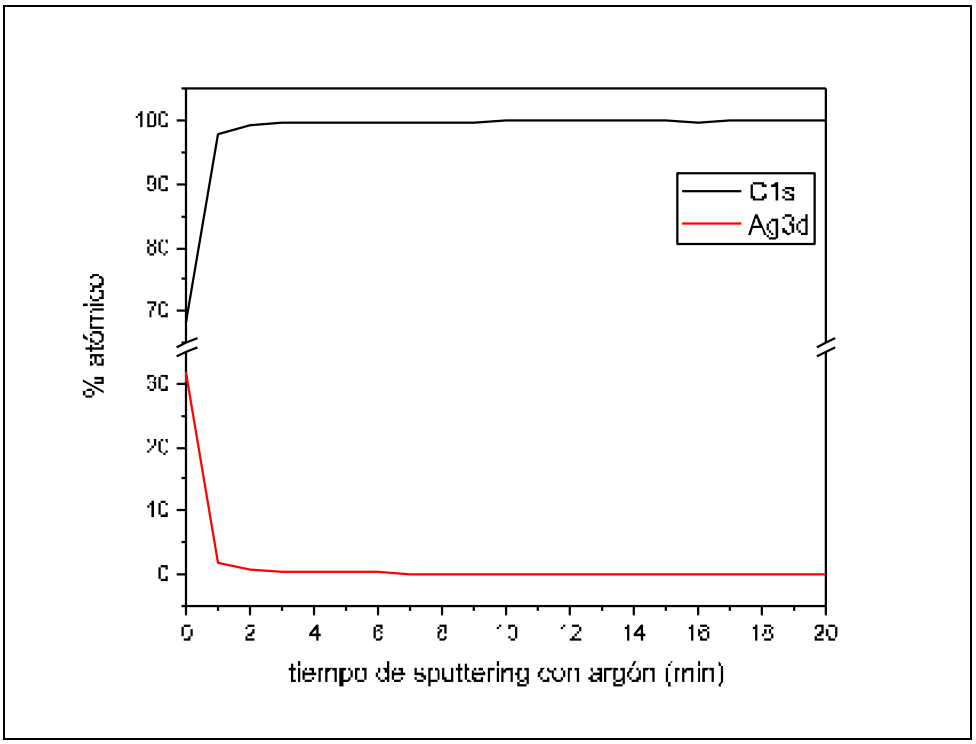


**Figure 7.9. Graph of the XPS measurements on the Ag+ implanted PC sample, showing a significant % of Ag3d onthe initial nanometers of sample's depth.**

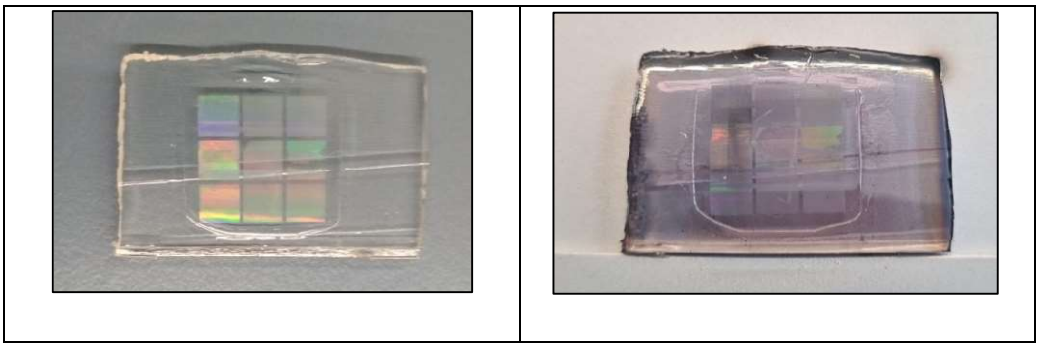

**Figure 7.10. Picture of the micro/nanotextured TPU sample before (left) and after (right) the ion implantation.**

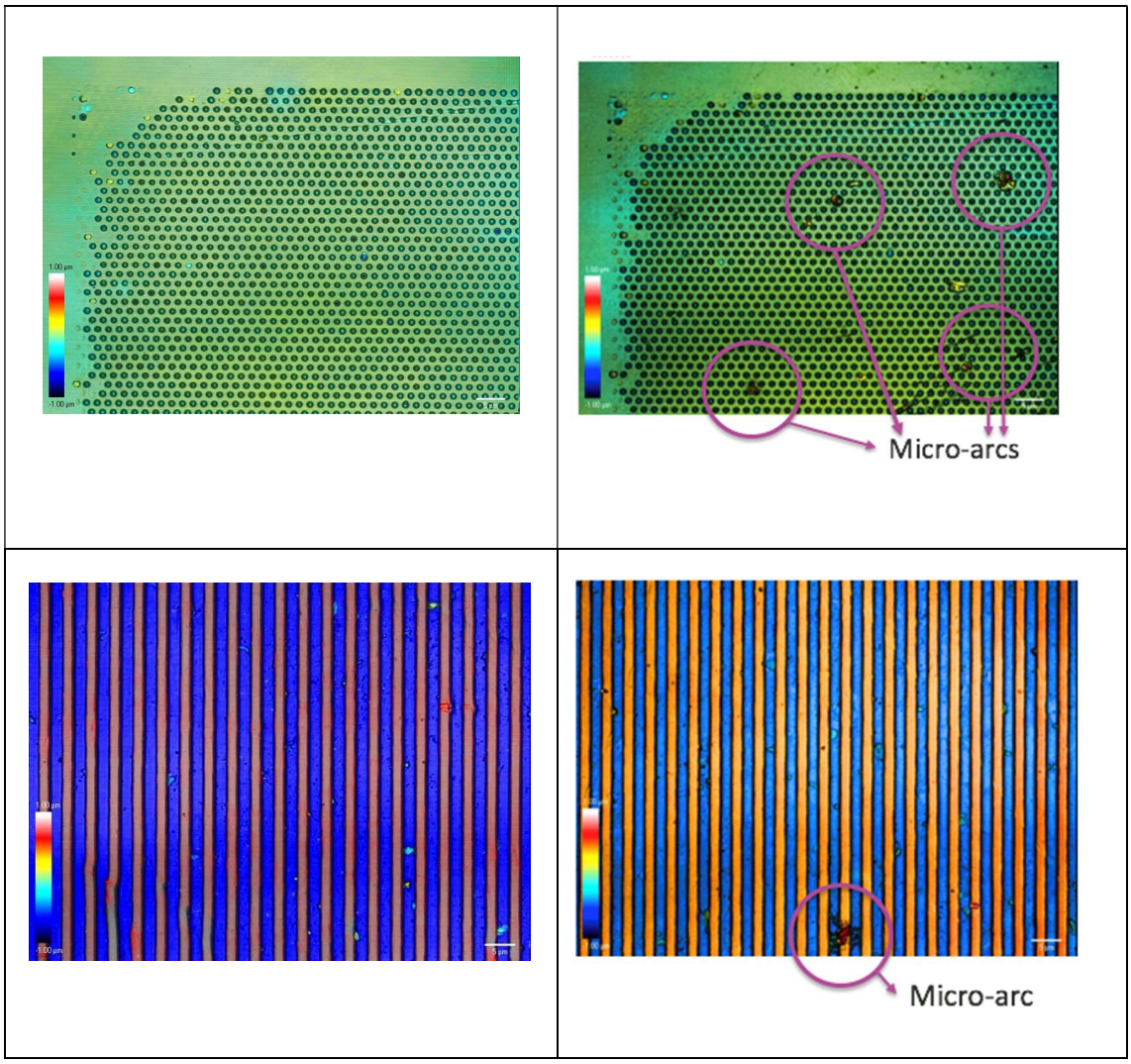


**Figure 7.11. CLSM images of the TPU sample before (left) and after (right) the ion implantation process. The images show the 1µm diameter micropillars (above) and the 2 µm width vertical lines (below) from the experimental stamps initially used in chapter 3.**

Also, profiles extracted out of CLSM images of these samples before and after the implantation process were extracted to compare for other potential disruptions. Those images for the horizontal 2 µm width lines and for the 1 µm diameter pillars, and the height profiles extracted from them, can be seen on Figure 7.12 and 7.13. Although no major disruption of the microtexture geometries is observed, it can be seen that there exists a certain flattening of the top section, in both the horizontal lines and the cylindrical pillars, which might be attributed to partial polymer degradation of the micro/nanofeatures due to the cleaning agents used on the sample preparation (Ethanol).

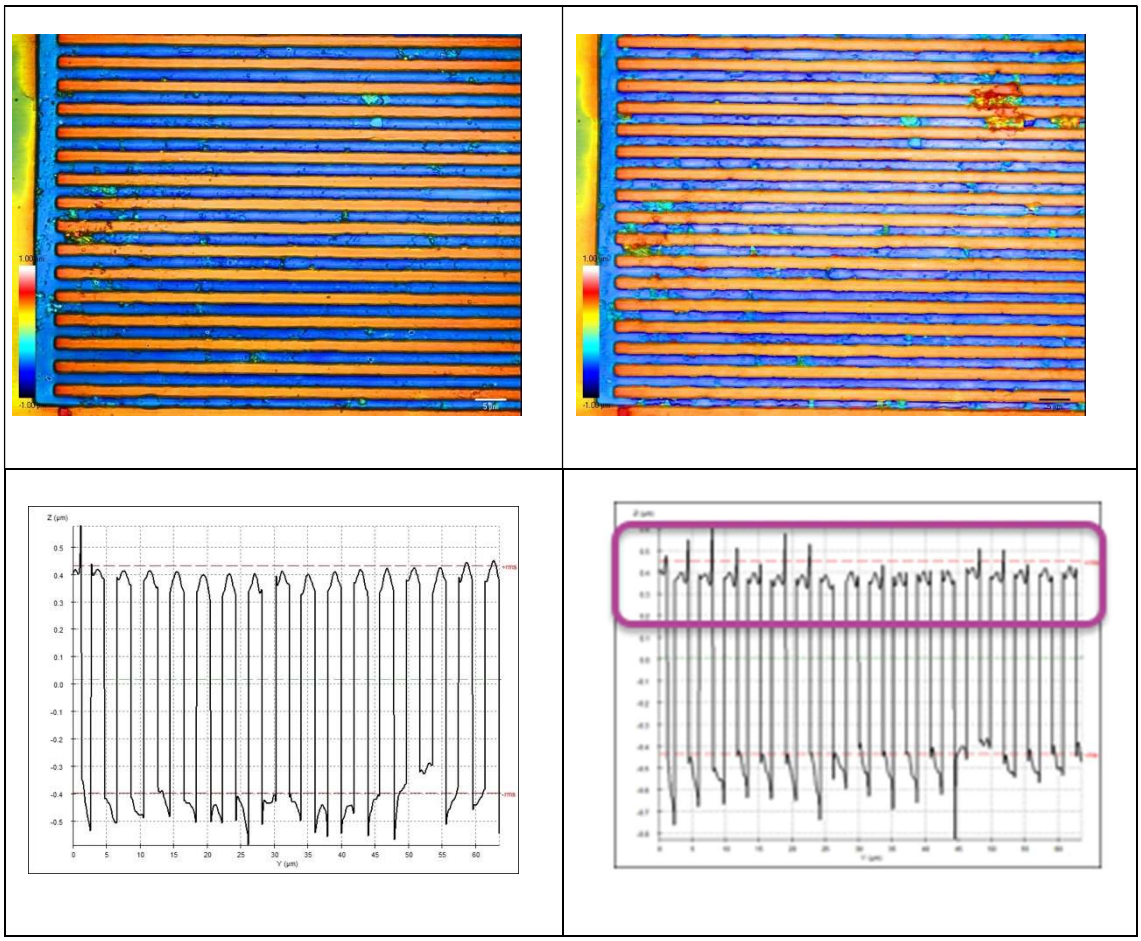

**Figure 7.12. CLSM images of the TPU sample before (left) and after (right) ion implantation, showing the subtle change of the top of the lines after implantation on the profiles extracted (below).**

To complete this section of the study, samples of PC and PMMA were implanted with Ar ions at different process conditions (time, bias voltage) and their nanomechanical properties, together with the resulting degradation that took place (if any) were analysed. The following samples, treatment conditions and resulting degraded/non degraded samples were used:

| Sample Nr. | Bias (kV) | T(min) | PC degraded? | PMMA degraded? |
|---|---|---|---|---|
| 025-21 | 25 | 45 | Y | N |
| 026-21 | 5 | 45 | N | N |
| 027-21 | 25 | 5 | N | N |
| 028-21 | 10 | 45 | N | N |
| 029-21 | 15 | 45 | N | N |
| 030-21 | 20 | 45 | N | N |
| 031-21 | 10 | 135 | N | N |

**Table 7.1.** Details of the process conditions applied and summary of the resulting degraded samples.

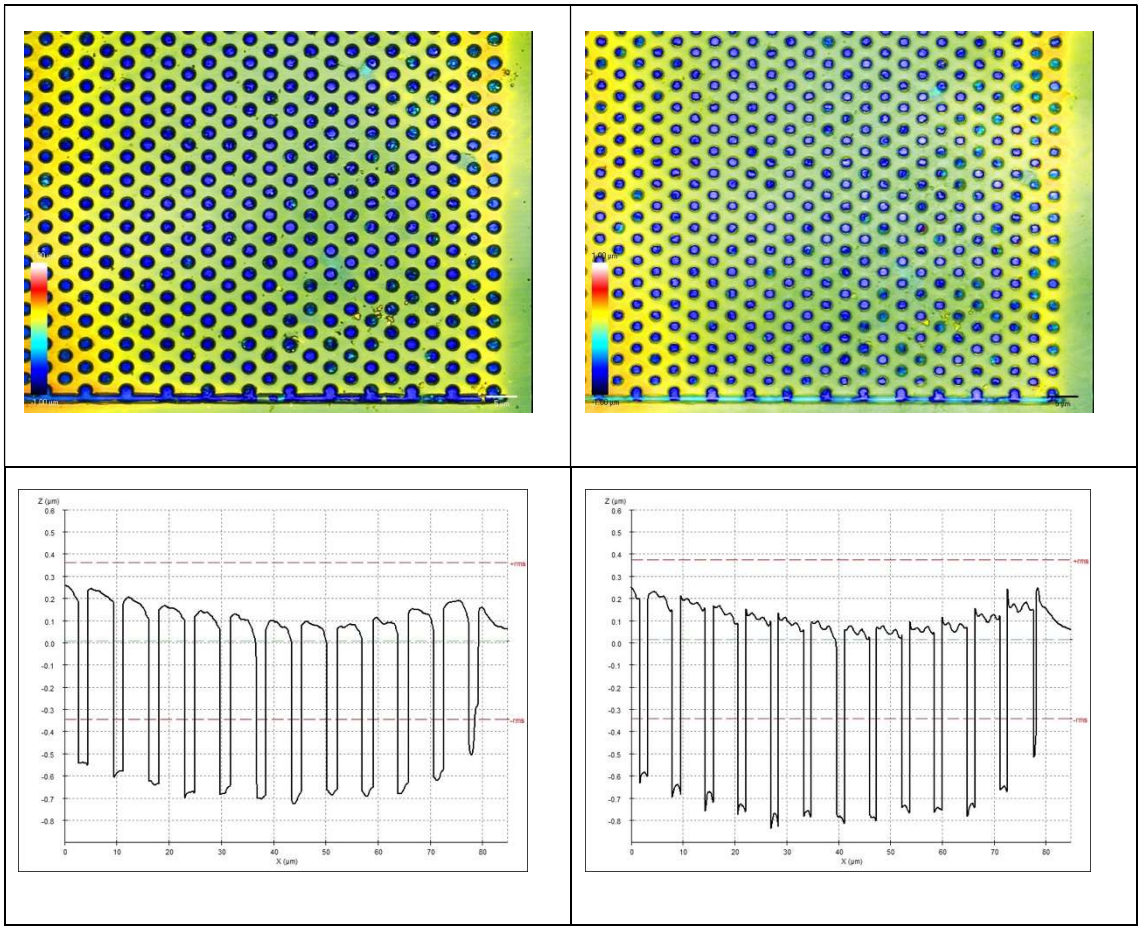


**Figure 7.13. CLSM images of the TPU sample before (left) and after (right) ion implantation, showing the subtle change of the top of the pillars after implantation on the profiles extracted (below).**

The results of the obtained storage modulus, loss modulus and loss factor for both polymers can be observed in the charts below.

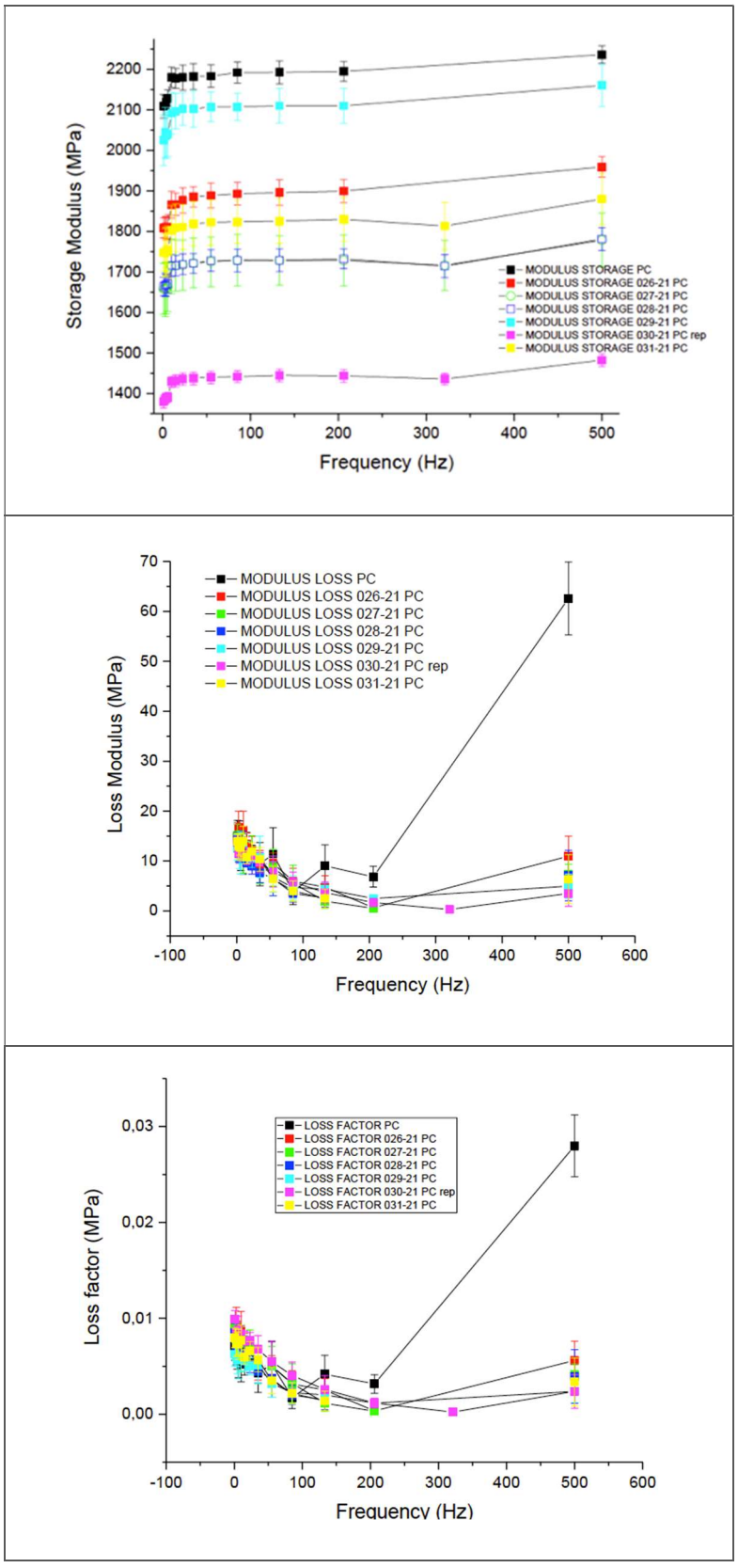


**Figure 7.14.** Storage modulus, Loss modulus and loss factor for the PC samples.

As it can be seen on Figure 7.14, all the implanted PC samples present a decay of their elastic component when compared to the non-implanted PC.

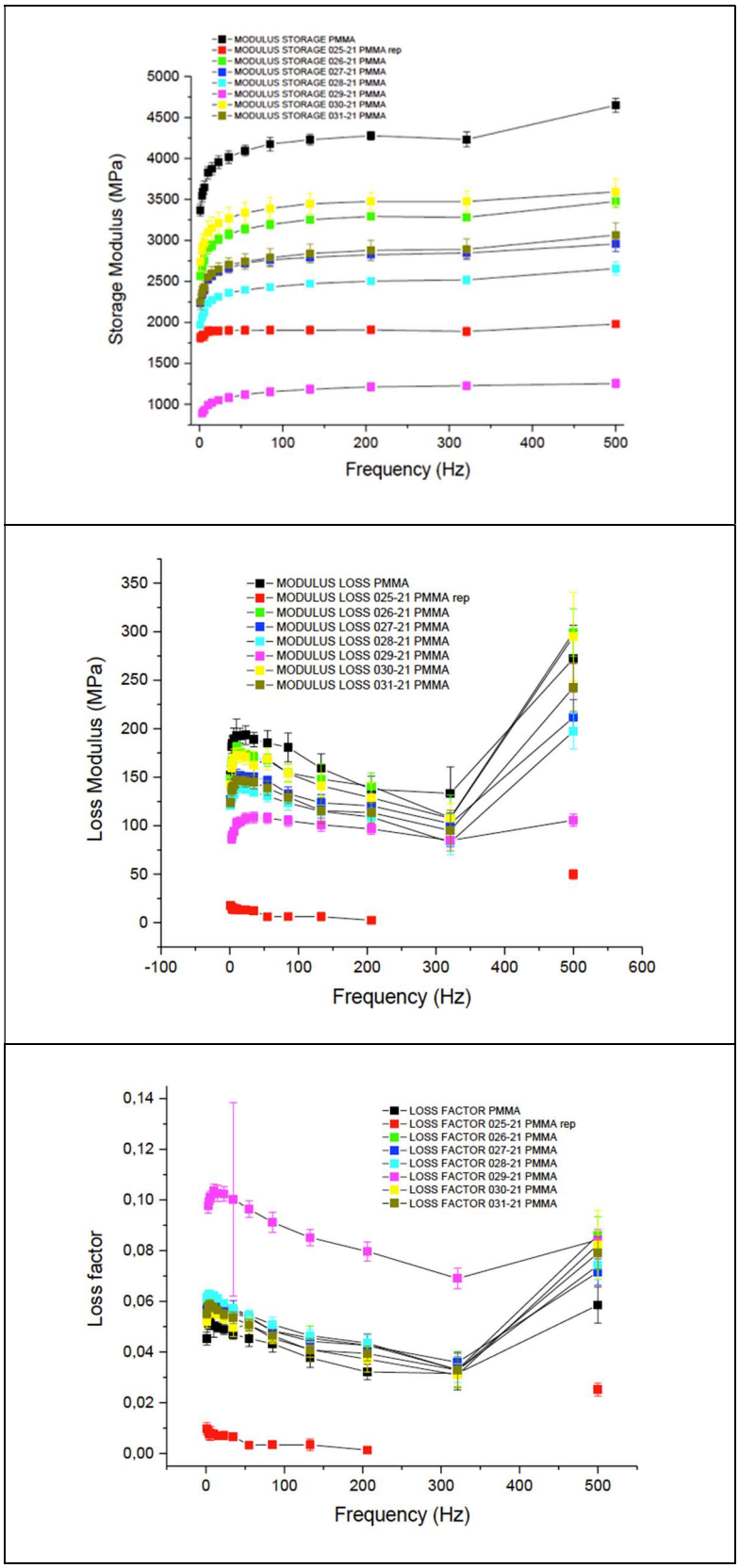


**Figure 7.15.** Storage modulus, Loss modulus and loss factor for the PMMA samples.

As it can be seen on Figure 7.15, all the implanted PMMA samples present a decay of their elastic component when compared to the non-implanted PMMA.

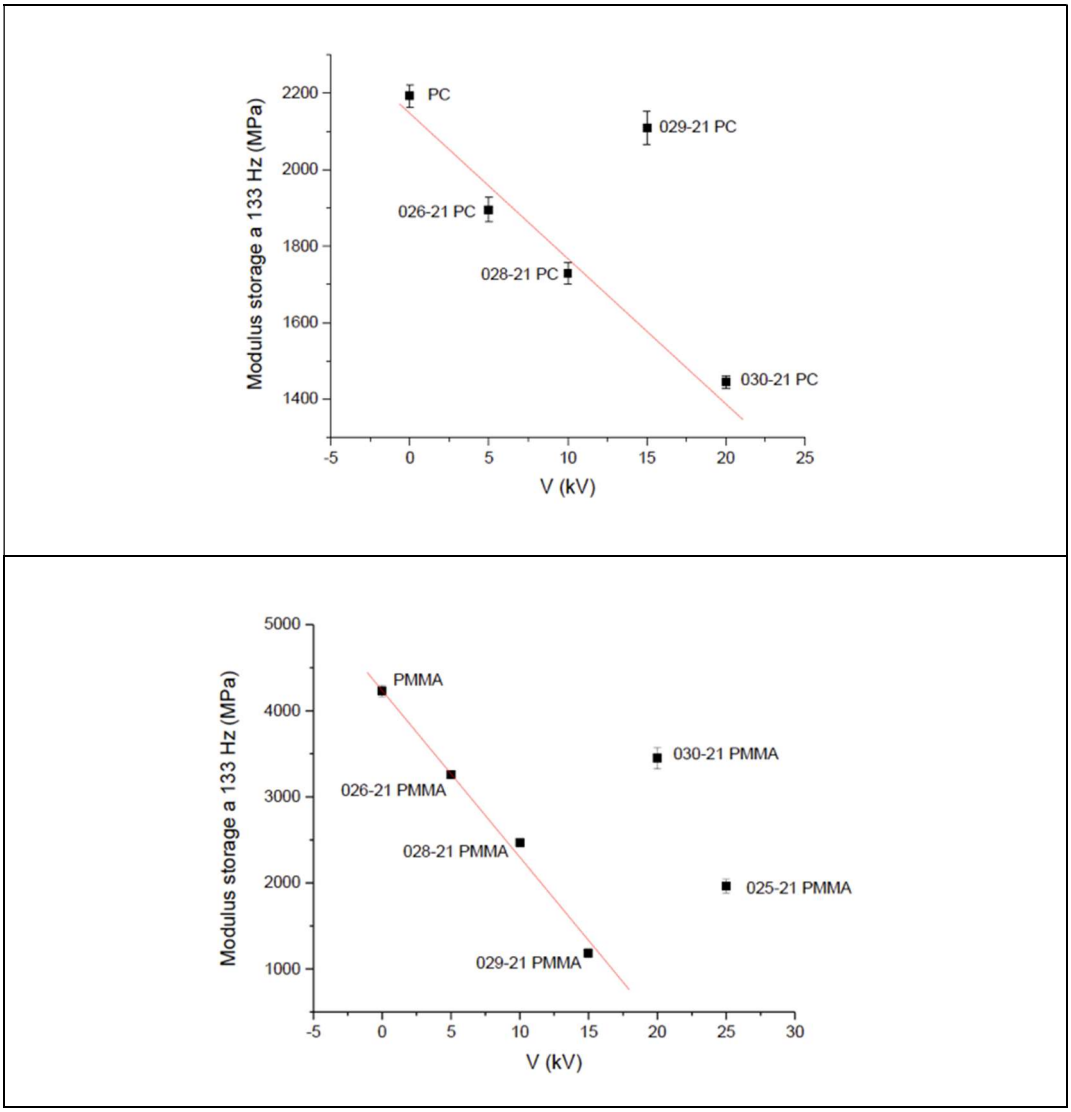


**Figure 7.16.** Evolution of the storage modulus with applied voltage for PC (above) and PMMA (below)

As observed in Figure 7.16, both PC and PMMA seem to experiment a linear decay of their respective storage moduli with increasing applied voltage (except for one sample in the case of PC and two for PMMA).

## CONCLUSIONS

The application of hard coatings to thermoplastic polymeric parts via PVD techniques was successfully demonstrated as a suitable technique to enhance the surface hardness (by an order of magnitude) and scratch resistance of polycarbonate samples. Nevertheless, the transparency of the sample was affected as expected.

Ion implantation tests with two different ions have been conducted as a process to potentially improve a wide range of properties of the thermoplastic materials. The applicability of these treatments on thermoplastic materials has been proven, showing only a small loss in transparency (that could vary as a function of the ion implanted) and a slight decay on their mechanical properties, shown by decays in both elastic and loss modulus components of their complex modulus has been observed. These losses in mechanical properties can nevertheless be minimised by the optimisation of the bias voltage and the exposure time depending on the specific ion implanted.

Also, when applying such treatments over micro/nanotextured surfaces, some small disruptions on the micro/nanotextures top surfaces were observed, most probably caused by small electric arcs produced during the application of the treatment. Nevertheless, the micro/nanotextured surface largely preserved its morphology undamaged, and the small defects produced by the electric arcs can probably be solved by careful fine tuning of the implantation conditions. These small disruptions might even be taken advantage of to further refine the micro/nanostructure morphology or introduce additional hierarchical levels on it.

# REFERENCES

[1] Popok, Vladimir. (2012). Ion implantation of polymers: Formation of nanoparticulate materials. Reviews on Advanced Materials Science. 30. 1-26.

[2] Di Benedetto F., & D'Amore A., Mosca M., Massaro M., Cassano G., Capodieci L., Esposito C., Tapfer L. (2015). Ion Implantation in thermoplastic polymers. https://doi.org/10.1109/NANOFIM.2015.8425354.

[3] Kavetskyy T., Stebeletska N., Borc J., Kravtsiv M., Graz K., Šauša O.,Švajdlenková H., Kleinová A., Kiv A., Tadeush O., Stepanov A.L., Long-range effect in ion-implanted polymers,Vacuum, Volume 200,2022,111038, https://doi.org/10.1016/j.vacuum.2022.111038.

# 8. FINAL DISCUSSION AND OVERALL CONCLUSIONS

## Final discussion and future outlook

The replication of micro- and nanotextured polymeric surfaces manufactured via injection moulding presents several challenges that need to be addressed before being completely industrialized in the future. Amongst those, the uniformity on the degree of replication (DR%) of the micro- and nanostructures and the development and adoption of tight quality-control methods are of paramount importance to guarantee consistent quality for serial produced goods.

During this study, it has been observed that several production methods can achieve the appropriate DR% of complex micro/nanostructures of high aspect ratio or multiple hierarchical levels, but there still remains significant uncertainty on achieving it over large surfaces. This is especially critical for the case of high- or very-high aspect ratio (HAR) micro/nanostructures, that will certainly require very tight control of the surface temperature and injection parameters (such as injection speed and holding pressure) across large surfaces.

The tight temperature control will probably require not only dynamic mould surface modulation, a typical capability of the existing variothermal injection moulding systems but will also need differential cooling or heating rates in different mould zones with independent modulation and controls. As we have previously discussed, the current variothermal mould technologies are positioned ahead than other injection moulding tooling options for the replication of complex micro/nanostructures due to their higher replication capability for HAR micro/nanostructures, but they haven´t yet been widespread applied in the industry. They still show a high implementation cost and lack the needed flexibility, mainly due to the fact that such systems are single-mould specific, which means a new system has to be custom designed and implemented every time a new geometry is to be manufactured via injection moulding.

In this sense, the approach using flexible polymeric micro/nanotextured films as mould insert templates, which has been studied during chapters 4,5 and 6 of this thesis, constitutes a potential alternative to VIM systems and reveals itself as very promising due to its low material cost, quick manufacturing, and potential applicability to a wide range of materials. These films start to be manufactured through roll-to-roll processes at pilot scale, specially for optical and medical applications, which will strongly lower their manufacturing costs. It is also foreseeable that an increase in the aspect ratios of the micro/nanotextures will be obtainable in the short-medium term.

Nevertheless, substantial work has still to be performed with these films in order to reduce the amount of manual labor associated with their manufacturing and make them more uniform. Also, the types of film materials and polymer coatings that can be used on them should be substantially extended, carefully considering them together with the polymers to be injected, and increasing the range of anti-stick treatments that can be applied on top of them. This will in turn greatly improve the coated-film’s durability due to the ease of demoulding obtained.

It is envisaged that, in the future, quartets of adequate polymer film material/micro-nanotextured polymer-coating/anti-stick treatment/injectable polymer combinations will

have to be defined and extensively tested in order to further push the implementation of this lower cost technology. This will achieve the best possible results in terms of DR% and uniformity. In any case, this technology will probably arrive to full application in sectors of lower volumes (such as for example medical devices or human protheses), high personalization and high-added value products, due to the cost savings associated with it.

For high-volume and lower added-value products, apart from other technologies outside the replication domain that rely on direct machining, controlled growth or coating or chemical etching, femtolaser mould micro/nanotexturing followed by ICM, VIM or VICM is the dominant route due to its robustness and higher uniformity of replication. This is achieved at the expense of high capital costs (in terms ox expensive equipment needed) and longer processing times. The relatively novel femtolaser technology for metallic mould microtexturing, apart from requiring a very high initial investment in equipment, also requires long calibration times and is still limited to the low micrometer range in terms of the microtexture dimensions, which hinders its wide applicability in the industry apart from high-added value optical and medical applications,

Other foreseeable challenge is the extension of the micro/nanotextured surfaces to complex 3D shapes, which can also be accelerated by the advantages of use of flexible mould inserts. While this is already a reality when for the femtosecond laser machining; it's still limited to only few materials (tool steels and few polymers) and low-micrometer range of texture dimensions. In the case of the flexible polymeric films, carefully designed handling, and pre-processing protocols (prior to be used as mould inserts) for several of the processes they undergo in their manufacturing will be crucial to ensure their quality.

These should for example include micro/nanofeature distortion and variation in the overall surface functionality caused by the forming processes aimed at producing a 3D film template. The variation in the functionalities caused by other processes such as coatings, ion implantation, cutting …etc., should also be researched and adequately defined to further favour the industrial application of the flexible film nanotextured inserts.

Another important challenge to be solved is the extension of these replication processes via injection moulding to a wide range of polymeric materials. It will be important to guarantee a consistent DR% for polymers of various configurations and masterbatches, such as those of low fluidity, added reinforcement agents such as short fibers or whiskers, those containing other additives such as high-molecualr weight ones…etc. A big portion of the existing research has been carried out for high-fluidity and low molecular weight polymers such as PP or PE, but other polymers of more complex processing and advanced properties (such as glass fiber-reinforced polyamides, PEEK, PEI, …etc., to cite some) should also be included in the research of these replication processes.

It is also important to mention that the optical characterization of the micro/nanotextured surfaces obtained will have to further improve the current existing methods in terms of accuracy and speed. Currently confocal microscopy and SEM techniques are the most applied methods, but both lack either sufficient resolution (lateral/oblique definition for the confocal microscopes) or processing speed (for the SEM). Both show some other limitations in terms of applicability on different materials, such as being limited to

conductive materials for SEM, or showing difficulties when applied to transparent materials such as the case of confocal microscopy. This creates the need for prior sample preparation that is very much time consuming and hinders their industrial implementation, also caused by the high cost of these equipments and by the fact that they are usually not suitable to be used in industrial environments but rather in laboratories.

In terms of the durability of micro/nanotextured surfaces, still a lot of work needs to be carried out to define the appropriate treatments (such as coatings, ionic implantations, PVD…etc.) that will maximize the durability of this type of surfaces in various applications and environments. This won't be an easy step due to the fact that many possible treatments might go in the opposite direction to that of the obtained functionalities, directly lowering them down or limiting their durability, and in this sense subsuperficial hardening and functionalization techniques such as ionic implantation are very promising.

The possibility of overcoming all these challenges at low cost and high throughput still remains to be fully proven. An increase in functionalities and potential application sectors observed during the last years of this technology's short lifetime (due to the reduction in the nanostructure dimensions and their increased complexity) has nevertheless created the general opinion that it is a matter of time until we see and extended presence micro/nanotextured functional surfaces in plastic objects commonly used in our daily lives.

Overall Conclussions

The path to obtain micro/nanotextured functional surfaces on thermoplastics using injection moulding techniques was explored in this thesis. Two main technical approaches for the production of such surfaces on thermoplastic parts were followed:

- injection moulding using laser-textured inserts, and
- injection moulding using NIL – textured film inlays.

Additionally, a third technique to bring micro/nanostructured thermoplastic thin films from 2D to 3D shapes via thermoforming techniques was also explored.

Various approaches using complementary technologies were tested in order to explore their potential benefits when applied to the replication processes via injection moulding (ICM, IR-heating) or to the enhancement of the properties of the micro/nanotextured surfaces produced (hard coatings, ion implantation).

**Injection Moulding (IM) Using Laser-Textured Inserts.**

The injection moulding of thermoplastic parts using laser-textured inserts was carried out with several microstructured inserts of various aspect ratios and functionalities:

- A $2^3$ DOE was carried out during the experiments to figure out the most influencing processing parameters between melt temperature, holding pressure and

injection speed. It was shown that melt temperature first, and the interaction between holding pressure and melt temperature in the second place are the dominant factors in the DR% response.

- The corresponding characterizations of the injected samples, both morphological and functional, showed the industrial applicability of this technology when using microstructures of low AR (>2) using regular isothermal injection moulding for the enhancement of properties of the surfaces of injected parts.

- These results and their potential industrialization were further demonstrated by the real application cases corresponding to two experimental interior car parts within the PLASTFUN project shown in the text.

- For higher ARs and therefore slenderer micro/nanofeatures, some kind of Advanced processing technique is required to overcome the frozen layer formation and guarantee the complete filling of the micro/nanocavities provided by a longer-lasting melt polymer flow during the injection process.

**Injection compression moulding (ICM)**

- Injection compression moulding techniques were tested with this purpose during this research, in order to analyse the potential mould filling improvements obtained. It was shown that no major improvements on the mould filling of a particular microstructure of AR~2 were obtained, and surprisingly some non-uniform replication across the sample width was obtained for the samples tested. Even if in the written literature [21,30,31] this type of process reveals the enhancement on the DR%'s obtained, an in-depth mould and microstructured cavity design review of the case researched should be performed in order to explore its full potential. Nevertheless, the process remains as an interesting alternative to enhance not only the DR% but also the homogeneity of the optical properties of parts produced with it, due to the uniform thicknesses and reduced warping parts it is able to provide.

**IM by IR-heating:**

- The other process enhancement application researched within this section was the mould surface heating using infrared heaters (IR-heating). The improvements on the DR% obtained for an AR of the microstructure of 2 (same as in the ICM study) were higher than 20%. These results demonstrate the validity of this technology to industrially replicate microstructured parts of high AR via injection moulding.

- The maximum potential of this technology seems nevertheless hindered by unwanted heat dissipations that could be minimised by isolating some parts of the injection mould, such as those containing the microstructured surface.

- In any case, to achieve the full potential of this technology, a design review of the mould and microstructure size, and its position on the mould surface in coordination with the heat source size utilized should be carried out in the future.

**Injection Moulding Using NIL – Textured Film Inlays.**

Concerning the second part of the research, the feasibility of replicating micro- and nanotextures on injection moulded polymeric surfaces using a coated polymeric film as mould inlay was demonstrated:

- This technique has lower cost and lower complexity approach (vs using textured metallic inserts) proved viable, yielding high DR%'s, even for amorphous thermoplastic polymers of low fluidity (PC, PMMA).

- A 23 DOE was also carried out in this case, that showed melt temperature as the dominating (and critical) processing factor, followed by the interaction between melt temperature and holding pressure.

- These results confirmed the feasibility of the method to obtain high micro/nanotexture DR%'s at the regular processing temperatures and pressures of the injected polymers. The main cause identified is the delay on the frozen layer formation and therefore the longer available time for the injected polymers to flow in the micro/nanocavities.

- Nevertheless, the low number of parts per polymeric inlay still needs to be dramatically increased towards the process industrialization, and therefore a lot of improvement needs to be implemented on the micro/nanotextured coated polymeric inlays. Those improvements should be carried out with the purpose of increasing coating-film adhesion and reducing film coating brittleness, which could therefore increase the satisfactory injected parts per film achieved.

- A high replication degree of hierarchical micro/nanostructures was also achieved with this method, and its extension to biopolymers of current interest proved to be favourable. The higher fluidity and lower melt temperatures of these materials can explain this high DR%. These polymer properties delay also in turn the film inlay degradation.

**To complete this chapter, three additional studies were carried out:**

i) the application of a multiscale finite element simulation method to the process of microcavity filling
ii) the study of the change in functionality of microtextured films upon large macroscopic deformations
iii) and the application of hard coatings and ion implantation treatments to the surface of micro/nanotextured polymeric parts.

i) In the finite element simulation, the multiscale approach followed by combining two commercial FEM softwares at macro- and microscale in order to simulate mould filling phenomena proved its feasibility, and the main influencing factors reasonably matched those observed in the real experiments.

ii) The change in surface functionality (hydrophobicity) of thermal-NIL microtextured thermoplastic films was studied, confirming a dramatic increase in hydrophobicity due to

the presence of the microtexture vs the flat polymeric surface. Then, the changes in the film surface functionality when it was subjected to a substantial macroscopic deformation were studied, developing later on a method to determine the change. The method was successfully tested. This method was based on a previously existing analytical method that predicts hydrophobicity change as a function of micropillar microdeformation and

completed with local macroscopic deformations obtained from DIC measurements. The model thus obtained can be used, for example, to define geometric parameters of patterns on the NIL stamps to bestow a given texture to the surface prior to thermoforming, knowing a priori the local deformation each area of the surface will experience. It can also provide clues of the maximum sustainable strain a thermoformed film can undergo while still retaining its functional properties.

iii) In the last stage of this research, post processing treatments of the micro/nanotextured polymeric surfaces were carried out. These treatments were twofold: hard coatings and ionic implantation. The main conclussions from the application of trhose treatments were:

a. The hard coating with CrN applied revealed an increase of the surface hardness of an order of magnitude, and the scratch resistance was clearly improved as denoted by the depth and 3D topography of the scratches obtained.

b. In the case of the ionic implantation treatments, the applicability of these treatments on thermoplastic materials was proven for two different ions, showing only a small loss in transparency and a slight decay on their mechanical properties. These losses in mechanical properties can nevertheless be minimised to remain under 15-20% by the optimisation of the specific ion implanted and the process parameters.

c. Also, when applying such treatments over micro/nanotextured surfaces, some small disruptions on the micro/nanotextures top surfaces were observed, although the micro/nanotextured surface preserved its overall morphology largely undamaged. Nevertheless, these small defects produced by the electric arcs can probably be solved by careful fine tuning of the implantation conditions and their effect could even be applied for the obtention of potential benefits such as further modification of the microtexture topographies or introduction of additional levels of hierarchy.

**Study of the shape and functionality variation of Micro/Nanostructured features on thin films by Thermoforming Techniques.**

The study of behaviour and dimensional variation of replicated micro/nanostructures on thermoplastic thin films bringing them from 2D to 3D shapes via thermoforming techniques was also explored:

• The reason to include this additional section within the research lies on the high industrial interest and compatibility of 3D micro/nanotextured functional films with IME products applications, that commonly rely on thermoformed films as part of their technologies.

• The combination of the achievable functionalities by using micro/nanotextured thermoplastic 3D films with those of the electronically printed films shows great potential

for applications such as automotive interior parts, consumer electronics, optics, and lighting, to cite some.

# ANNEXES

# 1. SUPPLEMENTARY INFORMATION TO "INJECTION MOULDING AND CHARACTERIZATION OF MICROTEXTURES ON POLYCARBONATE USING LASER TEXTURED INSERTS"

C. Sáez-Comet, E. Fontdecaba, N. Cuadrado, Eduard Vidales, Jordi Puiggali, L. J. del Valle

*Corresponding author: csaezcomet@gmail.com

## MORPHOLOGICAL CHARACTERIZATION

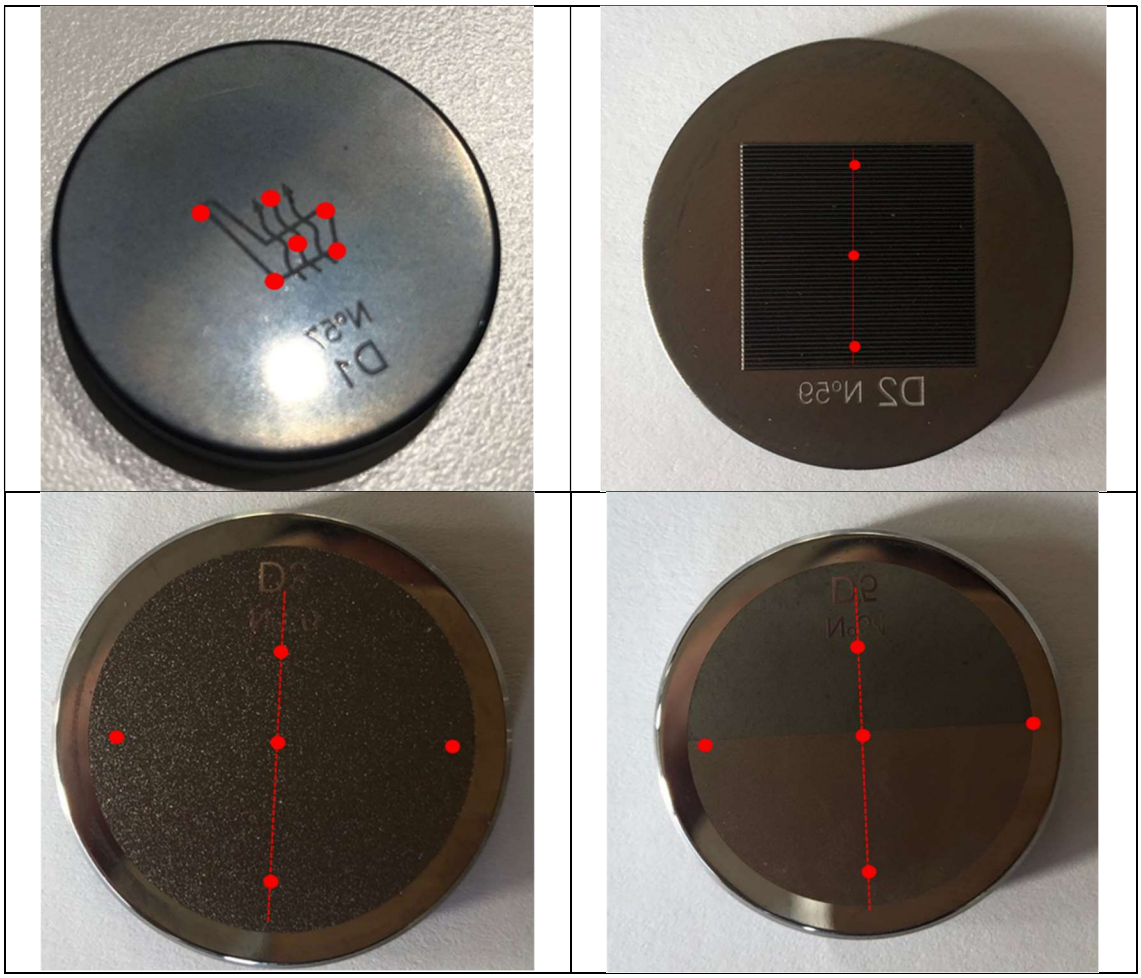

**Figure s1.1. Detail of the points (in red) on the microstructured surfaces of the disks that were used to check the overall morphological uniformity of the microstructure.** ***note that the points are marked on the original steel discs and not on the injected parts for a simpler representation and better contrast***

# DOE

| Exp.number | $T_m$ | $V_{inj}$ | P |
|---|---|---|---|
| 1 | 80 | 100 | 900 |
| 2 | 80 | 100 | 800 |
| 3 | 80 | 150 | 900 |
| 4 | 80 | 150 | 800 |
| 5 | 110 | 100 | 900 |
| 6 | 110 | 100 | 800 |
| 7 | 110 | 150 | 900 |
| 8 | 110 | 150 | 800 |

**Table s1.1.** Experimental design (doe) matrix used for the injection moulding experiments. $2^3$ experiments were established with taguchi method. $t_m$ = mould temperature; $v_{inj}$ = injection speed; and p = holding pressure.

## FUNCTIONAL CHARACTERIZATION

**Figure s1.2. Details of the test set-up utilized for the characterization of light-diffusive microstructures, in which it can be observed how the textured surface is illuminated**

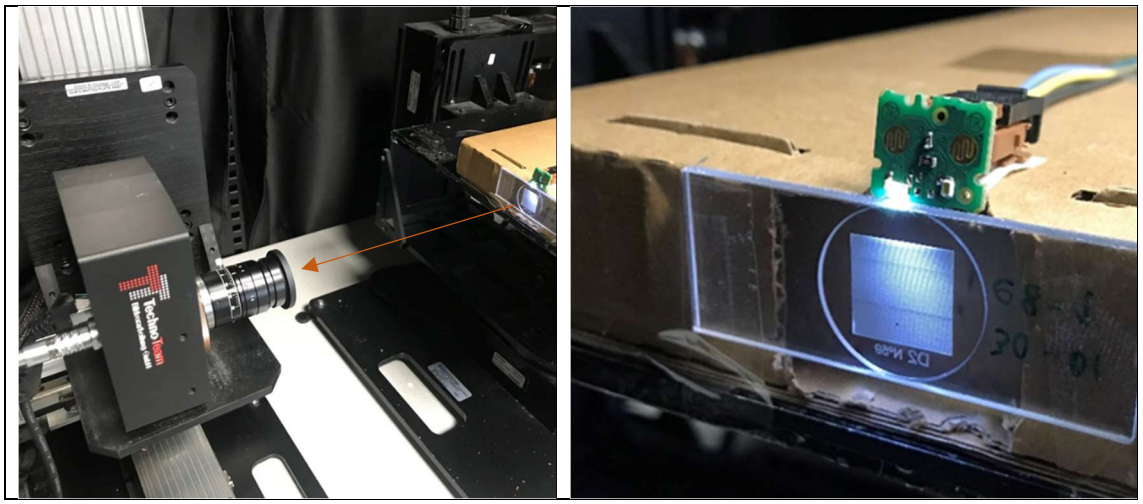

**Figure s1.3. Details of the test set-up utilized for the characterization of light-guiding microstructures.**

| Parameter | Definition | Application |
|---|---|---|
| $S_{tr}$ | *Str*, the Texture Aspect Ratio, is a measure of the spatial isotropy or directionality of the surface texture. For a surface with a dominant lay, the *Str* parameter will tend towards 0.00, whereas a spatially isotropic texture will result in a $S_{tr}$ of 1.00. | *Str* is useful in determining the presence of lay in any direction. For applications where a surface is produced by multiple processes, $S_{tr}$ may be used to detect the presence of underlying surface modifications. Str may find application in detecting subtle directionality on an otherwise isotropic texture |
| $S_a$ | The *Sa* parameter represents an overall measure of the texture comprising the surface. Sa is insensitive in differentiating peaks, valleys and the spacing of the various texture features. ... Sa is typically used for machined surfaces. | $S_a$ may be misleading in that many surfaces with grossly different spatial and height symmetry features (e.g., milled vs. honed) may have the same $S_a$, but function quite differently. Nonetheless, once a surface type has been established, the $S_a$ parameter may be used to indicate significant deviations in the texture characteristics. |
| $S_{dr}$ | $S_{dr}$, the Developed Interfacial Area Ratio, is expressed as the percentage of additional surface area contributed by the texture as compared to an ideal plane the size of the measurement region. | $S_{dr}$ may further differentiate surfaces of similar amplitudes and average roughness. Typically, $S_{dr}$ will increase with the spatial intricacy of the texture whether or not $S_a$ changes. $S_{dr}$ is useful in applications involving surface coatings and adhesion. $S_{dr}$ and may find relevance when considering surfaces used with lubricants and other fluids. $S_{dr}$ is affected by both texture amplitude and spacing. Thus, higher $S_a$, wider spaced texture may have actually a lower $S_{dr}$ value than a lower $S_a$ but finer spaced texture, as displayed above |

**Table s1.2** Surface roughness parameters chosen for the study (extracted from https://www.michmet.com/3d_s_spatial_parameters_sal.htm)

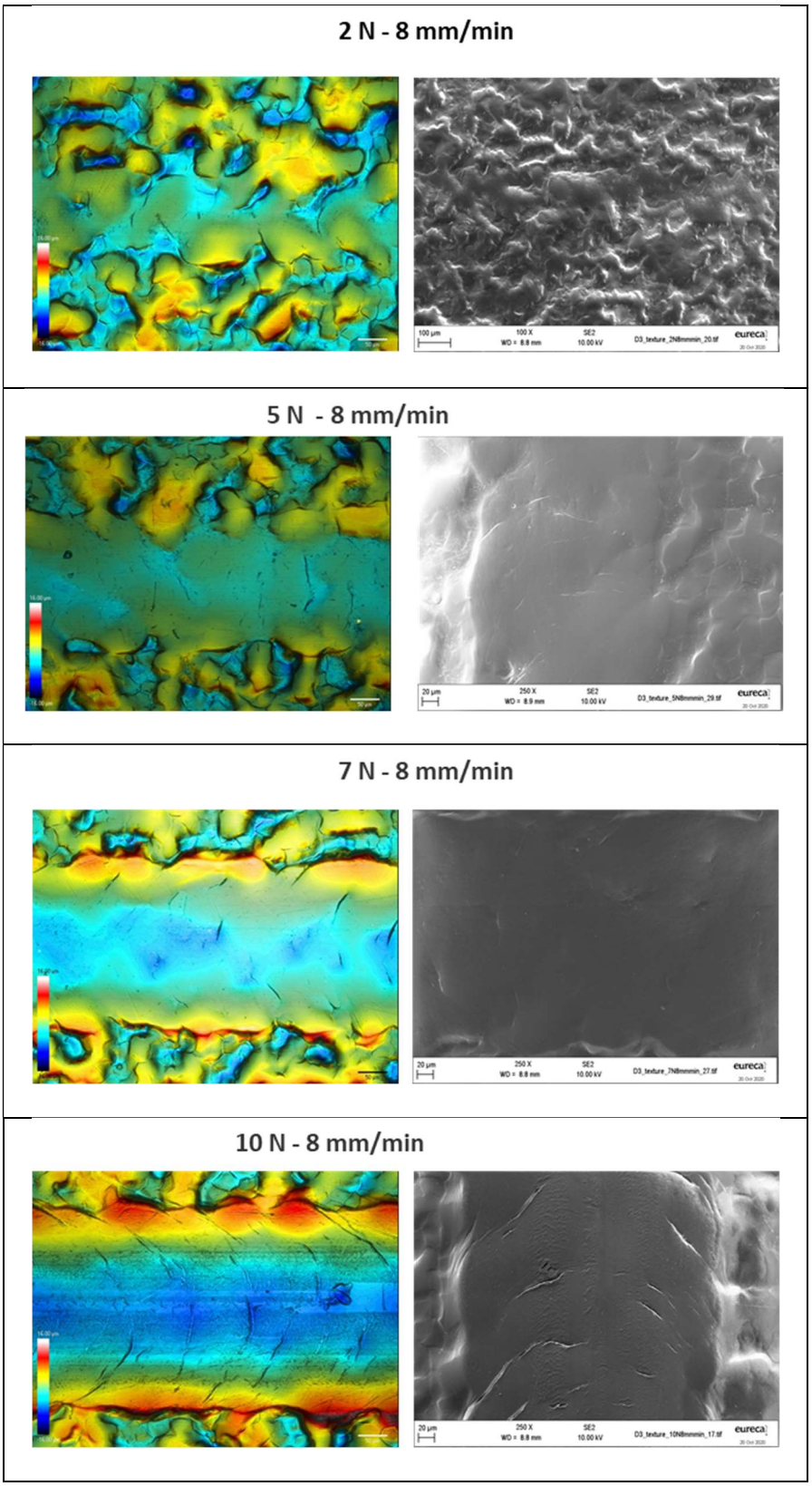


**Figure s1.4. Confocal (200X) and SEM images (250X) of the scratches produced on the D3 textured samples at load levels of 2, 5, 7 and 10 N and speed of 8 mm/min.**

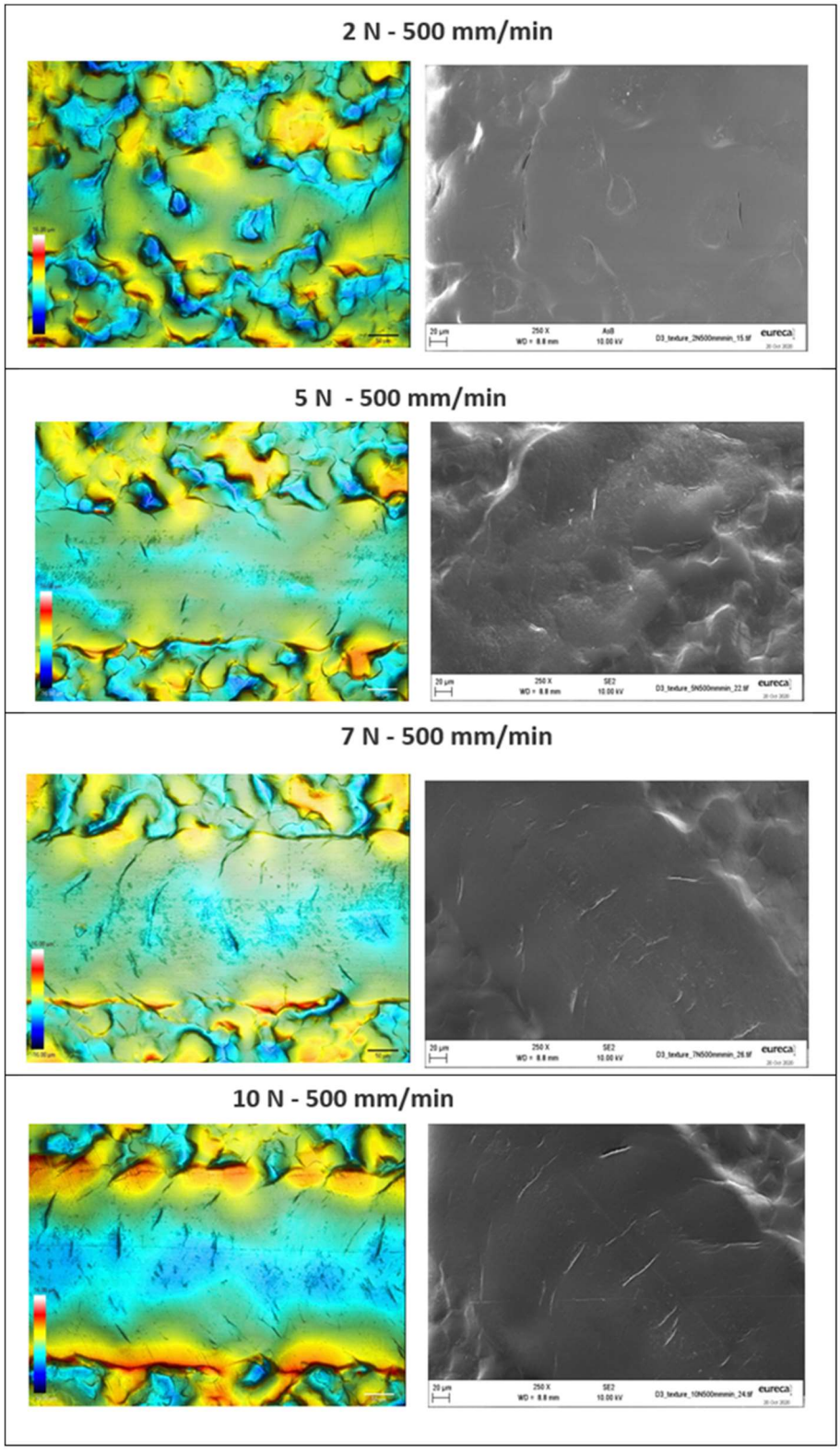


**Figure s1.5. Confocal (200x) and sem images (250x) of the scratches produced on the d3 textured samples at load levels of 2, 5, 7 and 10 n and a common speed of 500 mm/min.**

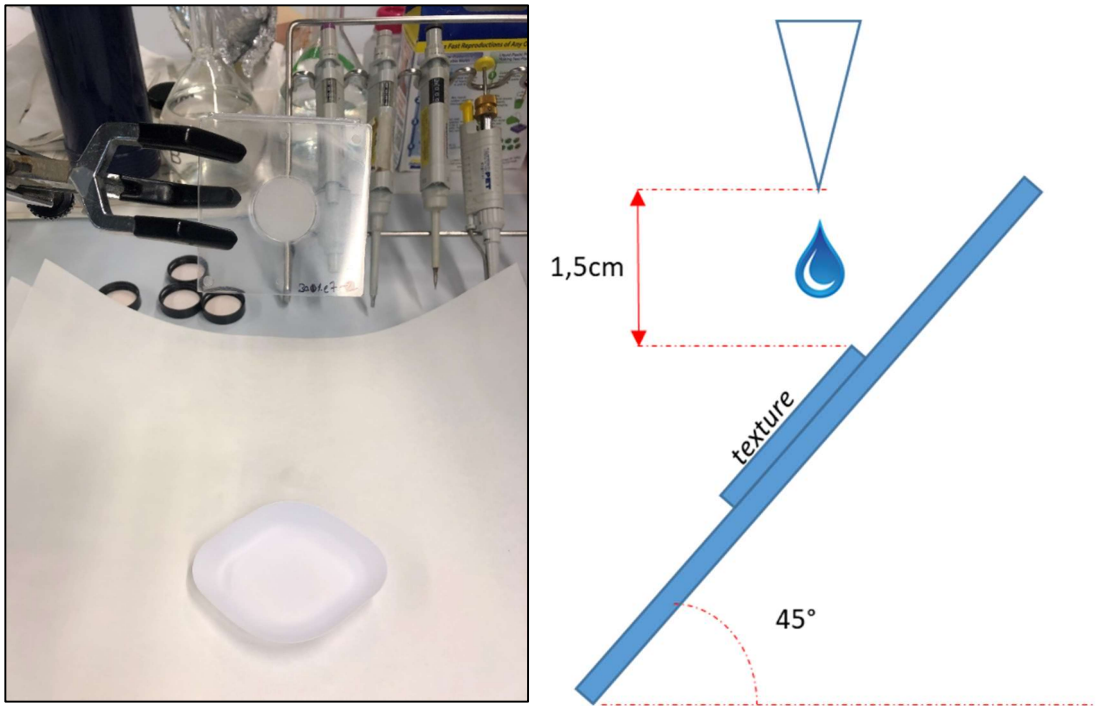


**Figure s1.6. Picture of the set-up used during the *easy to clean* functionality tests (left), and diagram showing the easy-to-clean test set-up.**

## 2.SUPPLEMENTARY INFORMATION ON "INFRARED MOULD-SURFACE HEATING EXPERIMENTS"

a

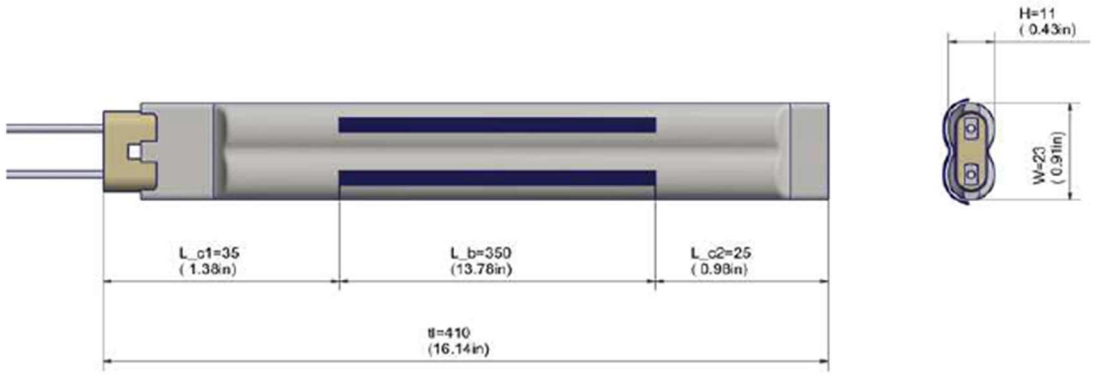

b

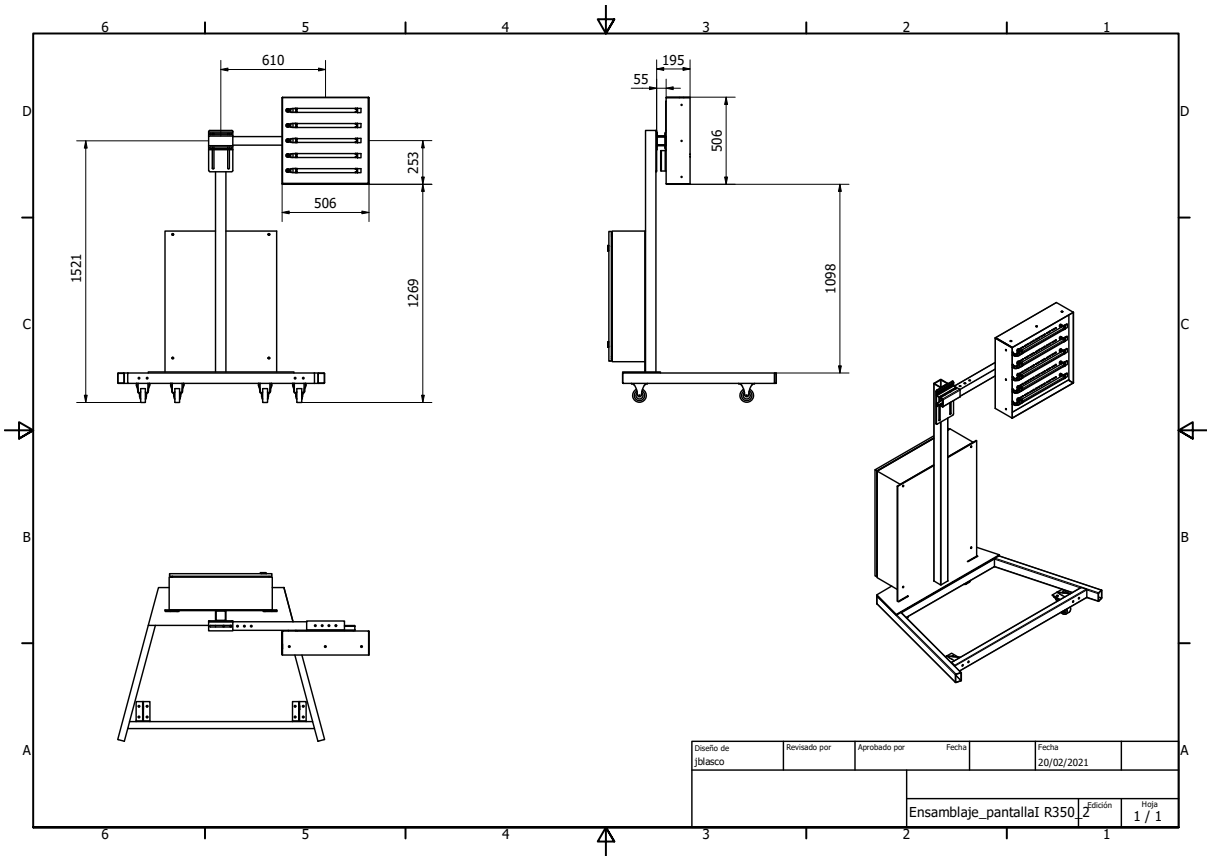
610
253
506
1521
1269
195
55
506
1098
Diseño de
jblasco
Revisado por
Aprobado por
Fecha
Fecha
20/02/2021
Ensamblaje_pantallaI R350_2
Edición
Hoja
1 / 1

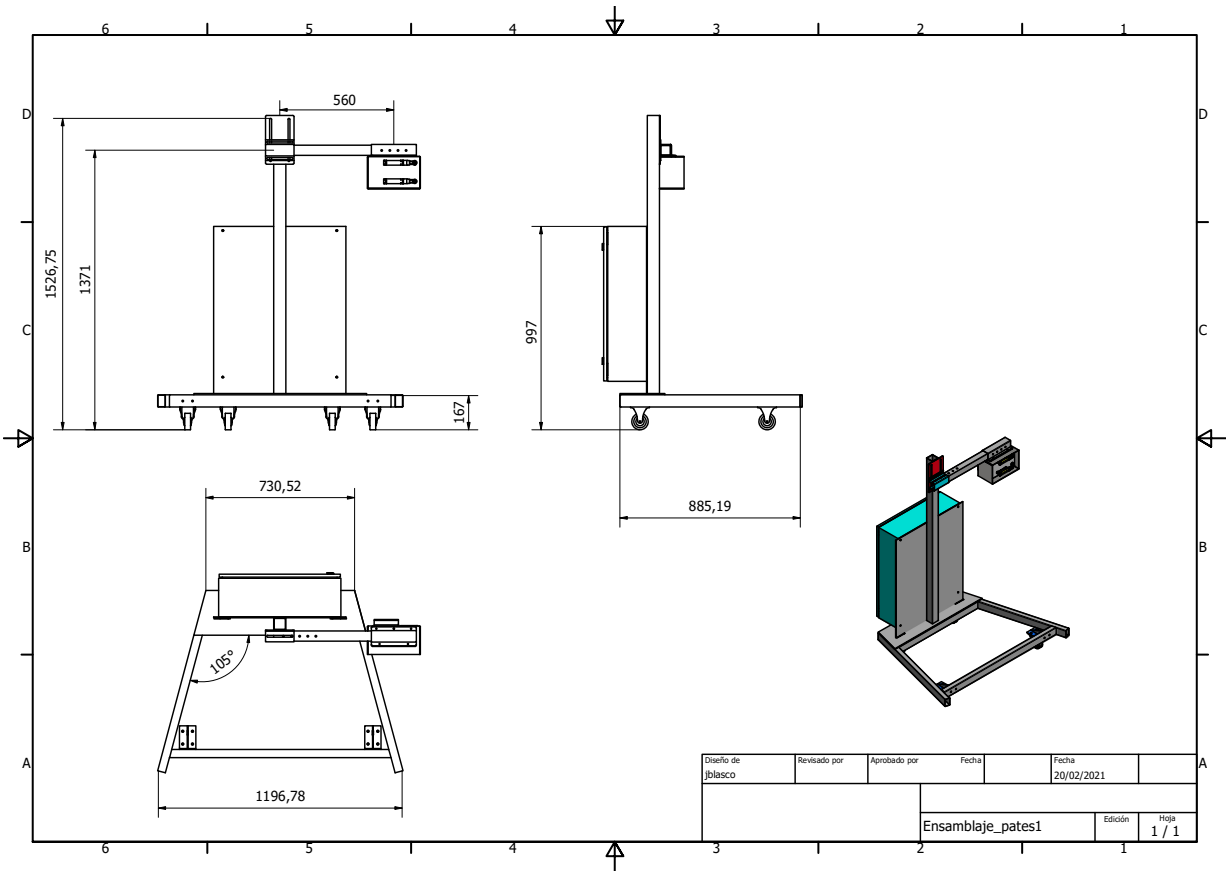
560
1526,75
1371
167
997
885,19
730,52
105°
1196,78
Diseño de
jblasco
Revisado por
Aprobado por
Fecha
Fecha
20/02/2021
Ensamblaje_pates1
Edición
Hoja
1 / 1

C

d

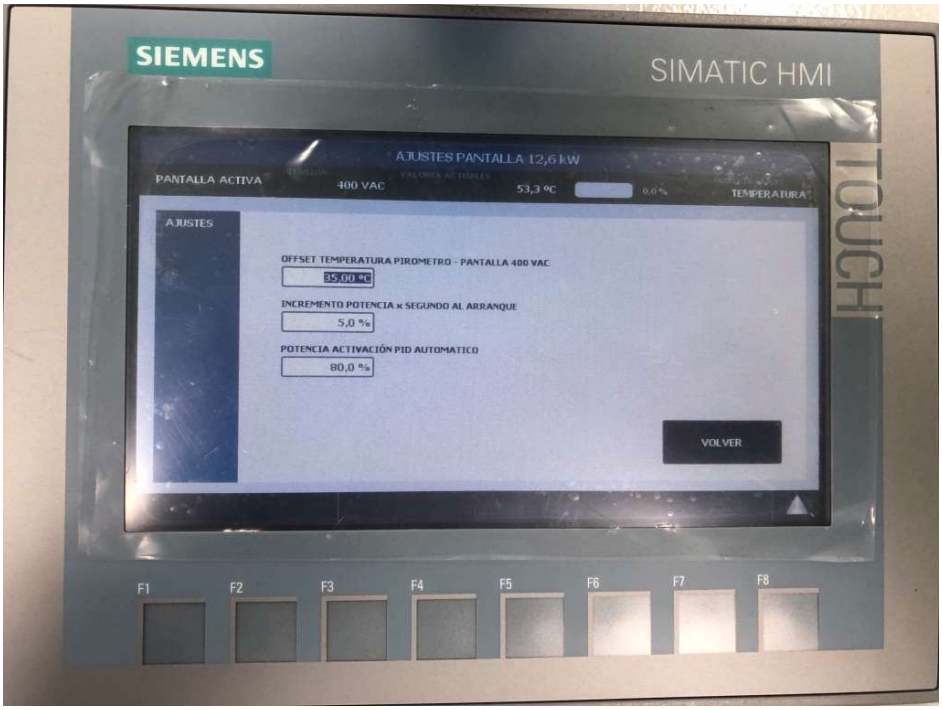


**Figure S6. Image showing a) the lamp type used for the IR-heater, b) the bigger sized heater mounted on the framework, c) the smaller sized heater mounted on the framework, d) the electronic command system. Source: EURECAT**

# 3.SUPPLEMENTARY INFORMATION TO “INTRODUCING SURFACE FUNCTIONALITY ON THERMOFORMED POLYMERIC FILMS”

## Supplemental information

### S1. Geometrical information of the pillar arrays.

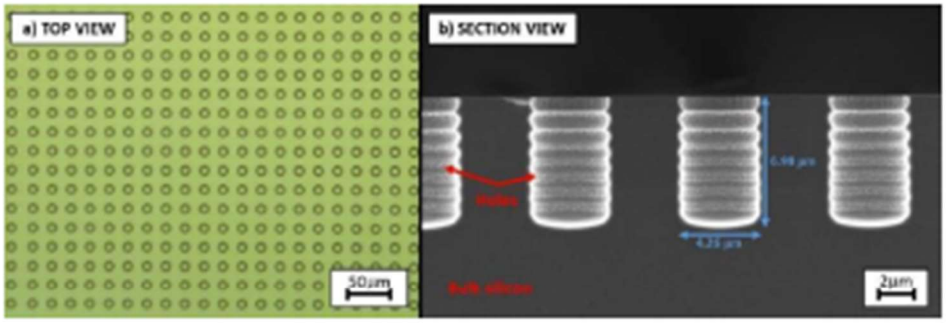


***Figure S1.*** *Finished silicon stamp. A) Top view optical microscopy image of the wells in the silicon. B) SEM image of the section of the wells craved into the silicon. The scalloping present in the contour of the wells is due to the Bosch modified etching process.*

*TableS 1 Nominal and obtained dimensions of the wells in the silicon stamps*

| | Design (µm) | 90º SEM characterization (µm) | |
|---|---|---|---|
| Quadrant | Diameter | Diameter | Depth |
| 1 | 4 | 4.3 | 7.0 |
| 2 | 6 | 6.5 | 7.8 |
| 3 | 8 | 8.9 | 8 |
| 4 | 10 | 9.8 | 8.7 |

## S2. Characterization of the imprinted arrays in the flat zone.

In the results presented in table 2, the 4 zones (size: 250x190 µm each) correspond to 4 different imprints performed with the same stamp.

*Table S2 Values of height (dZ) , diameter and pitch of the replicated patterns on the PC films at 4 different imprints.*

| Imprint | dZ histogram (µm) | Diameter (µm) |
|---|---|---|
| 1 | 10.4 | 6.6 |
| 2 | 9.5 | 6.6 |
| 3 | 9.9 | 6.6 |
| 4 | 9.4 | 6.6 |

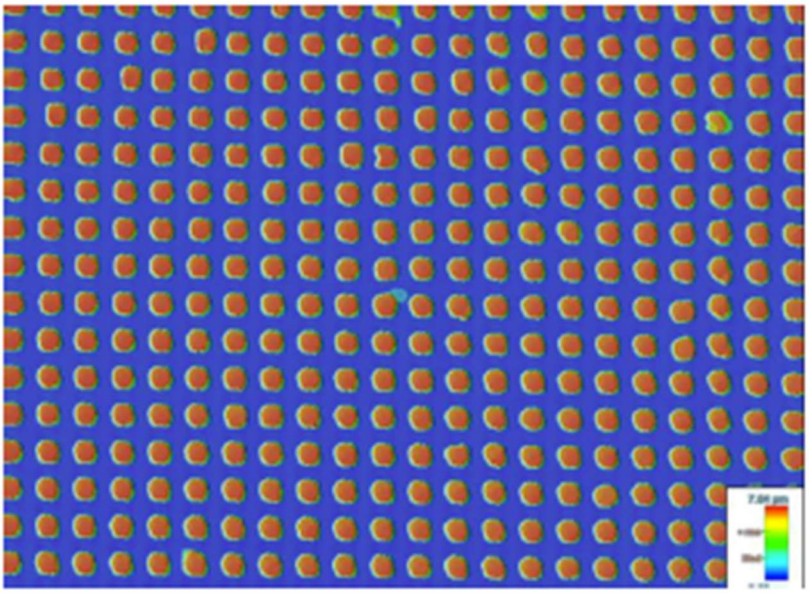

**Figure S2 Example of confocal characterization (a) Topography reconstruction (b) Height histogram**

## S3. Characterization of the imprinted arrays after thermoforming.

The local characterization of the zones 1-5 and the non-thermoformed micro-textured sample were performed by means of confocal microscopy.

*Table S3 Experimental Values for the deformed pillars*

| | Non-textured PC | Textured PC (flat) | Zone 1 | Zone 2 | Zone 3 | Zone 4 | Zone 5 |
|---|---|---|---|---|---|---|---|
| Water contact angle (°) | 77 | 150.6 | 147.7 | 146 | 135.9 | 127.1 | 107.1 |
| Standard Deviation (º) | ±5.3 | ±1.6 | ±4.3 | ±2.4 | ±8.0 | ±3.1 | ±5.1 |
| Curvature Radius (mm) | - | - | 314.5 | 211.3 | 59.8 | 58.6 | 50.1 |
| Linear Draw Ratio | - | - | 2.79 | 2.98 | 2.57 | 2.85 | 4.63 |
| AVG major strain (%) | - | - | 2.8 | 7.1 | 11.6 | 12.1 | 97.4 |
| AVG minor strain( %) | - | - | 0.3 | 1.2 | 4.6 | -1.8 | -15.5 |
| Pillar major radius top (µm) | - | 6.204 | 7.46 | 9.64 | 7.5 | 7.52 | 4.1 |
| Pillar minor radius top (µm) | - | 6.008 | 6.18 | 8.62 | 6.04 | 6.442 | 3.94 |
| Pillar major radius base (µm) | - | 7.55 | 8.97 | 10.97 | 8.3 | 9.02 | 11.84 |
| Pillar minor radius base (µm) | - | 7.64 | 7.62 | 9.97 | 7.45 | 7.65 | 7.78 |
| Array major period (mm) | - | 11.92 | 12.06 | 16.62 | 13.06 | 14.74 | 31.6 |
| Array minor period (mm) | - | 11.9 | 11.68 | 16.06 | 11.84 | 12.58 | 11.4 |
| Pillar height(mm) | - | 9.9 | 7.6 | 8.3 | 6.8 | 6.7 | 7.5 |
| Slope angle (º) (major) | - | 82.26 | 78.76 | 80.90 | 83.29 | 77.38 | 44.10 |
| Slope angle (º) (minor) | - | 80.64 | 79.27 | 80.76 | 78.29 | 79.78 | 62.89 |
| Slope angle (º) (average) | - | 81.45 | 79.02 | 80.83 | 80.79 | 78.58 | 53.49 |
| % Deformation ( major period) | - | 0.00 | 1.17 | 3.88 | 9.56 | 23.66 | 165.10 |
| % Deformation ( minor period) | - | 0.00 | -1.85 | 0.38 | -0.50 | 5.71 | -4.20 |
| % Deformation (major top) | - | 0.00 | 20.25 | 20.50 | 20.89 | 21.21 | -33.91 |
| % Deformation (minor top) | - | 0.00 | 2.86 | 7.75 | 0.53 | 7.22 | -34.42 |
| % Deformation (major bottom) | - | 0.00 | 18.81 | 37.13 | 9.93 | 19.47 | 56.82 |
| % Deformation (minor bottom) | - | 0.00 | -0.26 | 24.63 | -2.49 | 0.13 | 1.83 |

## S4. Determination of the contact angle from the Cassie-Baxter case

The method followed consisted in measuring the geometrical parameters described in Q. Zheng, C. Lü, Procedia IUTAM, Elsevier B.V., 2014: pp. 462–475. https://doi.org/10.1016/j.piutam.2014.01.04 1 for individual pillars in each of the five zones, which take into account the fact that when the dimensions shrink the perimeter/to area ratio increases.

In this model the Cassie-Baxter for an array of microstructures of arbitrary shape is defined as:

$$\cos\theta_{CB} = f\,(1+\cos\theta)\left(1-\frac{l_{cr}}{S}\right)-1$$

Where $f$ is the ratio between the top pillar area and the area of the unit cell of the array, and $S$ is the relation between the top area of the pillar and the perimeter of the top area of the pillar. $l_{cr}$ is a material dependent parameter and $\theta$ is the water contact angle of the flat non-textured surface. We have assumed $l_{cr}$ as 0.9 μm and θ = 77º (determined experimental). The overall behavior of the Cassie-Baxter values of the water contact angle are not critically dependent on $l_{cr}$ for a range of 0.1 μm – 1 μm and we have selected a value for which the absolute value of the water contact angle fit well with the experimental values for the cases of small strain. The values obtained in this way for the water contact angle are presented in Table S4 and displayed in figure 6 (red curve) of the main article.

*Table S4 Determination of the C-B contact angles following* Q. Zheng, C. Lü, Procedia IUTAM, Elsevier B.V., 2014: pp. 462–475. https://doi.org/10.1016/j.piutam.2014.01.04 1

| Zone | Pillar area ($\mu m^2$) | Array unit cell area ($\mu m^2$) | Perimeter (μm) | Fraction area | Size parameter | Contact angle C-B º |
|---|---|---|---|---|---|---|
| Flat | 29.3 | 141.8 | 19.2 | 0.21 | 1.53 | 153.7 |
| Zone 1 | 36.2 | 140.9 | 21.5 | 0.26 | 1.69 | 148.6 |
| Zone 2 | 65.3 | 266.9 | 28.7 | 0.24 | 2.27 | 145.0 |
| Zone 3 | 35.6 | 154.6 | 21.3 | 0.23 | 1.67 | 150.5 |
| Zone 4 | 38.0 | 185.4 | 22.0 | 0.21 | 1.73 | 151.6 |
| Zone 5 | 12.7 | 360.2 | 12.6 | 0.04 | 1.00 | 174.6 |

## Graphical Abstract of Manuscript " Introducing surface functionality on thermoformed polymeric films" by Carlos Saez et al.

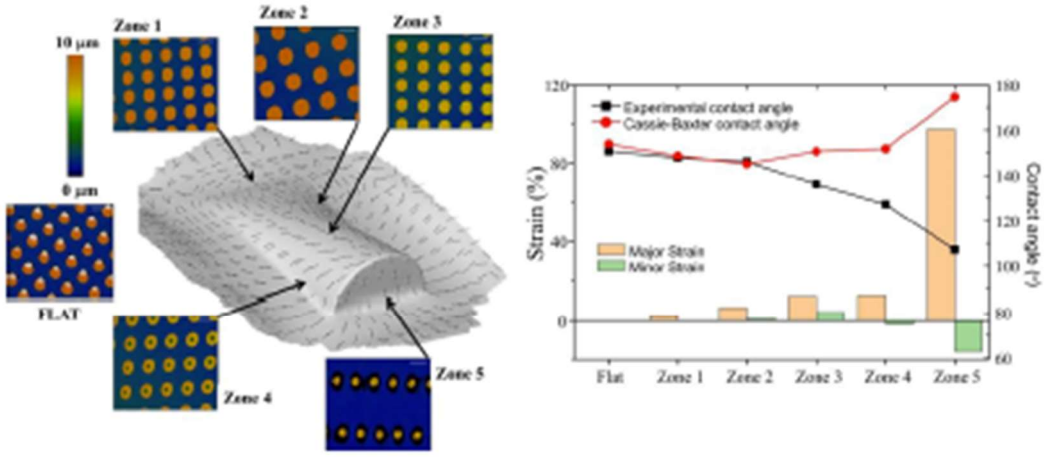

# 4. SUPPLEMENTARY INFORMATION TO "THREE-LEVEL HIERARCHICAL MICRO/NANOSTRUCTURES ON BIOPOLYMERS BY INJECTION MOULDING USING LOW COST POLYMERIC INLAYS"

C. Sáez-Comet [a], O. Muntada [b], N. Lozano [a], E. Fontdecaba[a], P. Sousa[c], J. Llobet[b], F.Perez-Murano [b] Jordi Puiggali[d], L. J. del Valle[d]
*Corresponding author: csaezcomet@gmail.com; Francesc.Perez@csic.es

## Silicon mould fabrication

The silicon mould consists of a 3-level hierarchical structure that is periodically repeated all across a 100 mm silicon wafer. The dimensions and periodicity of the elements in each level are shown in Table S1.

1L stands for the lower level, 2L the middle one and 3L the top level.

| Pattern | Lateral feature size (µm) | Pitch (µm) | Height (µm) |
|---|---|---|---|
| 1L | 0.6 | 1.58 | 0.5 |
| 2L | 6 | 15.8 | 4.8 |
| 3L | 35 | 107.44 | 26.9 |

**Table S4.1.** Dimensions of the three levels of the hierarchical array in the silicon mould

The overall process to fabricate the silicon mould is depicted in figure S1 and it consists of three sequences of photolithography and reactive ion etching.

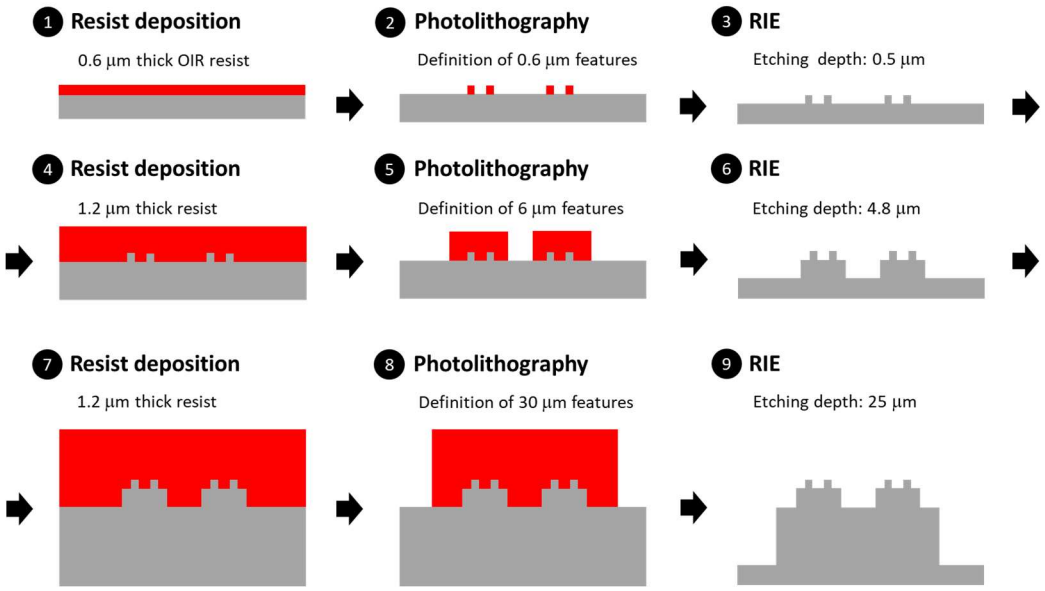


**Figure s4.1. Fabrication of the silicon mould containing 3-level hierarchical structures. Pattern 1L: steps 1-3; pattern 2L: steps 4-6; pattern 3L: steps 7-9**

As the dimensions of the final patterns are below 0.5 µm, we have used a step-and-repeat i-line photolithography system (Nikon NSR-2205i12D). We expose consecutive areas of 3.4 mm x 3.4

mm minimizing the stitching by a careful alignment procedure. Each of these areas contains a continuous array of structures according to the dimensions in Table S1.
The process starts with the deposition of a 0.6 □m thick OiR resist (FujiFilm) and a first photolithography exposition with the aim of defining the common alignment marks for the fabrication of all 3 levels. The marks are placed in two separated locations, approximately 1 cm from the wafer edge and are the key element for the sequential fabrication of each level while maintaining the correct alignment.
After the first exposition, the resist is developed and the 1L pattern is exposed in the same resist as the alignment marks. The area of each 1L repeating unit is 3.4 mm x 3.4 mm, so after each exposition the sample is displaced 3.4 mm precisely in order to maintain the periodicity between the features of one repeating unit and the following.
The resist is developed after the exposure of 1L. Then, a 500 nm depth silicon reactive ion etching (RIE) process is performed using an Alcatel 601E system with a modified Bosch process.
The 1st level structures (1L) are now covered with 1.2 □m thick HiPR 6512 (FujiFilm) resist, which is exposed with the 2L structures/features/element/component. In order to place them exactly in concordance with the position of the 1L features, the mask is positioned using the same exterior alignment marks as for the first level. Next, the exposition is repeated all across the wafer maintaining the periodicity of the features and the resist is developed.
The fabrication of the second level concludes with a 4.8 □m etching (deep RIE) of the 2L features. Note that during this etching step the previously defined 1L features remain protected by the resist. The fabrication of the 3L features is then performed in a similar manner. The first step is to protect the 1L and 2L features with the same 1.2 □m photoresist. Then the 3L repeating units are exposed with the reference of the exterior alignment marks and a constant periodicity. Once exposed, the motives are developed and etched ~25□m with a deep RIE. Figure S2 shows SEM image of the silicion mould.

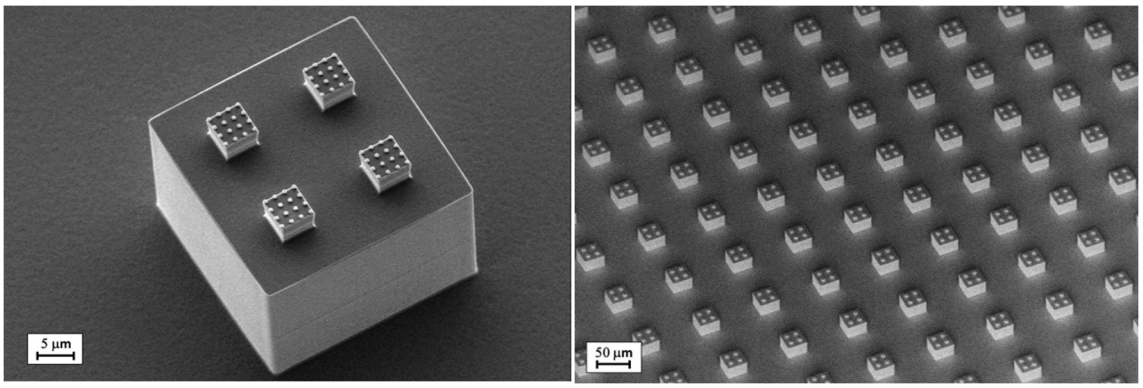


**Figure s4.2 (Left). SEM image of one of the 3-level structures of the silicon master mould. (Right) The basic structure is periodically repeated all across a 100 mm wafer.**

## Replication on polymeric films (inlays)

Step 1: silicon to PMMA
The process starts by applying an anti-sticking layer made of Teflon on the surface of the silicon master mould. Next, the mould is replicated into a 250 □m thick PMMA foil (GoodFellow) by means of thermal nanoimprint lithography in a Eitre® 8 system (Obducat). The first step consisted of heating the sample until it reaches 150 ºC and

keeping it under that temperature during 100s. Then a pressure of 40 bar was applied during 300 s, followed by the demoulding step, which was performed at 80 ºC.

Step 2: PMMA to PDMS

The next step is to replicate the PMMA copy into a Polydimethylsiloxane (PDMS) slab. The preparation of the PDMS (Sylgard® 184, Dow) follows the standard method: the base and the curing agent are mixed in a 10:1 ratio and the mixture was poured inside a recipient over the patterned PMMA foil. The mixture is degassed for 20 min to remove air bubbles and cured at stove during 1h at 80ºC. Finally, the fully cured PDMS is released.

Step 3: PDMS to OrmoStamp®

The PDMS slab is then replicated into OrmoStamp® using Plexiglas® PET films as a substrate.

The PDMS slab is placed on a hotplate at 50 ºC and uncured OrmoStamp® is spread evenly over the surface with the help of a spatula. Then, the PET foil is gently pressed against the PDMS and cured with UV light (wavelength = 365 nm; time = 120 s; power = 11 mW/cm$^2$). A soft post-bake is then performed at 50ºC during 10 min. After the release, an anti-sticking silanitzation treatment (Trichloro(1H,1H,2H,2H-perfluorooctylsilane) is applied to the OrmoStamp + PET plastic inlay during 10 min (figure S3).

**Mould Insert**

The insert provided adequate flatness, leaving the micro/nano textured face of the film exposed towards the interior of the cavity at a reduced depth of 1.25 mm with respect to the mould-insert surface. Also, below the films, an additional uncoated PC 200 mm film was used to enhance its mechanical support during the injection cycles. Thus, the injected specimen (a squared plate of 70 x 70 x 2.6 mm) has an elevation of 23 mm x 62 mm height that is centered on the specimen, on top of which the texture is replicated. Both insert and a replicated part representation can be seen in figure S3.

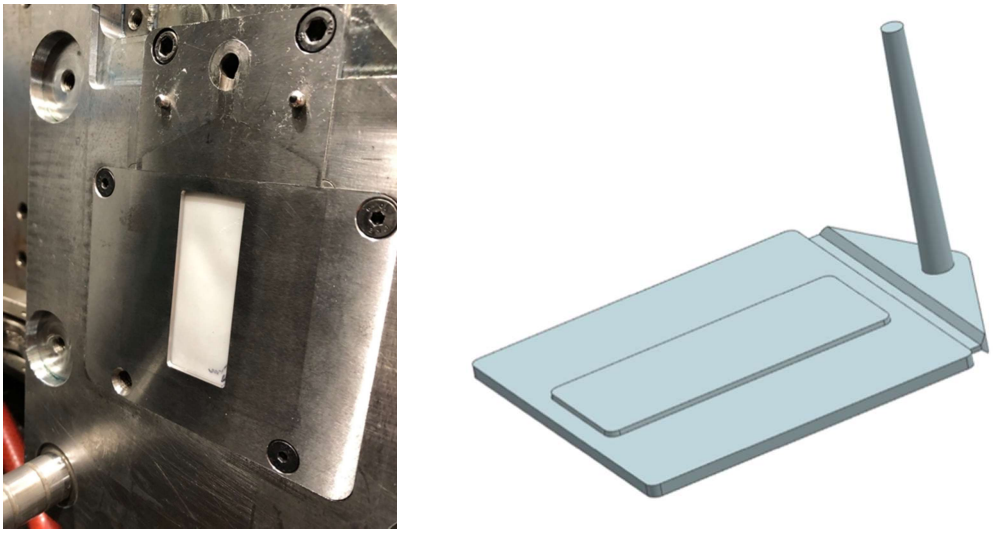

**Figure S4.3. Details of the injection mould insert and the model of the injected part to be obtained.**

## Quality of the replication

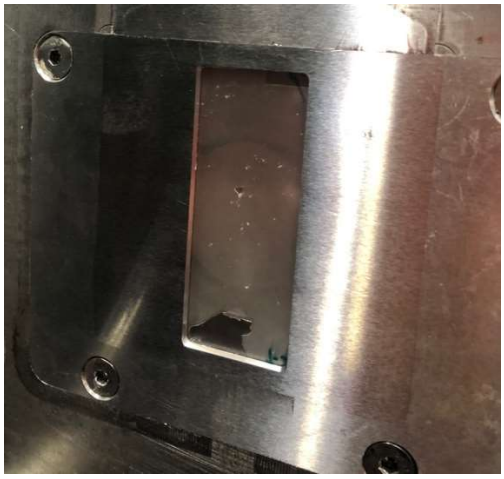

**Figure s4.4. Details of the deterioration of the inlay filmsafter various injection shots, showing coating delamination at its lower section.**

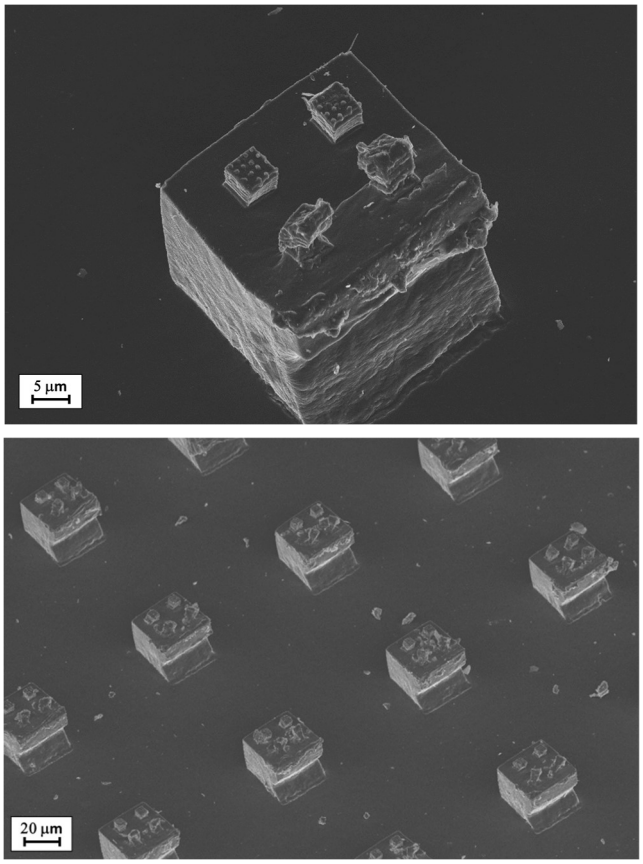


**Figure s4.5. SEM images of deformed micro/nano structures at different magnifications on a PP injected part.**